Facultad de Ciencias

Departamento de Quimica Organica

SYNTHESIS OF FULLERENE-BASED PHTHALOCYANINE AND SUBPHTHALOCYANINE HYBRIDS AND THEIR ELECTRON TRANSFER REACTIVITY

Memoria presentada por

OLGA TRUKHINA

Para optar al grado de

Doctor en Quimica Organica

Madrid, 2015

Entre las dificultades se esconde la oportunidad. (Albert Einstein)

This work was developed in the Department of Organic Chemistry of The Autonoma University of Madrid, under the supervision of Prof. Dr. Tomás Torres Cebada and Dr. Giovanni Bottari to whom I express my most sincere gratitude.

This work was presented in the following articles:

- "Tuning intramolecular electron and energy transfer processes in novel conjugates of $La_2@C_{80}$ and electron accepting subphthalocyanines". L. Feng, M. Rudolf, O. Trukhina, Z. Slanina, F. Uhlik, X. Lu, T. Torres, D. M. Guldi, T. Akasaka. *Chem. Commun.*, **2015**, 51, 330-333.
- "Taming C_{60} fullerene: tuning intramolecular photoinduced electron transfer process with subphthalocyanines". M. Rudolf, O. Trukhina, J. Perles, L. Feng, T. Akasaka, T. Torres, D. M. Guldi. *Chem. Sci.*, **2015**, 6, 4141-4147.
- "$Sc_3N@I_h$-C_{80} – dichotomy in electron transfer reactions". O. Trukhina, M. Rudolf, G. Bottari, T. Akasaka, L. Echegoyen, T. Torres, D. M. Guldi. *J. Am. Chem. Soc*. J. Am. Chem. Soc. **2015**, 137, 12914-12922.
- "Unprecedented regio-, stereo- and atropselective synthesis of an "elusive" *cis*-1 C_{60} fullerene bisadduct racemate by supramolecular-directed functionalization". G. Bottari, O. Trukhina, A. Kahnt, M. Frunzi, Y. Murata, A. Rodríguez-Fortea, J. M. Poblet, D. M. Guldi, T. Torres. **2015.** *Submitted*.

Pre-doctoral stays:

- My first research stay was performed in the group of Prof. A. Osuka in the Department of Chemistry, Graduate School of Science, Kyoto University, Japan, during July – October 2011, under kind guidance of Dr. N. Aratani, thanks to whom I profound my knowledge in chemistry of porphyrinoids.
- Photophysical measurements were carried out in the group of Prof. Dirk M. Guldi in the Department of Chemistry and Pharmacy of Friedrich-Alexander-Universität of Erlangen-Nürnberg, Germany, in September – October 2012, in close collaboration with Dr. M. Rudolf.
- Experience in chemistry of endohedral metallofullerenes was gained during research stay in the group of Prof. L. Echegoyen in the Dept. of Chemistry of the University of Texas at El Paso, EEUU, in April – May of 2013, with the help of his excellent co-workers – Dr. Marta Izquierdo y Maira Ceron.

Acknowledgements

I would like to express my most sincere gratitude to my research supervisors - *Prof. Tomás Torres* and *Prof. Giovanni Bottari* - for their continuous encouraging, support and guidance, as well as for being an infinite source of inspiration and vitality.

I would also like to thank a whole research group of Prof. Torres – in all its generations – that welcomed me during these years and provided excellent facilities for carrying out a doctoral stay. I dedicate a special acknowledgement to the core scientists – *Puri*, *Marivi*, *Gema*, *Salome*, *Gianni*, *David* – for being bright examples of expertise, persistence and commitment to science. Also, I want to thank *Andres*, *Ismael*, *Maxence* and *Miguel* for their dedication to the chemistry of porphyrinoids while helping the group in making it more interdisciplinary and multifaceted. I'd like to extend my thanks to those of friends and co-workers that have successfully defended their PhD thesis: *Juanjo*, *Beatriz*, *Anais*, *Angel*, *Mine*, *Irene*, *Maria Sanchez*, *Julia*, *Francesca* and *Carol*, with whom I spend the most of time sharing the lab. Special thanks for *Maria Medel* – for her kind friendship and help to *Maksim Filatov* during his research stay in the group. Many thanks and all the best wishes for current "active hands" of the lab: *Edu*, *German*, *Javi*, *Ettore*, *Lara*, *David*, *Eveline*, *Joana* and *Giulia*. Special regards to *Cinthya* and *Esmeralda* for becoming good friends.

I am very thankful to my close collaborators: *Prof. Luis Echegoyen* and *Prof. Takeshi Akasaka* – for their keen advices and precious samples of endohedral metallofullerenes. Thanks to *Prof. Dirk M. Guldi* and his team for performing time-resolved study which provided valuable data for this work. I also express my utmost thanks to *Prof. Mikhail Islyaikin* who has motivated and encouraged me for all scientific achievements up to date. I would also like to thank the faculty and staff of the Organic Chemistry Department and the Interdepartmental Research Service of UAM for their excellent work. I appreciate very much the FPI fellowship of UAM and the funding coming from projects coordinated by Prof. T. Torres.

I most certainly thank my family for their support and constant presence in my life.

Thank you all.

Abbreviations

Pc	phthalocyanine
SubPc	subphthalocyanine
EMF	endohedral metallofullerene
PET	photoinduced electron transfer
DIPEA	N,N-Diisopropylethylamine
TCAQ	tetracyanoanthraquinodimethane
ex-TTF	extended tetratiafulvalene
Por	porphyrin
CR	charge recombination
CS	charge separation
D-A	Donor-Acceptor
Por	porphyrin
CNT	carbon nanotubes
AgOTf	silver(I)triflate
COF	covalent organic framework
PPV	poly(*p*-phenylenevinylene)
NG	nanographene

Table of contents

Resumen en español

Resumen en español

El progresivo agotamiento de combustibles fósiles derivado de la ejecución de todo tipo de actividades humanas constituye una de las características más representativas de la sociedad moderna y hace imprescindible la búsqueda de fuentes de energía alternativas. De hecho, la energía es tan esencial para mantener y aumentar nuestros niveles económicos, que hoy en día uno de los retos más urgentes a los que se enfrenta nuestra sociedad viene dado por la búsqueda de nuevas fuentes para el desarrollo sostenible. Una de las líneas más atractivas para abordar este problema, y quizás la más prometedora para cubrir la demanda energética mundial a largo plazo, consiste en utilizar la luz solar.[1] La conversión de energía solar basada en materiales orgánicos es un campo de investigación y desarrollo relativamente joven en el área de la fotovoltaica.[2]

La explotación práctica de esta tecnología requiere finalmente la fabricación de dispositivos que exhiban tanto poder de conversión como largos tiempos de vida y, desafortunadamente, hasta ahora no ha sido posible combinar una eficiencia óptima de estos dispositivos con una buena estabilidad y procesabilidad. El reciente desarrollo en el área de dispositivos orgánicos emisores de luz, que enfrentan retos materiales y tecnológicos similares a los de las células solares, muestra que los pasos limitantes de los materiales orgánicos podrían superarse y el diseño de células solares orgánicas es, por tanto, viable.

Uno de los objetivos principales en este campo es el diseño de dispositivos compuestos de una unidad dadora y otra aceptora de electrones, ya que estos sistemas resultan cruciales en una de las etapas clave de la fotosíntesis como es la transferencia electrónica fotoinducida.[3] Los sistemas dador-aceptor (D-A) también se utilizan como componentes de dispositivos fotovoltaicos.[4] La comprensión de los procesos de transferencia electrónica y de energía que tienen lugar en dispositivos orgánicos entre dos especies químicas π-conjugadas, electroactivas, unidas covalente o no-covalente, son conceptos estimulantes en el ámbito de una ciencia emergente como es la electrónica molecular.

---

1 R. Eisenberg, D. G. Nocera, *Inorg. Chem.* **2005**, *44*, 6799-6801.

2 a) *Clean Electricity from Photovoltaics*, M.D. Archer y R. Hill, Eds. Imperial Collage Press, **2001**; b) *Organic Photovoltaics: Concepts and Realization,* C. Brabec, V. Dyakonov, J. Parisi, N.S. Sariciftci Eds. Springer, **2003**; c) St. D. Dimitrov, J. R. Durrant. *Chem. Mater*. **2014**, *26*, 616-630.

3 a) *Electron Transfer in Chemistry*, Ed. V. Balzani, Wiley-VCH: Weinheim, Germany, **2001**; b) S. Speiser *Chem. Rev.* **1996**, *96*, 1953-1976; c) Sh. Fukuzumi, K. Ohkubo, T. Suenobu, *Acc. Chem. Res.* **2014**, 47, 1455-1464.

4 M. Grätzel. *Inorg. Chem.* **2005**, *44*, 6841-6851.

Resumen en español

En el contexto en que se enmarca esta tesis, las sistemas D-A se emplearán para dar lugar a estados de separación de carga por tener una función captadora de fotones y dadora de electrones y una parte receptora de electrones, con el propósito de estudiar de manera efectiva y sencilla ciertos cromóforos que podrían participar en procesos fotoinducidos, produciéndose así una conversión de luz visible.

La ftalocianina (Pc) fue observada por primera vez en el 1928 como una impureza azul en el proceso de la producción de la ftalimida en la planta de Grangemouth perteneciente a Scottish Dyes. La estructura del cromóforo fue descubierta mas tarde por Sir Reginald Linstead del Imperial College de Londres.[5] Durante decadas, las Pcs[6] se utilizaron básicamente como colorantes. Finalmente, las Pcs se convertieron en los materiales de "amplio espectro" aplicables en la fabricación de dispositivos optoelectrónicos como consecuencia de sus propiedades semiconductoras[7] y ópticas no lineales[8], por lo que presentan un gran interés científico y tecnológico. La relevancia de las Pcs y compuestos relacionados radica en su excepcional estabilidad y su fuerte absorción óptica en la zona del rojo/infrarrojo cercano. Éstas poseen un sistema electrónico bidimensional, de carácter aromático con 18 electrones π, sobre el cual pueden llevarse a cabo múltiples modificaciones, introduciendo por ejemplo más de 70 átomos metálicos o no metálicos diferentes, sustituyendo una gran variedad de grupos funcionales en la periferia. Además, funcionalizando adecuadamente estos macrociclos pueden ajustarse sus propiedades redox, y obtener desde unidades oxidantes[9] hasta ftalocianinas con carácter reductor.[10]

---

5 R.P. Linstead. J. Chem. Soc. **1934**, 1016-1017.

6 a)"Phthalocyanines. Properties and Applications", Vols. 1-4 (Eds. C.C. Leznoff, A. B. Lever), VCH Publishers, Inc., Cambridge, 1996. b) "The Porphyrin Handbook", Vols. 15-20 (Eds. K.M. Kadish, K.M. Smith, R. Guilard), Academic Press, San Diego, 2003.

7 a) Ch. Qian, J. Sun, L. Zhang, H. Huang, J. Yang, Y. Gao. *J. Phys. Chem. C.* **2015**, 119, 14965-14971; b)P. Li, Y. J. Zhang, L. Cai, B. F. Ding, J. Xiang, G. Wang, K. Alameh, D. Ch. Zhou, Q. L. Song. *Org. Electron.* **2015**, 26, 75-80; c)G. de la Torre, M. Nicolau, T. Torres. *Phthalocyanines: Synthesis, Supramolecular Organization and Physical Properties* in "Supramolecular Photosensitive and Electroactive Materials" (Ed. H. Nalwa), Academic Press, New York, 2001.

8 a) O. M. Bankole, T. Nyokong. *J. Coord. Chem.* **2015**, 68, 3727-3740; b)G. de la Torre, P. Vázquez, F. Agulló-López, T. Torres, *Chem. Rev.* **2004**, *104*, 3723-3750.

9 X. Li, L. E. Sinks, B. Rybtchinski, M. R. Wasielewski, *J. Am. Chem. Soc.* **2004**, *126*, 10810-10811.

10 E. M. Maya, E. M. García-Frutos, P. Vázquez, T. Torres, G. Martín, G. Rojo, F. Agulló-Lopez, R. H. González-Jonte, V. R. Ferro, J. M. García de la Vega, I. Ledoux, J. Zyss, *J. Phys. Chem. A* **2003**, *107*, 2110-2117.

La subftalocianina (SubPc)[11] representa el menor homologo de la Pc y se conoce como macrociclo aromático con 14 electrones π que presenta una estructura cóncava formada por la unión de tres unidades de 1,3-diiminoisoindol fusionadas alrededor de un átomo de boro. Las SubPcs fueron descubiertas por Meller y Ossko en 1972, cuando estos investigadores intentaban obtener una Pc de boro.[12] En cuanto a sus propiedades, las SubPcs poseen de una intensa absorción en la región del UV-vis, y presentan propiedades fotofísicas y electroquímicas[13] que las hacen buenas candidatas para diversas aplicaciones en sistemas de transferencia de energía y de electrones (OLEDs, células solares, óptica no lineal, *etc*).[14]

A pesar de todo lo expuesto, sólo recientemente se ha comenzado a prestar atención a las propiedades de transferencia electrónica fotoinducida de las Pcs y SubPcs con potenciales aplicaciones en área de fotovoltaica. Aún se requiere un considerable esfuerzo sintético especialmente dirigido a la preparación de las sistemas D-A basados en Pcs y SubPcs y el estudio de las propiedades de los materiales basados en estos compuestos, permitiendo la realización de procesos iterativos de optimización de la propiedad física.

---

11 a) C. G. Claessens, D. Gonzalez-Rodriguez, T. Torres, *Chem. Rev*., **2002**, 102, 835-853; b) T. Torres, *Angew. Chem. Int. Ed*., **2006**, 45, 2834-2837. c) S. Shimizu, N. Kobayashi. *Chem. Commun.* **2014**, 50, 6949-6966.

12 A. Meller, A. Ossko, *Monatsh. Chem.* **1972**, 103, 150-155.

13 a) D. Gonzalez-Rodriguez, G. Bottari, *J. Porphyr. Phthalocya*. **2009**, 13, 624-636. b) B. del Rey, U. Keller, T. Torres, G. Rojo, F. Agulló-López, S. Nonell, C. Martí, S. Brasselet, I. Ledoux, J. Zyss, *J. Am. Chem. Soc*, **1998**, *120*, 12808-12817.

14 a) H. H. P. Gommans, T. Aernouts, B. Verreet, P. Heremans, A. Medina, C. G. Claessens, T. Torres *Adv. Funct. Mater*., **2009**, *19*, 3435-3439; b) B. Verreet, B. P. Rand, D. Cheyns, A. Hadipuor, T. Aernouts, P. Heremans, A. Medina, C. G. Claessens, T. Torres, *Adv. Energy Mat.*, **2012**, *1*, 565-568; c) Y. Zou, R. J. Holmes, *ACS Appl. Mater. Int*. **2015**, 7, 18306-18311. d) J. S. Castrucci, D.S. Josey, E. Thibau, Z.-H. Lu, T. Bender, *J. Phys. Chem. Lett.* **2015**, *6*, 3121-3125. e) K. Cnops, G. Zango, J. Genoe, P. Heremans, M. V. Martinez-Diaz, T. Torres, D. Cheyns. *J. Am. Chem. Soc.* **2015**, 137, 8991-8997.

Objetivos

El objetivo general de este proyecto es el desarrollo de materiales moleculares basados en derivados de Pc, capaces de dar lugar a procesos de transferencia electrónica fotoinducida. Modificaciones estructurales de las Pc y sus análogos como subftalocianinas (SubPcs) permiten la "confección a medida" de sus parámetros electrofísicos dentro de un amplio rango.

Así pues, los objetivos básicos son:

- Preparación de híbridos Pc y fullereno no covalentes, utilizando ambos - fullereno endohedrico $Sc_3N@I_h\text{-}C_{80}$ y fullereno C_{60}, aprovechando las amplias posibilidades de la quimica redox de estos compuestos.
- Preparación de conjugados de SubPc y fullereno covalentes, utilizando ambos - fullereno endohedrico $La_2@I_h\text{-}C_{80}$ y fullereno C_{60}, explorando las propiedades electron-aceptoras de las SubPc y raro comportamiento electron-dador de fullerenos.
- Estudio fotofísico de dichas sistemas con el objetivo de demostrar su capacidad de actuar como interrumptores moleculares.
- Síntesis y estudio de los bis-aductos de la Pc a C_{60} a través de la reacción de Prato y el estudio de los factores supramoleculares que afectan a la formación de los bisaductos.
- -Preparacion de los sistemas multicromóforos de Pc y C_{60}, que pueden dar lugar a procesos de transferencia electrónica fotoinducida.

Capítulo 1: Endohedral metallofullerene-based phthalocyanine and subphthalocyanine hybrids for tunable electron transfer.

Este capítulo se centra en el uso de las Pcs y SubPs como dadores y/o aceptores de electrones para reveler capacidad de los fullerenos de actuar como reductor u oxidante bajo la irradiación con la luz, así modulando la dirección de la transferencia electrónica fotoinducida, así realizando el concepto del interrumptor molecular.

En la primera parte del capítulo, se describe un estudio sistemático sobre autoensamblaje de los sistemas supramoleculares basados en las Pcs de distinto character electrónico y los derivados de fullerenos $Sc_3N@I_h$-C_{80} y C_{60}.[15] Para ello se prepararon las Pcs de zinc (II) simétricas con los sustituentes dadores de electrones (*tert*-butilos) o aceptores de electrones (grupos alquilsulfonil) en periferia de macrociclo, tratando de la sintesis de los ftalonitrilos y su posterior tetramerizacion. Los derivados piridil de $Sc_3N@I_h$-C_{80} y C_{60} han sido preparados con un buen rendimiento por reacción de tipo Prato que permite el control sobre el modo de adición a la bola en cada caso. Así, los fullerenos han sido funcionalizados por piridilglicina vía formación de iluros de azometino en presencia de formaldehido.

Los experimentos llevados a cabo, entre los que se cuentan ensayos de espectrometría de masas, Job's plots y valoraciones, permitieron determinar que la estequiometría del complejos Pc-fullereno autoensamblados corresponde a la composición 1:1 y no depende de la naturaleza electrónica de las Pcs ni fullerenos. La cinética del equilibrio de formación del complejo, tampoco se ha mostrado afectada por la composicion de este, dando las las constantes de asociación aproximadamente del mismo orden de magnitud (10^6 M^{-1}).

Por otro lado, experimentos fotofísicos pusieron de manifiesto que una vez formado el complejo, se produce un quencheo de fluorescencia de la unidad de la Pc, con una transferencia de energía fotoinducida desde el primer singlete excitado de la Pc al del fullereno en question. Importante, el character electron-dador o electron-aceptor de la Pc ha mostrando tener una influencia sobre la dirección de la transferencia electronica fotoinducida. Llendo más en detalle, bajo la fotoexcitacion, fullereno $Sc_3N@I_h$-C_{80} reveló su natiraleza dual, siendo un dador de los electrones en caso del complejo con la hexa(pentilsulfonil) Zn(II)Pc y un acceptor de los electrones en caso

[15] O. Trukhina, M. Rudolf, G. Bottari, T. Akasaka, L. Echegoyen, T. Torres, D. M. Guldi. *J. Am. Chem. Soc.* **2015**, 137, 12914-12922.

del complejo con la tetra(*tert*-butil) Zn(II)Pc. Según nuestros conocimientos en el área, el caso del piridil derivado de $Sc_3N@I_h$-C_{80} presenta el primer ejemplo del comportamiento dual en las reacciones de la transferencia electronica fotoinducida. Al contrario, fullereno C_{60} dió lugar al estado de separacion de cargas unicamente en caso del complejo con la Zn(II)Pc de character dadora de electrones. El complejo de hexa(pentilsulfonil) Zn(II)Pc y C_{60} reveló unicamente las caracteristicas de la transferencia de energía.

En la segunda sección del capítulo se utiliza el metodo covalente para unir las unidades de SubPcs y fullerenos $La_2@I_h$-C_{80} y C_{60}.[16] Se decidió emplear las SubPcs que poseen en su periféria los sustituentes del caracter fuerte electron-atrayente como los grupos de fluor y pentilsulfonil para revelar las propiedades reductoras de ambos fullerenos y forzar la transferencia electronica fotoinducida desde los fullerenos $La_2@I_h$-C_{80} y C_{60} hacia la unidad de SubPc. Según nuestro conocimiento, en la bibliografía no existe ningun ejemplo sobre la capacidade del fullereno C_{60} a actuar como dador de los electrones siendo activado unicamente por fotoexcitacion.

Sintesis de las SubPcs se llevo al cabo a travéz de ambos modos - la modificación periferica y la axial. La modificación periferica ha permitido formar las SubPcs con el fuerte caracter electron-atrayente. Modificacion en axial fue la clave para la sintesis de los derivados de SubPcs con grupo aldehido. Los derivados de SubPc con grupos formilfenoxi en axial han sido unidos a los fullerenos $La_2@I_h$-C_{80} y C_{60} a travez de la reaccion de tipo Prato, vía formación de iluros de azometino en presencia de N-metilglicina. Fullereno $La_2@I_h$-C_{80} dio lugar a dos regioisomeros de adicion que fueron aislados y caracterizados.

Importante, que en todos casos hemos sido capaces de justificar la transferencia electronica fotoinducida con los metodos mas avanzados de la espectroscopia ultra rápida de barrido (absorción y fluorescencia). Por otro lado, el diseño racional de los derivados de Pc y SubPc nos ha permitido la modulación de los parámetros fotofísicos de la manera precisa para conseguir los fines pretendidos. Finalmente, ambos modos de formación de los híbridos – covalente y no covalente – han sido realizados con exito.

[16] a) L. Feng, M. Rudolf, O. Trukhina, Z. Slanina, F. Uhlik, X. Lu, T. Torres, D. M. Guldi, T. Akasaka. Chem. Commun., **2015**, 51, 330-333; b) M. Rudolf, O. Trukhina, J. Perles, L. Feng, T. Akasaka, T. Torres, D. M. Guldi. Chem. Sci., **2015**, 6, 4141-4147.

Capítulo 2: C_{60} fullerene-based phthalocyanine systems: from dimers to multicomponent arrays

En este capítulo se sintetizan y se estudian las estructuras de Pc y fullereno C_{60} multicromóforas covalentes tales como los productos de bisadicion de las Zn(II)Pc a C_{60} y los sistemas octupolares basados en el anillo del benzene hexasustituido port res unidades de Pc y tres unidades de C_{60} alternados entre ellos.

Para llegar a los bisaductos de Pc a C_{60}, se han utilizado la reacción de Prato: una unidad de fullereno C_{60} ha sido funcionalizada con formil-derivados de Zn(II)Pc vía formación de iluros de azometino según la cicloadición 1,3-dipolar en presencia de N-metilglicina. La formacion de los bisaductos correspondientes a los agregados de tipo H con un elevado rendimiento, entre otros, ha sido justificada por un amplio espectro de los metodos tales como la espectroscopia de absorción, espectrometría de masas, resonancia magnetica nuclear y calculos teoricos. Adicionalmente, todos los sistemas han sido caracterizados con los metodos de electroquímica y fotofísica. En este estudio se ha demostrado por primera vez que las interacciones no covalentes de tipo apilamiento π-π entre las dos unidades de Pc no enlazadas pueden ser de utilidad para promover la sintesis regio- , estereo- y atroposelectiva de los bisaductos de C_{60}. Al pesar de que las interacciones supramoleculares han sido utilizado exstensivamente para construir los sistemas complejos a base de C_{60} ,[17] el nuestro estudio representa el primer caso cuando las fuerzas no covalentes dirigen la doble adicion a la bola de C_{60}.

La segunda sección de este capítulo está dedicada a la sintesis de los sistemas octupolares basados en el anillo del benzeno hexasustituido por tres unidades de Zn(II)Pc y tres unidades de C_{60} alternados. Para llegar a este fin, se ha utilizado una reacción de ciclotrimerización de alquinilderivado de Zn(II)Pc con un grupo de aldehido en terminal, catalizada por cobalto. Una vez preparado, el conjugado con tres Zn(II)Pcs y tres aldehidos en terminal alternados, ha sido funcionalizado con tres unidades de fullereno C_{60} vía formación de de iluros de azometino según la cicloadición 1,3-dipolar en presencia de N-octylglicina. Los compuestos correspondientes han sido caracterizados por las técnicas habituales cómo espectrometría de masas, resonancia magnética nuclear, espectroscopia de luz ultravioleta-visible, y otros.

[17]. E. M. Perez, N. Martin. *Chem. Soc. Rev.* **2008**, 37, 1512-1519.

Concluciones

Capítulo 1:

- Los experimentos fotofisicos permitieron revelar el caracter dual fullereno $Sc_3N@I_h$-C_{80}, siendo un dador de los electrones en caso del complejo con la hexa(pentilsulfonil) Zn(II)Pc y un acceptor de los electrones en caso del complejo con la tetra(*tert*-butil) Zn(II)Pc. Según nuestros conocimientos en el área, el caso del piridil derivado de $Sc_3N@I_h$-C_{80} presenta el primer ejemplo del comportamiento dual en las reacciones de la transferencia electronica fotoinducida.
- El uso de las SubPcs con caracter fuerte electron-atrayente por los grupos de fluor o/y pentilsulfonil en la periferia ayudó a revelar las propiedades reductoras de los fullerenos $La_2@I_h$-C_{80} y C_{60} y forzar la transferencia electronica fotoinducida desde la unidad fullerenica hacia la parte de SubPc. Según nuestro conocimiento, hemos reportado el primer ejemplo sobre la capacidad del fullereno C_{60} a actuar como dador de los electrones siendo activado unicamente por fotoexcitacion.

Capítulo 2:

- En este estudio se ha demostrado por primera vez que las interacciones no covalentes de tipo apilamiento π-π entre las dos unidades de Pc no enlazadas pueden ser de utilidad para promover la sintesis regio- , estereo- y atroposelectiva de los bisaductos de C_{60}. Al pesar de que las interacciones supramoleculares han sido utilizado exstensivamente para construir los sistemas complejos a base de C_{60} , el nuestro estudio representa el primer caso cuando las fuerzas no covalentes dirigen la doble adicion a la bola de C_{60}.
- Se han sintetizado nuevos sistemas octupolares rígidos no planares basados en múltiples unidades de Pc y fullereno alternadas unidas a un benceno hexasustituido que pueden dar lugar a procesos de transferencia electrónica fotoinducida. Los compuestos correspondientes han sido caracterizados por las técnicas habituales cómo espectrometría de masas, resonancia magnética nuclear, espectroscopia de luz ultravioleta-visible, y otros.

Introduction and Objectives

Introduction

Increasing global demand for energy, along with dwindling fossil fuel resources and a better understanding of the hidden costs associated with these energy sources, have spurred substantial political, academic and industrial interest in alternative energy resources.[18] Among them, solar energy is one of the most promising in the long term. Every hour, the Earth receives enough solar power to supply humans' energy consumption for one year.[19] Meanwhile, the energy consumption of the world reached 16 terawatts in 2006 and is predicted to rise to ≈30 terawatts by 2050.[20] The development of species that can harvest and convert sunlight efficiently is thus an extremely important mission. Organic chemistry plays a crucial role in the search for such systems, as proper positioning of the active components is a key point for the achievement of efficient devices.

In this regard, the photosynthetic system found in nature is the supramolecular photoactive device by excellence that has served as inspiration to many scientists. Much effort has been devoted to the understanding of the mechanism of light conversion in this system, with the aim of designing artificial systems that can behave similarly in human's profit. Photosynthesis[21] is the process employed by plants, algae and cyanobacteria to convert the radiant energy from the sun into chemical energy to fuel the activities of these organisms. The success of this conversion relies upon the efficient absorption and conversion of sunlight.

The main players in the process are chlorophylls and carotenoids with characteristic absorption features (Figure 1a). While the latter play mainly a photoprotective role, chlorophylls are involved in light harvesting and charge separation processes.[22] Photosynthetic systems present

---

18 a) S. Berardi, S. Drouet, L. Francas, C. Gimbert-Surinach, M. Guttentag, C. Richmond, T. Stolla, A. Llobet, *Chem. Soc. Rev.* **2014**, 43, 7501-7519; b) R. Wengenmair, T. Bührke, *Renewable energy: sustainable energy concepts for the future*, Wiley - VCH, Weinheim, **2013**, pp. 1-170; c) issue on "Artificial Photosynthesis and Solar Fuels", *Acc. Chem. Res*. **2009**, *42*, 1859-2029.

19 Q. Schiermeier, J. Tollefson, T. Scully, A. Witze, O. Morton, *Nature,* **2008**, *454*, 816-823.

20 M. I. Hoffert, K. Caldeira, A. K. Jain, E. F. Haites, L. D. D. Harvey, S. D. Potter, M. E. Schlesinger, S. H. Schneider, R. G. Watts, T. M. L. Wigley and D. J. Wuebbles. *Nature*, **1998**, 395, 881-884.

21 B. Gobets, R. van Grondelle, *Biochim. Biophys. Acta,* **2001**, *1507*, 80-99.

22 a) B. Alberts, A. Johnson, J. Lewis, M. Raff, K. K. Roberts, P. Walter, *Molecular Biology of the Cell*, 5th ed., Garland Science, New York, **2007**, pp. 813-878; b) R. E. Blankenship, *Molecular Mechanisms of Photosynthesis*, Blackwell Science, **2002**, pp. 1-321; c) R. Berera, R. van Grondelle, J. T. M. Kennis, *Photosynth. Res,* **2009***, 101*, 105-108.

two basic components: an antenna complex for light harvesting, and a reaction center for charge separation.

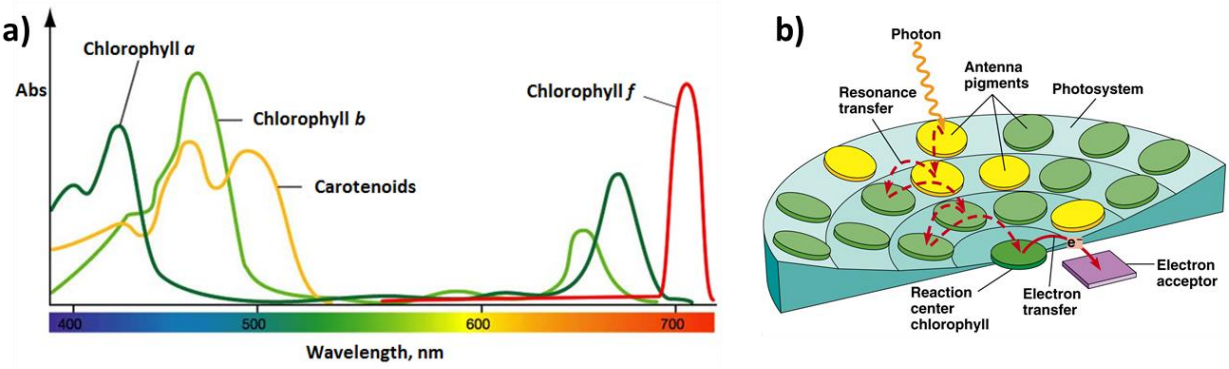

Figure 1. a) UV-vis absorption spectra of Chlorophylls (green and red lines) and carotenoids (yellow line); bSchematic representation of photosystem I.

The first step in photosynthesis is light absorption by the antenna complex. Photoinduced energy transfer is a process of great importance in the light harvesting complex, and, moreover, it acts as the trigger of charge separation process. The aim of this event is to progressively direct the energy from sunlight to the reaction centre. Energy transfer is a photophysical process where the excitation of a chromophore is transferred to a radiationless relaxation. Spectral overlap between the emission of the donor and the absorption of the acceptor is required for energy transfer to occur.

In the case of photosynthesis, energy transfer takes place through the dipolar coupling mechanism described by Theodore Förster in 1914. Förster resonance energy transfer (FRET) takes place when non-radiative excitation transfer occurs between two molecular entities separated by distances that exceed the sum of their Van der Waals radii.[23] This energy exchange happens via the electromagnetic field associated to the electron in the LUMO of the donor, which causes a perturbation on the electrons in the HOMO of the acceptor. The effectiveness of the energy transfer depends on the distance between the chromophores (the rate is proportional to R^{-6}) and the relative orientation of the chromophores. In this regard, organization of the chromophores is very important for an efficient photosynthetic process. A common feature of photosynthetic systems is a ring-like organization of the antenna (Figure 1 b) complex

[23] Helms, Volkhard. "Fluorescence Resonance Energy Transfer". Principles of Computational Cell Biology. Weinheim: Wiley-VCH. 2008. p. 202.

around the reaction center. Such degree of organization of the photosynthetic pigments addressed to ensure formation of efficient antennas and reaction centers is based on supramolecular interactions involving not only the pigments but also proteins and protein dimers.

Conversion of sunlight energy into chemical energy takes place through a cascade of unidirectional electron transfer reactions that will lead to the synthesis of carbohydrates. The success of this process relies on the effectiveness of these electron transfers and the lack of recombination reactions that would interrupt the process and cause a waste of the absorbed energy. In a similar manner, artificial self-assembly of supramolecular structures from photoactive components may be expected to modify the ground-state and/or excitedstate behaviour of the individual molecules. This fact may give rise to a number of processes (energy transfer, charge separation, perturbation of optical transitions and polarizabilities, modification of redox potentials, regulation of binding properties, photochemical reactions, etc.) that will depend on the arrangement of components in the supramolecular structure.

Resuming, in natural photosynthetic systems, cascades of energy- and electron-transfer reactions are triggered either directly by photoexcitation or indirectly by energy transfer from light-harvesting antenna systems. In terms of charge separation, the characteristics of the individual electron acceptors and electron donors are decisive to modulate its overall efficiency. In terms of charge recombination, the environment of the photosynthetic reaction center plays a crucial role to slow it down. Therefore, designing, synthesizing, and probing efficient energy capacitors as well as porphyrinoid chromophores featuring unique panchromatic absorptive, redox, and electrical properties is of a crucial importance.

Electron transfer and Marcus theory

In recent decades, the scientific community revealed a great interest towards non-covalent energy- and electron transfer processes, continuosly analyzing how the underlying interactions vary as a function of environment.[24]

[24] a) S. Fukuzumi, K. Ohkubo, F. D'Souza, J. L. Sessler. *Chem Commun.* **2012**, *48*, 9801-9815; b) J. L. Sessler, B. Wang, S. L. Springs, C. T. Brown. "Electron and Energy Transfer Reactions in Non-covalently Linked, Supramolecular Model Systems,"*Comprehensive Supramolecular Chemistry, Vol. 4*; Murakami, Y., Ed.; Pergamon: Oxford UK; Chapter 9, 1996; c) A. Takai, M. Chkounda, A.

Classically, energy- and electron transfer interactions can be divided into redox processes (full change in oxidation states of the components), charge transfer complexes (partial charge transfer as a result of favorable orbital overlap between the constituent donors and acceptors), and photoinduced energy- or electron transfer (i.e., charge transfer stimulated by spectroelectrical illumination). Electron transfer reactions, often referred to as redox reactions, consist of the transfer of an electron from one species (donor or reductant) to another species (acceptor or oxidant). Between discreet molecules, such ET events occur through one of two limiting pathways: inner sphere or outer sphere. In the inner sphere mechanism, the donor and acceptor are bridged during the electron transfer process, resulting in large changes to the coordination sphere of the products compared to the reactants, including alterations in the number, type, and lengths of bonds or the ligands surrounding the redox center. In outer sphere electron transfer reactions no bonds are formed or broken. Instead, upon close contact of the redox active species *via* e.g., diffusion or supramolecular complexation, an electron "hops" through space (tunnels) from the donor to the acceptor completing the ET process. Typically, outer sphere ET processes are preferred when the rate of electron transfer is faster than ligand substitution, when there are no suitable bridging ligands, or when one or both of the electroactive components is inert.

A number of rate expressions have been introduced to the literature that may be used to predict whether an outer shell ET reaction will take place in the forward or back directions and whether the resulting charge separated (CS) state will be stable. Of these, the "Marcus Theory", pioneered by Rudolf A. Marcus (for which he received the Nobel Prize in Chemistry in 1992), is the best known.[25] It relies on a transition-state theoretical approach and is accessible to the non-specialist. Unlike classical reaction mechanisms (such as S_N2) subject to microscopic reversibility, in ET, the electron undergoing reaction is quantized. It resides either fully on the donor or fully on the acceptor. Thus, the solvent and solvation state have enhanced importance. Specifically, the movement of electrons from donor to acceptor happens on a much faster time scale than the reorganization of large solvent molecules. Therefore, and according to the Franck-Condon

---

Eggenspiller, C. P. Gros, M. Lachkar, J.-M. Barbe and S. Fukuzumi, *J. Am. Chem. Soc.*, **2010**, 132, 4477-4489; d) T. Kojima, T. Honda, K. Ohkubo, M. Shiro, T. Kusukawa, T. Fukuda, N. Kobayashi and S. Fukuzumi, *Angew. Chem., Int. Ed.*, **2008**, 47, 6712-6716.

[25] a) R. A. Marcus, *Angew. Chem., Int. Ed.* **1993**, 32, 1111-1121; b) R. M. Metzger, *J. Mater, Chem,* **2008**,*18*, 4364-4396; c) P. E. Schween, K. Gui, Y. Zhang, P. L. Burn, P. Meredith, B. J. Powell, *Organic Electronics,* **2012**, *13*, 2538-2545.

principles,[26] the nuclear orientations of the reactants, products, and the solvent, must be degenerate. In other words their orientations must be identical before and after the electron "jumps." However, since energy must also be conserved during the ET process for any non-isoergic reaction, the solvent sphere of the reactants and the products cannot be the same; rather, its orientation must lie somewhere in between the two. Consequently, the energy required to reorganize the solvent shell into a state where ET can occur (corresponding to the hypothetical transfer of a partial electron) is equivalent to the activation barrier, $\Delta G^{\ddagger}$, of the ET reaction.

Marcus found that he could treat the complicated reaction coordinate diagram containing all of the coordinates for each individual solvent molecule within a single coordinate, the solvent polarization (P or Δe).[27] Using eq. 1, the Gibbs free energy of the system becomes a function of Δe, where r_D and r_A are the radius of the donor and acceptor, respectively, R_{DA} is the distance between the donor and acceptor, and ε_{op} and ε_s are the optical and static dielectric constants of the solvent, respectively. The physical meaning of Δe in this equation is equivalent to the amount of charge transferred from the donor to the acceptor.

$$G = \left(\frac{1}{2r_D} + \frac{1}{2r_A} - \frac{1}{R_{DA}}\right) \cdot \left(\frac{1}{\varepsilon_{op}} - \frac{1}{\varepsilon_s}\right) \cdot (\Delta e)^2 \quad (1)$$

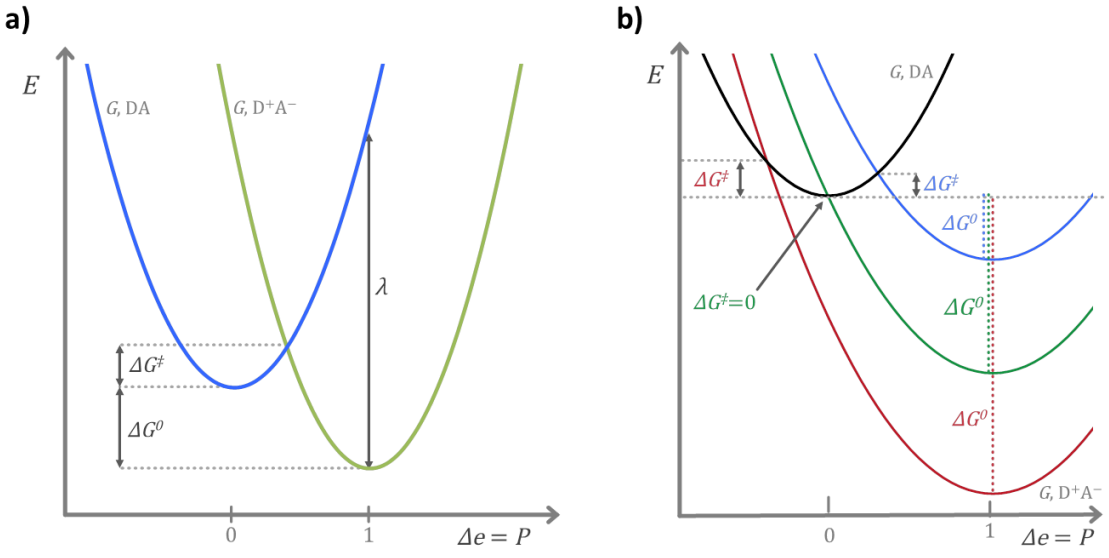

Figure 2. Schematic diagram according to Marcus Theory showing: a) the parabolic outer sphere reorganization energies for a general donor-acceptor ET system. The first parabola (G, DA in blue) denotes

[26] a) J. Franck, *Trans. Faraday Soc.* **1926**, 21, 536-542; b) E. Condon, *Phys. Rev.*, **1926**, 27, 640-646.

[27] R. A. Marcus, *J. Chem. Phys.*, 1956, **24**, 966-978.

the solvent polarization condition before the ET event while the second (G, D^+A^- in green) corresponds to the post ET situation. $\Delta G^{\ddagger}$, ΔG^0, and λ depict the activation energy, the free energy driving force, and the outer shell reorganization energy of the ET event, respectively; b) the effect of increasing the thermodynamic driving force ΔG^0 on the activation energy $\Delta G^{\ddagger}$. Increasing ΔG^0 (going from the blue to the green successor parabola) leads to a concurrent decrease in $\Delta G^{\ddagger}$, until $\Delta G^{\ddagger} = 0$. Subsequent increases of ΔG (from the green to red parabola) leads to an *increase* in the value $\Delta G^{\ddagger}$. The latter transformation depicts the so-called "inverted" region of Marcus theory.

Plots of eq. 1 are parabolic in nature, and represent the amount of energy required to perturb the solvent environment of a system to that of an arbitrary amount of transferred charge. Although for any given ET event the amount of charge is quantized, the perturbation of the solvent is not, and can be treated classically. Thus, plotting eq. 1 for both the precursor (D and A) and successor ($D^{\bullet+}$ and $A^{\bullet-}$) complexes on the same axis allows a semi-quantitative understanding of the ET process (Figure 2a). For instance, the point where the parabolas intersect corresponds to the activation energy ($\Delta G^{\ddagger}$) of the electron transfer process. Solving for this point (eq. 2), Marcus found $\Delta G^{\ddagger}$ as a function of the reorganization energy, λ_o (the value of G in eq. 1 when $\Delta e = 1$) and the driving force, ΔG^0, of the reaction.

$$\Delta G^{\ddagger} = \frac{(\lambda_o + \Delta G^0)^2}{4\lambda_o} \qquad (2)$$

Finally, substituting the activation energy into the Arrhenius equation, the rate constant is obtained (eq. 3):

$$k = Ae^{\frac{-(\Delta G^0 + \lambda_o)^2}{4\lambda_o RT}} \qquad (3)$$

where A is a pre-exponential factor dependent on the distance between the redox pair, and the damping factor, R is the ideal gas constant, and T is the temperature of the solution.

A further peculiarity of Marcus theory is the so-called Marcus "inverted" region.[28] In the "normal" region associated with Marcus theory, an increase in the free energy driving force, ΔG^0, results in a *decrease* of the activation energy, $\Delta G^{\ddagger}$ (Figure 2b). This trend continues until $\Delta G^{\ddagger} = 0$, or in other words, the point in which an electron can be transferred from the precursor to the successor complex without requiring the manipulation of the solvent environment of the

[28] R. A. Marcus, *Discuss. Faraday Soc.*, 1960, **29**, 21-31.

precursor complex. At this value of ΔG^{0}, the rate of electron transfer is at a maximum and approaches diffusion limits. However, further increasing the driving force leads to an *increase* in the activation barrier, $\Delta G^{\ddagger}$, and a retardation of the reaction rates. This portion is termed the "inverted" region in Marcus theory and upon experimental conformation,[29] became one of the hallmarks of ET theory.

This brief discussion of the dynamics of electron transfer is included to illustrate the elementary theory behind ET processes and to serve as a starting point for design considerations of efficient systems for charge separation. For a compound to ensure the charge separation, the shape and/or location of its parabolic Δe vs. G curve must be modified in a reversible (and ideally specific) manner upon exposure to outer factors. Similarly, photosynthetic systems achieve long-lived charge separation states because electron-transfer events are located in the "inverted region" of Marcus' parabola. Thus, modifying the solvation sphere, reorganizational energy, Gibbs free energy of the donor or acceptor, or the distance between the donor and acceptor should have an effect on the rate of ET.

Phthalocyanines and related compounds

Among the chromophores that have been used as molecular components in artificial photosynthetic systems, porphyrinoids, the ubiquitous molecular building blocks employed by Nature in natural photosynthesis, have been the preferred and obvious choice, due to their intense optical absorption and rich redox chemistry.[30]

Within the large family of porphyrinoid systems, phthalocyanines (Pcs) enjoy a privileged position (Figure 3a). These chromophores, which have a two-dimensional 18 π-electron aromatic

[29] J. R. Miller, L. T. Calcaterra, G. L. Closs, *J. Am. Chem. Soc.*, 1984, **106**, 3047-30149.

[30] a) P. K. Poddutoori, L. P. Bregles, G. N. Lim, P. Boland, R. G. Kerr, F. D'Souza, Francis. *Inorg. Chem.* **2015**, 54, 8482-8494; b) A. S. Konev, A. F. Khlebnikov, P. I. Prolubnikov, A. S. Mereshchenko, A. V. Povolotskiy, O. V. Levin, A. Hirsch. *Chem. Eur. J.* **2015**, 21 , 1237-1250; c) M. Fathalla, J. C. Barnes, R. M. Young, K. J. Hartlieb, S. M. Dyar, S. W. Eaton, A. A. Sarjeant, D. T. Co, M. R. Wasielewski, J. F. Stoddart. *Chem. Eur. J.***2014**, 20, 14690-14697; d) M. Urbani, S. Osati, S. Kuhri, D. M. Guldi, T. Torres. *J. Porph. Phthalocy*. **2013**, 17, 501-510; e) D. M. Guldi, G. M. A. Rahman, V. Sgobba, C. Ehli. *Chem. Soc. Rev*. **2006**, *35*, 471-487, and references therein; f) S. Fukuzumi, K. Ohkubo, O. Wenbo, Z. Ou, J. Shao, K. M. Kadish, J. A. Jutchison, K. P. Ghiggino, P. J. Sintic, M. Crossley. *J. Am. Chem. Soc*. **2003**, *125*, 14984-14985.

system isoelectronic with porphyrins, possess in fact unique physico-chemical properties which render these macrocycles valuable building blocks in materials science.[31]

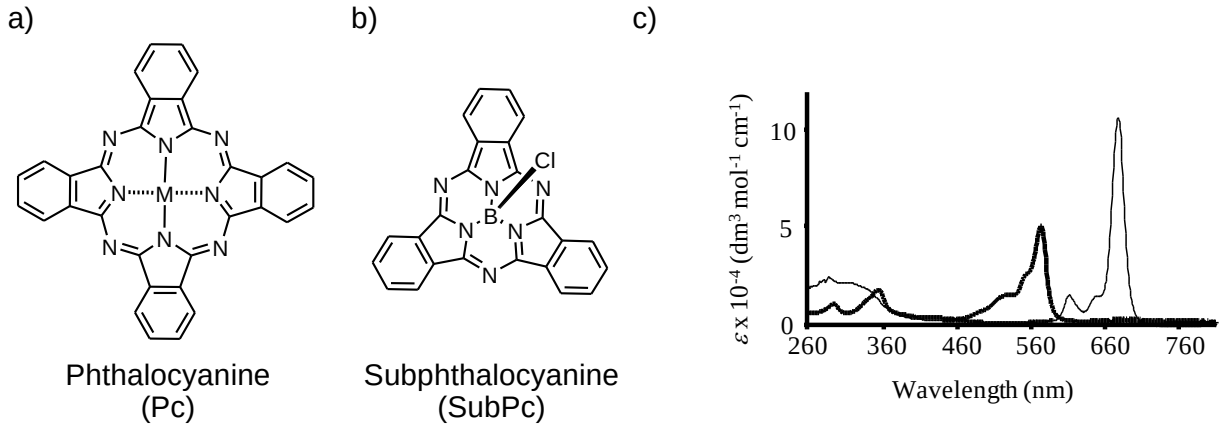

Figure 3. Molecular structures of a) a Pc and b) a SubPc. c) Typical UV/vis absorption spectra of Pcs (thin line) and SubPcs (thick line).

Pcs are thermally and chemically stable compounds which present an intense absorption in the red/near infrared (IR) region of the solar spectrum with extinction coefficients (as high as 200.000 $M^{-1}\,cm^{-1}$) and fluorescence quantum yields higher than that of Pors (Figure 3c), thus representing ideal light harvesting antenna systems. Moreover, these macrocycles are synthetically versatile compounds, in which the two hydrogen atoms of the central cavity can be replaced by more than 70 metals and a variety of substituents can be incorporated in their structure, at the axial and/or peripheral positions of the macrocycle.[32] These structural modifications allow tuning some of the physical parameters of these macrocycles, such as their aggregation status or their reducing/oxidizing characteristics. These features render Pcs ideal molecular components in donor-acceptor (D-A) ensembles where their role is twofold: First, they

[31] a) *Phthalocyanine Materials: Structure, Synthesis and Function*; McKeown, N. B., Ed.; Cambridge University Press: Cambridge, 1998; b) M. Hanack, H. Heckmann, R. Polley. In *Methods of Organic Chemistry (Houben-Weyl)*; Schaumann, E., Ed.; Georg Thieme Verlag: Stuttgart, 1998; vol. E 9d, p. 717; c) de la Torre, G., Nicolau, M., Torres, T. In *Supramolecular Photosensitive and Electroactive Materials*; Nalwa, H. S., Ed.; Academia Press: New Cork, 2001, p. 1; d) Kobayashi, N. *Coord. Chem. Rev.* **2002**, *227*, 129-232; e) Y. Rio, M. S. Rodriguez-Morgade, T. Torres. *Org. Biomol. Chem.* **2008**, *6*, 1877-1894.

[32] a) S. Singh, A. Aggarwal, N. V. S. D. K. Bhupathiraju, G. Arianna, K. Tiwari, C. M. Drain. *Chem. Rev.* **2015**, 115, 10261-10306; b) P. Gao, D. Konrad, S. Aghazada, M. K. Nazeeruddin. *Chimia*. **2015**, 69, 253-263; c) A. de la Escosura, O. Trukhina, T. Torres. *Struct. Bond*. **2014**, 159, 145-191; d) G. de la Torre, G. Bottari, M. Sekita, A. Hausmann, D. M. Guldi, T. Torres. *Chem. Soc. Rev.* **2013**, 42, 8049-8105; e) M. J. Heeney, Sh. A. Al-Raqa, A. Auger, P. M. Burnham, A. N. Cammidge, I. Chambrier, M. J. Cook. *J. Porph. Phthalocy*. **2013**, 17, 649-664, f) A. B. Sorokin, *Chem. Rev.* **2013**, 113, 8152-8191.

function as antennas, since they absorb very efficiently light in the visible region of the solar spectrum; and second, once photoexcited, they act as an electron donor for the acceptor moiety.[33] These latter characteristics make these macrocycles promising building blocks for their incorporation in photovoltaic and artificial photosynthetic devices.

Similarly, subphthalocyanines (SubPcs) (Figure 3b) are known as lower Pc homologues which present an 14 π-electron aromatic structure with an extended conjugation and a cone-shaped geometry. [34-] Owing to their intense absorption in the visible region of the solar spectrum (*i.e.*, with extinction coefficients as high as 60.000 $M^{-1}\,cm^{-1}$) (Figure 3c) and high optical and thermal stabilities, they have evolved as perfect light-harvesting building blocks.[36] Rich redox chemistry that may be tuned, even easier than in the case of Pcs, by the introduction of different peripheral functional groups.

The great interest in Pcs and SubPcs as molecular building blocks for the construction of artificial photosynthetic systems has led others and us to synthesize and study a wide range of covalent and non-covalent (Sub)Pc-based D-A systems incorporating electroactive acceptor units of diverse nature and redox character such as fullerene, carbon nanotubes (CNT), graphene, perylenediimide, anthraquinone, ferrocene, ruthenium bypyridine complexes, flavin, porphyrin and others.

Among the acceptor units employed for the preparation of such (non-)covalent systems, carbon nanostructures like fullerenes, carbon nanotubes and graphene deserve a special mention due to their excellent electron acceptor ability, which convert them as perfect molecular partners for photo- and electroactive systems. The extraordinary electron acceptor properties of fullerenes,[37]

---

33 a) V. Balevicius, A. Gelzinis, D. Abramavicius, L. Valkunas. *J. Phys. Chem. B* **2013**, 117, 11031-11041; b) H. Imahori, T. Umeyama, K. Kurotobi, Y. Takano. Chem. Commun. **2012**, 48, 4032-4045; c) H. Lemmetyinen, N. V. Tkachenko, A. Efimov, M. Niemi. Phys. Chem. Chem. Phys. **2011**, 13, 397-412; d) K. Ohkubo, S. Fukuzumi. *J. Porph. Phthalocy.* **2008**, 12, 993-1004; e) F. D'Souza, O. Ito. *Coord. Chem. Rev.* **2005**, *249*, 1410-1422.

34 Claessens, C. G.; Gonzalez-Rodriguez, D.; Torres, T. *Chem. Rev.* **2002**, *102*, 835-854.

35 Torres, T. *Angew. Chem. Int. Ed.* **2006**, *45*, 2834-2837.

36 C. G. Claessens, D. Gonzalez-Rodriguez, M. S. Rodriguez-Morgade, A. Medina, T. Torres, *Chem. Rev.* **2014**, 114, 2192-2277.

37 a) Diederich, F.; Gomez-Lopez, M. *Chem. Soc. Rev.* **1999**, *28*, 263; b) Fukuzumi, S.; Guldi, D. M. In *Electron Transfer in Chemistry*; Balzani, V., Ed.; Wiley-VCH, 2001, vol. 2, p. 270; c) *Fullerenes: From Synthesis to Optoelectronic Properties*; Guldi, D. M.; Martin, N.; Eds.; Kluwer Academic Publishers: Dodrech, 2002; c) *Fullerenes: Principles and Applications*; Langa, F., Nierengarten, J.-F.; Eds.; The Royal Society of Chemistry: Cambridge, 2007 (Nanoscience and Nanotechnology Series); d)

coupled with their small reorganization energy and their ability for promoting ultrafast CS together with very slow charge recombination (CR) features, have prompted the incorporation of these carbon nanostructures in a large number of D-A systems where photoinduced electron transfer (PET) processes and solar energy conversion are sought. Similarly, the outstanding properties of CNTs[38] have generated a tremendous interest towards the implementation of this novel carbon allotrope into D-A nanohybrids. CNTs in fact readily accept electrons, which, in turn, might be transported under nearly ideal conditions along its one-dimensional (1-D) tubular axis. In the recent time, special attention has been driven to modern 2D materials.[39] Among others, graphene, a single atomic layer composed of sp^2-hybridized carbon, is a rapidly rising star material, which has found very broad applications in recent years. Graphene was successfully isolated from graphite using a technique called mechanical exfoliation in 2004.[40] Since then, the study of graphene has been making a huge impact on many areas of science and technology due to its outstanding electronic, optical and mechanical properties.[41]

Up to date, a large variety of covalently-linked D-A (Sub)Pc-based conjugates, containing as acceptor units fullerene and CNTs, have been synthesized and their photophysical properties studied in solution and/or in the solid state, revealing the occurrence, in the majority of the cases, of PET events. In such systems, the nature of the bridging spacer has been varied both from the electronic (*i.e.,* conjugated/non-conjugated) and/or structural (*i.e.,* rigid/flexible) point

---

Giacalone, F.; Martin, N. *Chem. Rev.* **2006**, *106*, 5136; e) Delgado, J. L.; Herranz, M. A.; Martin, N. *J. Mater. Chem.* **2008**, *18*, 1417; f) Guldi, D. M.; Illescas, B. M.; Atienza, C. M.; Wielopolski, M.; Martin, N. *Chem. Soc. Rev.* **2009**, *38*, 1587.

38 a) *Carbon Nanotubes and Related Structures: New Materials for the Twenty-First Century*; Harris, P., Ed.; Cambridge University Press: Cambridge, 2001; b) Dresselhaus, M. S., Dresselhaus, G., Avouris, P. In *Carbon Nanotubes: Synthesis, Structure, Properties and Applications*; Springer-Verlag: Berlin, 2001; c) Reich, S., Thomsen, C., Maultzsh, J. In *Carbon Nanotubes: Basic Concepts and Physical Properties*; VCH: Weinheim, 2004; d) Tasis, D.; Tagmatarchis, N.; Bianco, A.; Prato, M. *Chem. Rev.* **2006**, *106*, 1105-1136; e) Kostarelos, K.; Lacerda, L.; Pastorin, G.; Wu, W.; Wieckowski, S.; Luangsivilay, J.; Godefroy, S.; Pantarotto, D.; Briand, J.-P.; Muller, S.; Prato, M.; Bianco, A. *Nat. Nanotechnol.* **2007**, *2*, 108-113; f) Sgobba, V.; Guldi, D. M. *J. Mater. Chem.* **2008**, *18*, 153-157; g) Sgobba, V.; Guldi, D. M. *Chem. Soc. Rev.* **2009**, *38*, 165-184.

39 a) Z. Liu, S. P. Lau, F. Yan. *Chem. Soc. Rev.*, **2015**, 44, 5638-5679; b) Z. Yang, J. Ren, Z. Zhang, X. Chen, G. Guan, L. Qiu, Y. Zhang, H. Peng. *Chem. Rev.*, **2015**, 115, 5159-5223.

40 K. S. Novoselov, A. K. Geim, S. V. Morozov, D. Jiang, Y. Zhang, S. V. Dubonos, I. V. Grigorieva and A. A. Firsov. *Science*, **2004**, 306, 666-669.

41 A. K. Geim. *Science*, **2009**, 324, 1530-1534.

of view, with the aim of identifying to which extent these changes would influence the PET dynamics.[42]

Recently, a general and versatile synthetic strategy for the preparation of chemically stable, segregated Pc-C_{60} alignments has been presented, which relies on the solvothermal synthesis of Pc-based covalent organic frameworks (COFs) and their postfunctionalization by a C_{60} derivative.[43] Pc-based COFs present a porous architecture formed by periodically ordered Pc columnar arrays, which generate aligned 1-D nanochannels. Jiang et al. demonstrated that the interior walls of these open channels, adequately functionalized with azide moieties, could be covalently "grafted" with an ethynyl-functionalized C_{60} derivative via a "click" reaction (Figure 4). By this strategy, the former electron-donating, Pc-based COF architecture is transformed into a photoresponsive COF structure constituted by segregated D-A alignments of stacked Pcs and electronaccepting buckyballs spatially confined into the nanochannels. Interestingly, laser stimulation of this D-A heterojunction triggers photoinduced electron transfer processes, giving rise to photogenerated charge separated species with lifetimes that are strongly affected by the delocalization of radical cation and anion species on the Zn(II)Pc and C_{60} moieties, respectively.

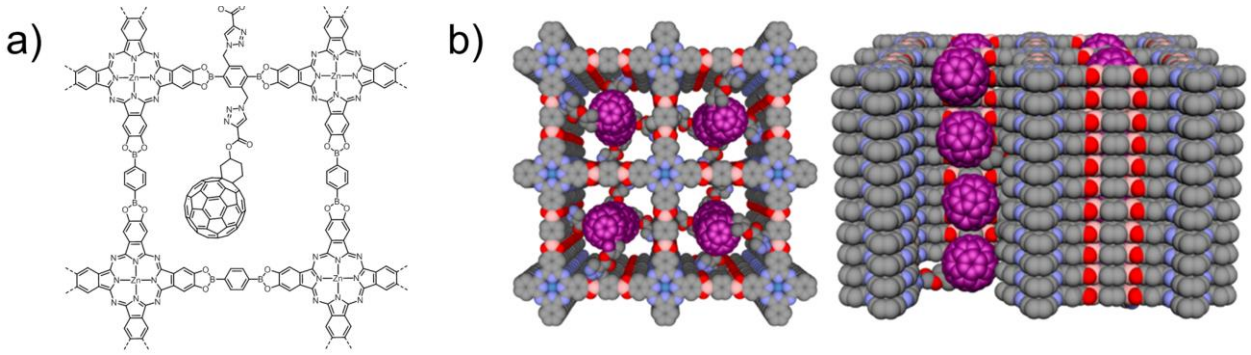

Figure 4. a) Molecular structure and b) top (left) and side (right) view of a fragment of D-A Pc-based COF with C_{60} units (purple) covalently linked to the nanochannels walls.

Supramolecular interactions have also been successfully employed for the construction of noncovalent Pc-C_{60} ensembles using Pc and C_{60} derivatives carrying out complementary recognition motifs with the aim of increasing the lifetime of the photoinduced charge separated states. In this context, metal-ligand coordination, hydrogen-bonding, D-A, or cation-crown ether

42 Y. Araki, O. Ito, *J. Photochem. Photobiol. C* **2008**, *9*, 93-156.

43 L. Chen, K. Furukawa, J. Gao, A. Nagai, T. Nakamura, Y. Dong, D. Jiang, *J. Am. Chem. Soc.* **2014**, 136, 9806-9809.

noncovalent interactions have been widely used, independently or in combination, for the preparation of Pc-C_{60} supramolecular systems.[44]

D-A, Pc/SWCNT supramolecular hybrids based on a series of dendritic (i.e., first to third generations), electron-donor Pcs have also been recently reported.[45] In such systems, the dendritic nature of the oligoethylene-functionalized macrocycles and the π-aromatic surface of the Pcs allow effective interaction between the Pc core and the surface of the SWCNTs without the requirement of any pyrene anchoring group. In the case of the third generation-dendrimer, Pc/SWCNT ensemble, a particularly stable complex was obtained as demonstrated by a series of optical and microscopy techniques (Figure 5a). Once again, transient absorption studies were carried out in order to shed light on the fate of the photogenerated products, suggesting the occurrence of a CT process between Pc and SWCNT with the formation of the $Pc^{\bullet+}$ and $SWCNT^{\bullet-}$ species, with lifetime of about 250 ps. It is interesting to notice that the presence of dendritic oligoethylene glycol end groups allowed dispersing SWCNTs in both common organic solvents and aqueous media.

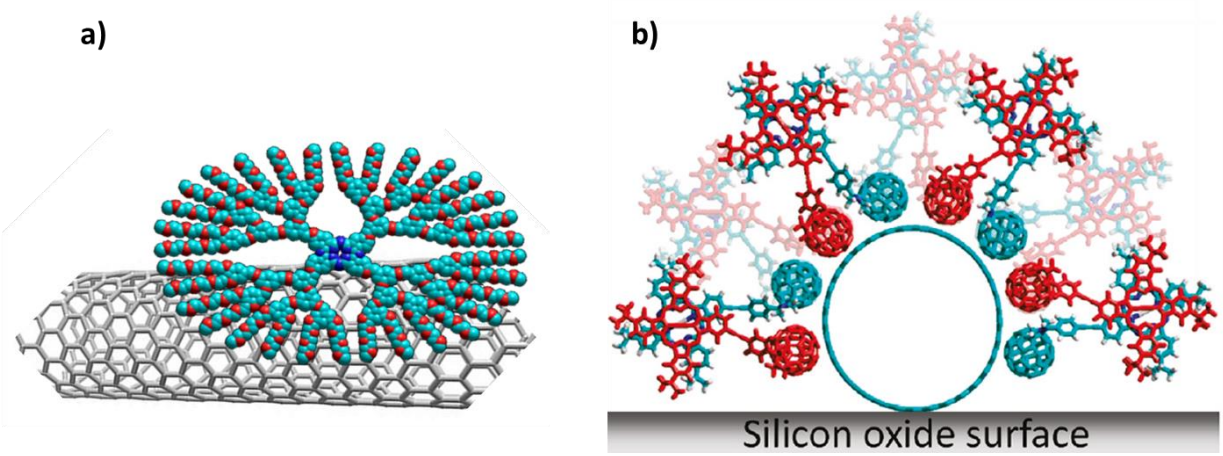

Figure 5. a) Schematic representation of the noncovalent assembly of a third-generation dendritic Zn(II) Pc onto a SWCNT; b) Frontal view of the proposed supramolecular organization of Pc-C_{60} dyad on a 2.5 nm SWCNT on a silicon oxide surface.

[44] a) G. Bottari, J. A. Suanzes, O. Trukhina, T. Torres. *J. Phys. Chem. Lett.*, **2011**, 905-913; b) G. Bottari, O. Trukhina, M. Ince, T. Torres. *Coord. Chem. Rev.*, **2012**, 256, 2453-2477.

[45] U. Hahn, S. Engmann, C. Oelsner, C. Ehl, D. M. Guldi, T. Torres, *J. Am. Chem. Soc.* **2010**, 132, 6392-6401.

The organization properties of a Pc-C_{60} dyad on SWCNTs grown by chemical vapor deposition directly on hydrophilic silicon oxide wafers have also been reported (Figure 5b).[46] In such a study, the strong affinity of a Pc-C_{60} dyad for graphitic surfaces coupled to the poor affinity of this conjugate for hydrophilic surfaces such as silica or mica has been exploited in order to promote the organization of Pc-C_{60} dyad on the curved 1-D graphite-like surface of these SWCNTs. AFM studies revealed that Pc-C_{60} conjugate is able to self-assemble with nanometer precision by means of noncovalent interactions on the outer wall of these SWCNTs. Several control experiments were performed with the aim of identifying some of the key factors responsible for the supramolecular organization of this Pc-C_{60} conjugate on these surface-grown SWCNTs. These experiments provided a series of "indirect proofs" which allowed proposal of an organization model for the dyad/SWCNT supramolecular heteroarray. In this model, the structurally rigid Pc-C_{60} dyads are arranged around the SWCNTs' 1-D axis, adopting a radial upright position, with the C_{60} fullerene moieties pointing downward toward the SWCNT interacting with its curved graphitic surface and the Pcs units π-π stacking between them (Figure 5b). The final goal for the preparation of such assemblies is to alter the electrical resistance of these SWCNTs "coated" with nanometer precision by a photoresponsive D-A, Pc-C_{60} dyad in response to appropriate photonic stimuli.

The electronic characteristics of graphene flakes were found to be detectibly altered by supramolecular association with a ZnPc poly(*p*-phenylenevinylene) polymer bearing cyano groups (ZnPc-PPV-CN) (Figure 6a).[47] ZnPc-PPV-CN, containing a string of pendant ZnPc units along its polymeric backbone, was found to associate strongly with nanographene (NG). ZnPc-PPV-CN assists in the exfoliation of graphite and stabilizes the newly formed flakes that were found to contain 2-3 layers of graphene. Surprisingly, evidence of strong electronic coupling between the individual components was seen in the ZnPc-PPVA-CN/NG aggregates even in the ground-state. Specifically, the absorption of the Q-band of ZnPc was shifted to 707 nm, in comparison with 675 nm for free ZnPc-PPV-CN in THF. Additionally, upon interaction with NG, the fluorescence of ZnPc was quenched. This was taken as evidence of electron transfer from ZnPc to graphene in the excited state. Additional evidence was obtained from transient absorption spectra of the ZnPc-

[46] G. Bottari, D.Olea, V. Lopez, C. Gomez-Navarro, FZamora, J. Gomez-Herrero, T. Torres. *Chem. Commun.* **2010**, 46, 4692-4694.

[47] J. Malig, N. Jux, D. Kiessling, J.-J. Cid, P. Vázquez, T. Torres, D. M. Guldi, *Angew. Chem., Int. Ed.*, **2011**, 50, 3561-3565.

PPV-CN/NG hybrid employing femtosecond flash photolysis in THF (700 nm). In these studies, the appearance of a peak at 840 nm was noted. Such a feature is characteristic of the one-electron oxidized form of ZnPc. Hence, in the current system photoexcitation of the ZnPc moieties leads to efficient PET from ZnPc to graphene, with the latter species acting as an electron acceptor.

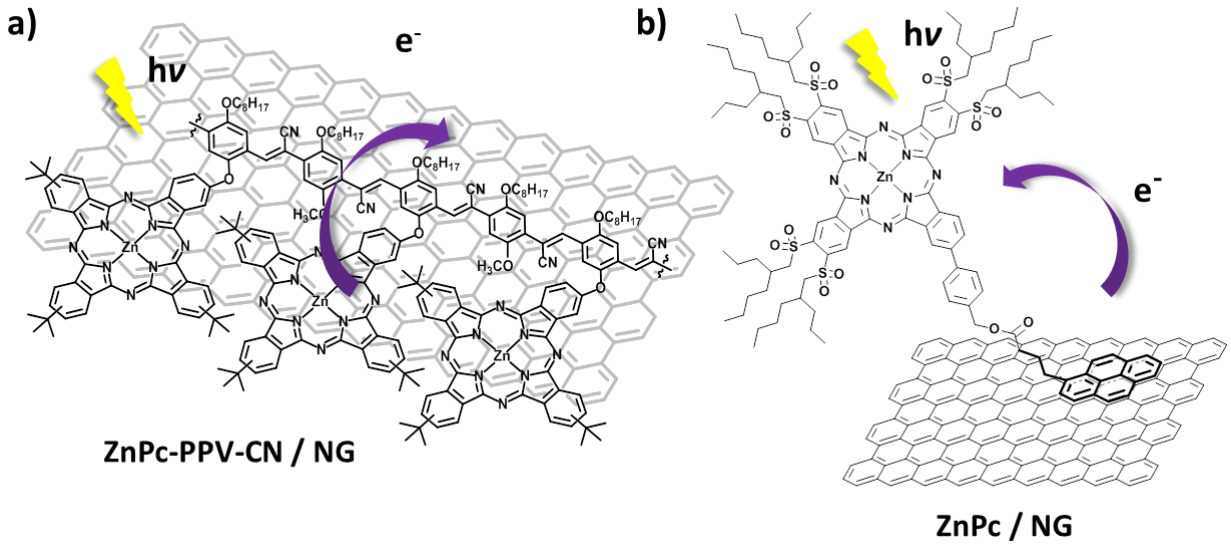

Figure 6. a) Proposed structure of an exfoliated graphene/ZnPc-PPV-CN nanohybrid; b) Proposed structure of an (alkylsulfonyl) ZnPc-pyrene/graphene nanohybrid.

Pc/NG systems have also helped shed light on the less-well explored electron donating features of graphene. For instance, by exploiting π-π interactions, a pyrene-functionalized (alkylsulfonyl) zinc(II) phthalocyanine (ZnPc-Py) could be bound to highly exfoliated graphite (Figure 6b).[48] The reduction potential of ZnPc-Py is relatively low, as would be expected given the electron withdrawing sulfonyl ester groups. As a result, this particular porphyrinoid species is electron deficient. It acts an electron acceptor when mixed with NG sheets. Evidence for strong electronic interactions was seen in both the ground and excited states. Upon photoexcitation of the ZnPc-Py/NG complex at 387 nm, a CS state was generated (i.e. ZnPc-Py$^{\bullet-}$-NG$^{\bullet+}$) that undergoes slow charge recombination. Transient absorption maxima at 485, 582, and 760 nm and minima at 460 and 640 nm were observed that were considered as "fingerprints" of the one-electron reduced radical anion ZnPc-Py$^{\bullet-}$, supporting the formation of the transient CS state. Other new features evolved during the transient decay, including broad maxima at 950 and 1070 nm that were interpreted in terms of the formation of new holes in the valence band of graphene. When

[48] A. Roth, M.-E. Ragoussi, L. Wibmer, G. Katsukis, G. de la Torre, T. Torres, D. M. Guldi, *Chem. Sci.*, **2014**, 5, 3432-3438.

considered in conjunction with the previous example involving ZnPc-PPV-CN, the studies with (alkylsulfonyl) ZnPc-Py provide support for the notion that sheets of NG may serve as an ambidirectional supramolecular PET partner when paired with appropriately tuned Pc compounds.

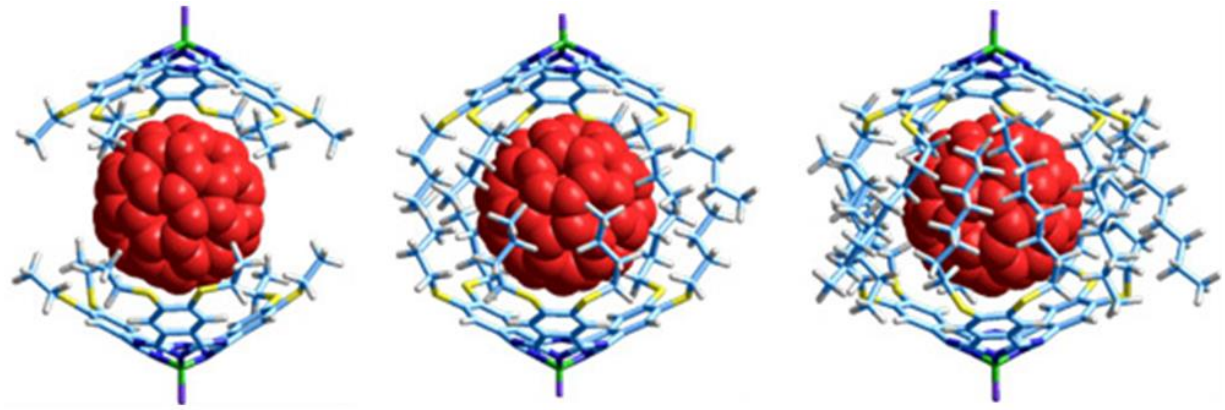

Figure 7. Models of the 2:1 supramolecular complexes of SubPcs and C_{60}.

In addition to having received attention for their unique photophysical properties, SubPc have attracted interest as easy-to-manipulate components for molecular self-assembly. For instance, SubPcs have been recently used to construct supramolecular jelly fish-like ensembles[49] (Figure 7) and for SubPc-based metallosupramolecular encapsulation.[50] In both cases, photoexcitation of the SubPc supramolecular hybrids is followed by singlet excited-state energy transfer to a complexed fullerene receptor. Additionally, covalent constructs containing SubPcs have been demonstrated to undergo efficient photoinduced electron transfer reactions, with the SubPcs acting as either electron donors or acceptors. Because of this latter duality, we predict that SubPcs will emerge as important constituents in PET-based electron switches, molecular sensors, and synthetic logic gates. However, to date this promise has yet to be realized.

Herein, the different synthetic strategies that have been pursued so far for the preparation of D-A Pc- and SubPc-carbon nanostructure systems, having the donor and the acceptor units connected either covalently or by using supramolecular interactions, have been resumed. A photophysical analysis of most of these systems helps in rationalizing which effect the structural and electronic features of these D-A systems have on the photoinduced electron/energy transfer

[49] I. Sanchez-Molina, C. G. Claessens, B. Grimm, D. M. Guldi, T. Torres, *Chem. Sci.*, **2013**, 4, 1338-1344.
[50] I. Sanchez-Molina, B. Grimm, C. Krick, M. Rafael, C. G. Claessens, D. M. Guldi, T. Torres, *J. Am. Chem. Soc.*, **2013**, 135, 10503-10511.

dynamics. The latter would shed the light onto the perspectives of utilization of Pcs and fullerenes in organic photovoltaics in terms of the different types of organic solar cell architectures and performance of the devices.

Objectives

General objectives

The main objective of this thesis is to explore the synthetic versatility of Pcs and their related structures towards fullerenes. This synthetic versatility allows the modulation of electron transfer events on supramolecular and intramolecular level, as well as disclosing the unique selectivity in Prato reactions of C_{60}. Moreover, synthesis and study of complex multicomponent systems opens new perspectives of their possible applications.

The basic objectives are the following:

a) Explore the possibilities of non-covalent interactions for the construction of supramolecular architectures based on Pc and endohedral metallofullerenes.

b) Construct covalent conjugates of SubPcPc and endohedral metallofullerenes.

c) Study the reaction of bisaddition of Pc to C60 and disclose the complex mixture of resulting products.

d) Study the photophysical and electrochemical properties of the fullerene-based systems with Pcs and SubPcs.

Methodology

In order to reach the aforementioned objectives, development of the following tasks is necessary:

a) Design and synthesis of Pc:

The synthesis of Pcs will be carried out by cyclotetramerization reaction of the corresponding phthalonitriles in the presence of zinc(II) acetate. Synthesis of asymmetrically substituted Pcs will

be undertaken, following by the use of Pd-catalyzed cross-coupling reactions until preparation of the desired module.

b) Design and synthesis of SubPcs:

The synthesis of SubPcs will be carried out by cyclotrimerization reaction of the proper phthalonitriles in the presence of boron trichloride. This will generate the desired macrocyclic structure as chloro-derivative. SubPcs thus obtained will be functionalized axially and/or peripherally if required. Axial functionalization of the chloro-SubPcs will be performed by nucleophilic substitution with 4-hydrohybenzaldehyde or phenol via preparation of triflate-substituted intermediates in situ.

c) Design and synthesis of fullerene-derivatives and their conjugates:

Empty and endohedral fullerenes will be functionalized according to Prato protocol in all cases, affording building blocks for supramolecular self-assembly or conjugates with other chromophores, such as dyads, bisadducts or multicomponent systems.

d) Study of the self-assembling and π-π stacking interactions:

Stoichiometric amounts of building-blocks in the proper conditions are expected to give rise to the desired compounds in high to quantitative yields.

π-π stacking interactions for the Pc bisadducts of C_{60} will be checked by titration experiments. Job Plot evaluation will allow determination of stoichiometry and titrations will afford information on the binding constants.

e) Study of photoinduced and electrochemical processes

Photophysical and electrochemical studies of the self-assembled systems as well as the host-guest complexes will be carried out in order to retrieve information on the interactions between the different components. Fluorescence quenching experiments, fluorescence quantum yields, time-resolved fluorescence and transient absorption spectroscopy will be carried out in the group of Prof. Dirk M. Guldi (Friedrich-Alexander Univertität Erlangen-Nürnberg).

Thesis distribution

The present Thesis has been organized in three parts. The first part of *Introduction and objectives* includes the inspiration and background of the work, as well as the current state-of-the-art of electron transfer theory and chemistry of phthalocyanine-related macrocycles. Special emphasis is made on the hybrid structures of Pc and Pcs with other carbon nanostructures, that will hold the leading roles along the discussion. *Chapter 2* is centered on the use of Pc and SubPcs for the construction of hybrids with fullerenes, empty and endohedrals. This chapter is, at the same time, divided in two sections. The first one is dealing with supramolecular systems of Pcs and endohedral fullerenes, giving rise to switchable electron transfer reactions. The second section is centered on covalent conjugates of endohedral fullerenes and SubPcs with strong electron-withdrawing character. First part of the *Chapter 3* contains the description of the unique case of regio-, stereo-, enantio-selectivity of the formation of Pc-based C_{60} bisadducts as a result of π-π stacking interactions between Pc cores. Finally, the second part shows the synthesis of octupolar, hexasubstituted benzene centered, tri-Pcs and tri-C_{60} system.

Chapter 1

(Sub)Pc-EMF hybrids for tunable electron transfer

1.1 Introduction

In modern society, a constantly growing demand for implementation of nanoelectronics has generated a significant interest towards electro- and photoactive molecular materials.[51] Organic electronics strongly depends on the preparation and study of donor-acceptor (D-A) supramolecular systems, whose relative success is directly connected with the efficiency of photoinduced charge separation – a fundamental process common to both natural photosynthesis and solar energy conversion.[52]

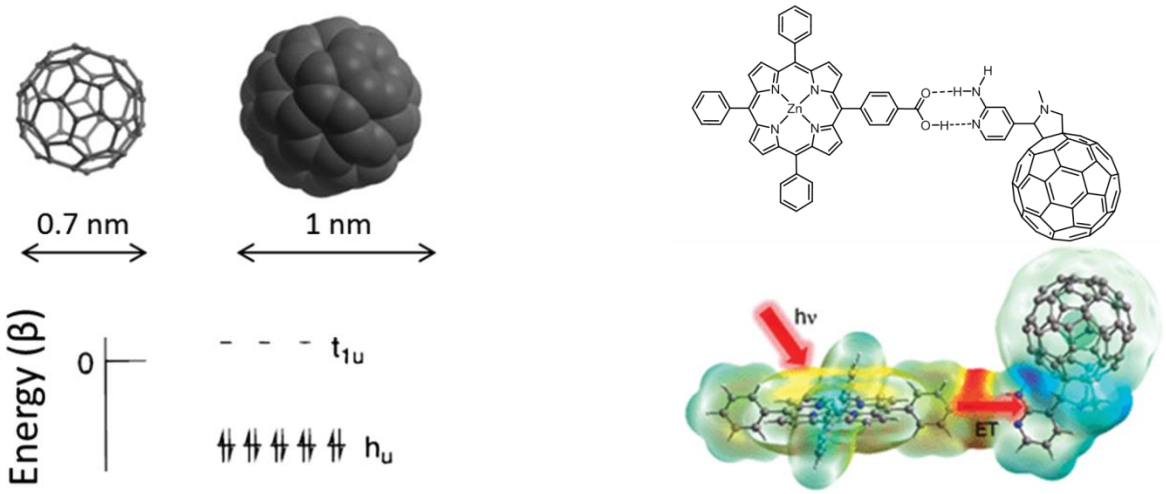

Figure 1.1 Crystallographic and van der Waals dimensions and molecular orbital diagram of C_{60} (left) and schematic representation of PET within hydrogen bonded porphyrin–fullerene conjugate (right)[53].

Due to their outstanding physicochemical properties, fullerenes have been identified as ones of the most promising candidates for nanoelectronics, promoting their incorporation in nanostructures where photoinduced electron transfer (PET) and solar energy conversion take

[51] a) Y. Liu, J. Zhao, Z. Li, C. Mu, W. Ma, H. Hu, K. Jiang, H. Lin, H. Ade, H. Yan *Nat. Commun*. **2014**, 5, 5293. b) S.-H. Liao, H.-J. Jhuo, P.-N. Yeh, Y.-S. Cheng, Y.-L. Li, Y.-H. Lee, S. Sharma, S.-A. Chen. *Sci. Rep*. **2014**, 4, 6813. c) L. Lu, T. Xu, W. Chen, E. S. Landry, L. Yu. *Nat. Photon.* **2014**, 8, 716 - 722. d) K. Cnops, B. P. Rand, D. Cheyns, B. Verreet, M. A. Empl, P. Heremans *Nat. Commun.* **2014**, 5, 3406.

[52] a)Y. Kawashima, K. Ohkubo, V. Blas-Ferrando, M. Vicente, H. Sakai, E. Font-Sanchis, J. Ortiz, F. Fernandez-Lazaro, T. Hasobe, A. Sastre-Santos, S. Fukuzumi, *J. Phys.l Chem. B* **2015**, 119, 7690 - 7697. b) G. D. Scholes, G. R. Fleming, A. Olaya-Castro, R. van Grondelle, *Nat. Chem.* **2011**, *3*, 763 - 774. c) R. J. Cogdell, T. H. P. Brotosudarmo, A. T. Gardiner, P. M. Sanchez, L. Cronin, *Biofuels* **2010**, *1*, 861 - 876. c) Special issue on "Artificial Photosynthesis and Solar Fuels", *Acc. Chem. Res.* **2009**, *42*, 1859 - 2029.

[53] F. D'Souza, G. M. Venukadasula, K. Yamanaka, N. K. Subbaiyan, M. E. Zandler and O. Ito, *Org. Biomol. Chem.*, **2009**, **7**, 1076 - 1080.

place.[54] The most abundant C_{60} fullerene is an electron-deficient spherical polyolefin with a crystallographic diameter of 0.7 nm and van der Waals diameter of 1 nm (Figure 1.1). It has a triply degenerate low-lying lowest unoccupied molecular orbital (LUMO) (Figure 1.1) and hence is an excellent electron acceptor able to accommodate up to six electrons per molecule.[55] On one hand, rigid aromatic structure of C_{60} fullerene evokes low reorganization energy in electron transfer reactions and, on the other hand, its extended π-conjugation affords efficient charge stabilization.[56,57]

Additionally, unique chemical versatility of fullerenes allow the fine-tuning of their physical and electrochemical properties by, for example, covalent modification of their exterior.[58,59] In light of the aforementioned, a myriad of electron donor-acceptor conjugates / hybrids have been designed featuring porphyrins,[60] (sub)phthalocyanines,[61,62] perylene-diimides[63] and other

---

54 a) Z. A. Page, Y. Liu, V. V. Duzhko, T. P. Russell, T. Emrick. *Science* **2014**, 346, 441 - 444. b) T. M. Clarke, J. R. Durrant, *Chem. Rev.* **2010**, *110*, 6736 - 6767. c) B. M. Savoie, A. Rao, A. A. Bakulin, S. Gelinas, B. Movaghar, R. H. Friend, T. J. Marks, M. A. Ratner. *J. Am. Chem. Soc.*, **2014**, 136, 2876 - 2884. d) S.-H. Liao, H.-J. Jhuo, Y.-S. Cheng, S.-A. Chen, *Adv. Mater.* **2013**, 25, 4766 - 4771. e) *Fullerenes: From Synthesis to Optoelectronic Properties*; Guldi, D. M., Martin, N., Eds.; Kluwer Academic Publishers: Dodrecht, The Netherlands, 2002.

55 L. Echegoyen, L. E. Echegoyen, *Acc. Chem. Res*. **1998**, 31, 593 - 601.

56 a) S. Kirner, M. Sekita, D. M. Guldi, *Adv. Mater.* **2014**, *26*, 1482 - 1493. b) A. J. Ferguson, J. L. Blackburn, N. Kopidakis, *Mat. Letters* **2013**, *90*, 115 - 125. c) Ch.-Z. Li, H.-L. Yip,A. K.-Y. Jen, *J. Mat. Chem.* **2012**, *22*, 4161 - 4177.

57 a) D. M. Guldi. *Chem. Soc. Rev.* **2002**, *31*, 22 - 36. b) D. M. Guldi, M. Prato. *Acc. Chem. Res.* **2000**, *33*, 695 - 703.

58 a) J. L. Delgado, P.-A. Bouit, S. Filippone, M. A. Herranz, N. Martin, *Chem. Commun.* **2010**, *46*, 4853 - 4865. b) A. Hirsch. *The Chemistry of the Fullerenes*, John Wiley & Sons, **2008**, pp. 1 - 215.

59 a) E. E. Maroto, M. Izquierdo, S. Reboredo, J. Marco-Martínez, S. Filippone, N. Martín. *Acc. Chem. Res.* **2014**, *47*, 2660 - 2670. b) S.-E. Zhu, F. Li, G.-W. Wang. *Chem. Soc. Rev.* **2013**, *42*, 7535 - 7570.

60 a) T. Hasobe, *Handbook of Carbon Nano Materials* (Eds.: F. D'Souza, K. M. Kadish), **2012**, *4*, 95 - 130. b) O. Ito, F. D'Souza, *Molecules* **2012**, *17*, 5816 - 5835. c) S. Fukuzumi, T. Kojima, *J. Mat. Chem.* **2008**, *18*, 1427 - 1439.

61 a) G. Bottari, M. Urbani, T. Torres, *Organic Nanomaterials: Synthesis, Characterization, and Device Applications* (Eds.: T. Torres, G. Bottari,), John Wiley & Sons, Inc., Hoboken, New Jersey, **2013**, pp. 163 - 187. b) G. Bottari, J. A. Suanzes, O. Trukhina, T. Torres, *J. Phys. Chem. Lett.* **2011**, 2, 905 - 913. c) G. Bottari, G. de la Torre, D. M. Guldi, T. Torres, *Chem. Rev.* **2010**, *110*, 6768 - 6816.

62 a) C. B. KC, G. N. Lim, M. E. Zandler, F. D'Souza, *Org. Letters* **2013**, *15*, 4612 - 4615. b) D. Gonzalez-Rodriguez, E. Carbonell, G. de Miguel Rojas, C. Atienza Castellanos, D. M. Guldi, T. Torres, *J. Am. Chem. Soc.* **2010**, *132*, 16488 - 16500. c) J.-H. Kim, M. E. El-Khouly, Y. Araki, O. Ito, K.-Y. Kay, *Chem. Letters* **2008**, *37*, 544 - 545. d) D. Gonzalez-Rodriguez, T. Torres, D. M. Guldi, J. Rivera, M. A. Herranz, L. Echegoyen, *J. Am. Chem. Soc.* **2004**, *126*, 6301 - 6313. e) D. Gonzalez-Rodriguez, T. Torres, D. M. Guldi, J. Rivera, L. Echegoyen, *Org. Lett.* **2002**, *4*, 335 - 338.

63 a) S. Pla, L. Martin-Gomis, K. Ohkubo, S. Fukuzumi, F. Fernandez-Lazaro, A. Sastre-Santos, *Asian J. Org. Chem.* **2014**, *3*, 185 - 197. b) P. Hudhomme, R. M. Williams, *Handbook of Carbon Nano Materials* (Eds.: F. D'Souza, K. M. Kadish,) **2011**, *2*, pp. 545-591. c) J. Baffreau, S. Leroy-Lhez, P.

chromophores. Interestingly, exohedral derivatization of these empty carbon cages with a wide variety of photo- and/or redox-active species hasn't caused an inversion in the direction of the charge transfer process. In all mentioned D-A systems, light-harvesting chromophors usually act as electron donors and empty fullerenes as electron acceptors. Notably, reports in which fullerenes are employed as electron donors remain, however, scarce.

The main reason for that is the fact that oxidation of empty fullerenes requires harsh conditions. Being more precise, it occurs only by treating those with, for example, strong oxidizing agents[64] or upon photo- or electron-induced ionization in the presence of electron transferring photosensitizers.[65] The first example of *intermolecular* electron-transfer oxidation of fullerenes was reported by Fukuzumi *et al.* in the presence of *p*-benzoquinone and radical-ion pair stabilizing scandium triflate $Sc(OTf)_3$.[66] The only case of *intramolecular* oxidation of C_{60} fullerene has been reported later by the same author. In a fullerene-trinitrofluorenone conjugate, photoexcitation and the presence of $Sc(OTf)_3$ afforded the formation of oxidized fullerenes, whereas only the triplet excited state of the fullerene was observed in the absence of $Sc(OTf)_3$.[67] No successful *intramolecular* oxidation of fullerenes by means of simple photoexcitation has been reported up to date.

On this connection, many efforts have been devoted to the design and synthesis of fullerene-based D-A systems that would allow the use of fullerenes as electron donors and, thus, afford an inversion in the direction of the charge transfer processes in photovoltaic devices in order to improve their performances. Thus, linking fullerenes to strong electron acceptors, which provide the means of charge stabilization within their extended π-system, could assist in shedding light onto the rare electron donating features of fullerenes. Another possible tool towards the change of the paradigm is an internal functionalization of empty fullerenes by an incorporation of

---

Hudhomme, M. M. Groeneveld, I. H. M. van Stokkum, R. M. Williams, *J. Phys. Chem. A* **2006**, *110*, 13123 - 13125.

64 a) F. Cataldo, S. Iglesias-Groth, A. in Manchado, *Fullerenes, Nanotubes and Carbon Nanostructures*, **2012**, *20*, 656 - 671. b) C. Bruno, I. Doubitski, M. Marcaccio, F. Paolucci, D. Paolucci, A. Zaopo, *J. Am. Chem. Soc.* **2003**, *125*, 15738 - 15739. c) C. A. Reed, K.-C. Kim, R. D. Bolskar, L. J. Mueller, *Science* **2000**, *289*, 101 - 104.

65 a) K. Ohkubo, R. Iwata, T. Yanagimoto, S. Fukuzumi, *Chem. Commun.* **2007**, 3139-3141. b) S. Fukuzumi, K. Ohkubo, H. Imahori, D. M. Guldi, *Chem. Eur. J.* **2003**, *9*, 1585 - 1593. c) L. Biczok, H. Linschitz, *J. Phys. Chem. A* **2001**, *105,* 11051 - 11056, and references therein.

66 S. Fukuzumi, H. Mori, H.Imahori, T. Suenobu, Y. Araki, O. Ito, K. M. Kadish, *J. Am. Chem. Soc.*, **2001**, *123*, 12458 - 12465.

67 K. Ohkubo, J. Ortiz, L. Martin-Gomis, F. Fernandez-Lazaro, A. Sastre-Santos, S. Fukuzumi, *Chem. Commun.* **2007**, 589 - 591.

molecular guests into their interior. Establishing flexibility of electron transfer events could open up new ways of using fullerenes in novel photoelectrochemical water splitting devices, operating under oxidative conditions; novel solar cells featuring larger open circuit voltages, or towards optoelectronic devices integrating novel *n*-type semiconductors.

1.1.1 Background and objectives

On this connection, endohedral metallofullerenes (EMFs) - carbon cages that encapsulate atoms, ions, or clusters – have received a special attention in scientific community due to their unique physicochemical properties. [68] Thus, these spherical molecules possess a flexible redox chemistry that significantly varies as a function of the encapsulated species. Moreover, EMFs exhibit higher absorption coefficients in the visible region of the electromagnetic spectrum and reduced HOMO-LUMO gaps compared to their analogues. All mentioned makes EMFs excellent candidates for optoelectronic applications.[69]

Similarly to their empty analogues, EMFs have been exstensively used as electron-accepting units in covalently-linked D-A systems with porphyrins,[70,71] phthalocyanines,[72] corroles,[73] extended tetrathiafulvalenes (ex-TTF),[74] thriphenilamines[75] and other photoactive conjugated molecules. More recently, a few examples of EMF-based, D-A conjugates have been reported in which the EMF acts as an electron-donor when being covalently-linked to electron-accepting moieties such

---

68 a) T. Wang, C. Wang, *Acc. Chem. Res.* **2014**, *47*, 450-458. b) J. Zhang, S. Stevenson, H. C. Dorn, *Acc. Chem. Res.* **2013**, *46*, 1548 - 1557. c) M. Rudolf, S. Wolfrum, D. M. Guldi, L. Feng, T. Tsuchiya, T. Akasaka, L. Echegoyen, *Chem. Eur. J.* **2012**, 18, 5136 - 5148.

69 R. B. Ross, C. M. Cardona, D. M. Guldi, S. S. Gayathri, M. O. Reese, N. Kopidakis, J. Peet, B. Walker, G. C. Bazan, E. van Keuren, B. C. Holloway, M. Drees, *Nature Mat.* **2009**, *8*, 208 - 212.

70 L. Feng, S.G. Radhakrishnan, N. Mizorogi, Z. Slanina, H. Nikawa, T. Tsuchiya, T. Akasaka, S. Nagase, N. Martín, D.M. Guldi. *J. Am. Chem. Soc.* **2011**, *133*, 7608 - 7618.

71 L. Feng, Z. Slanina, S. Sato, K. Yoza, T. Tsuchiya, N. Mizorogi, T. Akasaka, S. Nagase, N. Martín, D.M. Guldi, *Angew. Chem. Int. Ed.* **2011**, *50*, 5909 - 5912;

72 J. R. Pinzon, C. M. Cardona, M. A. Herranz, M. E. Plonska-Brzezinska, A. Palkar, A. J. Athans, N. Martin, A. Rodriguez-Fortea, J. M. Poblet, G. Bottari, T. Torres, S. S. Gayathri, D. M. Guldi, L. Echegoyen. *Chem. Eur. J.* **2009**, *15*, 864 - 877.

73 B. Liu, H. Fang, X. Li, W. Cai, L. Bao, M. Rudolf, F. Plass, L. Fan, X. Lu, D. M. Guldi. *Chem. Eur. J.* **2015**, *21*, 746 - 752.

74 Y. Takano; M. A. Herranz, N. Martín, S. G. Radhakrishnan, D. M. Guldi, T. Tsuchiya, S. Nagase, T. Akasaka. *J. Am. Chem. Soc.* **2010**, *132*, 8048 - 8055.

75 J. R. Pinzon, D. C. Gasca, S. S. Gayathri, G. Bottari, T. Torres, D. M. Guldi, L. Echegoyen, *J. Am. Chem. Soc.* **2009**, *131*, 7727 - 7734.

as perylene-diimide[76,77] and tetracyanoanthraquinodimethane (TCAQ).[78] Interestingly, both, reductive and oxidative PET processes, have been observed for the two of EMFs, namely $La_2@I_h$-C_{80} (Figure 1.2) and $Lu_3N@I_h$-C_{80} upon mixing the EMF moiety with the appropriate redox-active unit.

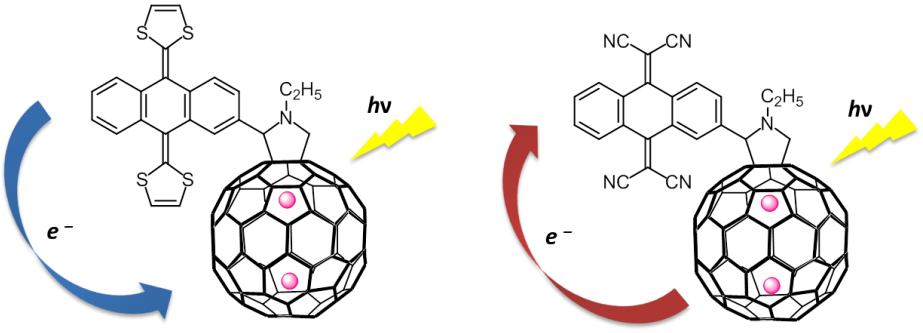

Figure 1.2. Covalent conjugates of $La_2@I_h$-C_{80} with electron-donor (ex-TTF) and electron-acceptor (TCAQ) molecules resulting in switching of the direction of PET.

Supramolecular approach to the construction of D-A EMF-based hybrids is another strategy that offers multiple advantages with respect to the covalent approach. Thus, it allows preparing and studying a large number of systems through the simple and rational combination of a given array of redox and/or photo-active molecules. Recently, supramolecular hybrids have been prepared in which EMFs act either as electron-acceptor ($La_2@C_{80}$[79a] and $Li^+@C_{60}$) or electron-donor ($M_3N@I_h$-C_{80}; M = Lu or Sc) moieties. As it is shown on the Figure 1.3, supramolecular constructs of tetraphenyl-Zn(II)porphyrin and $La@C_{82}$ revealed PET reactivity similar to that of their covalent conjugate. The use of supramolecular approach in the construction of these dimers significantly reduces the synthetic efforts and, theoretically, allows screening of the influence of different chromophors-guests on the direction of ET. However, to the best of our knowledge, no examples of bidirectional PET have been reported thus far for D-A supramolecular ensembles with identical

---

76 M. Rudolf, L. Feng, Z. Slanina, T. Akasaka, S. Nagase, D. M. Guldi, *J. Am. Chem. Soc.* **2013**, *135*, 11165 - 11174.

77 L. Feng, M. Rudolf, S. Wolfrum, A. Troeger, Z. Slanina, T. Akasaka, S. Nagase, N. Martín, N. T. Ameri, C. J. Brabec, D. M. Guldi, *J. Am. Chem. Soc.* **2012**, *134*, 12190 - 12197.

78 Y. Takano, S. Obuchi, N. Mizorogi, R. García, M. A. Herranz, M. Rudolf, D. M. Guldi, N. Martín, S. Nagase, T. Akasaka, *J. Am. Chem. Soc.* **2012**, *134*, 19401 - 19408.

79 a) T. Tsuchiya, M. Rudolf, S. Wolfrum, S. R. Gayathri, R. Aoyama, Y. Yokosawa, A. Oshima, T. Akasaka, S. Nagase, D. M. Guldi. *Chem. Eur. J.* **2013**, *19*, 558 - 565. b) T. Kamimura, K. Ohkubo, Y. Kawashima, H. Nobukuni, Y. Naruta, F. Tani, S. Fukuzumi. *Chem. Sci.*, **2013**, *4*, 1451 - 1461. c) B. Grimm, J. Schornbaum, C. M. Cardona, J. D. van Paauwe, P. D. W. Boyde, D. M. Guldi. *Chem. Sci.*, **2011**, *2*, 1530 - 1537.

fullerene species that show a dual electronic behavior, as previously observed for cyclo[8]pyrrole-based supramolecular systems.[80] In this respect, the rational choice of a chromophoric counterpart may play a decisional role in both, defining the direction of PET processes and enabling electron transfer dichotomy, characteristic for switching systems and sensors.

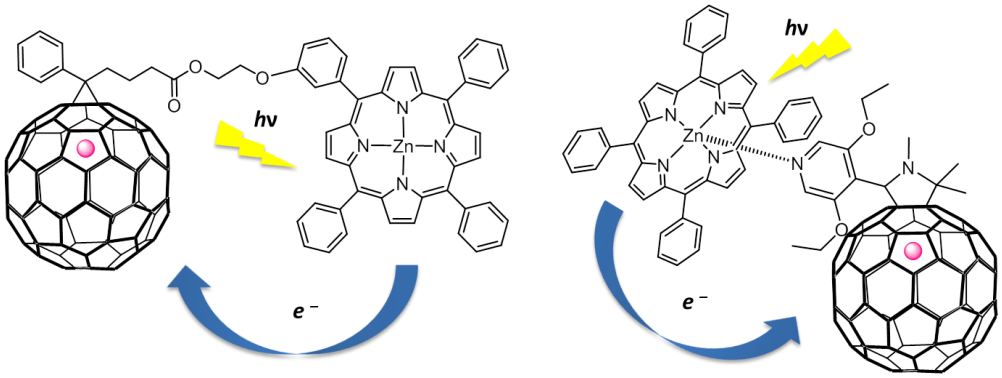

Figure 1.3. Covalent and supramolecular hybrids of La@ C_{82} with Zn(II)porphyrin (Por).

As it has been mentioned in introduction, phthalocyanines and their lower derivatives – subphthalocyanines – possess well-known chemical versatility and architectural flexibility that allows modulation of their electronic properties from electron donor – to electron acceptor, by simple peripheral modification of their molecules. Thus, Torres *et al*. reported a vast variety of (Sub)Pcs with low reduction potentials, which bear electron-withdrawing substituents.[**Ошибка! Закладка не определена.**, 81] Additionally, owing to the intense absorption of Sub(Pcs) in the visible region of the solar spectrum – complementary to that of fullerenes – and high optical and thermal stabilities, these robust molecules have evolved as perfect light-harvesting building blocks. All mentioned renders these chromophors ideal electron acceptors when linked to fullerenes and, thus, opens the possibility to test the dual behaviour of EMFs in PET processes and, maybe, even to switch the direction of electron transfer in conjugates, containing empty fullerenes.

The main aim of this chapter, as stated in the previous section, is the preparation of covalent and supramolecular constructs of fullerenes (empty and endohedral) and phthalocyanines/

[80] K. Ohkubo, K. Mase, E. Karnas, J. L. Sessler, S. Fukuzumi. *J. Phys. Chem. C* **2014**, *118*, 18436 - 18444.

[81] A. Roth, M.-E. Ragoussi, L. Wibmer, G. Katsukis, G. de la Torre, T. Torres, D. M. Guldi, *Chem. Sci.*, **2014**, *5*, 3432 - 3438.

subphthalocyanines of various electronic nature, and study of photopysical and electrochemical properties of the resulting systems.

Thus, at first, we intended to prepare supramolecular systems based on $Sc_3N@I_h$-C_{80} or C_{60} and phthalocyanines with strong electron-donor or electron-acceptor character, to switch the direction of photoindiced electron transfer.

In order to do so, we describe in the first section of this chapter the synthesis of pyridyl-derivatives of $Sc_3N@I_h$-C_{80} **4** or C_{60} **3** and the formation of their supramolecular complexes with an electron-donating **1** or an electron-accepting Zn(II)Pcs **2** by metal-ligand, axial coordination of the pyridyl moiety of the fulleropyrrolidine to the zinc metal center of the Pc macrocycle (Figure 1.4). We report on the study of the complexing abilities of the two counterparts in solution. In the first instance, we expect to reveal the intensity of the interaction of fullerene with Pc "companion" as a function of the electronic nature of Pcs macrocycle throught defining the correcpondidng bindidng constants.

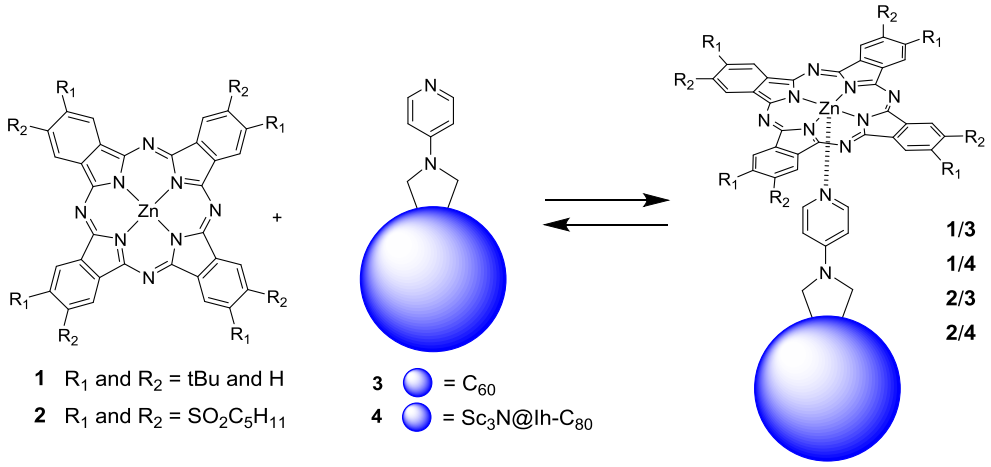

Figure 1.4. Metal-ligand, axial coordination of *N*-(*p*-pyridyl)-substituted fulleropyrrolidines **3** or **4** to Zn(II)Pcs **1** and **2** leading to supramolecular complexes **1/3** , **2/3** and **1/4**, **2/4**.

The choice of Zn(II)Pcs as supramolecular "counterparts" of fullerenes **3** and **4** was prompted by several reasons. Pcs are aromatic macrocycles which possess excellent light-harvesting capabilities, good thermal stability, and rich redox chemistry.[82] Moreover, and importantly, the optical and electrical properties of these macrocycles can be easily modulated by the careful

82 *Handbook of Porphyrin Science*; Kadish, K. M., Smith, K. M., Guilard, R., Eds.; Academic Press: San Diego, **2010**; Vols. 1 - 5.

choice of the metal center and/or the peripheral substituents making them perfect building blocks for light harvesting, photovoltaic, and molecular photonic applications.[83]

We chose tetra-*tert*-butyl Zn(II)Pc **1** as electron-donor due to its well-known electron-rich character, reasonable solubility in the most of organic solvents and its commercial availability. Four *tert*-butyl groups were expected to lower the tendency of Zn(II)Pcs towards aggregation caused by strong π-π interactions. Interestingly, the presence of different isomers of $_{tert}$Bu-substitution is known to not affect the physicochemical properties of the resulting systems. Octakis-(pentylsulfonyl) Zn(II)Pc **2** were selected as electron acceptor due to their well-know electron deficient nature and easy synthetic availability. More interestingly, $Sc_3N@I_h$-C_{80} was chosen as the most abundant and readily available endohedral fullerene of its family, with redox characteristics resembling those of empty C_{60} and only slightly shifted towards cathodic potentials. Importantly, $Sc_3N@I_h$-C_{80} is the only EMF which can be prepared[84] and separated in bulk quantities by non-HPLC methods[85] with a yield higher than C_{84}, the third most abundant empty fullerene.[86]

Finally, photoindiced ET processes occurring in the complexes were studied with pump probe techniques.

To the best of our knowledge, none example of SubPc-EMF system has been reported to date. Nevertheless, low reduction potentials of SubPcs and low reorganization energies in electron transfer reactions render them ideal electron acceptors when linked to fullerenes. Taking into account the experience of our group in the preparation of SubPc-based covalent systems,**Ошибка! Закладка не определена.**b,d,e, [87] in the second section of this chapter, we centered on the synthesis of

---

[83] a) G. Bottari, G. de la Torre, T. Torres. *Acc. Chem. Res.* **2015**, *48*, 900 - 910. b) N. L. Bill, O. Trukhina, J. L. Sessler, T. Torres. *Chem. Commun.* **2015**, *51*, 7781 - 7794. c) G. Bottari, O. Trukhina, M. Ince, T. Torres. *Coord. Chem. Rev.* **2012**, *256*, 2453 - 2477. d) G. Bottari, G. de la Torre, D. M. Guldi, Torres, T. *Chem. Rev.* **2010**, *110*, 6768 - 6816. e) F. D'Souza, O. Ito. *Coord. Chem. Rev.* **2005**, *249*, 1410 - 1422.

[84] a) S. Stevenson, M. A. Mackey, M. C. Thompson, H. L. Coumbe, P. K. Madasu, C. E. Coumbe, J. P. Phillips. *Chem. Commun.* **2007**, *41*, 4263 - 4265. b) S. Stevenson, M. C. Thompson, H. L. Coumbe, M. A. Mackey, C. E. Coumbe, J. P. Phillips. *J. Am. Chem. Soc.* **2007**, *129*, 16257 - 16262.

[85] a) S. Stevenson, M. A. Mackey, C. E. Coumbe, J. P. Phillips, B. Elliott, L. Echegoyen. *J. Am. Chem. Soc.* **2007**, *129*, 6072 - 6073. b) S. Stevenson, K. Harich, H. Yu, R. R. Stephen, D. Heaps, C. Coumbe, J. P. Phillips. *J. Am. Chem. Soc.* **2006**, *128*, 8829 - 8835. c) Z. Ge, J. C. Duchamp, T. Cai, H. W. Gibson, H. C. Dorn, *J. Am. Chem. Soc.* **2005**, *127*, 16292 - 16298. d) B. Elliott, L. Yu, L. Echegoyen, *J. Am. Chem. Soc.* **2005**, *127*, 10885 - 10888.

[86] W. Kratschmer, L. D. Lamb, K. Fostiropoulos, D. R. Huffman, *Nature,* **1990**, *347*, 354 - 358.

[87] a) C. R. Nieto, J. Guilleme, C. Villegas, J. L. Delgado, D. Gonzalez-Rodriguez, N. Martín, T. Torres, D. M. Guldi, *J. Mater. Chem.*, **2011**, *21*, 15914 - 15918. b) C. Romero-Nieto, J. Guilleme, J. Fernandez-Ariza,

conjugates of $La_2@I_h$-C_{80} and SubPcs of strong electron-withdrawing character **6** and **8**, as well as their corresponding C_{60}-based reference systems **5** and **7** (Figure 1.5).

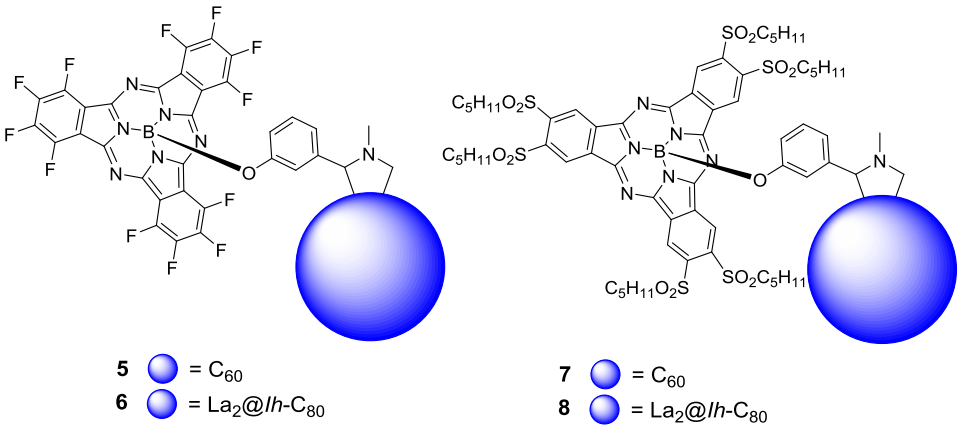

Figure 1.5. Conjugates of SubPcs and fullerenes (endohedral and empty).

We selected the perfluorinated SubPc and the hexa-(pentylsulfonyl)-SubPc as strongest, among easily available, electron acceptors, according to their redox characteristics. Whereas, $La_2@I_h$-C_{80} was chosen as fitting metallofullerene for it's relatively low HOMO-LUMO gap,[Ошибка! Закладка не определена.] if compared with other EMFs. Finally, the presence of photo- and electroactive chromophores in these systems motivated the photophysical studies, such as investigation of intramolecular electronic communication between SubPc and fullerenic moiety in ground and excited states as well as analysis of the correspondidng PET events.

S. M. Rodriguez-Morgade, D. Gonzalez-Rodriguez, T. Torres, D. M. Guldi, *Org. Lett.*, **2012**, *14*, 5656 - 5659.

1.1.2. Experimental techniques

Study of the D-A systems, described in this chapter, involves the knowledge of some techniques of supramolecular chemistry and phtotophysics. In this regard, some basic experiments required for the determination of quantitative aspects of the binding equilibrium (stoichiometry, binding constant) will be described. Afterwards, a brief explanation of the methods of the steady-state and pump-probe spectroscopy, usually employed for the study of photophysical properties of organic molecules, will be given.

Method of Continuous Variation

The method of continuous variation is a procedure commonly used to determine the stoichiometry of a binding event. It is generally associated with P. Job, who applied the procedure to the study of many coordination compounds.[88] The this method, the total molar concentration of the two binding partners – host and guest – is held constant, whereas their mole fractions vary. Hence, the detection parameter changes proportionally upon complex formation. This parameter is then plotted *vs* the mole fraction of one of the components. The maximum on the resulting plot indicates the stoichiometry of the two species (Figure 1.6).

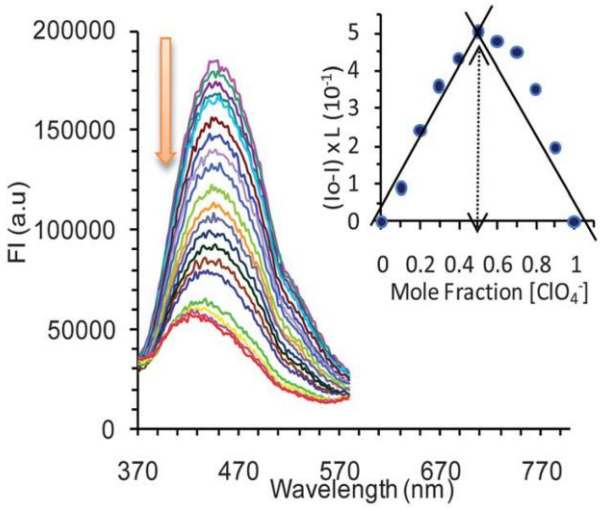

Figure 1.6. An example of the Job's plot with 1:1 stoichiometry (inset) built upon gradual addition of ClO_4^- to chemosensor, detecting changes of fluorescence.[89]

There are several conditions to be concidered when applying the Job's method:

[88] P. Job, *Annali di Chimica Applicata.,* **1928**, *9,* 113 - 203.
[89] R. Kumar, S. Kumar, P. Singh, G. Hundal, M. S. Hundal, S. Kumar. *Analyst*, **2012**, *137*, 4913 - 4916.

- the system must conform to the Lambert-Beer's law,
- one complex must predominate under the conditions of the experiment,
- the total concentration of the two binding motifs must be maintained constant,
- pH and ionic strength must be maintained constant,
- experiment should be carried out at different values of total concentration to ensure its reliability.

Moreover, Job's Plots of 1:1 complexes allow approximate determination of the binding constants.[90] For that purpose, the slope of the tangent lines to the Job Plot's curve at mole fraction χ = 0 and χ = 1 must be determined, and then, binding constants can be derived from the following equations:

$$a_0 = \frac{m}{m+1}$$

$$a_1 = \frac{-m}{(m+1)}$$

where: a_0 y a_1 – slopes of tangent lines at mole fraction χ = 0 and χ = 1; $m=K_{eq}\times[C]_0$.

Titrations

A titration is a volumetric technique in which a solution of one reactant – the titrand – is added to a solution of a second reactant – analyte – until the equivalence point will be reached. The equivalence point is the point at which titrant has been added in exactly the right quantity to react stoichiometrically with the analyte.[91]

Titration is the most common approach to quantify interactions between host and guest in supramolecular chemistry.[92] The changes of some physical parameter, affected upon addition of the titrand, can be tracked by various spectroscopic techniques such as NMR, UV-vis, fluorescence and others. The accuracy of the results relies on the right choice of concentration range, suitable technique, acquisition of a reasonable number of data points, and careful work during the experimental procedure as well as on the data analysis.

[90] E. Bruneau, D. Lavabre, G. Levy, J. C. Micheau, *J. Chem Educ.*, **1992**, *69*, 833 - 837.
[91] http://chemed.chem.wisc.edu/chempaths/GenChem-Textbook/Titrations-875.html
[92] P. Thodarson, *Chem. Soc. Rev.*, **2011**, *40*, 1305 - 1323.

In general, it is worthwhile to obtain as much information as possible prior to the titration experiment (stoichiometry, estimated value of binding constant), in order to ease the choice of the above mentioned parameters.

Supramolecular titration experiments are usually carried out maintaining the concentration of one component – host (H) – fixed. Then, the physical changes observed on the system can be plotted *vs* the added concentration of guest (G). The resulting titration curve is known as binding isotherm (Figure 1.7, inset), and its points can be fitted to a mathematical model which is deduced from the equilibrium taking place. From these data, the binding constant K_a, corresponding to the formation of supramolecular complex, can be determined.[93]

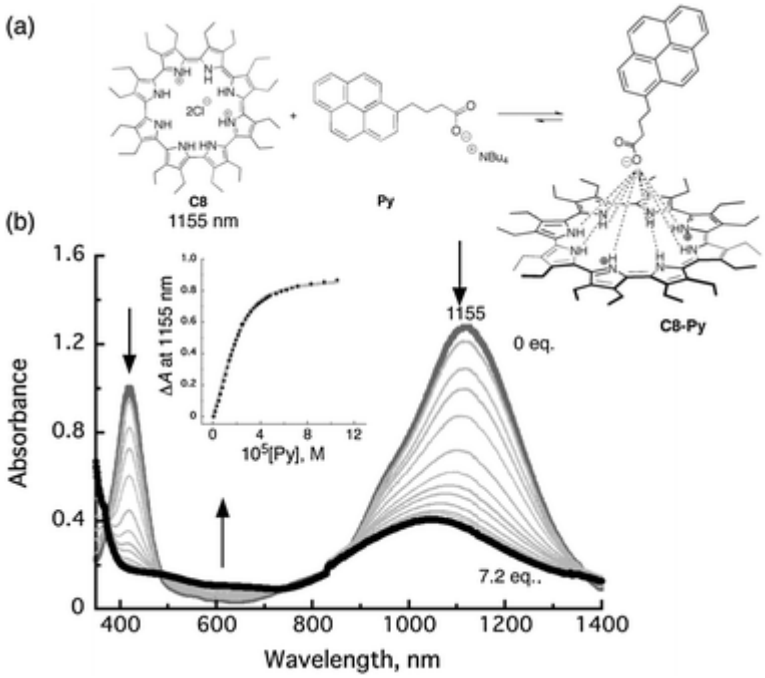

Figure 1.7. An example of the 1:1 bindidng isotherm produced from the change in absorbance at 1155 nm (inset) built upon UV-vis absorption titration of tetra-*n*-butylammonium 1-pyrenebutyrate (Py) into cyclo[8]pyrrole (C8) at 1.5×10^{-5} M in MeCN at 298 K (a,b).[94]

Electrochemistry

Electrochemical measurements of organic molecules in solution are employed to determine the energies of their frontier orbitals – HOMO and LUMO – and the bandgap between them

[93] K. A. Connors, *Binding Constants,* Wiley & Sons, New York, 1987.

[94] J. L. Sessler, E. Karnas, S. K. Kim, Z. Ou, M. Zhang, K. M. Kadish, K. Ohkubo and S. Fukuzumi, *J. Am. Chem. Soc.*, **2008**,*130*, 15256 - 15257.

corresponding to the energy of the first singlet excited state.[95] These are crucial parameters for the study of photoinduced transfer processes.

Within a material that the electrode is made of (platinum, gold or graphite) a continuum of levels is created with the available electrons filling a certain number of states. The Fermi-level corresponds to the energy at which the 'top' electrons sit. This level is not fixed, and its energy can be modified by supplying electric energy. That means, if we apply a positive potential, we are removing electrons from the material and, thus, the Fermi level will descend. When the Fermi level of the electrode goes below the energy of the HOMO of the analyte, the first oxidation of the molecule occurs (Figure 1.8). In contrast, when applying a negative potential, we are injecting electrons into the empty levels of the electrode, and thus, the Fermi level goes up. When the applied potential reaches an energy higher than the LUMO of the molecule, the first reduction takes place (Figure 1.8).

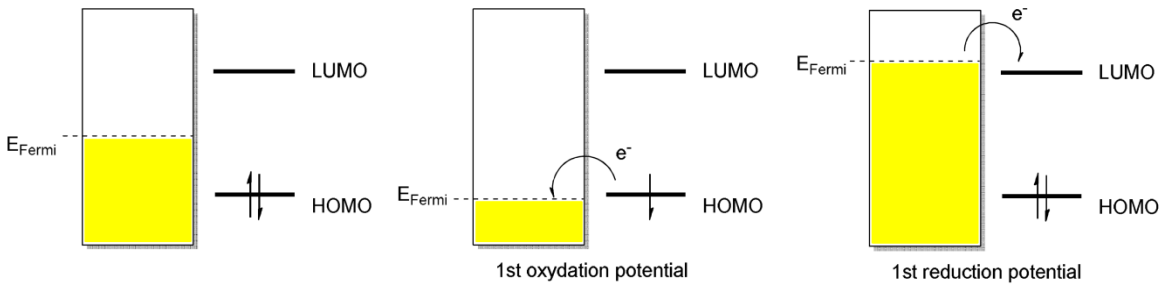

Figure 1.8. Schematic representation of the relationship between redox processes and frontier orbitals of compounds.

Cyclic voltammetry

Cyclic voltammetry (CV) is a type of potentiodynamic electrochemical measurement based on variation of the applied potential at a working electrode in both – forward and reverse – directions at a determined scan rate, while monitoring the current.[96] CV measurements must be carried out in a solutions with highest diffusion control. During the experiment, the potential is applied between the reference and the working electrodes, while the current intensity is measured between the working and the counter electrode. The current at the working electrode

[95] Electrochemical Methods: Fundamentals and Applications, A.J. Bard, L. R. Faulkner, Wiley & Sons, 2nd Ed., January 2001.

[96] P. T. Kissinger, W. R. Heinemann, *J. Chem. Educ.*, **1983**, *60*, 702-706; Handbook of instrumental Techniques for Analytical Chemistry, F. A. Settle (Chapter 37, S. P. Kounaves), Prentice Hall, 1997.

will increase when reductions (injection of electrons from the electrode to the empty orbitals of the analyte) or oxydations (injection of electrons from occupied orbitals of the analyte to the electrode) of the molecule in solution occur. The current falls off again as the concentration of analyte close to the electrode surface is depleted.

Cyclic voltammetry can distinguish reversible and irreversible electrochemical processes. A redox process is said to be reversible if the system remains in equilibrium throughout the whole potential scan. A typical voltammogram for a reversible process is shown in Figure 1.9. Generally, two conditions must be fulfilled to consider an oxidation or reduction reversible, at 25°C and any scan rate:

- the peak potential separation $\Delta E_p = (E_{pc} - E_{pa}) = 59.2/n$, mV,
- the peak-current ratio $i_{pa}/i_{pc} = 1$

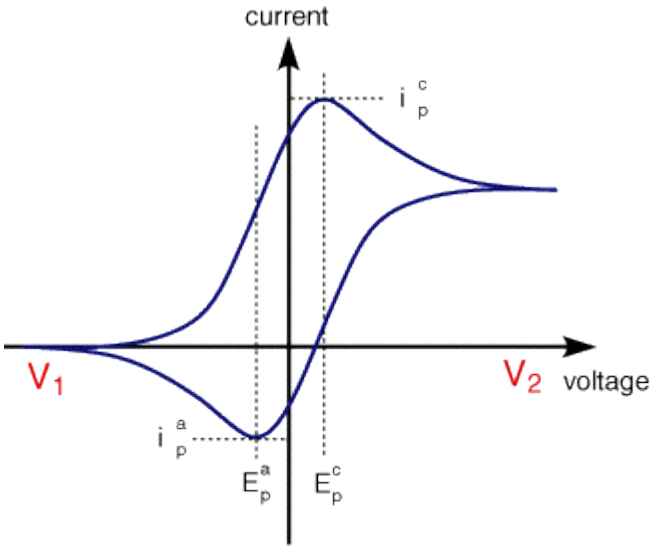

Figure 1.9. A typical cyclic voltammogram showing the important peak parameters.

On the other hand, irreversibility is caused by slow exchange of electrons between the analyte and the working electrode.

Square wave voltammetry

Square-wave voltammetry (SWV) is a pulse technique. The excitation signal in SWV consists of a symmetrical square-wave pulse of amplitude Esw superimposed on a staircase waveform of step height ΔE, where the forward pulse of the square wave coincides with the staircase step. The net current is obtained by taking the difference between the forward and reverse currents. The peak height in the voltammogram is proportional to the concentration of the electroactive species,

and allows limits of detection up to 10^{-8} M. In general, it is employed to obtain the exact values of the redox potentials.

This type of potential modulation presents important advantages as increased speed and sensitivity. However, it does not distinguish between reversible and non reversible redox processes.

Photophysics

The absorption of UV or visible light by an organic molecule causes the promotion of an electron from an initially occupied, low energy orbital to a higher energy, previously unoccupied orbital (Figure 1.10).[97] When such event happens, an excited state of the molecule is generated. Following light absorption, several processes contribute to the relaxation of the molecule and its return to the ground state. These processes can be either *radiative* (a photon is emitted during the transition) or *non-radiative* (the loss of energy is emitted as heat- infrared radiation- instead of UV-visible light).

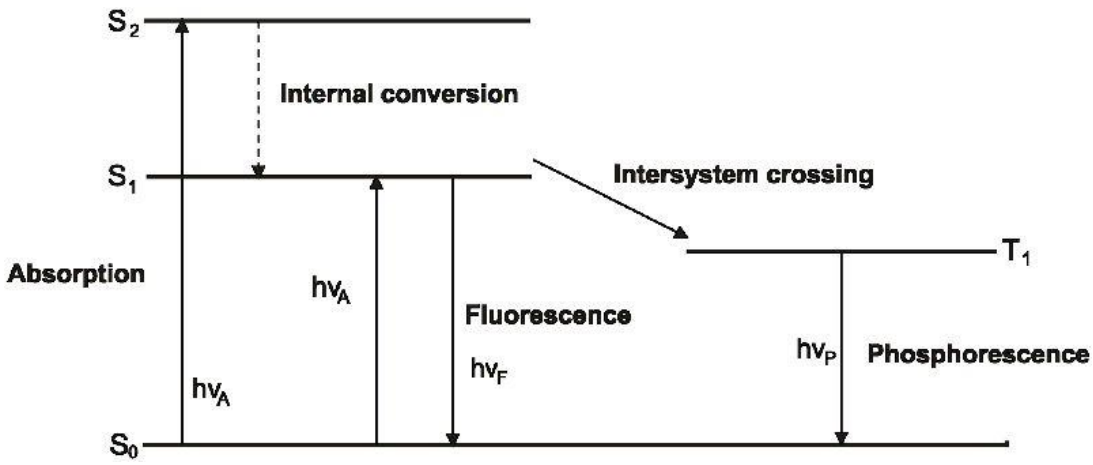

Figure 1.10. Yablonski diagram.

Molecules in condensed phases rapidly relax to the lowest vibrational state of S_1 (typically in 10^{-12} s or less). Fluorescence then results from a thermally equilibrated excited state. This radiative transition to the ground state generally occurs to excited vibrational levels within the ground state, which then reaches thermal equilibrium again through vibrational relaxation. As a consequence, fluorescent emission is bathocromically shifted with respect to absorption. This

[97] a) Modern Molecular Photochemistry, N. J. Turro, University Science Books, 1991. b) Principles of Fluorescence Spectroscopy, 3rd Ed., J. R. Lackowicz, Springer Science, 2006.

wavelength difference between both bands is called *Stokes shift*. Moreover, when the shape of the fluorescence spectrum mirrors the one of the absorption band, it means that the vibrational structure in both the ground state and the first excited state are similar. Actually, all transitions between electronic states occur without nuclear geometry being affected; they take place within times close to 10^{-15} s, which is a too short interval for nuclei displacement (Franck-Condon Principle).

Radiative emission from the first singlet excited state also occurs when the molecule interacts with an electromagnetic wave of the exact frequency of the transition. The photon thus generated has the same phase, frequency, polarization and direction of the incident light. In normal media at thermal equilibrium, absorption exceeds stimulated emission because there are more electrons in the lower energy states than in the higher energy states. However, when a population inversion is present the rate of stimulated emission exceeds that of absorption, and a net optical amplification can be achieved.

Molecules in the first singlet excited state can also undergo a spin flip of one electron to the first triplet state. This conversion is known as *intersystem crossing*. Spin flip is usually produced by spin-orbit coupling, and it is more favourable if the molecule possesses heavy atoms. Radiative emission from T_1 to the ground state is called phosphorescence, and it is usually shifted to longer wavelengths than fluorescence. Transitions involving a change of spin are optically forbidden, and as a consequence the rate constants for phosphorescence are several orders of magnitude lower than for fluorescence.

Relaxation from the S_1 or the T_1 to the ground state can also occur non-radiatively through the vibrational levels, which is known as *internal conversion*.

All the photophysical events described above are defined by their quantum yield and their lifetime. The quantum yield is the number of times a specific event occurs per photon absorbed by the system. For example, *fluorescence quantum yield* is defined as the number of molecules decaying from S_1 to S_0 through emission with respect to the number of photons absorbed. As both radiative and non radiative transitions can depopulate the first singlet excited state, the fluorescence quantum yield is given by:

$$\Phi_f = \frac{\Gamma}{\Gamma + k_{nr}}$$

Where Γ is the rate of fluorescence and k_{nr} contains the kinetic rates of all non radiative processes that deactivate the first singlet excited state.

The *lifetime of an excited state* is defined by the average time the molecule spends in that state prior to deactivation. Lifetime is the inverse of the total decay rate (sum of the kinetic rates corresponding to the processes that depopulate the excited state):

$$\tau = \frac{1}{\Gamma + k_{nr}}$$

Time-resolved fluorescence is a technique in which the fluorescence of a sample is monitored as a function of time after excitation by a flash of light. The width of the excitation pulse is made as short as possible, preferably much shorter than the decay time of the sample. Fluorescence lifetime is determined fitting the data to exponential decay models. For a single exponential decay, around 63% of the molecules have emitted prior to t = τ.

Lifetime of triplet states can be determined with laser flash photolysis. In this technique, a sample is firstly excited by a strong pulse of light of a laser. The pulse width ranges from nanoseconds to femtoseconds, depending on the laser. In this manner, an increased population of excited states is generated. Typically the light absorption of the sample (at the maximum of absorption of the triplet state) after excitation is recorded within short time intervals.

After light absorption, and in the presence of other molecules in solution, chromophores can also undergo transformations like energy transfer, photoinduced electron transfer or other chemical reactions. These events are among the fastest events in nature. They occur in time scales ranging from femtoseconds to nanoseconds. The development of ultrafast laser systems has enabled investigation of these events in real time. *Femtosecond transient absorption spectroscopy*, also referred to as *femtosecond pump-probe spectroscopy*, is one of the most common tools to investigate ultrafast photochemical reactions. In particular, this technique allows the observation of light-induced intra- and intermolecular processes on the time scale of the motion of atoms and electrons and, thus, provides one of the most effective methods for studying the behaviour of transient species like radicals, ions and excited states.[98]

[98] R. Berera, R. van Grondelle, J. T. M. Kennis, *Photosynth. Res.*, **2009**, *101*, 105 - 118.

The principle of *transient absorption spectroscopy* is shown in Figure 1.11a. Here, the absorbance at a particular wavelength or range of wavelengths of a sample is measured as a function of time after excitation by a flash of light. In a typical experiment, both the light for excitation – pump – and the light for measuring the absorbance – probe – are generated by a pulsed laser. In each measurement, the absorbance of the probe pulse by the sample is recorded twice, the second time after a certain delay with respect to the pump pulse. Thus, in the first shot, the absorbance of the sample in the ground state is recorded. In contrast, the second time the probe pulse hits the fraction of molecules that has been promoted to an electronically excited state by means of the pump pulse. A difference absorption spectrum is then calculated. By changing the delay, a ΔOD profile as a function of time and wavelength is obtained (Figure 1.11b). This profile contains information on the dynamic processes occurring in the system under study. Specifically, the analysis of the *differential absorption spectra* (ΔOD *vs* wavelength) allows identification of the excited states or transient species formed upon excitation of the chromophore. On the other hand, the study of *decay profiles* (ΔOD *vs* time) provides information on the kinetics of photophysical or photochemical processes.

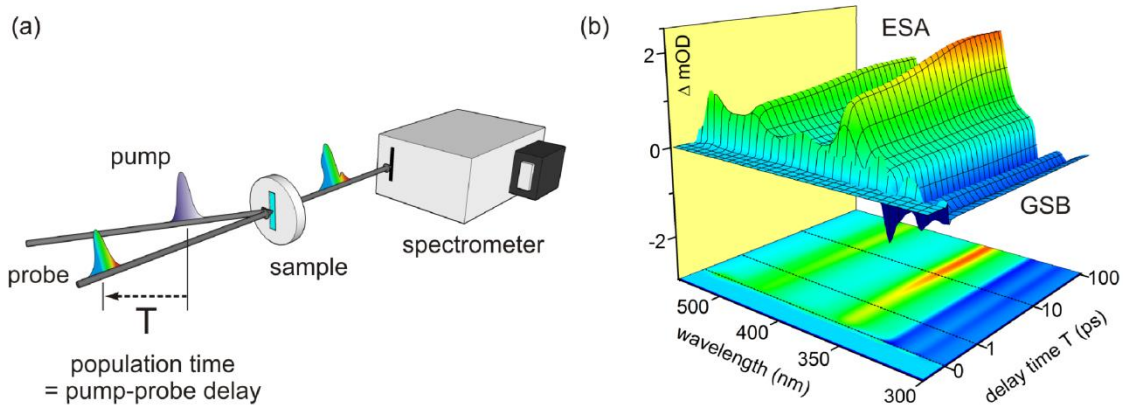

Figure. 1.11. (a) Schematic representation of transient absorption (pump-probe) spectroscopy. (b) UV-light-induced changes in optical density (ΔOD) of pyrene showing dynamics of the S_1 excited state absorption (ESA) and ground state bleach (GSB) contribution.

In general, the bands observed in a transient absorption spectrum arise from four kinds of contributions:

- *Ground-state bleach*: as a fraction of molecules has been promoted to the excited state through the action of the pump pulse, population of the ground state has decreased. As a consequence,

ground state absorption of the excited sample is lower than the non-excited. Hence, a negative signal in the ΔOD spectrum is observed. This signal appears in the region of the ground state absorption (it mirrors the UV-Vis absorption band).

- *Stimulated emission*: upon population of the first excited state, stimulated emission may take place when the second probe pulse passes through the sample. This process will occur only for optically allowed transitions, and its spectral profile generally reflects the fluorescence spectrum of the chromophore. The photon thus generated is emitted in the same direction as the one of the probe pulse, and both are detected. Hence, stimulated emission produces a negative ΔOD signal. Many chromophores present such a low Stokes shift that both ground state bleach and stimulated emission bands overlap and merge into one band.

- *Excited state absorption*: optically allowed transitions from the excited states (populated upon excitation with the pump pulse) to higher states might exist in certain wavelength regions. Absorption of the probe pulse at these regions is then observed as a positive band in the ΔOD spectrum.

- *Product absorption*: after excitation, photophysical or photochemical processes might give rise to long-lived states or transients, such as triplet, charge separation or isomerization states. These species appear as positive bands, and they are accompanied by bleaching at the bands corresponding to the excited states that lead to their formation. For example, as a triplet arises from intersystem crossing from a singlet excited state, bleaching will be observed in the bands of the latter.

1.2 Supramolecular ensembles of $Sc_3N@I_h$-C_{80} / C_{60} and Pcs

1.2.1 Synthesis and characterisation

A $Sc_3N@I_h$-C_{80} derivative **4** was prepared and connected to an electron-donating **1** or an electron-accepting **2** Zn(II) phthalocyanine (Pc) by metal-ligand, axial coordination of the pyridyl moiety of the fulleropyrrolidine to the zinc metal center in the Pc macrocycle (Figure 1.12). Similarly, a pyridyl-substituted C_{60} derivative **3** was synthetized and axially-coordinated to Zn(II)Pcs **1** and **2**.

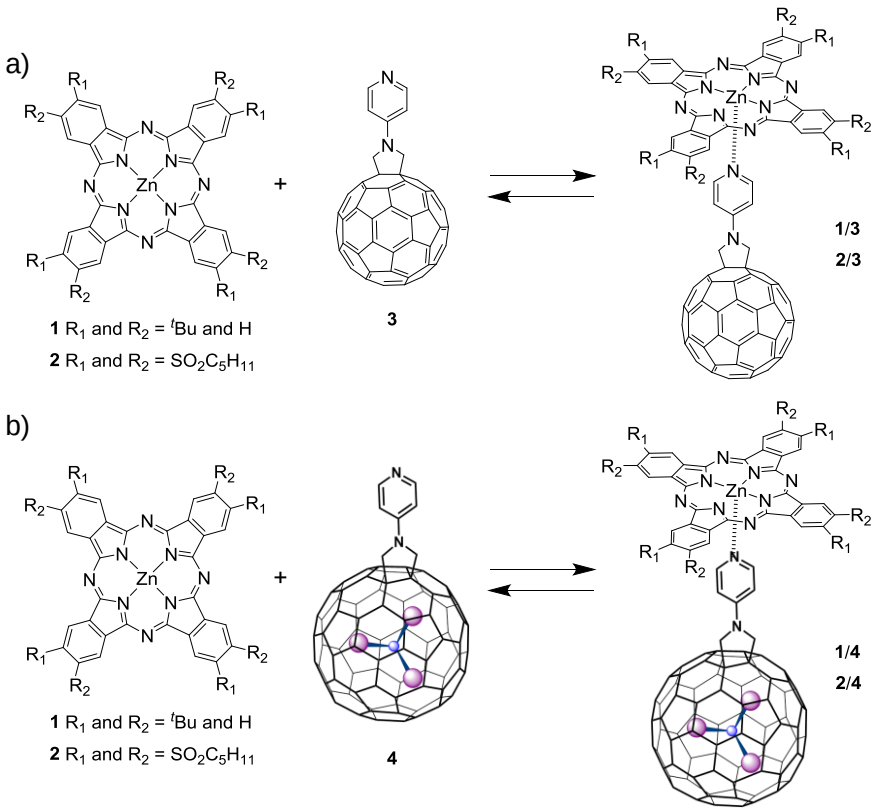

Figure 1.12. Metal-ligand, axial coordination of *N*-(*p*-pyridyl)-substituted fulleropyrrolidines **3** or 4 to Zn(II)Pcs **1** and **2** leading to supramolecular complexes **1**/**3** and **2**/**3** (a), and **1**/**4** and **2**/**4** (b).

Octakis-(pentylsulfonyl) Zn(II)Pc **2** was prepared in 54% yield by the cyclotetramerization reaction of 1,2-dicyano-4,5-bis(pentylsulfonyl)benzene **15** in a DMF/*o*-dichlorobenzene (*o*-DCB) mixture at 145 ^{o}C in the presence of zinc(II) acetate. Tetra-*tert*-butyl Zn(II)Pc **1** was purchased from Sigma Aldrich. On the other hand, pyridyl-substituted fulleropyrrolidines **3**[99] and **4** were prepared by the 1,3-dipolar cycloaddition of an azomethyne ylide, generated *in situ* by the reaction of *N*-

[99] F. T. Tat, Zh. Zhou, S. MacMahon, F. Song, A. L. Rheingold, L. Echegoyen, D. I. Schuster, S. R. Wilson. *J. Org. Chem.* **2004**, *69*, 4602 - 4606.

pyridylglycine and paraformaldehyde, to C_{60} and $Sc_3N@I_h$-C_{80}, respectively, in refluxing *o*-DCB under an argon atmosphere.

It is well-known that the 1,3-cycloaddition of the as-formed azomethyne ylide to C_{60} takes place exclusively at a [6,6]-carbon bond leading to the formation of an only product (when considering the mono-addition).**Ошибка! Закладка не определена.** In the case of $Sc_3N@I_h$-C_{80}, two possible regioisomers resulting from the azomethyne ylide addition at a [5,6]- or [6,6]-carbon bond of the EMF sphere are theoretically possible (Figure 1.13).

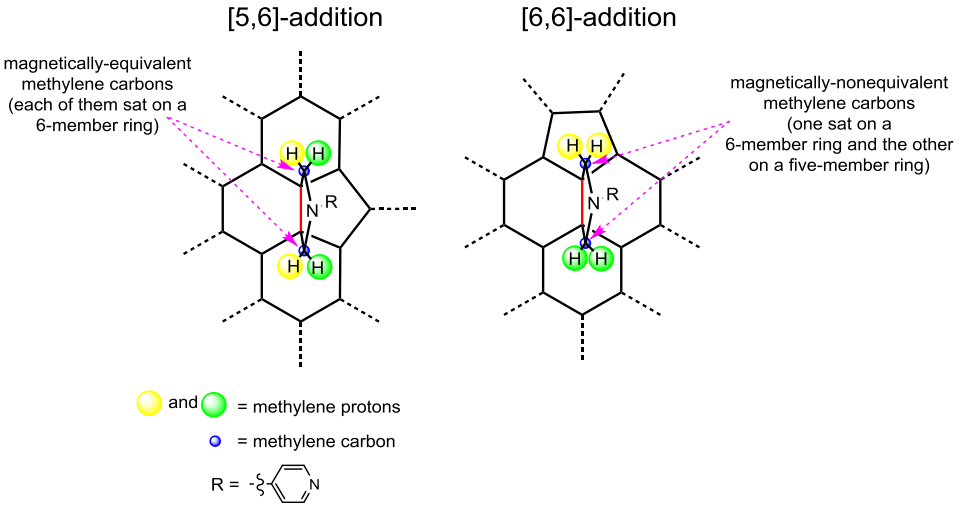

Figure 1.13: Schematic representation of the [5,6]- and [6,6]-addition patterns of the [5,6]- and [6,6]-*N*-(*p*-pyridyl)-3,4-$Sc_3N@Ih$-C_{80} fulleropyrrolidine isomers, respectively.

Thus, taking the above mentioned into account, the progress of the formation of $Sc_3N@I_h$-C_{80} derivative **4**, was monitored by HPLC. The concomitant formation of both a kinetic [6,6]- and a thermodynamic [5,6]- regioisomer was observed at the early stages of the Prato reaction (Figure 1.14). Thus, an aliquot of this reaction taken after 30 min. shows an 83/17 % ratio between the [6,6]-adduct and the [5,6]-adduct **4** (Figure 1.15a). Interestingly, the [6,6]-adduct was fully converted to the more stable [5,6]-adduct **4** after 12 h in refluxing *o*-DCB in an isomerization process involving the pirouetting of the pyrrolidine addend (Figure 1.15b). The ratio between the [5,6]- and the [6,6]-$Sc_3N@I_h$-C_{80} adducts was calculated by comparing the areas of their respective HPLC peaks assuming identical absorption coefficients for both fullerene isomers.

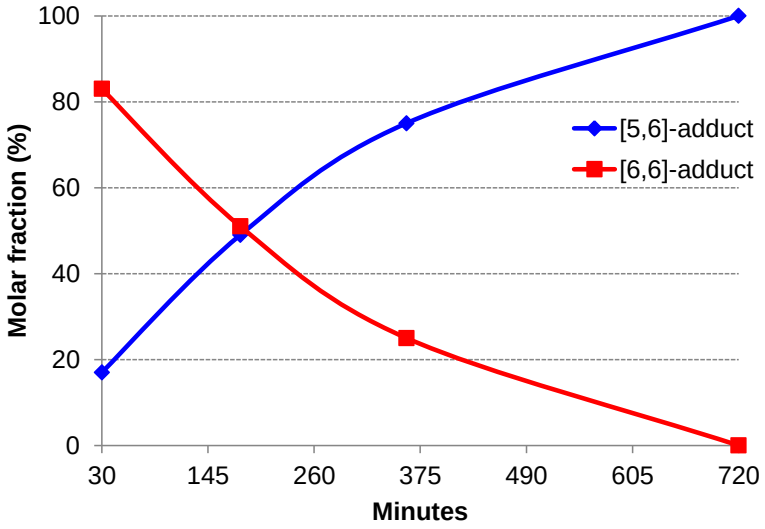

Figure 1.14. Molar fraction (as obtained by HPLC) of the kinetically-controlled [6,6]-adduct (blue rhombs) and the thermodynamically-controlled [5,6]-adduct (red squares) within the reaction mixture leading to $Sc_3N@I_h$-C_{80} derivative **4** as a function of the reaction time.

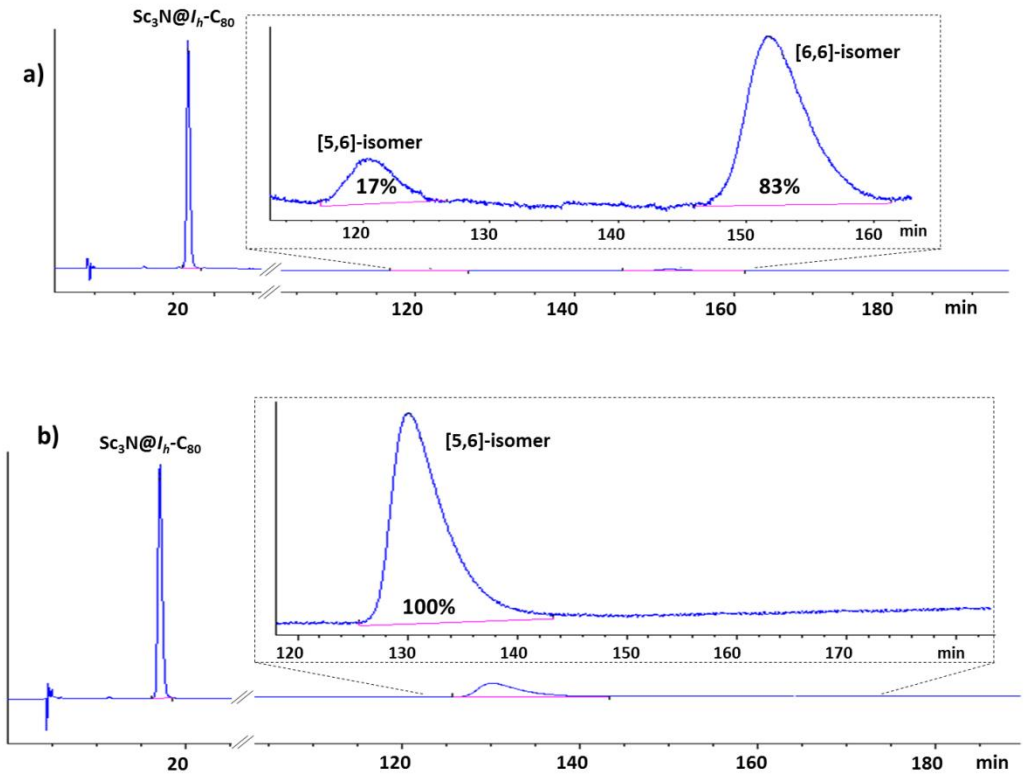

Figure 1.15. HPLC profiles of two aliquots taken from the reaction mixture leading to $Sc_3N@I_h$-C_{80} derivative **4** at 30 min (a) and 12 h (b).

The isolation of the [6,6]-adduct of $Sc_3N@I_h$-C_{80} derivative **4** was not pursued otherwise it would have implied to stop the reaction at early reaction times (*i.e.*, after 30 min) when the progress of

the Prato reaction is still extremely low in order to have the ratio between the [6,6] kinetic product and the [5,6] thermodynamic product at its maximum). Nevertheless, the formation of [6,6]-adduct was unequivocally determined by ^{1}H, COSY and HSQC (Figure 1.16) NMR experiments using a 25:75 mixture of the [6,6]-/[5,6]-$Sc_3N@I_h$-C_{80} isomers.

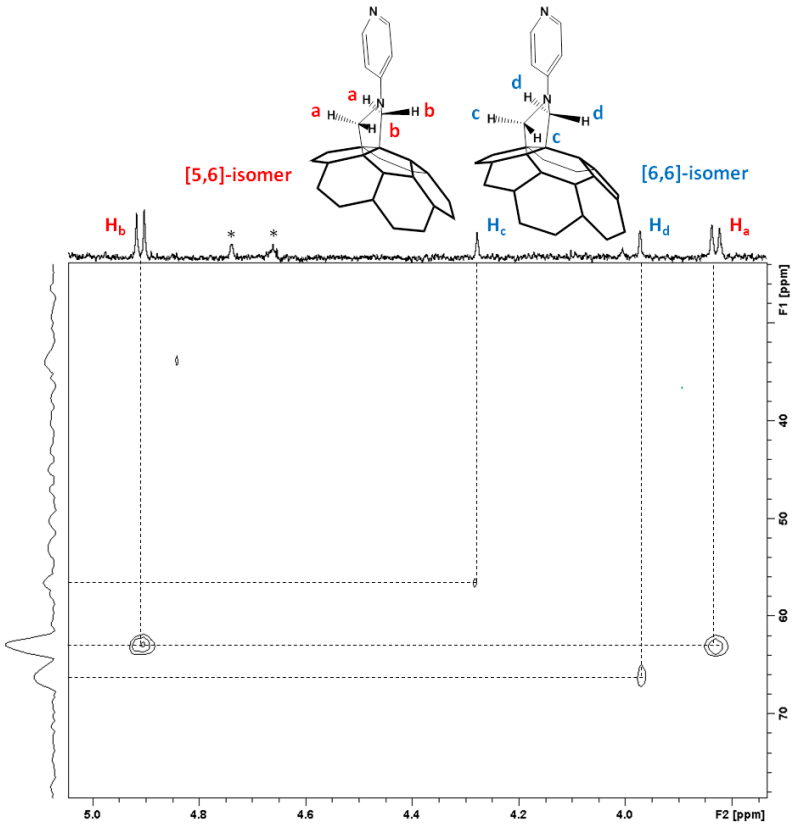

Figure 1.16*:* ^{1}H-^{13}C HSQC NMR spectrum (700 MHz, CS_2/CD_2Cl_2 (2:1), capillary) of a 25:75 mixture of [6,6]- and [5,6]-*N*-(*p*-pyridyl)-3,4-$Sc_3N@I_h$-C_{80} fulleropyrrolidine isomers.

To the best of our knowledge, this is the second time a [6,6]-adduct generated by 1,3-dipolar cycloaddition of an azomethyne ylide to $Sc_3N@I_h$-C_{80} fullerene has been observed and characterized.[100] Column chromatography of the reaction crude on silica gel was carried out after 12 h, resulting in the isolation of the [5,6]-isomer **4** in a 12% yield as the only mono-adduct, and negligible amounts of bisadducts.

The formation of pyridyl $Sc_3N@I_h$-C_{80} bisadducts, rarely observed in $Sc_3N@I_h$-C_{80} chemistry due to the poor reactivity of this EMF towards the 1,3-dipolar cycloaddition, was confirmed by a MALDI-

[100] T. Cai, C. Slebodnick, L. Xu, K. Harich, T. E. Glass, C. Chancellor, J. C. Fettinger, M. M. Olmstead, A. L. Balch, H. W. Gibson, H. C. Dorn. *J. Am. Chem. Soc.* **2006**, *128*, 6486 - 6492.

TOF peak at 1349.0 *m/z* corresponding to the $[C_{94}H_{16}N_5Sc_3]^-$ molecular ion. Considering the high thermal stability of the [6,6]-monoadduct, this observation agrees with recent results reported by Yamakoshi *et al.* [101]

$Sc_3N@I_h$-C_{80} derivative **4** was characterized by NMR and UV-vis spectroscopies, and mass spectrometry. The MALDI-TOF spectrum of derivative **4** shows a major peak at 1228.9 *m/z* corresponding to the molecular ion, together with some small peaks at lower intensities due to fragmentation.

The ^{1}H NMR spectrum of **4** in a CS_2/CD_2Cl_2 mixture shows two sets of doublets for both the pyridyl protons (8.44 and 6.91 ppm) and the two diastereotopic geminal protons of the pyrrolidine ring (4.98 and 3.82 ppm) (Figure 1.17). As expected for a [5,6]-addition to $Sc_3N@I_h$-C_{80}, these latter protons show a cross-peak correlation to the same pyrrolidine methylene carbon atom at 62.6 ppm as inferred by ^{1}H-^{13}C HSQC NMR (Figure 1.16). Whereas, in the case of the [6,6]-adduct, and differently from the [5,6]-adduct, the two methylene protons of the pyrrolidine ring at 4.28 and 3.97 ppm correlate to two magnetically-nonequivalent methylene carbon atoms of the pyrrolidine ring at 56.5 and 66.2 ppm, respectively (Figure 1.16).

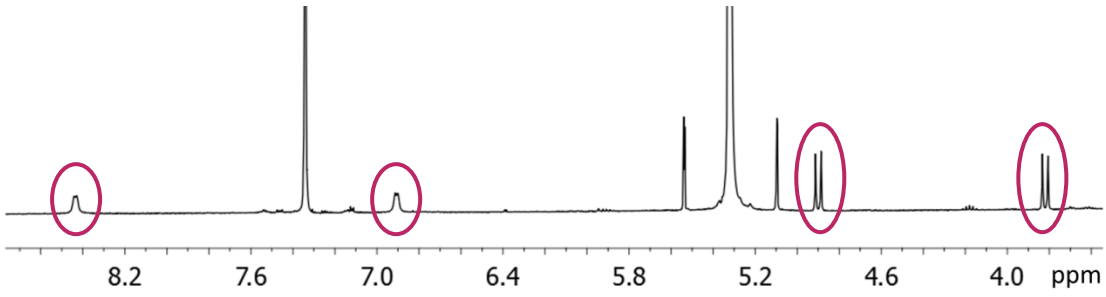

Figure 1.17. ^{1}H NMR spectrum (400 MHz, CS_2/CD_2Cl_2 2:1) of $Sc_3N@I_h$-C_{80} derivative **4.**

Moreover, the two methylene protons of the pyrrolidine ring of [5,6]-adduct show large chemical shift difference between themselves which arises from the different magnetic environments experienced by the two methylene protons (Figure 1.13) and the shielding of the α-methylene protons caused by the *trans*-lone pairs of the pyrrolidine nitrogen atom, according to Dorn *et al*.[102] Moreover, both geminal protons resonance is downfield shifted by almost 1 ppm with respect to the chemical shift of the same geminal pyrrolidine protons in *N*-methyl-3,4-[5,6]-

[101] S. Aroua, M. Garcia-Borras, M. F. Bölter, S. Osuna, Y. Yamakoshi. *J. Am. Chem. Soc.* **2015**, *137*, 58 - 61.
[102] T. Cai, Zh. Ge, E. B. Iezzi, T. E. Glass, K. Harich, H. W. Gibson, H. C. Dorn. *Chem. Commun*. **2005**, 3594 - 3596.

$Sc_3N@I_h$-C_{80} fulleropyrrolidine. This shift is probably due to a decreased ring current in fulleropyrrolidine **4** caused by the presence of the pyridyl unit.

1.2.2 Host-guest interactions

Supramolecular interactions in the ground state between Zn(II)Pcs **1** and **2**, on one hand, and fullerenes **3** and **4**, on the other hand, were investigated by visible/near-infrared absorption spectroscopy in chlorobenzene and in *o*-DCB.

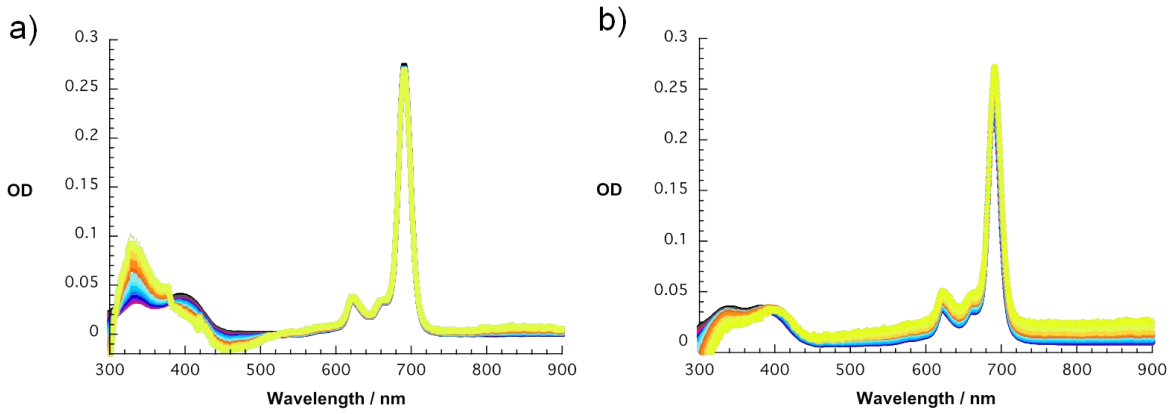

Figure 1.18. Steady-state absorption spectra of Zn(II)Pc **2** upon addition of C_{60} derivative **3** (a) $Sc_3N@I_h$-C_{80} derivative **4** (b) in chlorobenzene.

Absorption assays with solutions of Zn(II)Pcs **1** and **2** titrated with variable amounts of fullerene derivatives **3** and **4** were performed maintaining the total Zn(II)Pc concentration constant at 1.0 x 10^{-6} M. Absorption changes of the Soret- and Q-band were monitored at 350 and 680 nm for Zn(II)Pc **1** and at 360 and 690 nm for Zn(II)Pc **2**, respectively. However, only in the case of Zn(II)Pc **2** changes in its absorption features were observed upon addition of fullerene derivatives **3** and **4** (Figure 1.18). Well-defined isosbestic points at 307, 382, 522, and 706 nm for **2**/**3** and at 390 nm for **2**/**4** indicate the formation of Zn(II)Pc/fullerene supramolecular complexes and appreciable ground-state coupling. A 1:1 stoichiometry for both supramolecular complexes **2**/**3** and **2**/**4** was established by Job plot analysis (Figure 1.19).

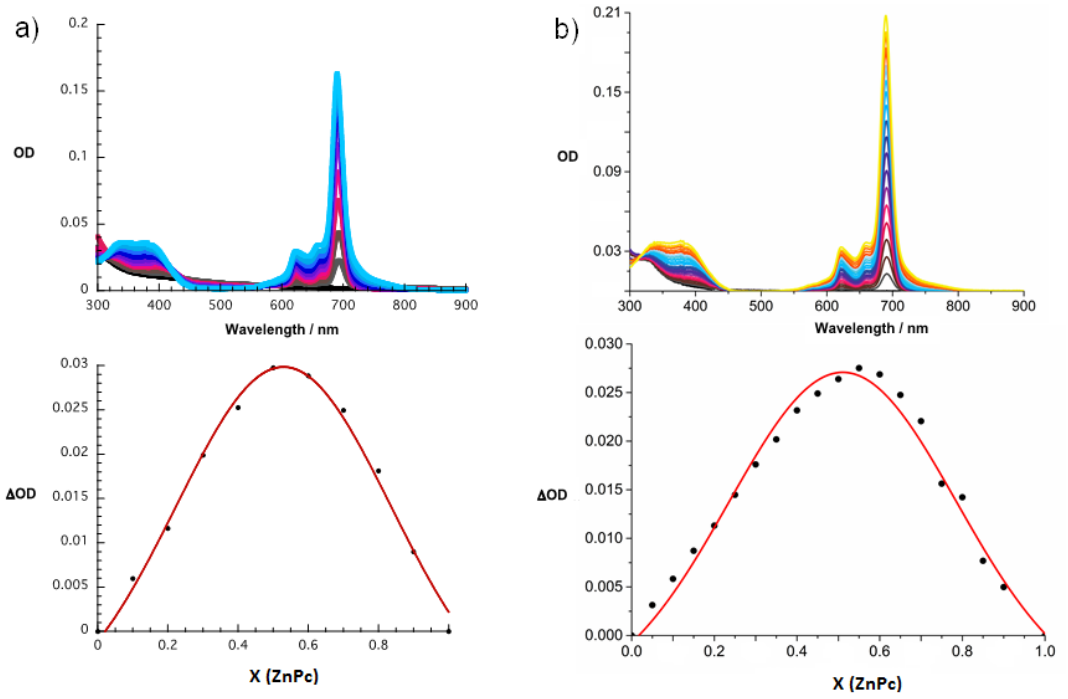

Figure 1.19. Job's plot analysis for the complexation of **2**/**4** (a) and **2**/**3** in (b) in chlorobenzene monitored at 694 nm and 693 nm, respectively.

1.2.3 Electrochemistry

The electrochemical properties of derivatives **1**–**4** and pristine $Sc_3N@I_h$-C_{80} fullerene were investigated by cyclic voltammetry (CV) and square wave voltammetry (SWV) in *o*-DCB containing *n*-Bu_4NPF_6 (0.05 M). Their corresponding redox potentials are summarized in Table 1. In the case of *N*-(*p*-pyridyl)-(3,4)-fulleropyrrolidines **3** and **4**, up to four reduction and two oxidation peaks are observed (Figure 1.20).

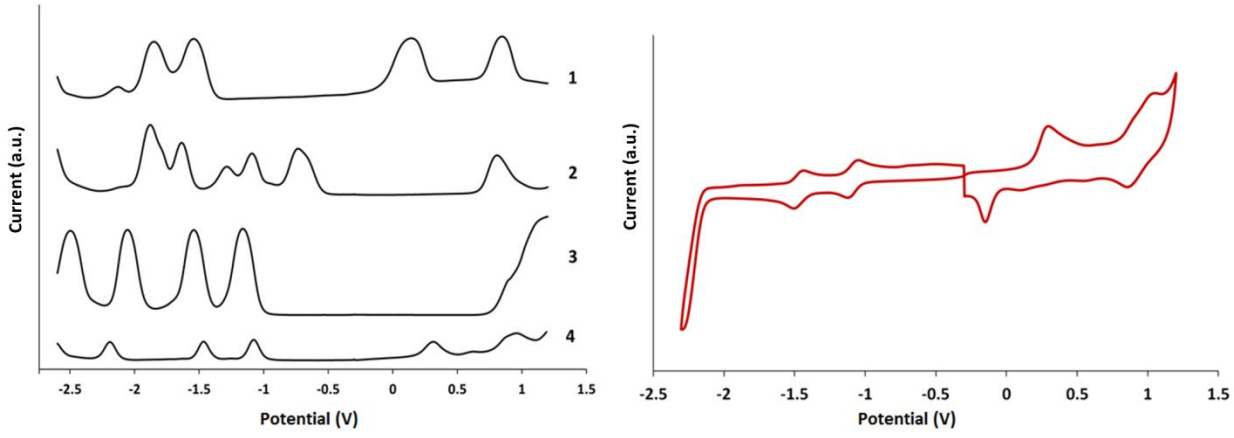

Figure 1.20: Square wave voltammogramms of derivatives **1**–**3** ($c \approx 10^{-3}$ M) and **4** ($c \approx 10^{-5}$ M) and cyclic voltammogram of **4** in *o*-DCB. Potential values are referred to $E_{(ox)1/2}$ of the Fc/Fc^+ redox couple.

More specifically, C_{60} derivative **3** displays four reversible reduction peaks at −1.12, −1.51, −2.02, −2.46 V, and two irreversible oxidation peaks at +0.89 and +1.09 V, in agreement with previous reports. Similarly, **4** reveals reversible reduction peaks at −1.04, −1.43, −2.15, −2.58 V, which are characteristic for [5,6]-$Sc_3N@I_h$-C_{80} fulleropyrrolidine adducts.[103] In the anodic scan, fulleropyrrolidine **4** displays two quasi-reversible oxidation processes at +0.29 and +0.94 V. The former is ascribed to the oxidation of the I_h-C_{80} cage. It is interesting to note that **4** shows both the first reduction and oxidation shifted toward more positive and negative potentials, respectively, with respect to C_{60} derivative **3** (80 and 600 mV, respectively) and pristine $Sc_3N@I_h$-C_{80} fullerene (220 and 300 mV). Considering the good electron-accepting and electron-donating features of derivative **4**, a possible electronic duality of this fulleropyrrolidine in PET reactions was anticipated. A study of the redox properties of Zn(II)Pcs **1** and **2** was also conducted. In this context, whereas derivative **1** shows two quasi-reversible reductions at −1.50 and −1.81 V and two quasi-reversible oxidations at +0.16 and +0.82 V, Zn(II)Pc **2**, featuring eight sulfonyl groups, shows seven anodically-shifted, irreversible reduction peaks at −0.65, −0.70, −1.06, −1.24, −1.61, −1.78, −1.85 V and one irreversible oxidation peak at +0.77 V (Figure 1.20).

Table 1. Redox potentials of derivatives **1**–**4** and pristine $Sc_3N@I_h$-C_{80} obtained by DPVs, E_p *vs* Fc/Fc^+, V.

Compound	E_p^4 (red)	E_p^3 (red)	E_p^2 (red)	E_p^1 (red)	E_p^1 (ox)	E_p^2 (ox)
1	---	---	−1.81	−1.50	+0.16	+0.82
2[a]	−1.24	−1.06	−0.70	−0.65	+0.77	---
3	−2.46	−2.02	−1.51	−1.12	+0.89	+1.09
4	−2.58	−2.15	−1.43	−1.04	+0.29	+0.94
$Sc_3N@I_h$-C_{80}	---	−2.37	−1.62	−1.26	+0.59	+1.09

[a] Only the first four reductions of octasulfonyl Zn(II)Pc **2** are reported.

Comparing the redox properties of Zn(II)Pcs **1** and **2** and $Sc_3N@I_h$-C_{80} derivative **4** it is possible to conclude that the EMF derivative is both easier to reduce and to oxidize than Zn(II)Pcs **1** and **2**, respectively. In other words, electron transfer from Zn(II)Pc **1** to **4** is theoretically feasible upon complexation. Moreover, a change of the supramolecular "partner" of derivative **4** from Zn(II)Pc

[103] C. M. Cardona, B. Elliott, L. Echegoyen, *J. Am. Chem. Soc*. **2006**, *128*, 6480 - 6485.

1 to **2** is expected to reverse the direction of the photoinduced charge transfer from the EMF to the electron-accepting, octasulfonyl Zn(II)Pc.

1.2.4 Photophysics

Insights into the excited-state interactions within the Zn(II)Pc-fullerene supramolecular ensembles were obtained from steady-state fluorescence measurements in chlorobenzene and *o*-DCB. The Zn(II)Pc-centered fluorescence of derivatives **1** and **2** with maxima at 685 and 694 nm, respectively, were monitored upon photoexcitation at either 610 or 630 nm. For both Zn(II)Pcs, an exponential decrease of their fluorescence is observed upon addition of derivative **4** until the endpoint of the titration is reached (*i.e.*, after the addition of 11 and 6 equivalents of **4** to Zn(II)Pcs **1** and **2**, respectively), a change associated with the quantitative formation of the Zn(II)Pc-fullerene hybrids (Figure 1.21a,b). A similar trend was observed upon replacing compound **4** for C_{60} derivative **3** (Figure 1.21c,d). The Zn(II)Pc fluorescence quantum yield in the supramolecular complexes **1**/**3**, **2**/**3**, **1**/**4**, and **2**/**4** is 0.02, 0.08, 0.11, and 0.06, respectively. These values are significantly lower than the 0.30 and 0.23 obtained for uncomplexed Zn(II)Pcs **1** and **2**, respectively. Taking into account a 1:1 complexation stoichiometry between the Zn(II)Pc and the pyridine-substituted fulleropyrrolidine, the Zn(II)Pc/fullerene binding constants for the four supramolecular complexes were calculated using the fluorescence titration data according to equation:

$$\frac{I}{I_0} = 1 - \frac{1}{2c_0}\left[\left(c_F + c_0 + \frac{1}{K_{ass}}\right) - \sqrt{\left(c_F + c_0 + \frac{1}{K_{ass}}\right)^2 - 4\,c_0\,c_F}\right]$$

where K_{ass} is the binding constant, c_0 is the concentration of Zn(II)Pc **1** or **2**, and c_F is the concentration of the fullerene derivatives **3** or **4**. Overall, the binding constants – log K_{ass} – were 6.1 ± 0.1 (**1**/**3**), 6.2 ± 0.2 (**2**/**3**), 5.5 ± 0.1 (**1**/**4**), and 5.9 ± 0.1 (**2**/**4**) in chlorobenzene (Figure 1.21a-d).

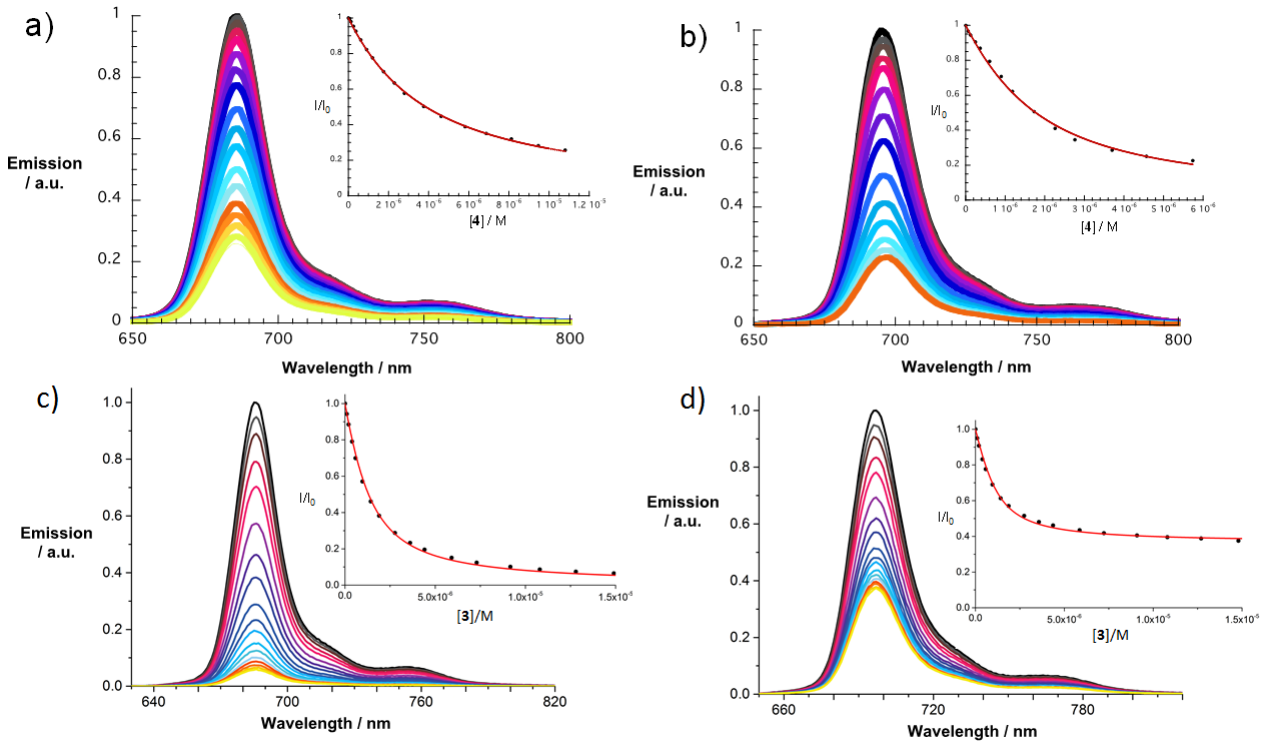

Figure 1.21. Steady-state fluorescence spectra of Zn(II)Pc **1** upon addition of $Sc_3N@I_h$-C_{80} derivative **4** (a) and C_{60} derivative **3** (c) and fluorescence spectra of Zn(II)Pc **2** upon addition of $Sc_3N@I_h$-C_{80} derivative **4** (b) and C_{60} derivative **3** (d) in chlorobenzene at room temperature. Inset: Plot of the change in fluorescence intensity of Zn(II)Pc as a ratio of I_F/I_0 *vs* the concentration of fullerene.

Spectroelectrochemical experiments were deemed necessary to assist in the interpretation of the excited-state spectral features of the four supramolecular complexes. To this end, the formation of the one-electron reduced form of electron-deficient Zn(II)Pc **2** and the one-electron oxidized forms of electron-rich Zn(II)Pc **1** and $Sc_3N@I_h$-C_{80} derivative **4** were monitored upon spectroelectrochemical reduction and oxidation, respectively, in deaerated *o*-DCB. The differential absorption spectrum of Zn(II)Pc **2** upon spectroelectrochemical reduction displays sets of maxima at 476, 605, 647, 769, 960, and 1100 nm, as well as minima at 426, 628, 665, and 695 nm (Figure 1.22a). On the other hand, spectroelectrochemistry of Zn(II)Pc **1** under oxidative conditions (Figure 1.22b) reveals differential absorption maxima at 442, 528, 728, and 836 nm as well as minima at 613, 650, and 680 nm. Similarly, spectroelectrochemical oxidation of $Sc_3N@I_h$-C_{80} derivative **4** shows differential absorption changes that include maxima at 715 and 880 nm and a broad tail that reaches out into the near-infrared region (Figure 1.23a). On the other hand, the absorption features of the reduced $Sc_3N@I_h$-C_{80} derivative **4** were obtained by pulse radiolytic studies which led to differential absorption spectra with a maximum at 830 nm and a

broad near-infrared tail (Figure 1.23b). The radical anion of the C_{60} fulleropyrrolidine derivative **3** reveals a characteristic maximum at 1010 nm upon pulse radiolytic reduction.[104]

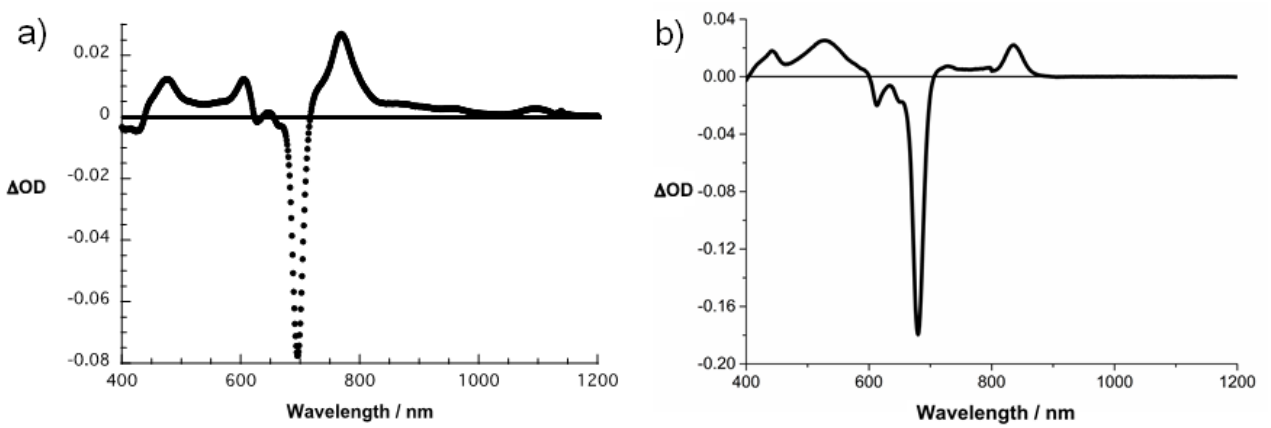

Figure 1.22. Differential absorption spectra obtained upon (a) electrochemical reduction of Zn(II)Pc **2** and (b) electrochemical oxidation of Zn(II)Pc **1** in argon-saturated *o*-DCB.

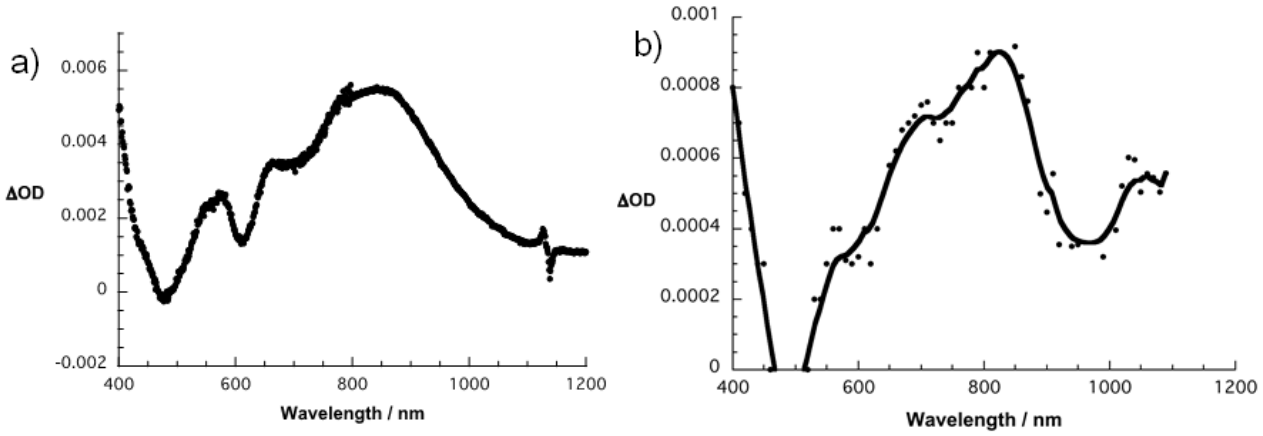

Figure 1.23. Differential absorption spectra obtained upon (a) electrochemical oxidation of $Sc_3N@I_h$-C_{80} derivative **4** in argon-saturated *o*-DCB and (b) pulse radiolytic reduction of $Sc_3N@I_h$-C_{80} derivative **4** in a deoxygenated solvents mixture containing toluene, 2-propanol and acetone with $(CH_3)_2$•COH and $(CH_3)_2$•CO^- radicals.

Insights about the formation, and decay, of photogenerated charge separated species for hybrids **1**/**3**, **2**/**3**, **1**/**4**, and **2**/**4** were derived from transient absorption studies following femtosecond and nanosecond excitation. Compounds **1**–**4** were individually investigated.

Upon excitation of C_{60} derivative **3** with a 387 nm laser pulse (Figure 1.24a,c), differential absorption spectra arise, which are attributed to the population of the singlet excited state of C_{60}

[104] D. M. Guldi, M. Maggini. *Gazz. Chim. Ital.* **1997**, *127*, 779 - 785.

with characteristic absorption maxima in the visible at 520 and in the near-infrared between 800 and 1200 nm. The C_{60} singlet excited state features undergo quantitative intersystem crossing with a lifetime of 1.5 ± 0.1 ns to afford its triplet manifold with a characteristic maximum at 700 nm and a lifetime up to 20 µs in oxygen-free chlorobenzene. Photoexcitation of a chlorobenzene solution of $Sc_3N@I_h$-C_{80} derivative **4** with a 387 nm laser pulse (Figure 1.24b,d) leads to differential absorption changes that include strong transient maxima at 480 and 1025 nm. The singlet excited state features of fullerene **4** decay fast with a lifetime of 25 ± 5 ps. The presence of the C_{80}-encapsulated Sc_3N cluster in **4** is likely to be responsible for the fast singlet excited state decay to yield the triplet manifold.

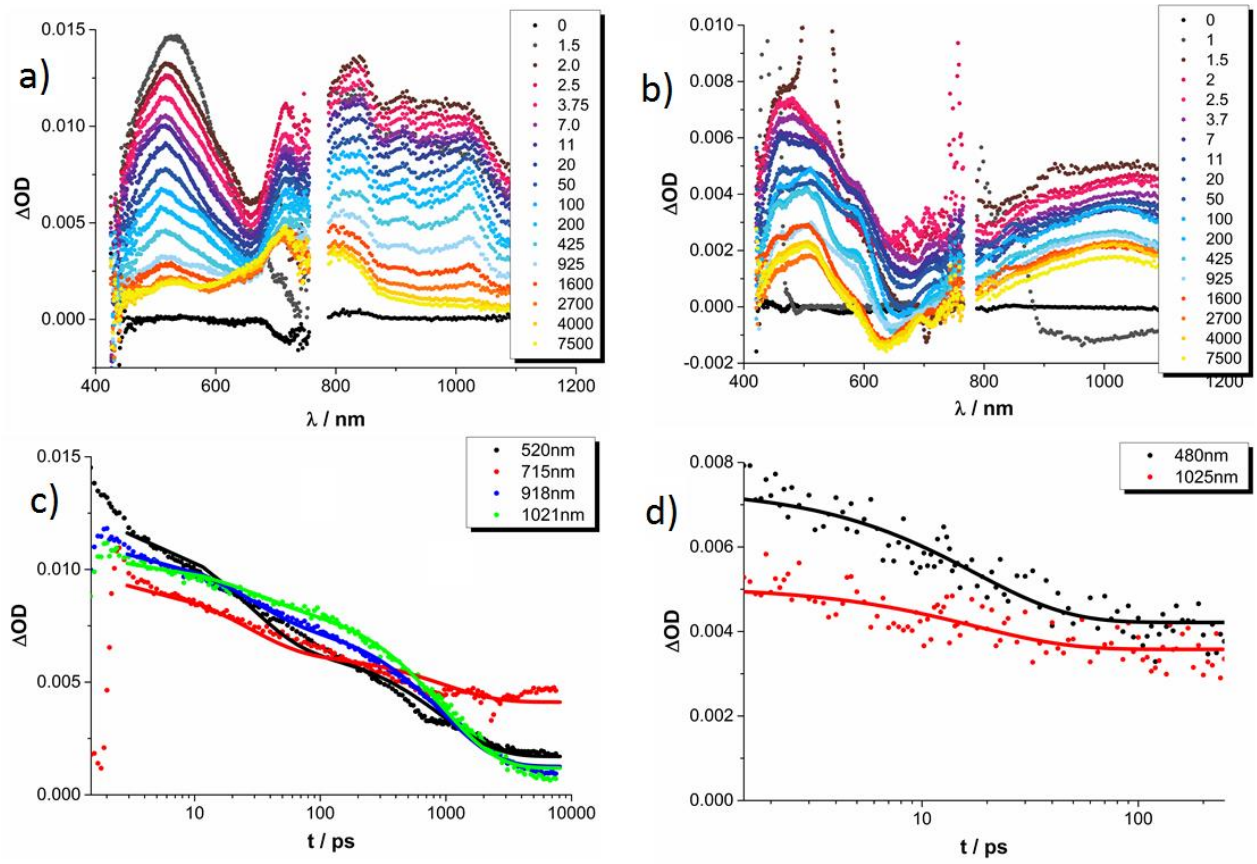

Figure 1.24. Differential absorption spectra obtained upon femtosecond flash photolysis (387 nm) of C_{60} derivative **3** (c = 1 x 10^{-5} M) (a) and $Sc_3N@I_h$-C_{80} derivative **4** (c = 1 x 10^{-5} M) (b) in argon-saturated chlorobenzene with several time delays between 0 and 7500 ps at room temperature. Time-absorption profiles of the spectra shown above monitoring intrinsic intersystem crossing of **3** (1.5 ± 0.1 ns) (c) and **4** (25 ± 5 ps) (d).

Turning to Zn(II)Pcs, derivative **1** (Figure 1.25a,c) reveals differential absorption changes that include transient maxima at 483, 598, 638, 739, and 825 nm as well as transient minima at 615

and 683 nm upon excitation at 676 nm. These transients correlate with the singlet excited state of Zn(II)Pc **1** and have an intrinsic lifetime of 2.8 ± 0.1 ns in chlorobenzene. In **1**, the singlet-singlet transitions undergo intersystem crossing to the corresponding triplet excited state with a transient maximum at 500 nm and transient minima at 615, 652, and 682 nm. For the chlorobenzene solution of sulfonyl-substituted Zn(II)Pc **2**, it was necessary to add small amounts of pyridine to circumvent Zn(II)Pc aggregation, which otherwise dominates the outcome of the femtosecond transient absorption experiments even at Zn(II)Pc concentrations as low as 1 x 10^{-5} M. The differential absorption spectrum of **2** reveals transient maxima at 521, 647, and 850 nm as well as transient minima at 624 and 695 nm upon 676 nm laser irradiation (Figure 1.25b,d). Similar to Zn(II)Pc **1**, we ascribe these differential absorption changes to the formation of the singlet excited state of **2**, which undergoes intersystem crossing with a time constant of 2.8 ± 0.1 ns to form the corresponding triplet excited state. The triplet excited state displays characteristic transient absorption maxima at 440 and 810 nm and minima at 624, 664, and 694 nm.

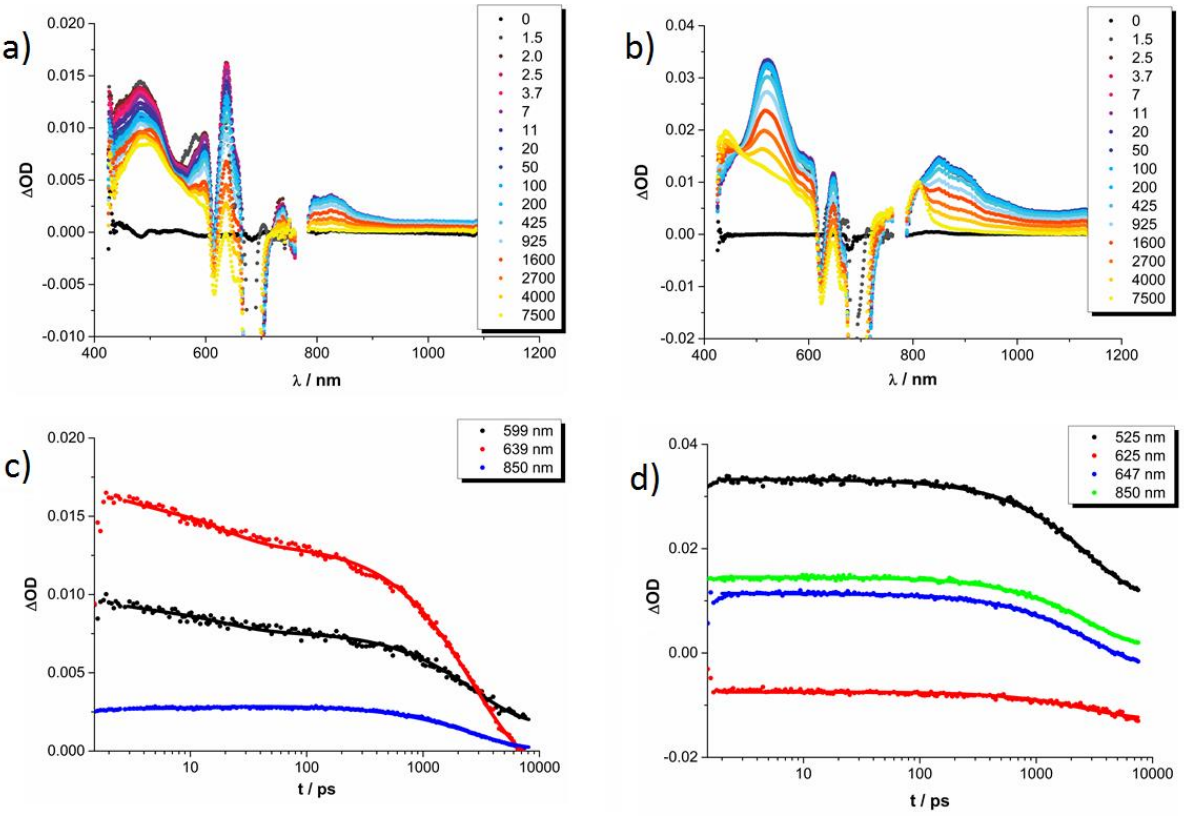

Figure 1.25. Differential absorption spectra obtained upon femtosecond flash photolysis (676 nm) of Zn(II)Pc **1** (c = 1 x 10^{-5} M) (a) and Zn(II)Pc **2** (c = 1 x 10^{-5} M) (b) in argon-saturated chlorobenzene. Time-absorption profiles of the spectra shown above monitoring intrinsic intersystem crossing of Zn(II)Pc **1** (2.8 ± 0.1 ns) (c) and Zn(II)Pc **2** (2.8 ± 0.1 ns) (d).

Next, transient absorption analysis of supramolecular complexes **1**/**3**, **2**/**3**, **1**/**4**, and **2**/**4** was carried out. Differential absorption spectra of hybrid **1**/**3** include transient maxima at 495, 600, 640, and 800 nm and minima at 616 and 680 nm which were observed directly after photoexcitation with 676 nm laser pulses (Figures 1.26a,c). These transient features relate to the singlet excited state features of Zn(II)Pc **1**. In contrast to **1**, in supramolecular ensemble **1**/**3** these features decay within 29 ± 1 ps and give rise to new transient maxima at 540, 720, 850, and 1024 nm as well as to transient minima at 617 and 680 nm. These features, especially those in the near-infrared, are reliable fingerprints of the one-electron oxidized Zn(II)Pc **1** and the one-electron reduced fullerene **3** species, that is, $\mathbf{1}^{\bullet+}/\mathbf{3}^{\bullet-}$. From a multiwavelength kinetic analysis, a lifetime of 9.0 ± 0.5 ns in chlorobenzene was deduced for the $\mathbf{1}^{\bullet+}/\mathbf{3}^{\bullet-}$ radical ion pair state. Notably, the product of charge recombination is the triplet excited state of electron-rich Zn(II)Pc **1**.

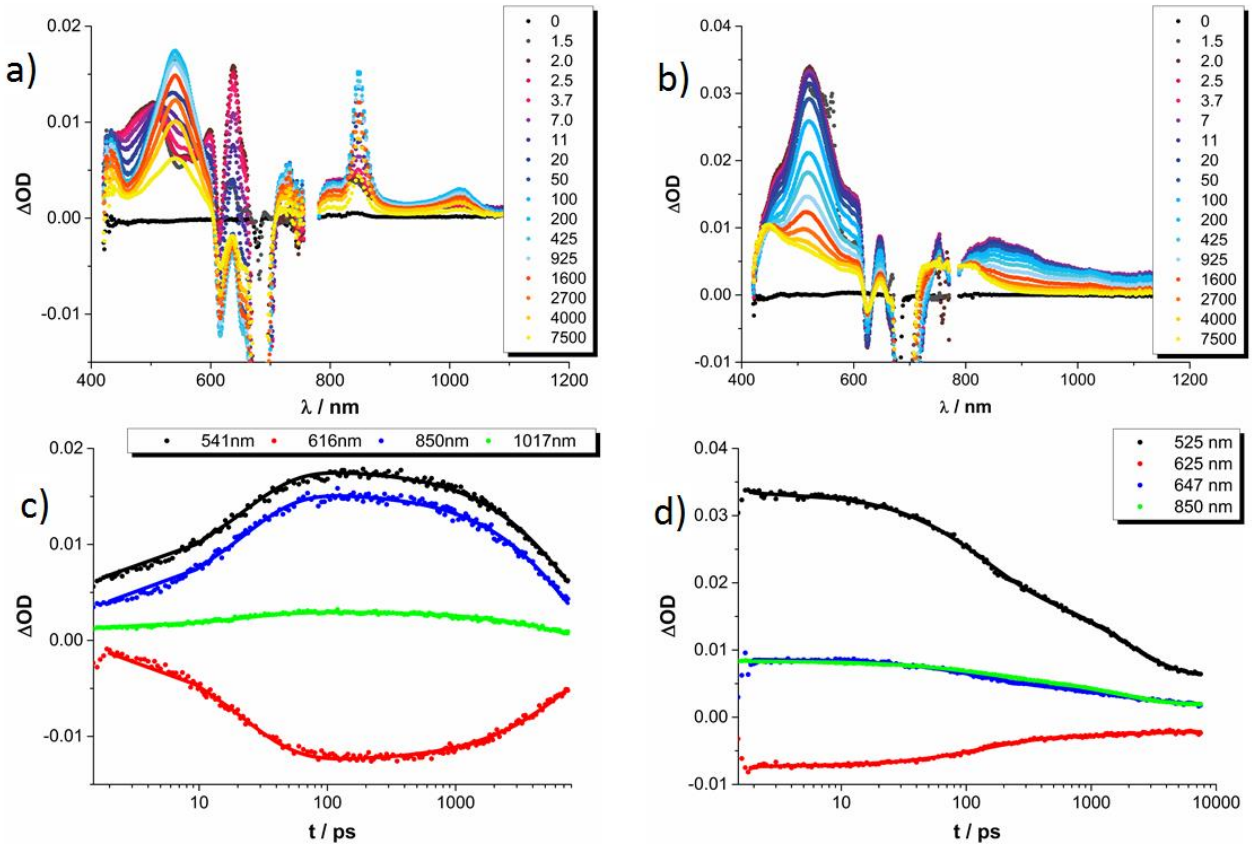

Figure 1.26. Differential absorption spectra obtained upon femtosecond flash photolysis (676 nm) of **1**/**3** (a) and **2**/**3** (b) (fullerene/Zn(II)Pc = 10:1) in argon-saturated chlorobenzene. Time-absorption profiles of the spectra shown above monitoring the charge separation (29 ± 1 ps) and the charge recombination (9.0 ± 0.5 ns) for **1**/**3** (c) and intrinsic Zn(II)Pc intersystem crossing (2.8 ± 0.1 ns) for **2**/**3**.

Photoexcitation of supramolecular hybrid **2**/**3** with 676 nm laser pulses leads to the exclusive population of the singlet excited state of electron-deficient Zn(II)Pc **2** with transient maxima at 521, 647, and 850 nm and minima at 624 and 695 nm (Figure 1.26b,d), in agreement with the transient absorption experiments of **2**. These latter transitions then decay to the corresponding triplet excited state features of **2** with maxima at 445, 647, and 810 nm and minima at 624, 664, and 693, similar to what was observed for uncomplexed Zn(II)Pc **2**. In the case of supramolecular complex **2**/**3** no evidence for any PET event is observed. An electron transfer from the singlet excited state of Zn(II)Pc **2**, with an energy of 1.79 eV, to C_{60} derivative **3** is ruled out on thermodynamic grounds due to the high radical ion pair state energy for $\mathbf{2}^{\bullet+}/\mathbf{3}^{\bullet-}$. From electrochemical experiments performed with the individual components **2** and **3**, a $\mathbf{2}^{\bullet+}/\mathbf{3}^{\bullet-}$ radical ion pair state energy of 1.89 eV was calculated. Notably, axial coordination of pyridyl derivatives to Zn(II)Pc **2** is known to shift the oxidation potential by ~0.2 eV.[105] In other words, electron transfer from the electron-accepting Zn(II)Pc **2** singlet excited state to the fullerene derivative **3** is energetically unfavorable.

Laser irradiation of D-A hybrid **1**/**4** at 676 nm leads to transient absorption spectra with maxima at 500, 600, 640, 739, and 825 nm and minima at 615 and 683 nm (Figure 1.27a-d). Overall, these features confirm the successful formation of the singlet excited state species of Zn(II)Pc **1**, which is located at 1.82 eV. With a lifetime of 6.8 ± 0.5 ps, these features decay giving rise to new transients with maxima at 440, 512, and 850 nm and minima at 615 and 683 nm. This result is indicative of the formation of the one-electron oxidized Zn(II)Pc **1**, in agreement with the spectroelectrochemical oxidation features of Zn(II)Pc **1** (Figure 1.25a,c). On the other hand, evidence of the formation of $\mathbf{4}^{\bullet-}$ is based on the broad near-infrared tail observed.[**Ошибка! Закладка не определена.**] Overall, these changes in transient absorptions of **1**/**4** can be assigned to a charge transfer from the electron-donating Zn(II)Pc **1** to the electron-accepting $Sc_3N@I_h$-C_{80} **4** to form the $\mathbf{1}^{\bullet+}/\mathbf{4}^{\bullet-}$ radical ion pair state with energy of 1.20 eV. The superimposed features of $\mathbf{1}^{\bullet+}$ and $\mathbf{4}^{\bullet-}$ are in sound agreement with those recorded for the $\mathbf{1}^{\bullet+}/\mathbf{4}^{\bullet-}$ radical ion pair (Figure 1.27d). The latter radical ion pair state consequently undergoes charge recombination within 180 ± 10 ps to the singlet ground state of Zn(II)Pc **1** (Figure 1.28a). At the conclusion of the 8 ns time scale, the triplet excited state of Zn(II)Pc is detected, whose formation is connected to a minor extend

[105] K. M. Kadish, K. M. Smith, R. Guilard. *The Porphyrin Handbook*, Academic Press, Amsterdam, **2003**.

to charge recombination and to a major extend to regular intersystem crossing in uncomplexed Zn(II)Pc **1**.

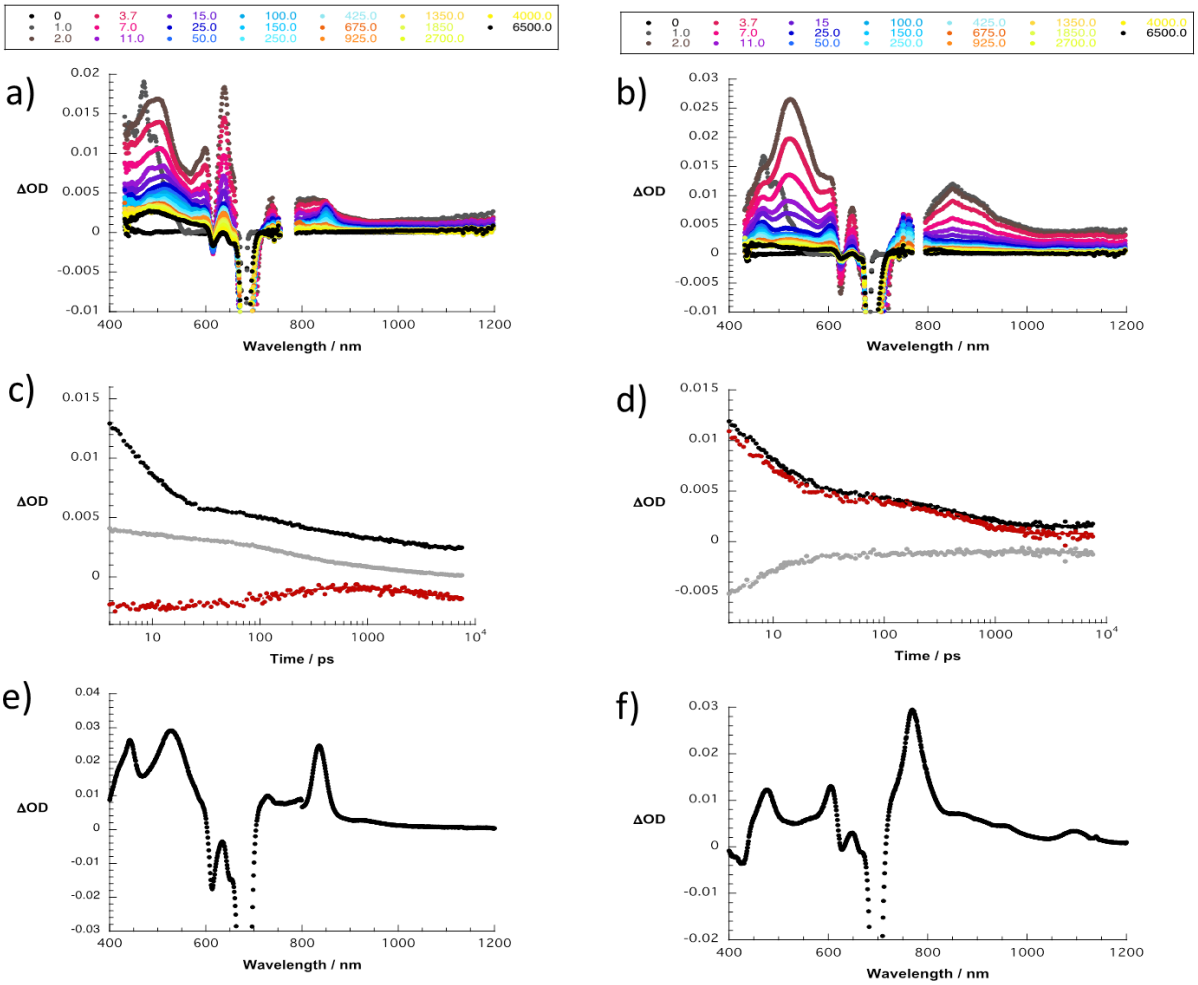

Figure 1.27. Differential absorption spectra obtained upon femtosecond flash photolysis (676 nm) of supramolecular ensemble **1**/**4** (a) and **2**/**4** (b) ([Zn(II)Pc] = 1 x 10^{-5} M, fullerene / Zn(II)Pc = 10:1) in argon-saturated chlorobenzene. Time-absorption profiles of the spectra shown above at 515 nm (black), 615 nm (red), and 850 nm (grey) monitoring the charge separation (6.8 ± 0.5 ps) and the charge recombination (180 ± 10 ps) for **1**/**4** (c) and those at 465 nm (black), 604 nm (red), and 624 nm (grey) monitoring the charge separation (6.6 ± 0.1 ps) and the charge recombination (505 ± 10) processes for **2**/**4** (d). Superimposed differential absorption spectra of $\mathbf{1}^{\bullet+}$ and $\mathbf{4}^{\bullet-}$ (e), and $\mathbf{2}^{\bullet-}$ and $\mathbf{4}^{\bullet+}$ (f).

Finally, supramolecular hybrid **2**/**4** was probed and the differential absorption spectra were recorded (Figure 1.27b-f). Upon 676 nm laser excitation, transient absorption maxima at 522, 647, and 850 nm and minima at 624 and 695 nm corroborate the population of the singlet excited state of Zn(II)Pc **2**. This singlet excited state decays rapidly with a lifetime of 6.6 ± 0.1 ps, followed by the formation of new maxima at 465, 603, 646, 760, and 1060 nm and minima at 625

and 695 nm. From a comparison of these transient spectra with the spectrum obtained from the spectroelectrochemical reduction of **2** (Figure 1.22a), it is possible to assign the visible bands in the former spectra to the one-electron reduced form of Zn(II)Pc **2**, namely $\mathbf{2}^{\bullet-}$. Due to the ratio of approximately 56:1 in terms of extinction coefficients between the 760 nm maximum of $\mathbf{2}^{\bullet-}$ and the 880 nm maximum of $\mathbf{4}^{\bullet+}$, it was not possible, with our instrumental setup, to observe any meaningful contribution from the radical cation signature of $Sc_3N@I_h$-C_{80} in the differential absorption spectra. On the other hand, the features of the $Sc_3N@I_h$-C_{80} derivative **4** radical cation species, namely $\mathbf{4}^{\bullet+}$, could be identified by comparison with the spectrum obtained upon spectroelectrochemical oxidation of **4** (Figure 1.23a). In accordance with these results, and differently from ensemble **1**/**4**, a PET process from the electron-donating $Sc_3N@I_h$-C_{80} **4** to the photoexcited electron-accepting Zn(II)Pc **2** must be occurring to yield the $\mathbf{2}^{\bullet-}/\mathbf{4}^{\bullet+}$ radical ion pair state at 0.94 eV instead of the energetically unfavorable uphill $\mathbf{2}^{\bullet+}/\mathbf{4}^{\bullet-}$ species at 1.81 eV. Notably, the superimposed features of $\mathbf{2}^{\bullet-}$ and $\mathbf{4}^{\bullet+}$ are in sound agreement with those recorded for the $\mathbf{2}^{\bullet-}/\mathbf{4}^{\bullet+}$ radical ion pair (Figure 1.27f). The photogenerated $\mathbf{2}^{\bullet-}/\mathbf{4}^{\bullet+}$ charge separated state, which has a lifetime of 505 ± 10 ps in chlorobenzene, then recombines to give rise to the ground state of Zn(II)Pc **2** (Figure 1.28b).

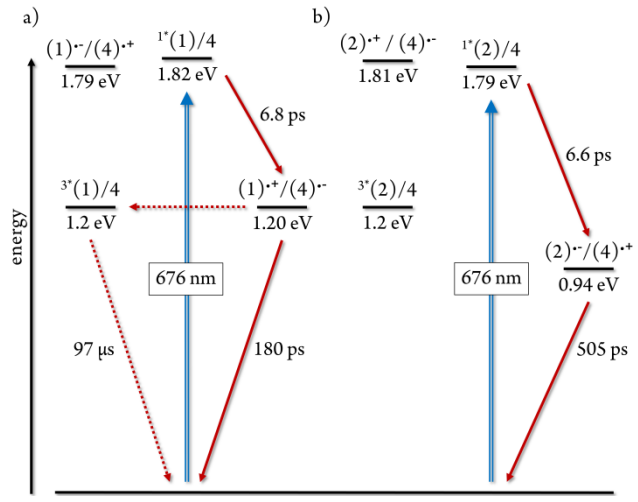

Figure 1.28. Energy level diagrams for supramolecular ensembles **1**/**4** (a) and **2**/**4** (b) in chlorobenzene reflecting major (solid arrows) and minor (dashed arrows) energetic pathways of charge separation and charge recombination. The energy of the $\mathbf{1}^{\bullet+}/\mathbf{4}^{\bullet-}$ and $\mathbf{2}^{\bullet-}/\mathbf{4}^{\bullet+}$ radical ion pairs were derived by the simple addition of the corresponding redox potentials, that is oxidation of **1** / reduction of **4**, and reduction of **2** / oxidation of **4**.

In the case of ensemble **1**/**4**, a competition between radical ion pair deactivation to the singlet ground state as the main pathway, on one hand, and to the triplet excited state of the Zn(II)Pc as the minor pathway, on the other hand, without thermodynamic driving force could also possibly occur. The Zn(II)Pc triplet excited state features observed in the transient absorption measurements of **2**/**4** likely result from uncomplexed Zn(II)Pc **2** in solution.

From the time-resolved absorption assays, it is possible to conclude that Pc-to-fullerene and fullerene-to-Pc electron transfer dictates the excited state deactivation in supramolecular complexes **1**/**3** and **1**/**4** (Pc-to-fullerene), and **2**/**4** (fullerene-to-Pc), while in **2**/**3** no evidence for an electron transfer was observed. Moreover, in Zn(II)Pc/$Sc_3N@I_h$-C_{80} hybrids **1**/**4** and **2**/**4**, charge separation is accelerated by an order of magnitude relative to the C_{60} hybrid **1**/**3** – 1.5 x 10^{11} s^{-1} *vs* 3.4 x 10^{10} s^{-1}. Nevertheless, the Zn(II)Pc/C_{60} hybrid **1**/**3** outperforms both Zn(II)Pc/$Sc_3N@I_h$-C_{80} hybrids **1**/**4** and **2**/**4** in terms of charge separated state lifetime by one order of magnitude as inferred by analyses of the transient absorption measurements which afforded charge recombination rate constants of 1.1 x 10^8, 5.6 x 10^9, and 2.0 x 10^9 s^{-1} for complexes **1**/**3**, **1**/**4**, and **2**/**4**, respectively.

1.3 Conjugates of electron accepting SubPcs with fullerenes $La_2@C_{80}$ and C_{60}

1.3.1 Synthesis and characterisation

(Perfluoro) SubPc **13** and hexa(pentylsulfonyl) SubPc **14** bearing chlorine atom at axial position were synthesized by cyclotrimerization reaction[106] of the corresponding perfluorophthalonitriles **15** or hexa(pentylsulfonyl) phthalonitrile **16** in the presence of 1M solution of boron trichloride in *p*-xylene at reflux under argon atmosphere (Scheme 1.1). Further modification of SubPcs **13** and **14** at axial position could become a non trivial task. Indeed, electron-deficient chloro-(alkylsulfonyl) SubPcs are known as the least reactive SubPc in terms of axial substitution of the chlorine atoms.[107] In fact, examples of conjugates involving (alkylsulfonyl) SubPcs are limited to a single case, namely a hexa(octylsulfonyl) SubPcs-ferrocene conjugate reported by our group.[108] This issue has been solved in this work with the help of the procedure recently developed in our group.[109]

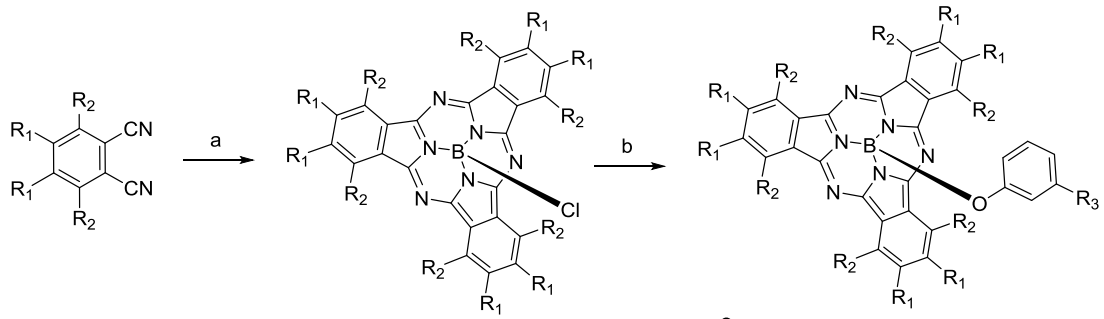

15 R_1, R_2 = F,
16 $R_1 = SO_2C_5H_{11}$, R_2 = H

13 R_1, R_2 = F,
14 $R_1 = SO_2C_5H_{11}$, R_2 = H

9 R_1, R_2 = F, R_3 = COH
10 $R_1 = SO_2C_5H_{11}$, R_2 = H, R_3 = COH
11 R_1, R_2 = F, R_3 = H
12 $R_1 = SO_2C_5H_{11}$, R_2 = H, R_3 = H

Scheme 1.1. Synthesis of SubPc conjugates **9-13**. Conditions: a) 1M BCl_3 in *p*-xylene, reflux; b) AgOTf, 3-hydroxybenzaldexyde/phenol, toluene.

[106] C. G. Claessens, T. Torres, *Angew. Chem. Int. Ed.* **2002**, *41*, 2561 - 2565.
[107] J. Guilleme, L. Martinez-Fernandez, D. Gonzalez-Rodriguez, I. Corral, M. Yanez, T. Torres. *J. Am. Chem. Soc.*, **2014**, 136, 14289 - 14298.
[108] D. Gonzalez-Rodriguez, T. Torres, M. M. Olgmstead, J. Rivera, M. A. Herranz, L. Echegoyen, C. A. Castellanos, D. M. Guldi, *J. Am. Chem. Soc.*, **2006**, *128*, 10680 - 10681.
[109] J. Guilleme, D. Gonzalez-Rodriguez, T. Torres, *Angew. Chem. Int. Ed.* **2011**, *50*, 3506 - 3509.

In the present work, (perfluoro) and hexa(pentylsulfonyl) derivatives of (formylphenoxy) substituted SubPcs precursors **9**[110] and **10** as well as (phenoxy)-substituted reference SubPcs **11**[111] and **12** were synthesized through triflate-substituted intermediates, generated by treating (chloro) SubPcs **13** and **14** with AgOTf (Scheme 1.1). Presence of six electron-withdrawing pentylsulfonyl groups on the periphery of SubPc **10** hampers nucleophilic substitution of the axial group at the boron atom even stronger than twelve fluorine substituents of SubPc **9**, causing the need of using of high temperatures. This is the reason why the corresponding triflate-containing SubPc intermediates were subjected to *in situ* substitution of triflyl group by 3-hydroxybenzaldehyde or phenol in toluene at 100 ^{o}C. Worthy to note, that the reaction proceeds as well at lower temperatures during longer times, giving lower yields of the product of nucleophilic substitution and higher amount of side- and decomposition products.

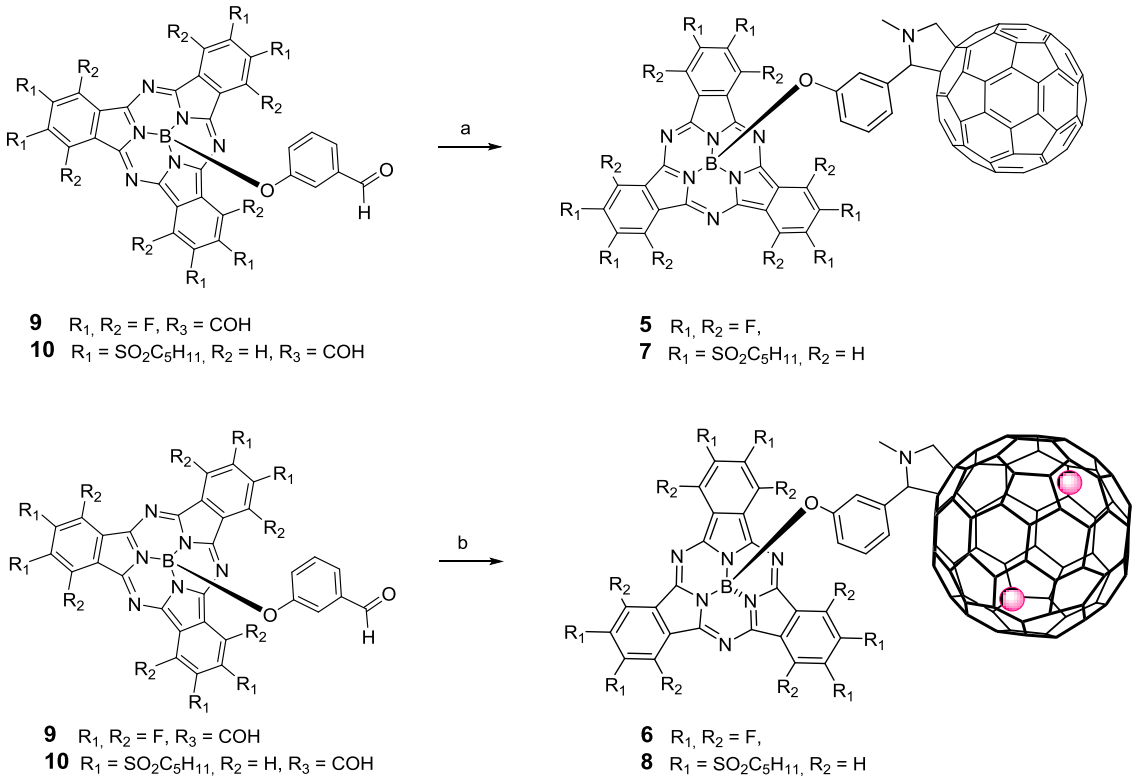

9 R_1, R_2 = F, R_3 = COH
10 R_1 = $SO_2C_5H_{11}$, R_2 = H, R_3 = COH

5 R_1, R_2 = F,
7 R_1 = $SO_2C_5H_{11}$, R_2 = H

9 R_1, R_2 = F, R_3 = COH
10 R_1 = $SO_2C_5H_{11}$, R_2 = H, R_3 = COH

6 R_1, R_2 = F,
8 R_1 = $SO_2C_5H_{11}$, R_2 = H

Scheme 2.2. Synthesis of SubPc-C_{60} conjugates **1a-b**. Conditions: a,b) N-methylglycine, C_{60}, toluene or *o*-DCB, reflux.

[110] SubPc **9** was synthesized previously in our group using a different protocol: a) M. Ince, A. Medina, J. H. Yum, A. Yella, C. G. Claessens, M. V. Martinez-Diaz, M. Graetzel, M. K. Nazeeruddin, T. Torres, *Chem. Eur. J.* **2014**, 20, 2016 - 2021. b) C. G. Claessens, D. Gonzalez-Rodriguez, B. del Rey, T. Torres, G. Mark, H. P. Schuchmann, C. von Sonntag, J. G. MacDonald, R. S. Nohr, *Eur. J. Org. Chem.* **2003**,14,2547 - 2551.

[111] a) G. E. Morse, M. G. Helander, J. F. Maka, Zh.-H. Lu, T. P. Bender, *ACS Appl. Mat. Int.* **2010**, *2*, 1934 - 1944. b) M.E. El-Khouly, J. B. Ryu, K.-Y. Kay, O. Ito, S. Fukuzumi, *J. Phys. Chem. C* **2009**, *113*, 15444 - 15453.

Further, SubPcs **9** and **10** bearing aldehyde functionality at axial position were used for the preparation of covalent systems with fullerenes. So, dimers with empty fullerene SubPcs-C_{60} (**5**, **7**) and those with endohedral fullerene SubPcs-$La_2@I_h$-C_{80} (**6**, **8**) were obtained by the 1,3-dipolar cycloaddition of azomethyne ylides generated *in situ* in a reaction of (3-formylphenoxy) SubPcs **9** or **10** and N-methylglycine, to C_{60}.or $La_2@I_h$-C_{80} (Scheme 2.2), according to procedure reported previously for **5**.

The reactions of the formation of conjugates **5** and **7** were stopped once no precursor SubPcs were detected by TLC and HPLC (Figure 1.31). Thus, TLC and HPLC analyses infered that the formation of SubPcs-C_{60} conjugate **7** was completed in 2h. In contrast, perfluorinated SubPc **9** reacts with C_{60} in 8h and reveals, as such, reactivity similar to that seen previously for other SubPcs in Prato protocols. This reflects the perturbation stemming from the six pentylsulfonyl substituents on the electronic properties of SubPc **10** and its corresponding intermediates. Futher purification of conjugate **5** was carried out by column chromatography on silica gel. Subsequent size exclusion separation on Bio-Beads yielded pure conjugate **5** in 63% yield and bis-adducts in moderate amounts of 6%. Efficient purification of **7** was, nevertheless, hampered by its degradation on silica gel and formation of decomposition products with similar polarities. Performing column chromatography on cyanopropyldichlorosilyl-modified silica gel as a solid support[112] allowed the successful separation of the conjugate **7** in somewhat lower yields of 24% followed by the final separation of bis-adducts by GPC.

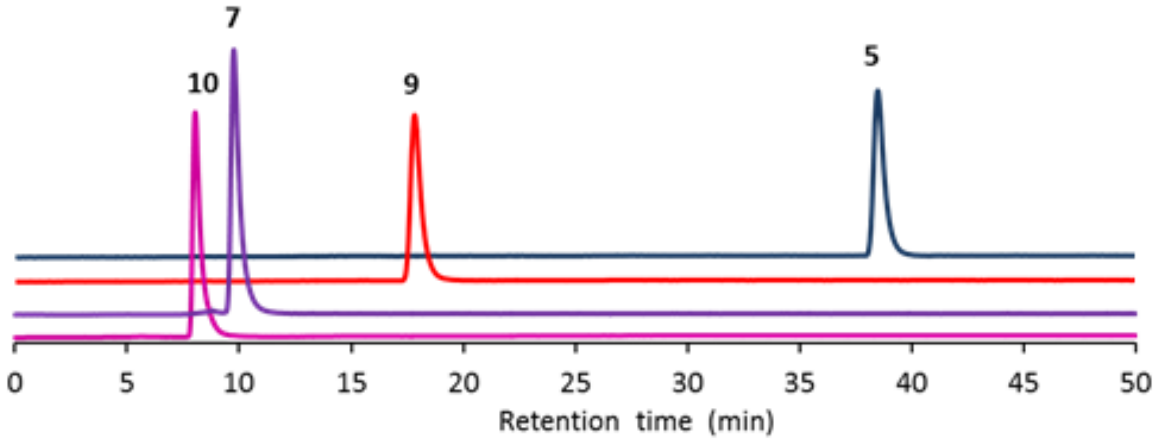

Figure 1.31. HPLC profiles of the isolated **5** and **7** and their precursors **9** and **10**.

[112] K. Okusa, H. Tanaka, M. Ohira, *J. Chromatogr. A* **2000**, *869*, 143 - 149.

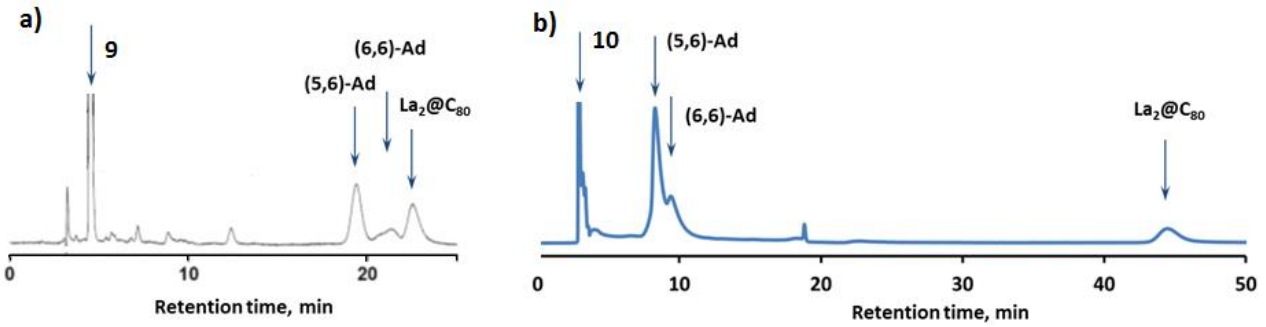

Figure 1.32. HPLC profiles of the reaction mixtures showing the formation of conjugates **6** after 80 min (a) and **8** after 15 min (b) as a mixture of [5,6]- and [6,6]- isomeric adducts.

Covalent conjugates of (perfluoro)SubPcs and hexyl(sulfonyl)SubPc with $La_2@I_h$-C_{80} were obtained *via* Prato reaction. In contrast, the corresponding reaction times were limited by the stability of newly formed conjugates **6** and **8**. Thus, product **6** could be maximally accumulated after 80 min of the reaction, with minimal amounts of decomposition products formed, and with approx. 10% of $La_2@I_h$-C_{80} remaining unreacted (Figure 1.32a). Maximum yield of the formation of conjugate **8** was reached already after 15 min, as it has been referred from HPLC profiles (Figure 1.32b). Interestingly, both dimers – **6** and **8** – were generated as a mixture of [5,6]- and [6,6]- pyrrolidine adducts to $La_2@I_h$-C_{80} cage (similar to what has been described for the Prato reaction of $Sc_3N@I_h$-C_{80} in the previous section of this chapter). Both products – **6** and **8** – were isolated by semi-preparative HPLC as a mixture of [5,6]- and [6,6]- isomers in 35% and 2% yield, respectively (based on consumed $La_2@I_h$-C_{80}), being hardly separable on a Buckyprep column.

Compounds were fully characterized by MALDI-MS spectrometry and ^{1}H and ^{13}C NMR, UV-vis, and FTIR spectroscopy. Saying that, conjugate **8** requires a special remark. Thus, MALDI-MS and UV-vis were the only techniques useful for the characterization of hexyl(sulfonyl)SubPc - $La_2@I_h$-C_{80} dimer **8** due to its low stability. Nevertheless, its formation was unumbigously proved by the presence of a peak at 2585.1 *m/z* of low intensity corresponding to the $[La_2C_{143}S_6H_{82}BN_7O_{13}]^-$ molecular ion. Peaks of higher intensities were ascribed to the products of decomposition due to the loss of fullerene moiety.

As it has been reffered from HPLC profiles, both dimers – **6** and **8** – were generated as a mixture of [5,6]- and [6,6]- pyrrolidine adducts to $La_2@I_h$-C_{80} cage. ^{1}H NMR spectroscopy additionally confirmed this finding. The ^{1}H NMR spectrum of **6** exhibits two sets of signals originating from phenyl protons and pyrrolidine protons, indicating the presence of two conformers of **6** in a 3:1 ratio (Figure 1.33a). Thus, doublets of higher intensity at 4.41 ppm and 3.14 ppm can be ascribed

to the geminal protons of the pyrrolidine moiety of [5,6]-adduct. Whereas, doublets of lower intensity at 4.10 ppm and 2.90 ppm correspond to geminal protons of the pyrrolidine moiety of [6,6]-adduct. Confirmation for this assignment was obtained from COSY experiments, revealing a cross coupling relationship between these two sets of signals. Methyne protons of pyrrolidine rings of [5,6]- and [6,6]-adducts appear at 3.65 and 3.50 ppm, respectively. Finally, N-methyl protons of [5,6]- and [6,6]-adducts resonate at 2.82 and 2.39 ppm. Signals at 6.17 and 6.08 ppm can be attributed to the phenyl protons of [5,6]-adduct located in *ortho*- and *para*- positions towards pyrrolidine moiety. Whereas, peaks at 5.98 and 5.81 ppm – to those of [6,6]-adduct. Signals of the *metha*- phenyl protons could not be observed due to their overlap with signals of *o*-DCB-d_4 protons. However, their chemical shifts were determined by COSY NMR as 7.05 and 7.30 ppm for [5,6]- and [6,6]-adduct, respectively. Characterization of **8** by ^{1}H NMR was, however, hampered by the small amounts of the isolated material and its poor stability.

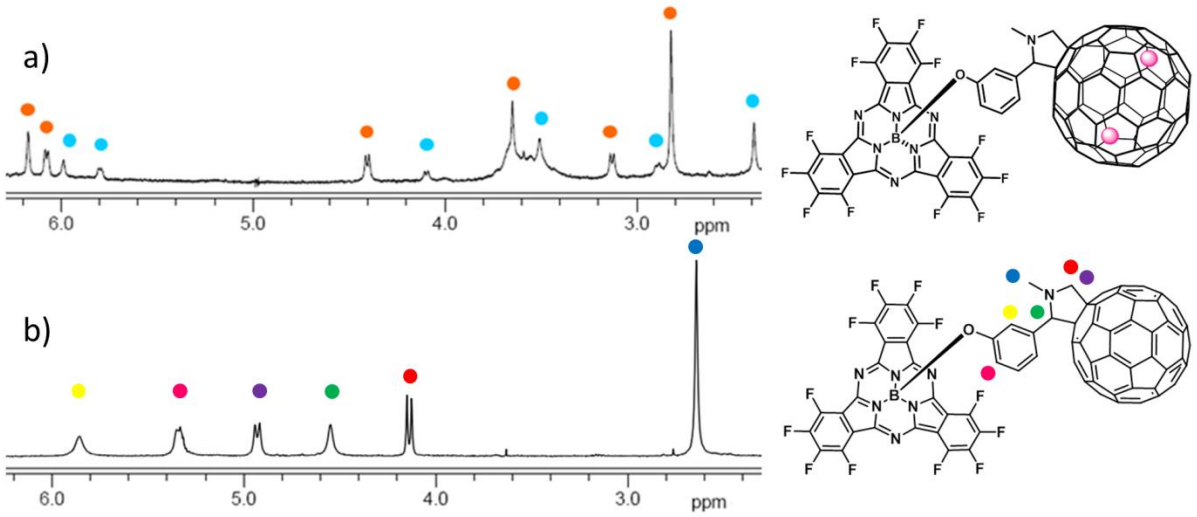

Figure 1.33. ^{1}H NMR spectra of (a) conjugate **6** (700 MHz, *o*-DCB-d_4) showing a mixture of [5,6]- and [6,6]-adducts, and (b) conjugate **5** (400 MHz, CS_2/CD_2Cl_2 2:1)**.**

^{1}H NMR spectrum of conjugate **5** confirms the formation of an only [6,6]-adduct that is characteristic for Prato reactions of C_{60}, and confirms the assignement made in ^{1}H NMR spectrum of the conjugate **6** (Figure 1.33b). However, it's worthy to note that conjugates **5** and **7** (as well as adducts of **6** and **8**) were obtained as a mixture of two diastereoisomers,[113] inseparable by conventional column chromatography or by HPLC. Their presence is manifested only by the broadening of signals in the ^{1}H NMR spectra (Figure 1.33).

[113] M. Prato, M. Maggini. *Acc. Chem. Res.* **1998**, *31*, 519 - 526.

1.3.2 Electrochemistry

The electrochemical properties of SubPc-C_{60} dyads **5** and **7**, and SubPc- $La_2@I_h$-C_{80} dimer **6** as well as their reference compounds were examined by CV and SWV (Figure 1.34) in *o*-DCB containing 0.05 M $(n\text{-Bu})_4NPF_6$.and compared with the redox characteristics of their references, that are, SubPcs **11**, **12**, N-methyl-3,4-fulleropyrrolidine and $La_2@C_{80}$-NTrt. The corresponding data are summarized in Table 2. Characterization of **8** by electrochemical techniques was, however, hampered by the small amounts of the isolated material and its poor stability.

Overall, **5** - **7** exhibit up to seven reductions and two oxidations in the cathodic and the anodic directions, respectively, which were assigned upon comparison with SubPcs **11** and **12**. Thus, (perfluoro) SubPc **11** reveals three reversible reductions at -1.09, -1.71, and -2.30 and one reversible oxidation at 1.02 V. Similarly, four reversible reductions at -0.81, -1.34, -1.73, and -2.19 V and one irreversible oxidation at 1.18 V are noted for hexa(pentylsulfonyl) SubPc **12**.

As to F_{12}SubPc- $La_2@I_h$-C_{80} dimer **6**, the first and second reductions, which are seen as a one-electron process at -0.47 and -1.12 V, coincide well with the reductions of $La_2@I_h$-C_{80} and F_{12}SubPc, respectively.

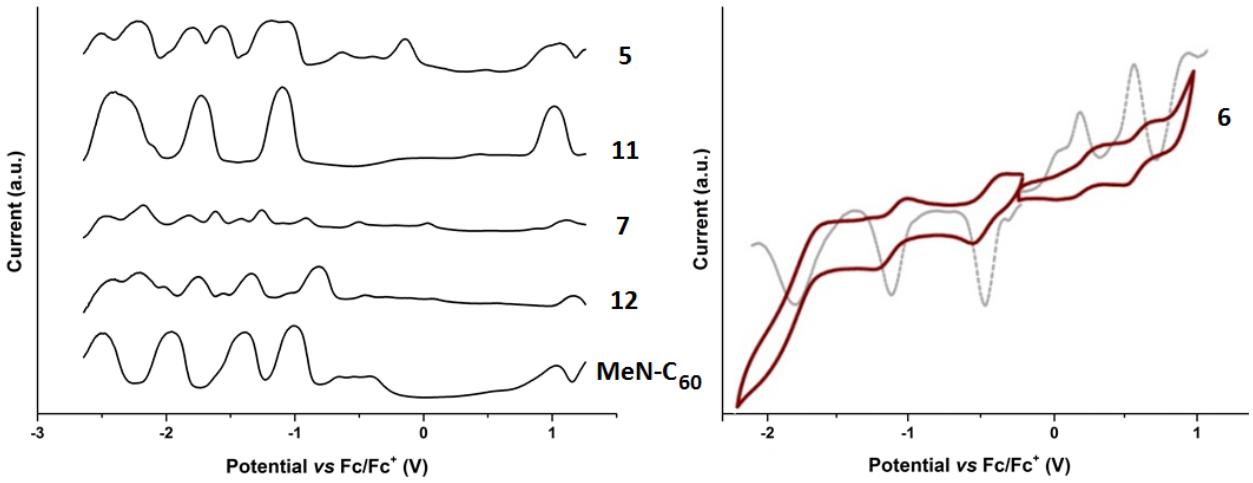

Figure 1.34: Square wave voltammogramms of dyads and their reference compounds ($c \approx 10^{-3}$ M) and cyclic voltammogram of **6** in *o*-DCB. Potential values are referred to $E_{(ox)1/2}$ of the Fc/Fc^+ redox couple. MeN-C_{60} = N-methyl-3,4-fulleropyrrolidine.

Table 2. Redox potentials[a] of dyads **5**-**7** and their reference compounds, E_p *vs* Fc/Fc^+, V.

Compound	E_p^4 (red)	E_p^3 (red)	E_p^2 (red)	E_p^1 (red)	E_p^1 (ox)	E_p^2 (ox)
6		-1.80[b]	-1.12	-0.47	+0.20	+0.58
5	-1.79	-1.57	-1.18	-1.06	+0.99	+1.08
7	-1.42	-1.26	-1.10	-0.91	+1.04	+1.12
11		-2.30	-1.71	-1.09	+1.02	
12	-2.19	-1.73	-1.34	-0.81	+1.18	
MeN-C_{60}[b]		-1.95	-1.40	-1.01	+1.04	
Trt$NLa_2@I_h$-C_{80}[c]		-2.13	-1.70	-0.44	+0.20	+0.59

[a]Values obtained by SWV; only the first four reductions of pentylsulfonyl-containing compounds **7** and **12** are reported. [b]MeN-C_{60} = N-methyl-3,4-fulleropyrrolidine. [c]$La_2@C_{80}$-NTrt (Trt = triphenylmethyl)[114].

The third reduction at -1.80 V appears as a two-electron process, involving the second reduction of $La_2@I_h$-C_{80} and the second reduction of F_{12}SubPc. In addition, three oxidations are visible. The first and second oxidations are fully reversible one-electron processes, which agree well with those of $La_2@I_h$-C_{80} (Table 2). The third oxidation is a two-electron process, corresponding to the first oxidation of F_{12}SubPc and the third oxidation of $La_2@I_h$-C_{80}. Notably, the ground state interactions between the electroactive constituents of **6** are negligible. The remarkable oxidative features of **6** underline the strong electron donor character of $La_2@I_h$-C_{80}.

Turning to the conjugates **5** and **7**, we can also see rich redox behavior. Thus, the reductions of F_{12}SubPc-C_{60} conjugate **5** evolving at -1.18, -1.79, and -2.21 V are ascribed to F_{12}SubPc centered processes, whereas those at -1.06 and -1.57 V relate to processes involving C_{60}. Oxidations at +0.99 and +1.08 V are C_{60} and F_{12}SubPc centered, respectively. In **7**, the presence of two strong acceptors, namely hexa(pentylsulfonyl) SubPc and C_{60}, leads to a coalescence and irreversibility of the reductions likely based on electron density rearrangements. As such, seven reductions at -0.91, -1.10, -1.26, -1.42, -1.62, -1.81, and -2.17 V plus two oxidations at +1.04 and +1.12 V evolve. Those at +1.04, -1.10, -1.42, and -1.81 V are C_{60} centered, while those at +1.12, -0.91, -1.26, -1.62, and -2.17 V correlate with either the oxidation or the reduction of hexa(pentylsulfonyl) SubPc.

[114] M. Yamada, M. Okamura, S. Sato, I. C. Someya, N. Mizorogi, T. Tsuchiya, T. Akasaka, T. Kato, S. Nagase, *Chem. Eur. J.* **2009**, *15*, 10533 - 10542.

From Figure 1.34 and Table 2, we conclude that hexa(pentylsulfonyl) SubPc **12** is more easily reduced and more difficult to be oxidized than F_{12}SubPc **11**. In other words, the alkylsulfonyl groups impose stronger electron withdrawing character than the fluorine atoms. A corroborating trend is found in **7** that is more easily reduced and more difficult to be oxidized than **5**, where the differences in reduction and oxidation are 150 and 50 mV, respectively. On the other hand, the corresponding first reduction in **5** and **7** are considerably 30 and 100 mV shifted if compared to those of the reference SubPcs **11** and **12**, suggesting stronger ground-state interactions between the electron donor and the electron acceptor subunits in **7**. If compered to its C_{60} analogue **5**, conjugate **6** undergoes 60 mV lower reduction and 80 mV lower oxidation that is similar to $La_2@I_h$-C_{80} redox behaviour.

1.3.3 Photophysics

To gain further insight into the ground state features of SubPc-$La_2@I_h$-C_{80} conjugates **6** and **8**, as well as their SubPc-C_{60} reference systems **5** and **7**, we turned to absorption spectroscopy. At a first glance, the absorption spectra of (pentylsulfonyl)SubPc-fullerene dimers **7** and **8** are best described as a simple superimposition of the spectra of the individual components, namely SubPc **12**, on one hand, and N-methyl-[5,6]-$La_2@I_h$-C_{80}-fulleropyrrolidine or N-methylfulleropyrrolidine, on the other hand. (Figure 1.35). This results in no shift if the absorption maxima in **7** and **8** as compared with that of SubPc **12**, indicating the lack of ground-state interaction between the individual components. In the contrary, **7** containing hexa(pentylsulfonyl) SubPc reveals strong absorption at 582 nm, which is 7 nm red-shifted in comparison with the absorption of perfluorinated **5** at 575 nm, thus, inferring the stronger electron-acceptor properties of sulfonated SubPcs than of fluorinated one (Figure 1.35).

In line with what was observed in steady state absorptions, the nature of the peripheral substituents influences the singlet excited state properties of **5** and **7** (Figure 1.35). In fluorescence experiments, a solvent independent fluorescence quantum yield of 0.17 is determined for SubPc **11**. In contrast, SubPc **12** exhibits solvent dependent quantum yields of 0.15, 0.07 and 0.06 in toluene, THF and benzonitrile, respectively. In reference to the aforementioned, fluorescence assays with **5** and **7** give rise to strong quenching of the SubPc fluorescence with values from 0.0007 to 0.0012.

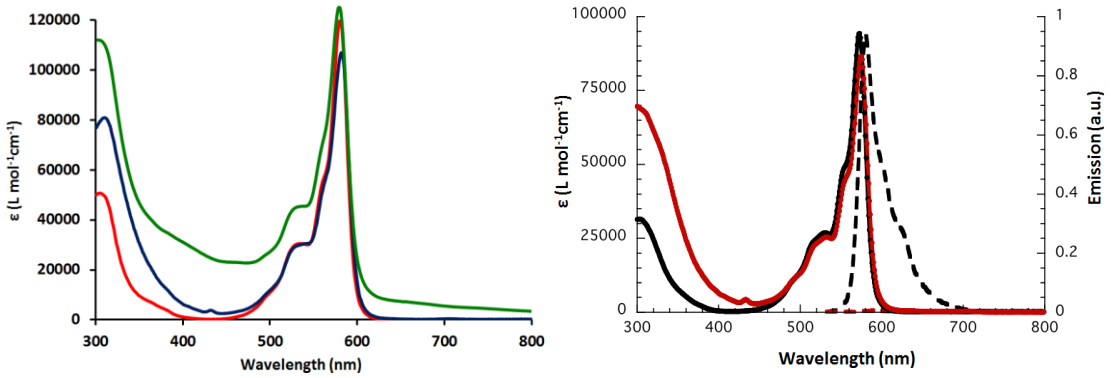

Figure 1.35. Absorption spectra of SubPc **12** (red line), its conjugates with $La_2@I_h$-C_{80} **8** (green line), and with C_{60} **7** (blue line) in toluene (left). Absorption (solid lines) and fluorescence spectra (dashed lines) of SubPc **11** (black lines) and conjugate **5** (red lines) in toluene (right).

To attribute our spectral observation, spectroelectrochemical experiments on $(F_{12}SubPc)^{\bullet-}$ and $((SO_2C_5H_{11})_6SubPc)^{\bullet-}$as well as $(La_2@I_h\text{-}C_{80})^{\bullet+}$ were deemed important (Figure 1.36). On one hand, the differential absorption spectra of the electrochemically reduced **11** reveal two broad features with maxima at 455 and 655 nm, which are accompanied by shoulders at around 475 and 610 nm, as well as a minimum at 570 nm. Upon spectroelectrochemical reduction of **12**, spectral characteristics including maxima at 480, 545, 620, and 735 nm complemented by minima at 534 and 581 nm evolved. Notably, pulse radiolytic reductions with **11** or **12** in deaerated toluene/2-propanol/acetone mixtures (8:1:1 v/v) results in quantitatively similar spectra with characteristic fingerprints at 610 and 620 nm, respectively. On the other hand, a characteristic maximum at 900 nm and a broad near infrared tail evolve as spectroscopic characteristics upon spectroelectrochemical oxidation of $La_2@I_h$-C_{80}.

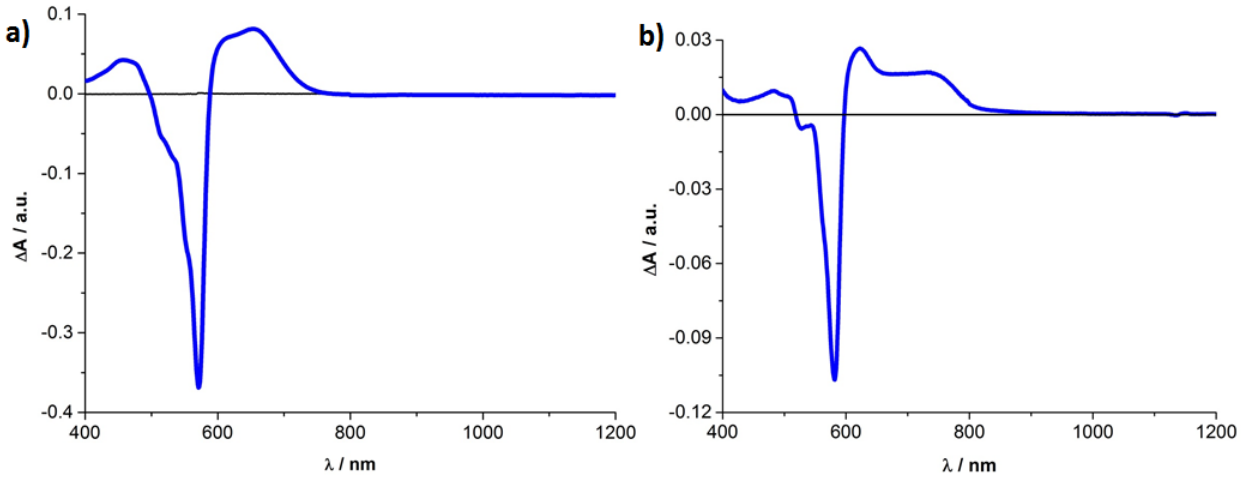

Figure 1.36. Differential absorption spectra obtained upon electrochemical reduction of SubPcs **11** (a) and **12** (b) at an applied bias of −0.5 and −0.3 V in argon-saturated toluene/acetonitrile mixtures (4/1 v/v) at room temperature.

Insights into the excited state deactivation in SubPc-La_2@I_h-C_{80} conjugates **6** and **8**, as well as their SubPc-C_{60} reference systems **5** and **7**, the corresponding (perfluoro)SubPc **11** and (pentylsulfonyl)SubPc **12** and La_2@I_h-C_{80} in general, and into the corresponding photoproducts, in particular, came from transient absorption measurements following femtosecond and nanosecond excitation. Excitation of La_2@I_h-C_{80} at 387 nm leads to the population of its singlet excited state (1.4 ± 0.2 eV), which features ground state bleaching at 465 nm and well-resolved fine structure with maxima at 516, 466, 614, 735, 800, and 900 nm. The latter is subject to a fast intersystem crossing – 60 ± 30 ps – to the triplet manifold due to the presence of the $(La_2)^{6+}$ cluster, which promotes efficient spin orbit coupling. Following the singlet excited state decay, a weak and broad absorption in the 800–1200 nm region, along with broad features that appear at 550 nm, are discernible. These features relate to the La_2@I_h-C_{80} triplet excited state (1.0±0.1 eV). For N-methylfulleropyrrolidine, differential absorption changes evolve immediately after the 387 nm laser excitation, which are characterized by maxima at 500 and 900 nm. The C_{60} singlet excited state (1.8 eV) decays with 1.4 ± 0.1 ns to afford the energetically lower lying triplet excited state (1.5 eV), whose characteristics are a transient maximum at 700 nm and a transient lifetime of up to 20 μs in the absence of molecular oxygen.

F_{12}SubPc **11** reveals upon excitation at 530 nm differential absorption changes, which include transient maxima at 440 and 600 nm as well as transient minima at 514, 575, and 635 nm – Figure 1.37a,c. In addition, a broad near-infrared feature spans from 650 to 1200 nm, which peaks around 710 nm. These features relate to the singlet excited state (2.16 eV) of **11**, which transforms with 1.9 ± 0.1 ns into the corresponding triplet excited state (1.4 eV). Transient absorption spectra of the latter maximize at 470 and 610 nm and minimize at 532 and 570 nm.

Commencing with the conclusion of the 530 nm excitation, SubPc **12** reveals differential absorption changes in the form of transient maxima at 424, 474, 623, 660 nm, a broad tail extending far into the near infrared, as well as transient minima at 533 and 583 nm (Figure 1.37b,d). These SubPc singlet excited state (2.12 eV) related transient absorption features undergo intersystem crossing to the corresponding triplet excited state (1.4 eV), which exhibits a broad transient in the visible part of the spectrum. The latter maximizes at 470 and 620 nm and

minimizes at 533 and 583 nm. Owing to the presence of sulfur, which facilitates spin-orbit coupling, the intersystem crossing is accelerated relative to what is seen for **11** with lifetimes of 1220 ± 20 ps, 420 ± 10 ps, 415 ± 10 ps in toluene, THF, and benzonitrile, respectively.

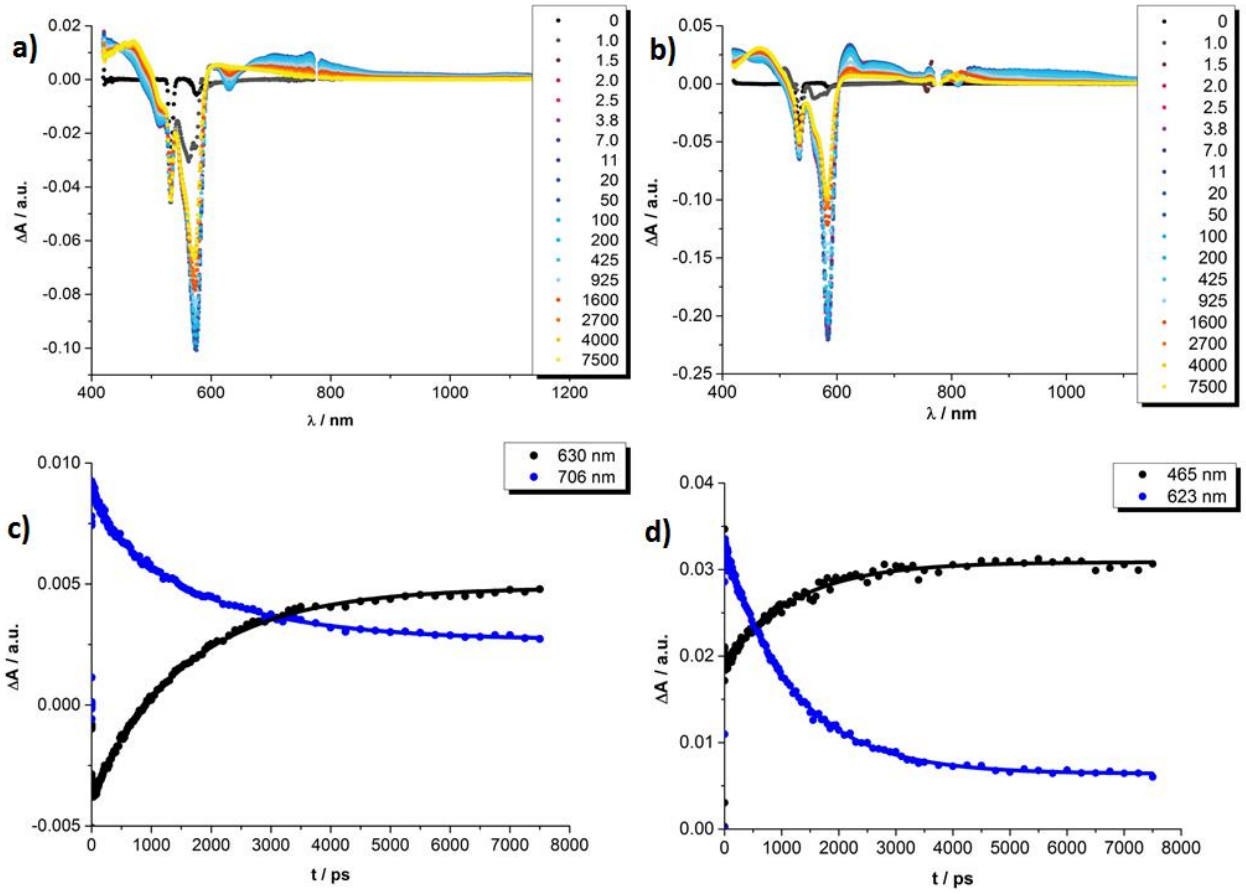

Figure 1.37. Differential absorption spectra obtained upon femtosecond flash photolysis (530 nm) of **11** (10^{-5} M) in argon-saturated THF (a) and those of **12** (10^{-5} M) in argon-saturated toluene (b). Time-absorption profiles of the spectra shown above for **11** (c) and **12** (d) monitoring the intersystem crossing.

Upon 530 nm excitation, conjugate **6** gives rise to differential absorption changes in the form of transient maxima at 450, 600, and 720 nm as well as transient minima at 575 and 635 nm (Figure 1.38a,c). In line with the reference experiments, namely with **11**, we assign these changes to the F_{12}SubPc singlet exited state. Instead of seeing the slow intersystem crossings, the SubPc singlet excited state decays ultrafast with lifetimes of 3.0 ± 0.4 ps (toluene), 2.2 ± 0.2 ps (THF), and 2.0 ± 0.2 ps (benzonitrile). Simultaneously, new transitions develop in the visible and the near-infrared regions. Importantly, the new transients do not match the signature of the SubPc triplet excited state. Instead, maxima at 480 and 590 nm as well as minima at 515 and 570 nm are discernable. These features bear great resemblance with the pulse radiolytic findings in the context of reducing SubPc and, as such, relate to its π-radical anion – $(F_{12}SubPc)^{\bullet-}$. In the near-infrared, a

broad tail is attributable to the $La_2@I_h$-C_{80} π-radical cation, that is, $(La_2@I_h\text{-}C_{80})^{\bullet+}$. Taking the aforementioned into concert, we conclude that an energetically low lying radical ion pair state (1.32 eV), namely $(La_2@I_h\text{-}C_{80})^{\bullet+}$-$(F_{12}SubPc)^{\bullet-}$, is formed. Both fingerprints served as reliable probes to determine the lifetime of the metastable $(La_2@I_h\text{-}C_{80})^{\bullet+}$-$(F_{12}SubPc)^{\bullet-}$ radical ion pair state. All decays were well fit by a single exponential fitting function throughout the femtosecond time scale. In particular, lifetimes of 34 ± 2 ps (toluene), 32 ± 2 ps (THF), and 35 ± 2 ps (benzonitrile) were derived.

Singlet oxygen quantum yields for **6** are as low as 0.010 in THF and support the assignment that any other state than the $F_{12}SubPc$ triplet excited state evolves as the product of charge recombination. Please note singlet oxygen yields in **11** of 0.31 (toluene), 0.10 (THF), and 0.35 (benzonitrile).

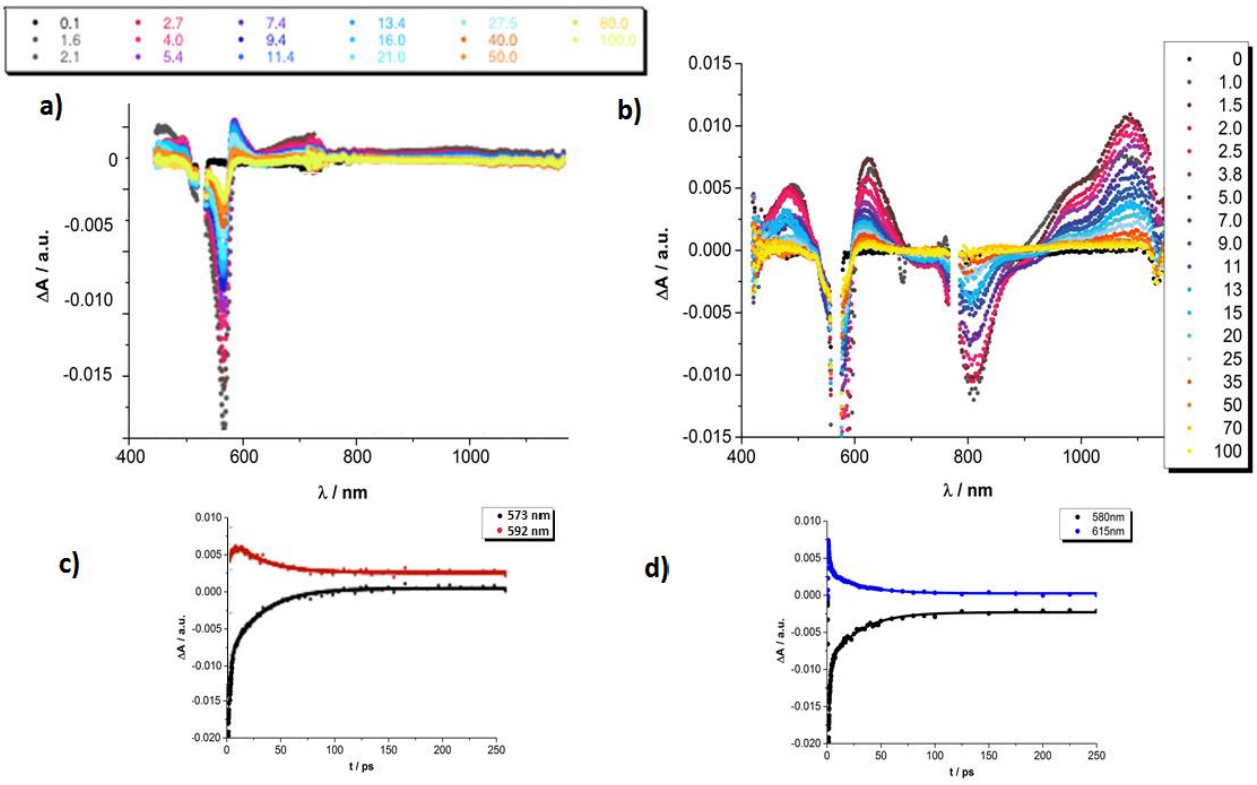

Figure 1.38. Differential absorption spectra obtained upon femtosecond flash photolysis (530 nm) of **6** (10^{-5} M) in argon-saturated THF (a) and those of (568 nm) of **8** (10^{-5} M) in argon-saturated benzonitrile (b). Time-absorption profiles of the spectra shown above for **6** (c) and **8** (d) monitoring the charge separation and the charge recombination.

Laser excitation of **8** in benzonitrile at 568 nm results immediately after excitation in differential absorption maxima at 485 and 623 nm and a minimum at 583 nm (Figure 1.38b,d). Although

these transient features relate to the singlet excited state of SubPc they decay ultrafast with a lifetime of 1.4 ± 0.1 ps. New transients evolve which maximize at 480 and 610 nm and minimize 583 nm. A spectral comparison with the results from the spectroelectrochemical / pulse radiolytic investigations supports the notion that the new transients are attributed to the π-radical anion – $((SO_2C_5H_{11})_6SubPc)^{\bullet-}$. Taking the aforementioned into concert, we postulate an electron transfer from $La_2@I_h\text{-}C_{80}$ to the SubPc singlet excited state to afford $(La_2@I_h\text{-}C_{80})^{\bullet+}$-$((SO_2C_5H_{11})_6SubPc)^{\bullet-}$ (1.36 eV). It is worth mentioning that the detection of $(La_2@I_h\text{-}C_{80})^{\bullet+}$ in the near infrared is hampered by the thermal decomposition of SubPc. This is seen to form a product with absorptions in the 700 - 850 nm range. Nevertheless, the metastable $(La_2@I_h\text{-}C_{80})^{\bullet+}$-$((SO_2C_5H_{11})_6SubPc)^{\bullet-}$ radical ion pair state decays with 28 ± 2 ps to the singlet ground state.

Likewise, 530 nm excitation of $F_{12}SubPc\text{-}C_{60}$ **5** results in the exclusive formation of the SubPc singlet excited state (Figure 1.39a,c). In particular, transient maxima at 450, 600, and 720 nm as well as transient minima at 515, 575, and 635 nm are formed and decay rapidly with 1.5 ± 0.3 ps (toluene), 1.5 ± 0.3 ps (THF), and 1.4 ± 0.3 ps (benzonitrile). As the SubPc singlet excited state decay comes to an end a broad near-infrared transient, which maximizes at 910 nm, is noted, suggesting a C_{60} singlet excited state. Interestingly, we did not find the characteristic C_{60} triplet feature at 700 nm at the end of the C_{60} singlet excited state deactivation. On the contrary, maxima at 470 and 615 nm as well as a minimum at 575 nm were concluded, pointing to the SubPc triplet excited state. From this we infer that the C_{60} triplet excited state (1.5 eV) undergoes a thermodynamically allowed transfer of triplet excited state energy to SubPc (1.4 eV). The kinetics at the 470 and 615 nm maxima further furnishes the kinetic assignment, namely the rate-determining step in the SubPc triplet excited state formation is the C_{60}centered intersystem crossing. A global analysis reveals kinetics that is very similar (1.6 ± 0.1 ns) to the inherent intersystem crossing dynamics seen for C_{60}. In this context, it is reassuring that the transients seen at the end of the femtosecond experiments matches that at the beginning of the nanosecond experiment.

Moreover, maxima at 470 and 610 nm, minima at 532 and 570 nm, and an excited state lifetime of 36 μs without oxygen perfectly agree with the SubPc triplet excited state of **11**. Likewise, singlet oxygen quantum yields of **5** were found as high as 0.28 (toluene), 0.13 (THF), and 0.41 (benzonitrile) and support the assignment that the triplet excited state evolves as the product of charge recombination. Singlet oxygen yields in **11** are as high as 0.35.

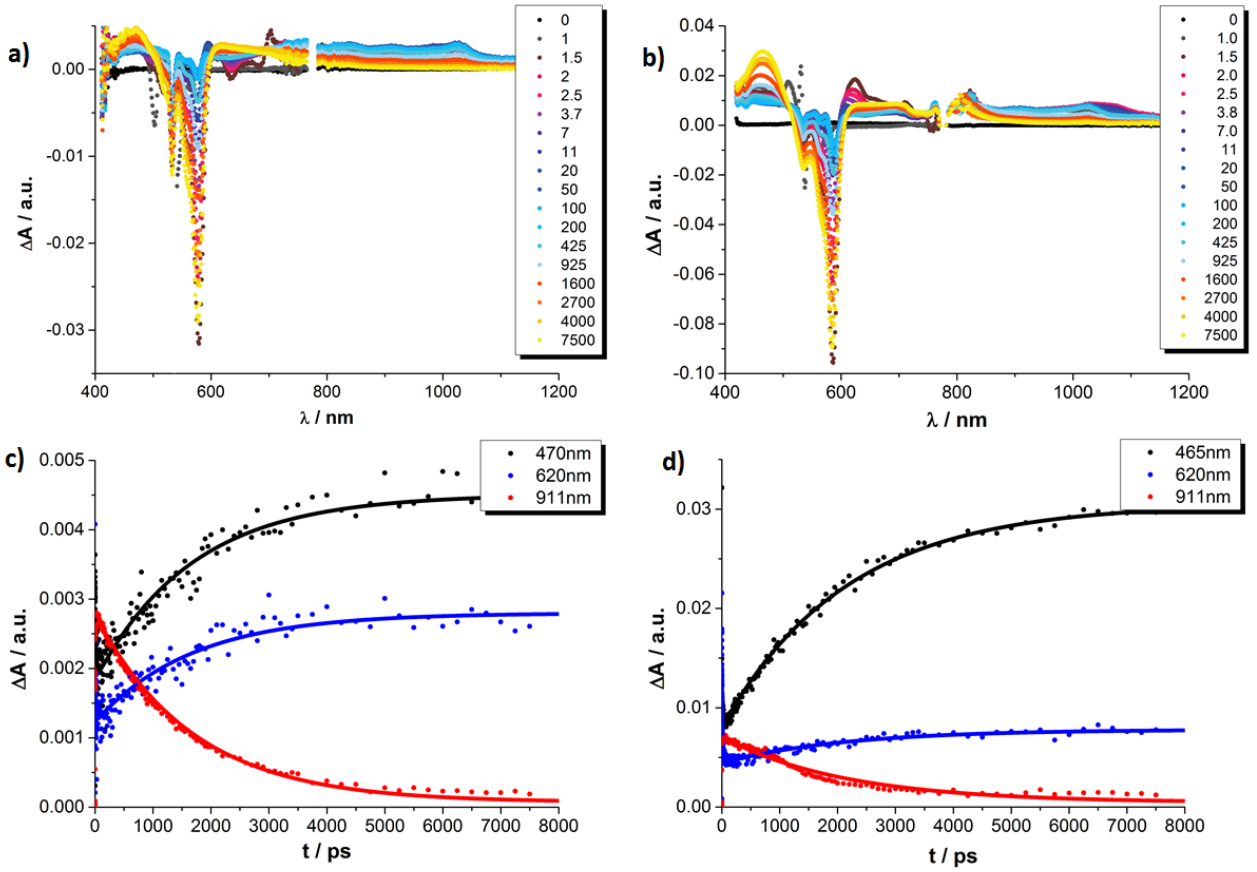

Figure 1.39. Differential absorption spectra obtained upon femtosecond flash photolysis (530 nm) of **5** (10^{-5} M) (a) and those of **7** (10^{-5} M) (b) in argon-saturated toluene. Time-absorption profiles of the spectra shown above for **5** (c) and **7** (d) monitoring the energy transfer.

When turning to **7**, excitation at 530 nm is accompanied by the formation of its singlet excited state (Figure 1.39b,d). Evidence stems from monitoring maxima at 427, 474, 623, and 660 nm and minima at 535 and 585 nm. These decay in the presence of C_{60} rapidly with 1.5 ± 0.3 ps (toluene), 1.5 ± 0.3 ps (THF), and 1.4 ± 0.3 ps (benzonitrile) to form accordingly the C_{60} singlet excited state with its 910 nm maximum. Like for **5**, we did not find the characteristic C_{60} triplet feature. Instead, maxima at 470 and 625 nm as well as minima at 535 and 585 nm of the SubPc triplet excited state were concluded. In other words, the triplet excited state of SubPc (1.4 eV) evolves from a thermodynamically allowed transfer of triplet excited state. The kinetics at the 470 and 625 nm maxima and the 585 nm minimum document that the rate-determining step is C_{60} centered intersystem crossing (1.6 ± 0.1 ns). In the absence of oxygen, the SubPc triplet excited state lifetime is 20 ± 5 µs in agreement with what was found for in **12**.

Exciting **5** at 320 or 387 nm populates higher lying singlet excited states (S_2: 3.4 ± 0.1 eV) of SubPc directly – the light partitioning at, for example, 320 nm is 1:1 (Figure 1.40). The latter are

discernable with maxima at 430, 600, and 995 and minima at 515 and 570 nm, which transform within 7 ± 1 ps to the lowest-energy singlet excited state in the absence of C_{60}. In contrast to that, in **5** the lifetime is shortened to 4.1 ± 0.2 ps (toluene), 3.5 ± 0.2 ps (THF), and 2.6 ± 0.5 ps (benzonitrile) by the bear presence of C_{60}. The product of an instantaneous transformation includes maxima at 590, 840, 910, and 1020 nm and a minimum at 575 nm. These are in sound agreement with those noted upon pulse radiolytical generation of $(C_{60})^{\bullet+}$. In the visible, a transient maximum at 595 nm and a transient minimum at 578 nm are clear fingerprints of $(SubPc(F_{12}))^{\bullet-}$. In other words, the close spectral resemblance between radiolytical and photophysical experiments prompts to the unprecedented formation of the $(C_{60})^{\bullet+}$-$(SubPc(F_{12}))^{\bullet-}$ (2.17 eV) radical ion pair state, as a product of charge separation (Figure 1.41). Both fingerprints served as reliable probes to determine the lifetime of the metastable $(C_{60})^{\bullet+}$-$SubPc(F_{12})^{\bullet-}$ radical ion pair state. Charge recombination proceeds with time constants of 31 ± 5 ps (toluene), 35 ± 5 ps (THF), and 38 ± 10 ps (benzonitrile) to populate the SubPc triplet excited state as the only discernable component. The singlet excited state of C_{60} (1.8 eV), which is partly excited at excitation wavelengths like 320 and 387 nm, is, however, insufficient in terms of thermodynamics to drive a charge transfer. Instead, the C_{60} singlet excited state related transient absorptions with maxima at 500 and 900 nm transform with a time constant of 1.6 ± 0.1 ns into the SubPc triplet excited state via triplet excited state energy transfer.

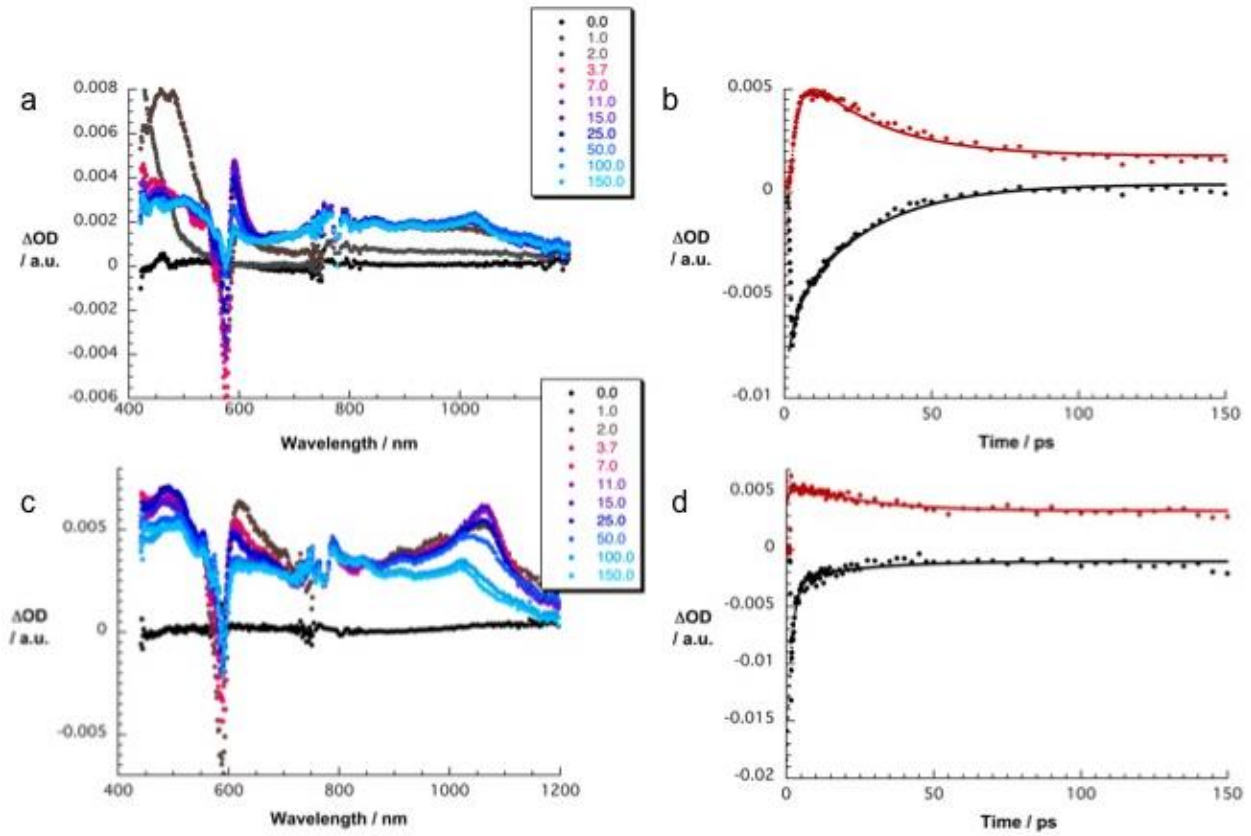

Figure 1.40. Differential absorption spectra obtained upon femtosecond flash photolysis (320 nm) of **5** (10^{-5} M) (a) and those of (387 nm) **7** (10^{-5} M) (c) in argon-saturated toluene. Time-absorption profiles of the spectra shown above (b) at 576 nm (black) and 591 nm (red), and (d) at 589 nm (black) and 608 nm (red) monitoring the charge separation and the charge recombination processes.

Experiments with 387 nm excitation of **7**, where the light partitioning is 2.6:1, leads to the formation of the singlet excited states of C_{60} and higher lying singlet excited states of SubPc (Figure 1.40). The C_{60} singlet excited state (1.8 eV) related transient absorption features with maxima at 500 and 900 nm transform with a time constant of 1.6 ± 0.1 ns into the SubPc triplet excited state via triplet excited state energy transfer, similar to the 530 nm excitation experiments. However, the higher lying singlet excited SubPc states (S_2: 3.3 ± 0.2 eV) are able to drive an ultrafast electron transfer evolving from C_{60} to SubPc. As a matter of fact, maxima at 481, 623, 655, and 1065 nm and minima at 532 and 585 nm decay fast in toluene, THF, and benzonitrile with lifetimes of around 0.6 ± 0.2, 1.4 ± 0.5, and 1.7 ± 0.5 ps, respectively. Simultaneously with the latter decay, new transitions develop in the visible and the near-infrared regions. Importantly, the new transients do not match the signature of the SubPc triplet excited state. Instead, maxima at 480, 550, 610, 840, 910, and 1025 nm as well as a minimum at 590 nm are discernable. Upon spectral comparison we ascribe the transitions in the visible to

$(SubPc(SO_2C_5H_{11})_6)^{\bullet-}$, while those in the near-infrared correspond to $(C_{60})^{\bullet+}$. In light of the aforementioned, we conclude an electron transfer from C_{60} to, for example, the SubPc singlet excited state to yield $(C_{60})^{\bullet+}$-$(SubPc(SO_2C_5H_{11})_6)^{\bullet-}$ (1.95 eV). The $(C_{60})^{\bullet+}$-$(SubPc(SO_2C_5H_{11})_6)^{\bullet-}$ radical ion pair state is short lived and decays with lifetimes of 16 ± 5, 21 ± 5, and 26 ± 5 ps in toluene, THF, and benzonitrile, respectively. At the end of this decay, the SubPc triplet excited state with maxima at 470 and 625 nm as well as minima at 535 and 585 nm emerges as the product of charge recombination. Singlet oxygen quantum yields of **7** were found to be as high as 0.49 (toluene), 0.24 (THF), and 0.65 (benzonitrile) and support the assignment that the triplet excited state evolves as the product of charge recombination. The singlet oxygen yields in **12** are 0.39 (toluene), 0.09 (THF), and 0.26 (benzonitrile).

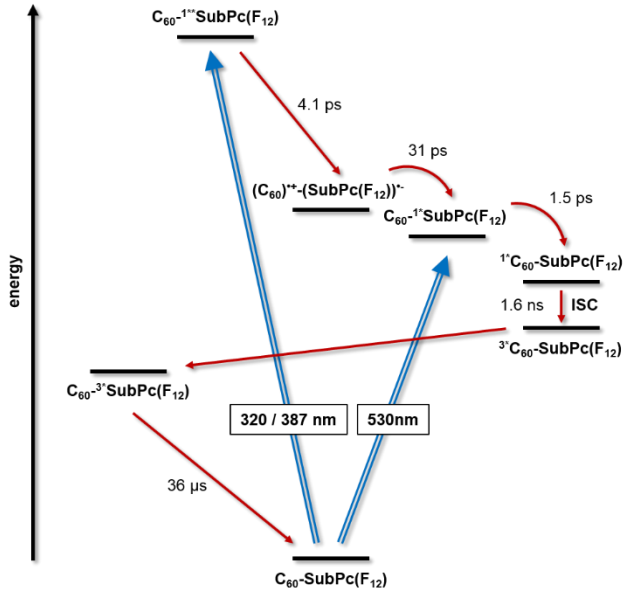

Figure 1.41. Energy level diagram of **5** reflecting the different pathways of energy and electron transfer.

1.4 Summary and conclusions

Along this chapter, synthesis and study of (Sub)Pc – EMF hybrids for tunable electron transfer has been discussed.

In the first section, we have successfully prepared four electron D-A ensembles built on metal-ligand coordination between C_{60} or $Sc_3N@I_h$-C_{80} featuring a pyridyl moiety, on one hand, and electron-donating or electron-accepting Zn(II)Pcs, on the other hand. Composition of supramolecular ensembles was Full-fledged photophysical assays with those two ensembles that contain $Sc_3N@I_h$-C_{80} **4** axially coordinated either to the electron-donating Zn(II)Pc **1** or to the electron-accepting Zn(II)Pc **2** revealed a switchable electron transfer reactivity.

Namely, spectroscopic and kinetic evidence for a Zn(II)Pc-to-$Sc_3N@I_h$-C_{80} a $Sc_3N@I_h$-C_{80}-to-Zn(II)Pc electron transfer – upon light excitation – was established as the major deactivation pathways in time–resolved pump probe experiments. In the case of the complexes between Zn(II)Pc **1** and fullerene derivatives **3** or **4**, PET from the Zn(II)Pc macrocycle to the fullerene moiety dominates the deactivation dynamics. Whereas, a $Sc_3N@I_h$-C_{80}-to-Pc charge transfer is observed for complex **2**/**4**, and no evidence of electron transfer was observed for complex **2**/**3**, in perfect agreement with electrochemical results obtained for derivatives **1**–**4**. This is, to the best of our knowledge, the first time that a fullerene-based molecular building block shows an electron transfer dualism. In the case of supramolecular complexes **1**/**4** and **2**/**4**, a switchable PET process is observed involving, for the first time, a fullerene-based molecule (**4**), which acts both as electron-acceptor or electron-donor as a function of the electronic nature of its supramolecular counterpart. Additionally, and importantly, this work involves, for the first time, the use of $Sc_3N@I_h$-C_{80} as an electron-accepting/-donating redox moiety, an EMF which is considered as the most abundant and readily available in bulk quantities by non-HPLC methods.

These findings, in combination with the small reorganization energy of fullerenes in electron transfer reactions, is likely to pave the road to the preparation of novel switching devices, solar energy conversion schemes, and logic gates based on $Sc_3N@I_h$-C_{80}, one of the most abundant and easy-to-purify fullerene. Particularly interesting is also the use of self-assembly *en-route* towards the preparation and study of a plethora of easy-to-prepare D-A constructs showing switchable electron transfer features.

In the second section, electron accepting SubPcs, bearing fluorine (**11**) or pentylsulfonyl substituents (**12**) on their periphery, have been used in combination with $La_2@I_h$-C_{80} and C_{60} fullerenes to prepare a series of novel electron donor-acceptor conjugates by means of the Prato reaction. We have documented the comprehensive study of their photophysical properties by means of several steady-state and time-resolved assays.

In terms of electrochemical and steady-state absorption, our results reveal no appreciable electronic interactions between SubPcs and $La_2@I_h$-C_{80} / C_{60}fullerene moieties in the ground state. In the excited state, an intramolecular electron-transfer evolves from $La_2@I_h$-C_{80} to photo excited (perfluoro) or (pentylsulfonyl) SubPc unit upon photoexcitation at 530 or 568 nm, respectively.

Regarding SubPcs-C_{60} reference conjugates **5** and **7**, only a singlet-singlet energy transfer from SubPc to C_{60} takes place upon photoexcitation at 530 nm. Whereas, unambiguous intramolecular ultrafast charge separation (in the range from 0.6 to 4.1 ps) occurs between SubPcs and C_{60} moieties upon photoexcitation at either 320 or 387 nm to form the one-electron oxidized form of C_{60} and the one-electron reduced forms of the two different SubPcs. This is, to the best of our knowledge, the first case of an *intramolecular* oxidation of C_{60} as part of an electron donor-acceptor conjugate for advanced solar energy conversion schemes by means of only photoexcitation. The charge separated state lifetime is at this state rather short lived with values of up to 38 ps. Radical ion pair state lifetime could be extended by, possibly, changing the energetics / thermodynamics of charge recombination.

Resuming, subphthalocyanines were proved to be successful candidates for tuning electron transfer reactivity of fullerenes. Thus, replacing $La_2@I_h$-C_{80} by C_{60} in SubPc hybrids provided a promising way to tune electron-transfer *vs* energy-transfer. Most importantly, energy transfer within SubPc-C_{60} conjugates could be switched back to electron transfer of the opposite direction by a simple change of the excitation strength from 530 nm to 320 nm. Considering the short separations between the electron donors and acceptors in the reported systems, further optimisation of the charge-separated state lifetimes seems achievable through the tailored design of linkers between $La_2@I_h$-C_{80} and SubPcs.

1.5 Experimental Section

1.5.1 Materials and methods

Chemicals (reagent grade) as well as solvents (anhydrous, deuterated and HPLC grade) were purchased from Aldrich Chemical, Alfa Aesar and Scharlau and used as received without further purification. Glassware was oven-dried at 110 ^{o}C overnight before use. All manipulations were carried out using Schlenk techniques under an atmosphere of dry argon.

Chromatography: column chromatography was carried out using silica gel Merck-60 (230-400 mesh, 60 Å) as the solid support. Thin layer chromatography (TLC) analyses were performed on aluminum sheets precoated with silica gel 60 F_{254} (Merck). Size-exclusion chromatography (GPC) was carried out using Bio-Beads S-X1 support (BIO-RAD) as a stationary phase and toluene as a mobile phase. High-performance liquid chromatography (HPLC) was performed on an Agilent 1100 LC (Agilent Technologies), using ø 4.6 × 250 mm Buckyprep column (Cosmosil). A mixture of toluene/o-dichlorobenzene (o-DCB)/methanol/NEt_3 = 75:25:1:1, vol %, at 0.7 mL/min flow rate and detection wavelength of 390 nm was employed in the section **1.2**. A mixture of toluene/dichloromethane/acetonitrile = 89:10:1, vol %, at 0.5 mL/min flow rate was employed in the section **1.3**.

Mass-spectrometry (MS): matrix-assisted laser desorption ionization time-of-flight (MALDI-TOF) experiments were carried out using Bruker Ultraflex III mass spectrometer, equipped with Nd:YAG laser operating at wavelength of 355 nm, in both positive and negative ionisation modes. A convenient matrix for these measurements is indicated for each compound.

Nuclear magnetic resonance: ^{1}H and ^{13}C NMR spectra were measured on a Bruker ASCEND-400, Bruker DRX-500 or a Bruker AVANCE 3HD NMR-700 spectrometer, locked on deuterated solvents. Carbon chemical shifts are measured in *ppm* relative to trimethylsilane (TMS), using the resonance of the deuterated solvent as an internal standard[115]. The assignment of the NMR signals was supported, in some cases, by 2D-NMR spectra such as COSY, HSQC, HMBC.

Ultraviolet-visible spectroscopy: UV-Vis spectra were recorded on a Varian Cary 50 Conc spectrophotometer or a Jasco V-660-spectrophotometer using spectroscopic grade solvents in 1 cm path length quartz cell, in spectrophotometric grade solvents.

Infrared spectroscopy: IR spectra were collected on Bruker Vector 22 spectrophotometer.

[115] G. R. Fulmer, A. J. M. Miller, N. H. Sherden, H. E. Gottlieb, A. Nudelman, B. M. Stoltz, J. E. Bercaw, K. I. Goldberg. *Organometallics*, **2010**, *29*, 2176 - 2179.

Steady-State Emission: the spectra were recorded on a FluoroMax 3 fluorometer (HORIBA JobinYvon). The measurements were carried out at room temperature.

Time-Resolved Absorption: *femtosecond transient absorption studies* were performed with 387 and 676 nm laser pulses (for compounds described in the section **1.2**) and with 320, 387, 530, and 568 nm laser pulses (1 kHz, 150 fs pulse width) (for compounds described in the section **1.3**) from an amplified Ti:Sapphire laser system (CPA-2101 and CPA-2110 from Clark-MXR, Inc.), the laser energy was 200 nJ. *Nanosecond laser flash photolysis* experiments were performed with 355 and 532 nm laser pulses from a Quanta-Ray CDR Nd:YAG system (6 ns pulse width) in a front face excitation geometry.

Photoinduced Oxidation of C_{60}-Py: a deaerated benzonitrile solution containing N-methylfulleropyrrolidine (1.5×10^{-4} M) and *p*-chloranil (0.04 M) in the presence of $Sc(OTf)_3$ (0.11 M) was excited with the help of the Quanta-Ray CDR Nd:YAG system at 532 nm (10 mJ per pulse).

Electrochemistry: *cyclic voltammetry* (CV) and *square wave voltammetry* (SWV) studies were performed on an Autolab PGSTAT30 potentiostate/galvanostate, in a home-built one-compartment cell using a three-electrode configuration, *o*-DCB as a solvent and 0.05 M tetra-*n*-butylammonium hexafluorophosphate (*n*-Bu_4NPF_6) as supporting electrolyte. A Pt electrode was used as the working electrode, a Pt wire as a counter electrode, $Ag/AgNO_3$ non-aqueous electrode as a reference. All potentials were recorded against a $Ag/AgNO_3$ non-aqueous electrode and corrected against Fc^+/Fc redox couple. CV was measured at scan rates of 100 mVs^{-1} and 50 mVs^{-1}, SWV was measured at scan rates of 50 mVs^{-1} and 20 mVs^{-1}. Prior to each voltammetric measurement, the cell was degassed by bubbling with argon for about 20 min. Electrochemical measurements were performed using a concentration of approximately 1×10^{-3} M for the compound in question. Compensation for internal resistance was not applied.

Materials: $Sc_3N@I_h$-C_{80}[116] (>99%) and $La_2@I_h$-C_{80} (>99%) fullerenes were prepared according to the synthetic procedures reported elsewhere; tetra-*tert*-butyl Zn(II)Pc **1** was purchased from Sigma Aldrich and used as reference compound in some of the photophysical and electrochemical measurements. *N*-methyl-3,4-fulleropyrrolidine was synthesized following a reported procedure.[117]

---

116 M. R. Ceron, F.-F. Li, L. Echegoyen. *Chem. Eur. J.* **2013**, *19*, 7410 - 7415.

117 M. Maggini, G. Scorrano, M. Prato. J. Am. Chem. Soc. **1993**, *115*, 9798 - 9799.

1.5.2 Synthetic procedures

- *N*-(*p*-Pyridyl)-3,4-C_{60} fulleropyrrolidine **3**:

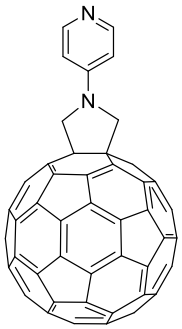

A mixture of 35 mg (0.05 mmol, 1 eq) of C_{60}, 22 mg (0.7 mmol, 14 eq) of paraformaldehyde, and 15 mg (0.1 mmol, 2 eq) of N-pyridylglycine in 21 mL of *o*-DCB was sonicated for 30 min at r.t. and then heated at reflux under argon for 9 h under argon. The solution was washed with dist. water and dried over Na_2SO_4. The solvent was partially removed under reduced pressure. The residue was purified by flash column chromatography (eluant toluene, then toluene/triethylamine = 100:1). Solvent was evaporated under reduced pressure, residue was suspended in hexane, filtered, washed with hexane, dried under vacuum, affording 15 mg (37%) of the compound as a brown powder. ^{1}H-NMR (CD_2Cl_2, 400 MHz): δ (ppm) = 8.51 (d, *J* = 8.0 Hz, 2H), 7.20 (d, *J* = 4.0 Hz, 2H), 5.35 (s, 4H).

- [5,6]-*N*-(*p*-Pyridyl)-3,4-Sc_3N@*Ih*-C_{80} fulleropyrrolidine **4**:

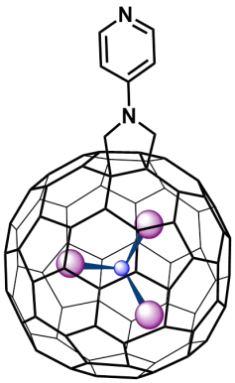

Argon was bubbled through a mixture of 3.0 mg of Sc_3N@*Ih*-C_{80} (2.7 µmol, 1 eq) and 15.0 mg of *N*-pyridylglycine (98 µmol, 35 eq) in 12 mL of *o*-DCB upon sonication for 15 min. After this time, the mixture was heated to reflux under argon for 10 minutes and a slurry of 15 mg of

paraformaldehyde (0.5 mmol, 185 eq) in 4 mL of *o*-DCB added in three portions every 15 min. Once the addition was complete the reaction mixture was heated to reflux for the next 12 h, following the reaction by HPLC (aliquots were taken every 15 minutes in order to estimate the ratio between the [5,6] and the [6,6] monoaddutcs). The reaction was stopped when the presence of the [6,6]-adduct was not observed anymore by HPLC. The resulting reaction mixture was then allowed to cool down to room temperature and charged onto silica gel column, eluting first with *o*-DCB in order to remove the unreacted $Sc_3N@I_h$-C_{80} fullerene, followed by a 10:1 mixture of *o*-DCB/NEt_3 in order to elute [5,6]-adduct **4**. The column chromatography fractions containing **4** were then reduced in volume under vacuum until reaching a volume of 10 mL. This latter solution was then washed with 15 mL of saturated solution of sodium bicarbonate (x 1 time) and 15 mL of distilled water (x 3 times). The resulting organic layer was dried over Na_2SO_4 and filtered. The filtrate was then reduced in volume until dryness and the obtained solid washed with diethyl ether and hexane, and the product finally dried under vacuum. Yield: 0.4 mg (12%; 20% on the basis of the recovered $Sc_3N@I_h$-C_{80} fullerene). HPLC retention time = 120 min;

A negligible formation of $Sc_3N@Ih$-C_{80} bisadducts could be detected by TLC on silica plates eluting with *o*-DCB/NEt_3 (10:1) once the reaction was stopped. These bisadducts were not detected by HPLC, probably, due to their long retention times. During the column chromatography, after the eluting mixture was changed to *o*-DCB/DMF 1:1, a negligible amount of a very polar fullerene-based compound was collected. The MALDI-TOF mass spectrometry spectrum of this column chromatography fraction confirmed, beside the presence of monoadduct **4**, the presence of $Sc_3N@Ih$-C_{80} bisadducts and minor amounts of product degradation, a degradation probably occurring during the mass spectrometry experiment.

^{1}H-NMR (CS_2:CD_2Cl_2 2:1, 400 MHz): δ (ppm) = 8.44 (m, 2H), 6.91 (m, 2H), 4.89 (d, *J* = 10.8 Hz, 2H), 3.82 (d, *J* = 10.8 Hz, 2H); MALDI-TOF MS (negative ionization, 9-nitroanthracene): found: 1228.9 *m/z,* calc. for $C_{87}H_8N_3Sc_3$, $[M]^-$: 1228.9, found: 1108.9 *m/z,* calc. for $C_{80}NSc_3$, $[M]^-$: 1108.9, found: 1165.9 *m/z,* calc. for $C_{83}H_7N_2Sc_3$, $[M]^-$: 1165.9; UV-vis (*o*-DCB): λ_{max} (nm) (log ε) = 316 (4.2), 372 (sh), 420 (sh), 471 (sh).

- [6,6]-*N*-(*p*-pyridyl)-3,4-Sc_3N@*Ih*-C_{80} fulleropyrrolidine:

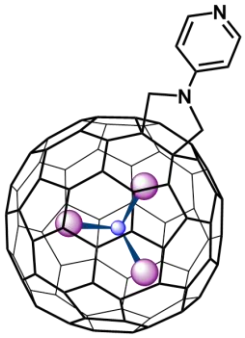

The [6,6]-adduct of *N*-(*p*-pyridyl)-3,4-Sc_3N@*Ih*-C_{80} fulleropyrrolidine, being the kinetically controlled product, was detected by HPLC as the major product 15 min after the reaction started, together with minor amounts of the [5,6]-adduct **4** (*i.e.*, [5,6]/[5,6] ratio 87/13). The isolation of the [6,6]-adduct was not performed due to its full conversion into the [5,6]-isomer **4** along the reaction course (12 h at reflux). However, the ^{1}H-NMR spectral features of the [6,6]-adduct were obtained from a 25/75 mixture of the [6,6]-/[5,6]-isomers sampled 6h after the beginning of the reaction. HPLC retention time = 160 min.; ^{1}H-NMR (700 MHz, CS_2/CD_2Cl_2 (2:1), capillary): δ (ppm) = 8.34-8.32 (m, 2H), 6.74-6.72 (m, 2H), 4.28 (s, 2H), 3.97 (s, 2H).

- 2,3,9,10,16,17,23,24-octakis-pentylsulfonyl Zn(II)Pc **2**:

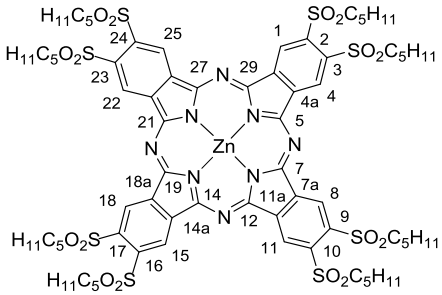

A mixture of 50 mg of 1,2-dicyano-4,5-bis(pentylsulfonyl)benzene **15** (0.126 mmol, 2.7 eq) and 8.5 mg of $Zn(OAc)_2$ (0.046 mmol, 1 eq) was heated to 145 ^{o}C in 1.2 mL of a *o*-DCB/DMF (5:1) mixture under argon atmosphere. The reaction completed in 26 h being followed by TLC. After being cooled to room temperature, the reaction mixture was evaporated to dryness under vacuum and the residue was triturated in hexane. The suspension was then filtered and the solid dissolved in 3 mL of $CHCl_3$. This chloroform solution was then charged onto silica gel column eluted with a mixture of $CHCl_3$/ethyl acetate (100:1) which allowed to obtain Zn(II)Pc **2** as a green

solid compound after solvent removal. Finally, electron-donating Zn(II)Pc **2** was recrystallized from DCM with a small addition of hexane, filtered, washed with cold hexane and dried under vacuum. Yield: 28 mg (54%). ^{1}H-NMR (400 MHz, THF-d_8): δ (ppm) = 10.36 (s, 8H; H-1, H-4, H-8, H-11, H-15, H-18, H-22, H-25), 4.25-3.91 (m, 16H; SO_2CH_2), 2.23-1.95 (m, 16H; $SO_2CH_2C\underline{H}_2$), 1.66-1.36 (m, 32H; $SO_2(CH_2)_2(C\underline{H}_2)_2$), 0.97-0.94 (m, 24H; CH_3); ^{13}C-NMR (THF-d_8, 100.6 MHz): δ (ppm) = 154.52 (8C; C-5, C-7, C-12, C-14, C-19, C-21, C-26, C-28), 142.37 (8C; C-2, C-3, C-9, C-10, C-16, C-17, C-23, C-24), 141.73 (8C; C-4a, C-7a, C-11a, C-14a, C-18a, C-21a, C-25a, C-28a), 128.95 (8C; C-1, C-4, C-8, C-11, C-15, C-18, C-22, C-25), 57.68 (8C; SO_2CH_2), 31.39 (8C; $SO_2CH_2\underline{C}H_2$), 23.00 (8C; $SO_2(CH_2)_2\underline{C}H_2$), 22.64 (8C; $SO_2(CH_2)_3\underline{C}H_2$), 14.04 (8C; CH_3); MALDI-TOF MS (positive mode, DCTB): found: 1648.3 *m/z,* calc. for $C_{72}H_{96}N_8O_{16}S_8Zn$, $[M]^+$: 1648.4, found: 1671.3 *m/z,* calc. for $C_{72}H_{96}N_8NaO_{16}S_8Zn$, $[M+Na]^+$: 1671.4, found: 3296.9 *m/z,* calc. for $C_{144}H_{192}N_{16}O_{32}S_{16}Zn_2$, $[2M]^+$: 3296.8, found: 3319.9 *m/z,* calc. for $C_{144}H_{192}N_{16}NaO_{32}S_{16}Zn_2$, $[2M+Na]^+$: 3319.8; UV-vis (THF): λ_{max} (nm) (log ε) = 683 (5.5), 659 (sh), 622 (4.6), 431 (sh), 378 (4.7), 341 (4.7).

- 3´-(N-Methyl-3´´,4´´[$La_2@I_h$-C_{80}]fulleropyrrolidine-2´´-yl)phenoxy-[1,2,3,4,8,9,10,11,15,16,17,18-dodecafluorosubphthalocyaninato]boron(III) **6**

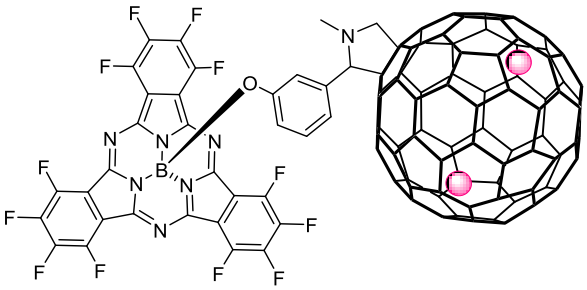

A mixture of $La_2@I_h$-C_{80} (2 mg, 1.6 µmol), F_{12}SubPc **9** (2.8 mg, 3.8 µmol) and N-methylglycine (5 mg, 56 µmol) was refluxed in 30 ml toluene for 85 min under argon atmosphere. Then, the mixture was separated by a two-step HPLC procedure, yielding 35% of **6** (based on consumed $La_2@I_h$-C_{80}).

^{1}H NMR (500 MHz, *o*-DCB-d_4): **6** (major conformer) δ= 6.17 (s (br), 1H), 6.08 (d (br), ^{2}J= 7.6 Hz, 1H), 4.41 (d, ^{2}J = 9.4Hz, 1H), 3.65 (s (br), 1H), 3.14 (d (br), ^{2}J = 8.9 Hz,1H), 2.82 (s (br), 1H); the phenyl protons are not identifiable in the ^{1}H NMR spectrum because of the overlap with the proton signals of *o*-DCB. However, their chemical shifts were determined according to the COSY

spectrum; **6'** (minor conformer) δ = 5.98 (s (br), 1H), 5.81 (d (br), ^2J = 8.0 Hz,1H), 4.10 (d, ^2J = 9.2Hz, 1H), 3.50 (s (br), 1H), 2.90 (d (br), ^2J = 8.9 Hz, 1H), 2.39 (s (br), 1H); the phenyl protons are not identifiable in the ^{1}H NMR spectrum because of the overlap with the proton signals of *o*-DCB. However, their chemical shifts were determined as δ = 7.30 ppm according to the COSY spectrum. MALDI-TOF MS (negative mode, TPB): found: 1997 *m/z,* calcd for $La_2C_{113}F_{12}H_{10}N_7OB$, $[M]^-$: 1996.9; UV-vis (toluene): λ_{max} (log ε) =300 (4.7), 574 (4.7).

- 3´-(N-Methyl-3´´,4´´-[La_2@I_h-C_{80}]fulleropyrrolidine-2´´-yl)phenoxy-[2,3,9,10,16,17-hexa(pentylsulfonyl)-subphthalocyaninato]boron(III) **8**

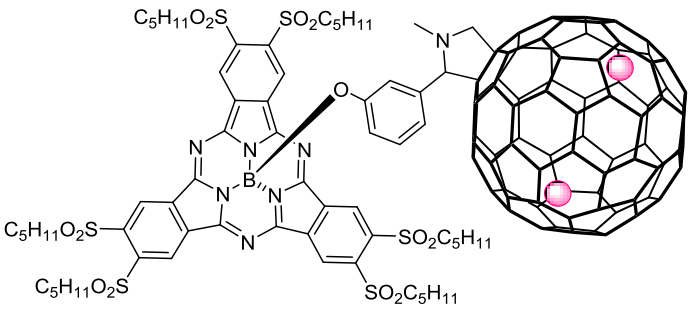

A mixture of La_2@C_{80} (2 mg, 1.6 µmol), $(SO_2C_5H_{11})_6$SubPc **10** (30.0 mg, 30.8 µmol) and N-methylglycine (5 mg, 56 µmol) was stirred in 15 ml of *o*-DCB at 115°C for 15 min under argon atmosphere. Then, **8** was isolated by one-step HPLC in a yield of 2% (based on consumed La_2@C_{80}).

MALDI-TOF MS (negative mode, TPB): found: 2585.1 *m/z,* calcd for $La_2C_{143}S_6H_{82}BN_7O_{13}$, $[M]^-$: 2585.3; UV-vis (toluene): λ_{max}=300, 530, 580 nm (study of the extinction coefficient of **8** was hampered by negligible amounts of isolated compound and its poor stability).

- 3´-(N-Methyl-3´´,4´´-[60]fulleropyrrolidin-2´´-yl)phenoxy-[1,2,3,4,8,9,10,11,15,16,17,18-dodecafluorosubphthalocyaninato]boron(III) **5**

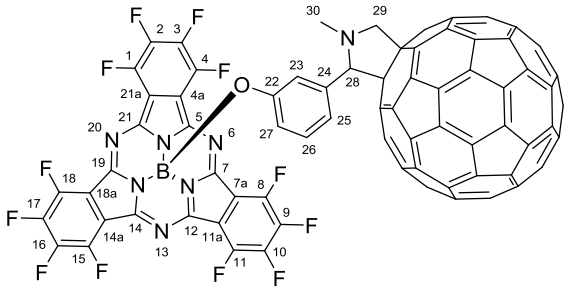

A mixture of (formylphenoxy) F_{12}SubPc **9** (22 mg, 0.03 mmol), C_{60} fullerene (43 mg, 0.06 mmol), N-methylglycine (8 mg, 0.09 mmol) in dry toluene (30 mL) was sonicated for approx. 10 min, until all the C_{60} got dissolved. The reaction mixture was stirred at reflux under argon atmosphere for 8 hours until no **9** was detected by TLC. The solution was then cooled to room temperature and poured onto a silica gel column, followed by the elution of products with toluene in the following sequence: unreacted C_{60}, monoadduct **5**, bisadducts. Final purification of **5** from bisadducts was achieved by using a Bio-Beads column and toluene as an eluting solvent. Rotary evaporation of toluene resulted in a purple residue, that was suspended in hexane, filtered, dried in vacuum, yielding **5** as a purple solid: 28 mg (63%). R_f = 0.8 (toluene).

^{1}H NMR (300 MHz, $CDCl_3$): δ (ppm) = 7.13-6.92 (m, 1H; H-25), 6.87-6.81 (dd, $J_o = J_{o'}$ = 7.6 Hz, 1H; H-26), 5.95-5.85 (m, 1H; H-23), 5.37-5.34 (d (br), J_o = 7.6 Hz, 1H; H-27), 4.91 (d (br), ^2J = 9.4 Hz, 1H; H-29), 4.54 (s (br), 1H; H-28), 4.13 (d, ^2J = 9.5 Hz, 1H; H-29'), 2.67 (s, 3H; H-30); ^{13}C NMR (100.6 MHz, $CDCl_3$): δ (ppm) = 155.9, 153.7, 152.9, 152.8, 148.5 (6C; C-5, C-7, C-12, C-14, C-19, C-21), 146.1, 145.9, 145.7, 145.5, 145.2, 145.1, 145.0, 144.3, 144.1, 143.7, 143.0, 142.8, 142.5, 141.8, 141.4, 141.3, 139.9, 139.1, 138.6, 135.8, 135.6, 135.4 (C_{60}^{sp2}, C-F), 129.6 (1C; C-26), 128.3 (1C; C-25), 123.3 (1C; C-27), 122.3 (1C; C-24), 118.4 (1C; C-23), 115.1 (6C; C-4a, C-7a, C-11a, C-14a, C-18a, C-21a), 82.5 (1C; C-28), 69.8 (1C; C-29), 68.7 (2C; C_{60}^{sp3}), 39.8 (1C; C-30); MALDI-TOF MS (negative mode, DCTB): found: 1497.1 *m/z,* calc. for $C_{93}H_{10}B_1F_{12}N_7O_1$, $[M]^-$: 1497.1; IR (KBr): ν (cm^{-1}) = 2924 (C-H), 2785, 1651 (C=N), 1605 (C=C), 1535, 1475 (C-F), 1381, 1265 (C-N), 1219, 1173, 1113 (C-C), 1063 (B-O), 970, 716, 600 (C-H), 530; UV-vis (toluene): λ_{max} (nm) (log ε) = 575 (4.9), 559 (sh), 534 (4.4), 520 (sh), 498 (sh), 435, 312 (4.8).

- 3´-(N-Methyl-3´´,4´´-[60]fulleropyrrolidin-2´´-yl)phenoxy-[2,3,9,10,16,17-hexa(pentylsulfonyl)-subphthalocyaninato]boron(III) **7**

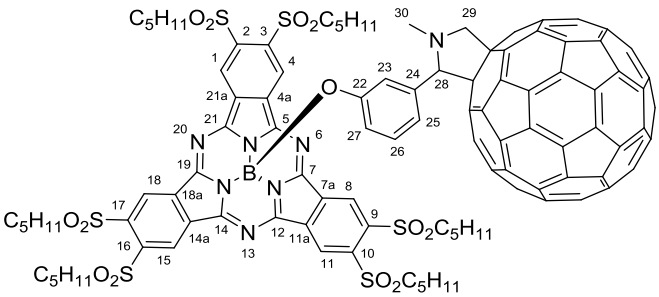

A mixture of (formylphenoxy) $(SO_2C_5H_{11})_6$SubPc **10** (37 mg, 0.03 mmol), C_{60} fullerene (43 mg, 0.06 mmol), N-methylglycine (8 mg, 0.09 mmol) in dry toluene (40 mL) was sonicated for approx. 10 min, until all the C_{60} got dissolved. The reaction mixture was stirred at reflux under argon atmosphere for 2 hours until no **10** was detected by TLC. The solution was then cooled to room temperature and poured onto a silica gel column, followed by the elution of products with a mixture of toluene-dicloromethane (1:1 vol), containing 0,8 % vol of ethanol, in the following sequence: unreacted C_{60}, monoadduct **7**, bisadducts. Due to high instability of sulfonyl-substituted SubPc on silica gel, an additional chromatography on cyanopropyldichlorosilyl-modified silica gel as a solid support, eluting with a mixture of toluene-dicloromethane (1:1 vol), was needed to eliminate SubPc decomposition products. Final purification from bisadducts was achieved by using a Bio-Beads column and toluene-dicloromethane (1:1) as an eluting mixture. Rotary evaporation of solvents resulted in a violet residue, that was suspended in hexane, filtered, dried in vacuum, yielding **7** as a violet solid: 14 mg (24%). R_f = 0.5 (toluene-ethylacetate = 3:1, vol).

^{1}H NMR (500 MHz, $CDCl_3$): δ (ppm) = 9.75-9,74 (ss, 6H; H-1, H-4, H-8, H-11, H-15, H-18), 7.1-6.9 (m, 1H; H-25), 6.88-6.70 (m, 1H; H-26), 5.90-5.60 (m, 1H; H-23), 5.50-5.20 (m, 1H; H-27), 4.88 (d (br), ^2J = 7.90 Hz, 1H; H-29), 4.52 (s (br), 1H; H-28), 4.12 (d (br), ^2J = 9.1 Hz, 1H; H-29'), 3.84-3.58 (m, 12H; $SO_2C\mathbf{H_2}$), 2.61 (s, 3H; H-30), 1.99-1.82 (m, 12H; $SO_2CH_2C\mathbf{H_2}$), 1.46-1.26 (m, 24H; $SO_2(CH_2)_2(\mathbf{CH_2})_2$), 0.88-0.85 (m, 18H; $SO_2(CH_2)_4\mathbf{CH_3}$); ^{13}C NMR (75.5 MHz, $CDCl_3$): δ (ppm) = 156.3, 153.9, 153.3, 153.1, 152.2 (6C; C-5, C-7, C-12, C-14, C-19, C-21), 152.1 (1C; C-22), 146.2 (6C; C-2, C-3, C-9, C-10, C-16, C-17), 141.9, 141.1, 139.6, 139.1, 138.7, 137.9, 132.8 (6C; C-4a, C-7a, C-11a, C-14a, C-18a, C-21a), 129.0 (1C; C-26), 128.9 (1C; C25), 128.3, 125.4, 124.7 (1C; C-27), 118.7 (1C; C-23), 82.5 (1C; C-28), 69.7 (1C; C-29), 68.9 (2C; C_{60}^{sp3}), 57.39 (6C; SO_2CH_2), 39.9 (1C; C-30), 30.6, 22.2, 22.0 (18C; $SO_2CH_2(\mathbf{CH_2})_3$), 13.9 (6C; CH3); MALDI-TOF MS (negative mode, DCTB): found:

2067.4 *m/z,* calc. for $C_{123}H_{82}B_1N_7O_{13}S_6$, $[M]^-$: 2067.4; HR MALDI-TOF MS (DCTB, PMMANa2100, NaI) found: 2067.4380 *m/z,* calc. for $C_{123}H_{82}B_1N_7O_{13}S_6$, $[M]^+$: 2067.4400; found: 2090.4274 *m/z,* calc. for $C_{123}H_{82}B_1N_7Na_1O_{13}S_6$, $[M+Na]^+$: 2090.4298; IR (KBr): *v* (cm^{-1}) = 2959, 2866 (C-H), 1605 (C=C), 1466, 1383, 1312, 1285, 1177 (S=O), 1149, 1097 (B-O), 710, 652; UV-vis (toluene): λ_{max} (log *ε*) = 582 (5.0), 566 (sh), 544 (sh), 534 (sh) 436, 314 (4.9).

- 3'-Formylphenoxy-[1,2,3,4,8,9,10,11,15,16,17,18-dodecafluorosubphthalocyaninato]boron(III) **9**

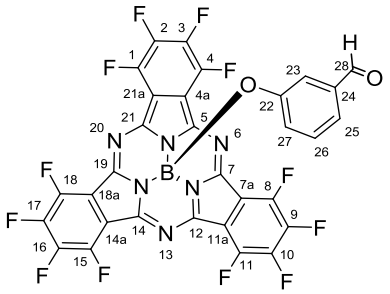

A mixture of F_{12}SubPcCl **13** (130 mg, 0.2 mmol) and silver (I) trifluoromethanesulfonate (AgOTf) (77 mg, 0.3 mmol) were stirred in dry toluene (3 mL) at room temperature under argon atmosphere protected from light. After 12 h, when no unreacted **13** was detected by TLC, 3-hydroxybenzaldehyde (49 mg, 0.4 mmol) was added under argon flow, following by the addition of N,N-diisopropylethylamine (DIPEA) (52 µL, 0.3 mmol) via syringe. The stirring was continued at 80 ^oC under argon atmosphere, and stopped after 4 h when no intermediate SubPcOTf was observed by TLC.[118] The reaction mass was diluted with 20 mL of toluene, passed through celite pad to eliminate impurities of inorganic salts, and thoroughly collected with toluene. Resulted solution was reduced in volume to approx. 8mL and charged onto silica gel column. Elution with a mixture of toluene-ethylacetate = 3:1 (vol) and evaporation of solvents resulted in a dark brown residue that was suspended in hexane, filtered, dried in vacuum, yielding 125 mg of **9** (85%). R_f = 0.5 (hexane-ethylacetate = 6:1, vol).

^{1}H NMR (300 MHz, $CDCl_3$): *δ* (ppm) = 9.59 (s, 1H; H-28), 7.20 (dd, J_o = 7.6 Hz, J_m = 1.6 Hz, 1H; H-25), 6.98 (dd, J_o = 7.6 Hz, $J_{o'}$ = 8.2 Hz, 1H; H-26), 5.91 (dd, J_m = $J_{m'}$ = 1.5 Hz, 1H; H-23), 5.56 (dd, $J_{o'}$

[118] SubPcs with electron-withdrawing groups are known to require longer reaction time and higher reaction temperatures in reactions of nucleophilic substitution at boron atom, compared to non-substituted SubPcs.

= 8.2 Hz, J_m = 1.6 Hz, 1H; H-27); ^{13}C NMR (75.5 MHz, $CDCl_3$): δ (ppm) = 191.3 (1C; C-28), 152.2 (1C; C-22), 148.6 (6C; C-5, C-7, C-12, C-14, C-19, C-21), 144.7-144.4 (m, 6C; C-F), 141.3-140.9 (m, 6C; C-F), 137.8 (1C; C-24), 130.2 (1C; C-26), 124.94, 124.87 (2C; C-25, C-27), 119.1 (1C; C-23), 115.1-114.6 (m, 6C; C-4a, C-7a, C-11a, C-14a, C-18a, C-21a); MALDI-TOF MS (positive mode, DCTB): found: 732.1 *m/z,* calc. for $C_{31}H_5B_1F_{12}N_6O_2$, $[M]^+$: 732.0; IR (KBr): ν (cm^{-1}) = 2947, 1697 (C=N), 1533, 1483 (C-F), 1387, 1269, (C-N), 1221, 1163, 1115, 1088 (B-O), 970, 714, 609; UV-vis (toluene): λ_{max} (nm) (log ε) = 574 (4.9), 558 (sh), 534 (4.4), 520 (sh), 499 (sh), 306 (4.5).

- 3'-Formylphenoxy-[2,3,9,10,16,17-hexa(pentylsulfonyl)-subphthalocyaninato]boron(III) **10**

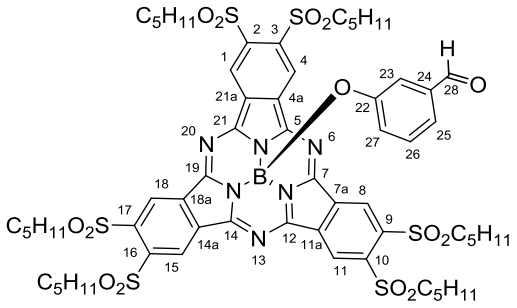

A mixture of $(SO_2C_5H_{11})_6$SubPcCl **14** (865 mg, 0.7 mmol) and Ag triflate (257 mg, 1.0 mmol) were stirred in dry toluene (10 mL) at room temperature under argon atmosphere protected from light. After 12 h, some unreacted **14** could be still detected by TLC. Nevertheless, 3-hydroxybenzaldehyde (171 mg, 1.4 mmol) was added under argon flow, following by the addition of DIPEA (174 µL, 1.0 mmol) via syringe. The stirring was continued at 115 ^{o}C under argon atmosphere, and stopped after 1 h when no unreacted **14** or intermediate SubPc triflate were observed by TLC.[119] The reaction mass was diluted with 20 mL of dichloromethane, passed through celite pad, and thoroughly collected with dichloromethane. Resulted solution was rotary evaporated till dryness. The residue was dissolved in 25 mL of dichloromethane and charged onto a silica gel column. Dichloromethane containing 0.1% of ethanol was used as an eluting solvent, affording the compound as a main zone. Additional purification of the compound on Bio-Beads, eluting with toluene, afforded pure **10**, allowing the separation of the main compound

[119] Presence of six electron-withdrawing sulfonylpentoxy groups on the periphery of SubPc **14** hampers nucleophilic substitution of the axial group at the boron atom even stronger than twelve fluorine substituents of **13**, causing the need of using of high temperatures. Worthy to note, that the reaction proceeds as well at lower temperatures during longer times, giving lower yields of the product of nucleophilic substitution and higher amount of side- and decomposition products.

from (sulfonyl)SubPc decomposition products formed on silica gel. Evaporation of solvents resulted in a magneta-color solid that was suspended in hexane, filtered, dried in vacuum, yielding 125 mg of **10** (25%). R_f = 0.5 (dichloromethane-ethanol, 0.1 vol %).

^{1}H NMR (300 MHz, $CDCl_3$): δ (ppm) = 9.82 (s, 6H; H-1, H4, H-8, H-11, H-15, H-18), 9.66 (s, 1H; H-28), 7.23 (dd (br), 1H; H-25), 7.01 (dd, J_o = 8.2 Hz, $J_{o'}$ = 8.6 Hz, 1H; H-26), 5.93 (dd (br), J_m = 7.6 Hz, $J_{m'}$ = 1.6 Hz, 1H; H-23), 5.59 (dd, J_o = 8.2 Hz, J_m = 1.6 Hz, 1H; H-27); ^{13}C NMR (75.5 MHz, $CDCl_3$): δ (ppm) = 191.4 (1C; C-28), 152.31 (6C; C-5, C-7, C-12, C-14, C-19, C-21), 152.28 (1C; C-22), 141.96 (6C; C-2, C-3, C-9, C-10, C-16, C-17), 138.02 (1C; C-24), 132.89 (6C; C-4a, C-7a, C-11a, C-14a, C-18a, C-24a), 130.49 (1C; C-26), 129.13 (2C; C-25), 125.48 (6C; C-1, C-4, C-8, C-11, C-15, C-18), 125.05 (1C; C-27), 118.57 (2C; C-23), 57.49 (6C; SO_2CH_2), 30.66, 22.60, 22.39 (18C; SO_2CH_2(**CH_2**)$_3$), 14.04 (6C; CH3); MALDI-TOF MS (positive mode, DCTB): found: 1320.4 *m/z,* calc. for $C_{61}H_{77}B_1N_6O_{14}S_6$, $[M]^+$: 1320.4; IR (KBr): ν (cm^{-1}) = 2959, 2935 (C-H), 1697, 1616 (C=C), 1466, 1385, 1315, 1292, 1177 (S=O), 1140, 1068 (B-O), 918, 710, 652; UV-vis (toluene): λ_{max} (nm) (log ε) = 581 (5.1), 566 (sh), 536 (4.5), 311 (4.7).

- Phenoxy-[2,3,9,10,16,17-hexa(pentylsulfonyl)-subphthalocyaninato]boron(III) **12**

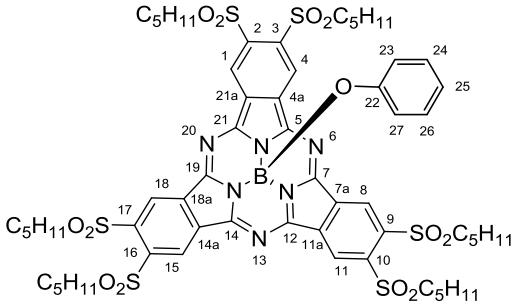

A mixture of $(SO_2C_5H_{11})_6$SubPcCl **14** (494 mg, 0.4 mmol) and AgOTf (154 mg, 0.6 mmol) were stirred in dry toluene (7 mL) at room temperature under argon atmosphere protected from light. After 12 h, some unreacted **14** could be still detected by TLC. Nevertheless, phenol (75 mg, 0.8 mmol) was added under argon flow, following by the addition of DIPEA (91 µL, 0.6 mmol) via syringe. The stirring was continued at 115 ^{o}C under argon atmosphere, and stopped after 1 h when no unreacted **14** or intermediate SubPcOTf were observed by TLC. The reaction mass was diluted with 20 mL of dichloromethane, passed through celite pad, and thoroughly collected with dichloromethane. Resulted solution was rotary evaporated till dryness. The residue was

dissolved in 15 mL of dichloromethane and charged onto a silica gel column. Dichloromethane containing 0.1% of ethanol was used as an eluting solvent, affording the compound as a main zone. Additional purification of the compound on Bio-Beads, eluting with toluene, allowed pure **12**, allowing the separation of the main compound from (sulfonyl)SubPc decomposition products formed on silica gel. Partial evaporation of a solvent and further precipitation of the compound with hexane afforded the compound in the form of magneta-color single crystals suitable for X-Ray diffraction analysis. Crystalline solid was filtered from hexane, dried in vacuum, yielding 181 mg of **12** (35%). R_f = 0.8 (dichloromethane-ethanol, 0.1 vol %).

^{1}H NMR (300 MHz, $CDCl_3$): δ (ppm) = 9.80 (s, 6H; H-1, H-4, H-8, H-11, H-15, H-18), 6.82 (dd, J_o = 7.1 Hz, $J_{o'}$ = 7.6 Hz, 2H; H-24), 6.73 (t, J_o = 7.6 Hz, 1H; H-25), 5.36 (d, J_o = 7.1 Hz, 2H; H-23), 3.90-3.70 (m, 12H; SO_2CH_2), 2.0-1.73 (m, 12H; SO_2CH_2**CH_2**), 1.47-1.25 (m, 24H; $SO2(CH_2)_2$(**CH_2**)$_2$), 0.88-0.83 (m, 18H; CH_3); ^{13}C NMR (75.5 MHz, $CDCl_3$): δ (ppm) = 152.19 (6C; C-5, C-7, C-12, C-14, C-19, C-21), 151.45 (1C; C-22), 141.81 (6C; C- 2, C-3, C-9, C-10, C-16, C-17), 132.94 (6C; C-4a, C-7a, C-11a, C-14a, C-18a, C-24a), 129.81 (2C; C-24), 129.08 (6C; C-1, C-4, C-8, C-11, C-15, C-18), 123.11 (1C; C-25), 118.95 (2C; C-23), 57.51 (6C; SO_2CH_2), 30.67, 22.64, 22.40 (18C; SO_2CH_2(**CH_2**)$_3$), 14.03 (6C; CH_3); MALDI-TOF MS (positive mode, DCTB): found: 1292.4 *m/z,* calc. for $C_{60}H_{77}B_1N_6O_{13}S_6$, $[M]^+$: 1292.4; HR MALDI-TOF MS (DCTB, PPGNa1000, PPGNa2000) found: 1292.3963 *m/z,* calc. for $C_{60}H_{77}B_1N_6O_{13}S_6$, $[M]^+$: 1292.3971; found: 1315.3896 *m/z,* calc. for $C_{60}H_{77}B_1Na_1N_6O_{13}S_6$, $[M+Na]^+$: 1315.3868; IR (KBr): ν (cm^{-1}) = 2959, 2935 (C-H), 1744, 1593 (C=C), 1464, 1385, 1310, 1283, 1177, 1149 (S=O), 1097 (B-O), 710, 640, 536; UV-vis (toluene): λ_{max} (nm) (log ε) = 581 (5.1), 563 (sh), 534 (4.5), 505 (sh), 308 (4.7).

- Chloro-[2,3,9,10,16,17-hexa(pentylsulfonyl)-subphthalocyaninato]boron(III) **14**

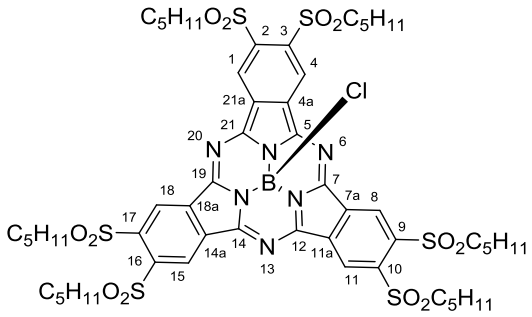

A 1M BCl_3 in *p*-xylene (10 mL, 10 mmol) was added to a 1,2-dicyano-4,5-bis(pentylsulfonyl)benzene **15** (3.9 g, 10 mmol), and the reaction mixture was stirred vigorously

at reflux for 30 min under argon atmosphere. Then the reaction was stopped, allowed to reach room temperature and flushed with argon. Xylene was rotary evaporated till dryness. The dark purple residue was dissolved in 10 mL of dichloromethane and subjected to column chromatography on silica gel using a dichloromethane containing 0.5% of ethanol as an eluent. Rotary evaporation of solvents and precipitation of the product with hexane gave a dark blue solid that was filtered, washed with hexane, dried in vacuum, yielding the pure compound **14** in an amount of 2.7 g (65%). R_f = 0.8 (dichloromethane-ethanol, 0.1 vol %).

^{1}H NMR (300 MHz, $CDCl_3$): δ (ppm) = 9.86 (s, 6H; H-1, H-4, H-8, H-11, H-15, H-18), 3.92-3.72 (m, 12H; SO_2CH_2), 1.97-1.73 (m, 12H; $SO_2CH_2\mathbf{CH_2}$), 1.47-1.25 (m, 24H; $SO2(CH_2)_2(\mathbf{CH_2})_2$), 0.88-0.83 (m, 18H; CH_3); ^{13}C NMR (75.5 MHz, $CDCl_3$): δ (ppm) = 150.70 (6C; C-5, C-7, C-12, C-14, C-19, C-21), 141.88 (6C; C-2, C-3, C-9, C-10, C-16, C-17), 132.81 (6C; C-4a, C-7a, C-11a, C-14a, C-18a, C-24a), 129.05 (6C; C-1, C-4, C-8, C-11, C-15, C-18), 57.31 (6C; SO_2CH_2), 30.47, 22.51, 22.20 (18C; $SO_2CH_2(\mathbf{CH_2})_3$), 13.84 (6C; CH_3); MALDI-TOF MS (positive mode, DCTB): found: 1234.3 *m/z,* calc. for $C_{54}H_{72}B_1Cl_1N_6O_{12}S_6$, $[M]^+$: 1234.3[120]; IR (KBr): ν (cm^{-1}) = 2959, 2947 (C-H), 2866, 1744, 1466 (C=C), 1383, 1312, 1298, 1177, 1149 (S=O), 798, 706, 648, 532; UV-vis (toluene): λ_{max} (nm) (log ε) = 583 (5.0), 565 (sh), 539 (4.4), 315 (4.6).

- 1,2-Dicyano-4,5-bis(pentylsulfonyl)benzene **15**

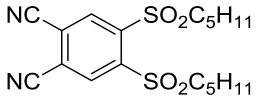

1,2-Dicyano-4,5-bis(pentylthio)benzene **16** (3 g, 9 mmol) was dissolved in 55 mL of acetic acid at 90 °C. A total amount of 43 mL of 33% H_2O_2 was added to the stirred solution as 5 mL portions every 15 min in the course of 2 h. The resulting turbid mixture was stirred at 90 ^{o}C for 2 h, until no **16** could be detected by TLC. After that, the reaction was stopped and allowed to cool to room temperature. The reaction mass was diluted with 100mL of brine, and the organic phase was extracted with 75 mL of dichloromethane (×2). Joined organic layer was washed with 150 mL of H_2O and 150 mL brine in a separation funnel. After that, it was dried over Na_2SO_4, filtered,

[120] The most intense peak corresponds to the $[M]^+$ ion, followed by the [M – axial group]$^+$ ion. Its observation in MS experiments (i.e. the loss of the axial group giving $SubPc^+$ cation) together with the [M – axial group + OH]$^+$ ion (i.e. $SubPcOH^+$) is common for chlorosubstituted SubPcs.

rotary evaporated till dryness, affording a crude product as yellow oil. Column chromatography on silica gel with a mixture of dichloromethane-ethyl acetate (30:1, vol) yielded yellow-pale oil. Finally, the product was recrystallized from 40 mL of methanol, filtered, dried under vacuum. Compound **15** was obtained as a crystalline pale-yellow solid: 3.03 g (85%).

M. p.: 75 °C. ^{1}H NMR (300 MHz, $CDCl_3$): δ (ppm) = 8.68 (s, 2H), 3.69-3.63 (m, 2H; SO_2CH_2), 1.81-1.71 (m, 2H; $SO_2CH_2\mathbf{CH_2}$), 1.46-1.28 (m, 8H; $SO_2(CH_2)_2(\mathbf{CH_2})_2$), 0.92-0.87 (m, 6H; CH_3); ^{13}C NMR (75.5 MHz, $CDCl_3$): δ (ppm) = 144.61, 137.60, 121.29, 113.19, 57.26, 30.36, 29.83, 22.13, 13.77.

- 1,2-Dicyano-4,5-bis(penylthio)benzene **16**

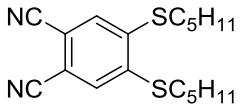

4,5-Dichloro-1,2-dicyanobenzene (1 g, 5 mmol), dry K_2CO_3 (2.0 g, 15 mmol), and 10 mL of dimethylformamide (DMF) were placed in a 50-mL round-bottom flask, equipped with a magnetic stirrer, rubber seal, and globe. After that, 1-pentanethiol (1.5 mL, 12 mmol) was added via syringe, and the reaction was stirred at 100 ^{o}C for 4 hours when no precursor phthalonitrile or a product of mono-substitution could be detected by TLC. Reaction mass was allowed to reach r.t., and further poured into 50 mL of water. Formed precipitate was filtered, washed with water and air dried. Crude product was then dissolved in 50 mL of dichloromethane and filtered. Dichloromethane was rotary evaporated in a presence of celite till dryness. Resulting solid was used to charge the column filled with silica gel. The product was eluted with a mixture of hexane-ethylacetate (10:1, vol). After solvents were rotary evaporated, the product was recrystallized from methanol, filtered and vacuum dried. Compound **16** was obtained as a white crystalline solid: 1.5 g (85%).

Mp: 64 °C. ^{1}H NMR (300 MHz, $CDCl_3$): δ (ppm) = 7.42 (s, 2H), 3.01-2.99 (m, 2H; SO_2CH_2), 1.78-1.73 (m, 2H; $SO_2CH_2\mathbf{CH_2}$), 1.48-1.39 (m, 8H; $SO_2(CH_2)_2(\mathbf{CH_2})_2$), 0.94-0.89 (m, 6H; CH_3); ^{13}C NMR (75.5 MHz, $CDCl_3$): δ (ppm) = 144.39, 128.29, 115.81, 111.22, 32.85, 31.14, 27.90, 22.32, 14.00.

Chapter 2

Pc/C_{60} systems: from dimers to multicomponent arrays

2.1 Introduction

The preparation of multicomponent architectures in which organic compounds present a high degree of order due to very specific functionalization is highly desirable and represents a key issue within the fast-growing fields of nanoscience and nanotechnology.[121] In this context, the utilization of self-assembly appears as an attractive and efficient strategy for the construction of such ordered structures as it can allow preparation of complex, multifunctional systems in an efficient and controlled way through the use of noncovalent interactions. On the other hand, the organic compounds with π-conjugated systems, such as Pcs and carbon nanoforms, are ideal candidates for the construction of covalent systems due to their exceptional chemical versatility.

In 1997, the first Pc-C_{60} conjugate was reported in which the macrocycle and the spherical carbon nanostructure were covalently linked through a Diels-Alder reaction between a Ni(II)Pc bearing a butadiene fragment and C_{60} fullerene.[122] Since then, many covalent and supramolecular Pc-C_{60} systems have been prepared and studied. In these ensembles, parameters such as (i) the electronic features of the macrocycle, (ii) the nature of the spacer connecting the Pc and C_{60} moieties in covalently linked systems (short/long, rigid/flexible, conjugated/ nonconjugated), and (iii) the supramolecular interaction motif(s) used to assemble the two moieties in noncovalent Pc-C60 systems have been varied, with the aim of rationalizing how these changes affect the formation and recombination of the photogenerated charged species.[123]

Since that first report, a large number of covalently-linked Pc-C_{60} systems (*i.e.*, dyads, triads, tetrads, etc.) have been reported. A compound frequently used for the preparation of several of these Pc-C_{60} systems is tris(*tert*-butyl)iodo Zn(II)Pc, which has established itself as an interesting building block for the preparation of such D-A systems (Scheme 2.1). It can be prepared *via* statistical condensation of 4-*tert*-butylphthalonitrile and 4-iodophthalonitrile using zinc(II)acetate as templating reagent. There are several factors that have contributed to the extensive use of tris(*tert*-butyl)iodo Zn(II)Pc for the preparation of D-A Pc-based systems such as the possibility to

---

121 a) Special Issue on "Supramolecular Chemistry and Self-Assembly". *Science* **2002**, 295, 2395-2421; b) Special Issue on "Supramolecular Approaches to Organic Electronics and Nanotechnology". *Adv. Mater*. **2006**, 18, 1227-1329.

122 K. Durr, S. Fiedler, T. Linssen, A. Hirsch, M. Hanack. *Chem. Ber.* **1997**, 130, 1375-1378.

123 a) G. Bottari, G. de la Torre, D. M. Guldi, T. Torres. *Chem. Rev.* **2010**, 110, 6768-6816; b) G. Bottari, G. de la Torre, T. Torres. *Acc. Chem. Res*., **2015**, 48, 900-910.

prepare it in reasonable yields (> 20%) and its easy purification. Moreover, the *tert*-butyl groups that decorate the macrocycle periphery confer to this molecule high solubility, and help to reduce the strong self-aggregation tendency typical of the Pcs. Besides the above mentioned points, probably the most important feature this precursor is the presence of an iodine atom directly attached to the Pc framework, which allows the easy functionalization of this macrocycle with, virtually, any functional group through the use of metal-catalyzed reactions.

Among a vast variety of inspiring examples of Pc-C_{60} dyads, we will center on the one reported relatively recently. Structurally-rigid, triple-bond-containing Pc-C_{60} dyad has been prepared starting from tris(*tert*-butyl)iodo Zn(II)Pc (Scheme 5).[124] Palladium-catalyzed Sonogashira coupling reaction between tris(*tert*-butyl)iodo Zn(II)Pc and ethynyl benzaldehyde has been used to directly attach a triple-bond group to the Pc ring, resulting in the formation of formyl Zn(II)Pc in 92% yield.

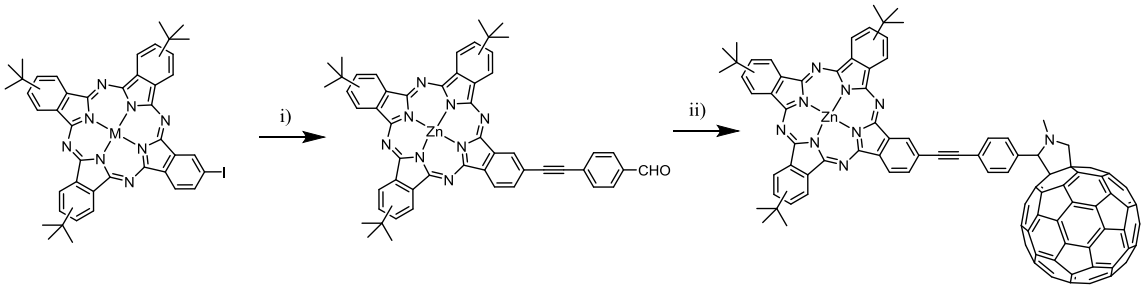

Scheme 2.1. Synthesis of the structurally-rigid, Pc-C_{60} conjugate. i) 4-ethynylbenzaldehyde, CuI, $PdCl_2(PPh_3)_2$, NEt_3, dry toluene, reflux. ii) C_{60} fullerene, *N*-methylglycine, dry toluene, reflux.

This latter compound was then reacted under the standard Prato reaction conditions, affording Pc-C_{60} dyad in 36% yield. Surprisingly, this dyad was able, when drop casted from toluene solutions, to self-organize on highly ordered pyrolytic graphite (HOPG) and graphite-like (i.e., graphite oxide) surfaces giving rise to the formation of micrometer long, fibers and films as revealed by AFM experiments. Conductive AFM measurements were carried out on such supramolecular fibers and films in order to address the electrical properties of these nanostructures obtaining electrical conductivity values as high as 30 μA for bias voltages ranging from 0.30 to 0.55 V. Control experiments revealed that the high electrical conductivity values

[124] G. Bottari, D. Olea, C. Gomez-Navarro, F. Zamora, J. Gomez-Herrero, T. Torres, *Angew. Chem. Int. Ed.* **2008**, *47*, 2026-2031.

observed for the solid-supported, self-assembled Pc-C_{60} conjugate are strongly related to the supramolecular order of the dyad within the nanostructures.

A hint about possible composition of the fibers could be taken from another recent work reporting on a similar system. Thus, Pc-C_{60} dyad with a short and semiflexible bridge has also been used in a Pc-C_{60} dyad, which forms a liquid crystalline material that exhibits efficient photocurrent generation and good short-range and long-range ambipolar charge transport properties.[125] Interestingly, preheated samples of this dyad showed a 5-fold increase in the charge mobility with respect to the unheated material, a phenomenon attributed to a better alignment of the Zn(II)Pc-C_{60} columns upon thermal treatment, which, in turn, may facilitate the charge transport.

2.1.1 Background and objectives

During the last decade, the preparation and study of C_{60} fullerene bisadducts has gained increasing interest in the field of fullerene chemistry and materials science.[126] In this context, an important issue related to the preparation of such derivatives is how to promote their regio- or, in some cases, stereocontrolled synthesis, not a trivial task considering that C_{60} presents 30 reactive double bonds distributed over its spherical structure. In one of the simplest cases such as the cycloaddition to C_{60} of two highly symmetrical and non-prochiral chemical species, a maximum of eight C_{60} bisadduct regioisomers could theoretically form accordingly to the eight C_{60} addition patterns (Figure 2.1a)[127], providing that additions occur exclusively on [6,6]-bonds. However, the isolation of these bisadducts is often difficult, necessarily involving the use of tedious HPLC chromatographic separation.

An important step forward towards the controlled synthesis of C_{60} bisadducts has been made possible by the use of the tether-directed remote functionalization introduced by Diederich and

125 H. Hayashi, W. Nihashi, T. Umeyama, Y. Matano, S. Seki, Y. Shimizu, H. Imahori. *J. Am. Chem. Soc.* **2011**, 133, 10736-10739.

126 a) R. K. M. Bouwer, J. C. Hummelen, *Chem. Eur. J.* **2010**, 16, 11250-11253; b) Meng, X., Zhang, W., Tan, Z., Du, C., Li, C., Bo, Z., Li, Y., Yang, X., Zhen, M., Jiang, F., Zheng, J., Wang, T., Jiang, L., Shu, C., Wang, C. *Chem. Commun.* **2012**, 48, 425-427; c) Kitaura, S., Kurotobi, K., Sato, M., Takano, Y., Umeyama, T., Imahori, H. *Chem. Commun.* **2012**, 48, 8550-8552; d) Miller, N. C., Sweetnam, S., Hoke, E. T., Gysel, R., Miller, C. E., Bartelt, J. A., Xie, X., Toney, M. F. & McGehee, M. D. *Nano Lett.* **2012**, 12, 1566-1570; e) Zhang, C., Chen, S., Xiao, Z., Zuo, Q., Ding, L. *Org. Lett.* **2012**, 14, 1508-1511; f) Li, Y. *Chem.-Asian J.* **2013**, 8, 2316-2328; g) He, Y., Chen, H.-Y., Hou, J., Li, Y. *J. Am. Chem. Soc.* **2010,** 132, 1377-1382.

127. Hirsch, A., Lamparth, I. & Karfunkel, H. R. *Angew. Chem. Int. Ed. Engl.* 1994, 33, 437-438.

co-workers[128]. This synthetic methodology consists in covalently linking the two residues that will ultimately add to C_{60} by a spacer which structural and conformational features lead to the preferred formation of certain C_{60} bisadducts (Figure 2.1b)[129]. This strategy, used almost exclusively in cyclopropanation reactions, has been successfully employed for the preparation of C_{60} bisadducts with excellent regioselectivity and, in some cases, high stereoselectivity[130]. Using this methodology, sterically-demanding *cis*-1 C_{60} bisadducts, usually obtained in very low-yield by untethered reactions, have also been obtained[131].

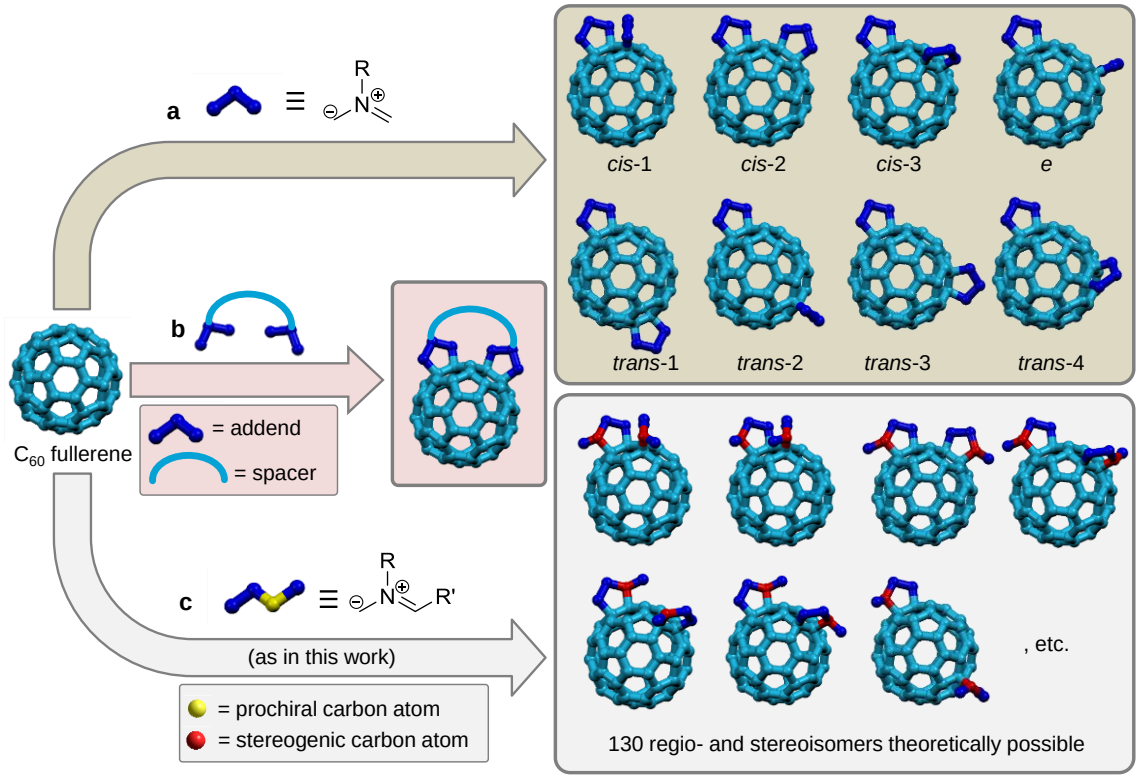

Figure 2.1. Bisaddition of tethered/untethered, prochiral/non-prochiral chemical species to C_{60} fullerene.

---

128. Isaacs, L., Haldimann, R. F. & Diederich, F. Tether-directed remote functionalization of buckminsterfullerene - Regiospecific hexaadduct formation. *Angew. Chem. Int. Ed. Engl.* **33,** 2339-2342 (1994).

129. a) Thilgen, C., Sergeyev. S.,Diederich, F. *Top. Curr. Chem*. **2004**, 248, 1-61; b) Nakamura, Y., Asami, A., Ogawa, T., Inokuma, S. & Nishimura, J. *J. Am. Chem. Soc.* **2002**, 124, 4329-4335; c) Reuther, U., Brandmuller, T., Donaubauer, W., Hampel, F.,Hirsch, A. *Chem. Eur. J.* **2002**, 8, 2261-2273; d) Prato, M.,Maggini, M. *Acc. Chem. Res.* **1998**, 31, 519-526; e) Diederich, F., Kessinger, R. *Acc. Chem. Res.* **1999**, 32, 537-545; f) Hino, T.,Saigo, K. *Chem. Commun.* **2003**, 402-403; g) Burley Glenn, A., Keller Paul, A., Pyne Stephen, G.,Ball Graham, E. *J. Org. Chem.* **2002**, 67, 8316-30.

130. Isaacs, L., Diederich, F. & Haldimann, R. F. *Helv. Chim. Acta* **1997,** 80, 317-342.

131. a) Da Ros, T., Prato, M., Lucchini, V. Additions of azomethine ylides to fullerene C_{60} assisted by a removable anchor. *J. Org. Chem.* **2000**, 65, 4289-4297; b) Izquierdo, M., Cerón, M. R., Alegret, N., Metta-Magaña, A. J., Rodríguez-Fortea, A., Poblet, J. M., Echegoyen, L. *Angew. Chem. Int. Ed.* **2013**, 52, 12928-12931; c) Cerón, M. R., Izquierdo, M., Aghabali, A., Valdez, J. A., Ghiassi, K. B., Olmstead, M. M., Balch, A. L., Wudl, F., Echegoyen, L. *J. Am. Chem. Soc.* **2015**, 137, 7502-7508.

Significantly more difficult, and to the best of our knowledge unprecedented, is the possibility to carry out a controlled synthesis of C_{60} bisadducts using untethered and prochiral (or low-symmetry) residues. In this case, a large number of C_{60} bisadducts could be formed with no regio- and stereocontrol due to the lack of any bias able to "guide" the cycloaddition of the two residues at specific positions of the C_{60} cage. For example, in the case of the 1,3 dipolar cycloaddition reaction of untethered, prochiral azomethine ylides to C_{60} fullerene – one of the most straightforward C_{60} functionalization method[132] and the reaction employed in this work – up to 130 C_{60} bisadducts having different regio- and stereochemistry could theoretically form and virtually impossible to separate from each other due to the expected similarity in their physicochemical properties (Figure 2.1c).

In the first section of this chapter, we report on the synthesis of two "untethered" C_{60} bisadduct enantiomers using a conceptually novel, "supramolecular-directed" functionalization approach. The corresponding bisadducts of Pc to C_{60} were synthesized according to Prato protocol. To reveal the role of non-covalent interactions between two Pcs, we plan to vary the two parameters: the length of the spacer and peripheral substituents, employing tert-butyl groups and bulky functionalities (Figure 2.2). We expect to take advantage of noncovalent interactions between untethered phthalocyanine (Pc) species to boost the selective formation of a pair of Pc_2-C_{60} bisadduct enantiomers. We plan to determine their structure by a combination of experimental techniques and theoretical calculations. We expect to disclose the case of atropselectivity of the formation of bisadducts as a result of the restricted rotation of the two Pc macrocycles in the products. Thus, we hope to reveal the first example of atropselective reaction in fullerene chemistry.

[132]. Maggini, M., Scorrano, G., Prato, M. *J. Am. Chem. Soc.* **1993**, 115, 9798-9799.

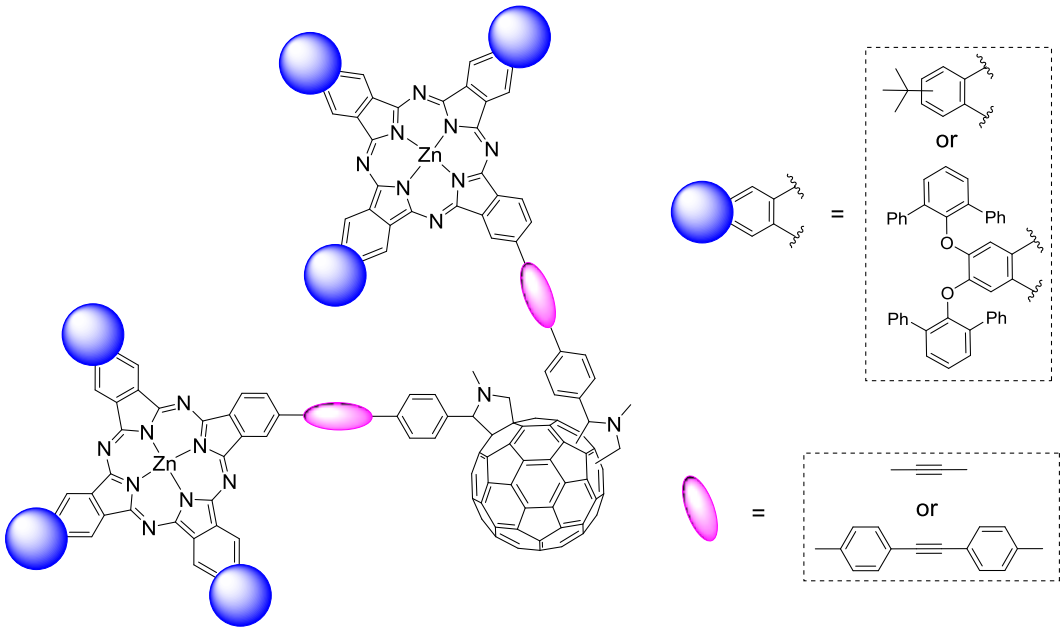

Figure 2.2. Pc-based C_{60} bisadducts.

Multicomponent systems involving porphyrinoids and fullerenes have also been reported and represent significant synthetic interest. Thus, a heptad (Figure 2.3) featuring a central hexaphenylbenzene unit substituted with two bis(phenylethynyl)anthracene moieties that absorb light in the 400-500 nm range, two Bodipy entities with absorption in the 450-550 and 330-430 nm range and two Zn(II)Por macrocycles has been prepared.[133] This complex hybrid also comprise a C_{60} sphere substituted with two pyridine ligands which coordinate to the two Por macrocycles via metal-ligand coordination interactions. It was demonstrated that in such system, which harvests light from the ultraviolet throughout the visible region up to 650 nm, singlet excitation energy is efficiently funneled from all four antenna units to the Por moieties. This energy transfer process is then followed by electron donation from the excited Pors to C_{60} to generate a charge-separated species which has a lifetime of 230 ps and an overall quantum yield close to unity.

[133] Y. Terazono, G. Kodis, P. A. Liddell, V. Garg, T. A. Moore, A. L. Moore, D. Gust, *J. Phys. Chem. B* **2009**, 113, 7147-7155.

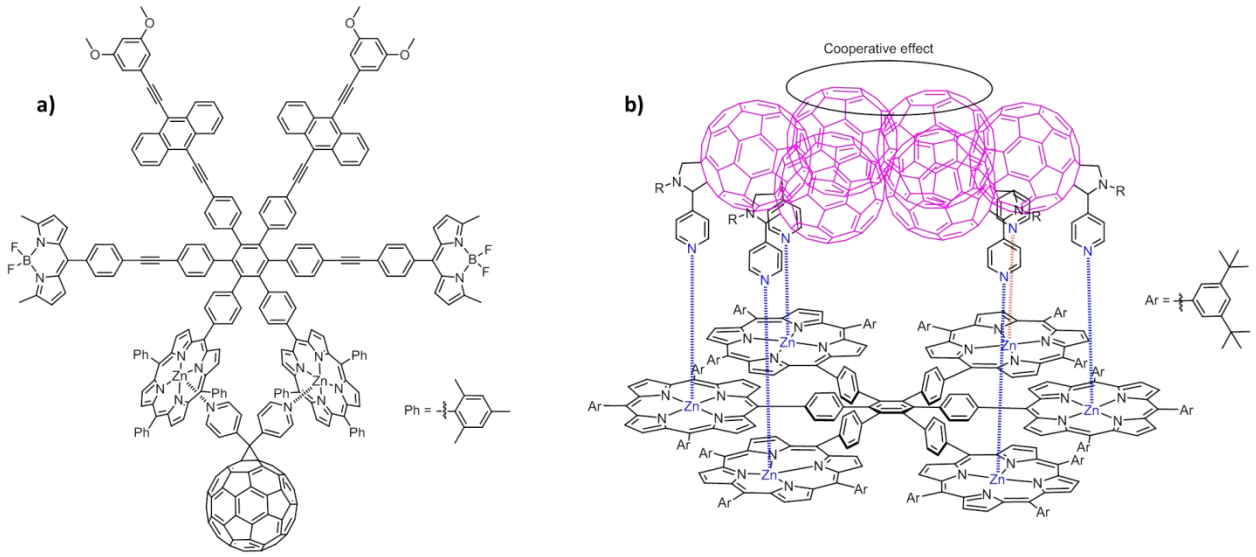

Figure 2.3. a) Molecular structure of heptamer; b) Molecular structure of a hexameric Por derivative complexing six, pyridine-substituted C_{60} units leading to supramolecular complex.

A similar, multicomponent system consisting in a central benzene unit surrounded by six Zn(II)Por macrocycle, each of them coordinating to a pyridine-substituted fulleropyrrolidine moiety has been reported (Figure 2.3b)[134]. The aggregation ability of this system has been demonstrated by UV-vis studies whereas fluorescence experiments indicate that the emission of the Por receptors is dramatically quenched by the coordinated fullerene units. Binding studies carried out by fluorescence titration experiments revealed a positive cooperative effect for the assembly of the C_{60}-pyridine derivatives with the polytopic Por receptor probably as a result of intramolecular C_{60}-C_{60} interactions between the different guests assembled onto the multi-Zn(II)Por platform.

In the second section of this Chapter, we describe the synthesis of novel multi-Pc, multi-C_{60} molecular systems in which alternating Pc and fullerene units are covalently attached to a central benzene moiety (Figure 2.4). The presence of a central hexaphenylbenzene unit is expected also allow further oxidative planarization of the compounds leading to hexabenzocoronene (HBC)-centered functional materials, interesting for photovoltaic applications. Benzene-centered Pc-C_{60} systems will be prepared by cobalt-catalyzed cyclotrimerization reaction of Pc derivatives containing a diphenylacetylene moiety, following the experimental conditions reported for the

134 A. Trabolsi, M. Urbani, J. L. Delgado, F. Ajamaa, M. Elhabiri, N. Solladie, J.-F. Nierengarten, A.-M. Albrecht-Gary, *New J. Chem*. **2008**, 32, 159-165.

preparation of a hexasubstituted Pc system.[135] The physic-chemical properties of the multicomponent systems, in which several photo- and redox-active Pc and C_{60} fullerene units are closely arranged around a central benzene moiety will be studied.

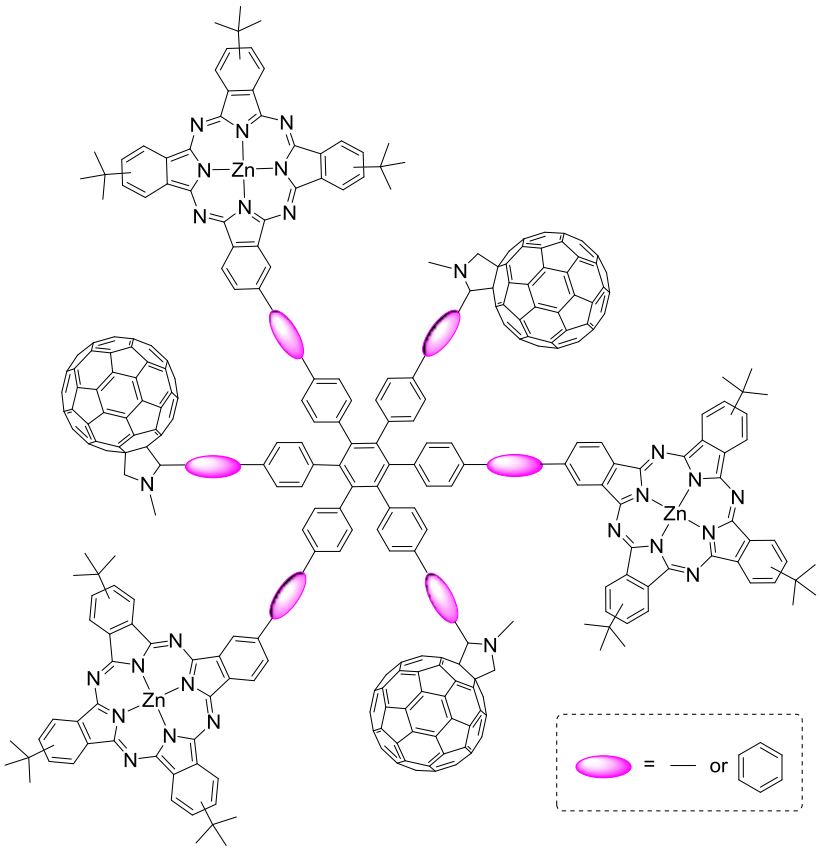

Figure 2.4. Multicomponent systems based on Pc and C_{60}.

[135] G. Bottari Giovanni, T. Torres . *Chem. Commun*. **2004**, 2668-2669.

1.1.2 Experimental techniques

Study of the D-A systems, described in this chapter, involves the knowledge of some techniques of supramolecular chemistry. In this regard, some basic concepts required for the distinction of H- and J-aggregates will be given.

UV-vis absorption of H- and J-aggregates

In addition to being a powerful tool to study the aggregation of chromophores, UV-vis absorption experiments may provide valuable hints about the topology of the aggregates[136,137]. The direction and magnitude of the transition shifts due to chromophoric stacking is generally interpreted by the molecular exciton approximation developed by Kasha[138]. This model, which neglects electronic overlap of the π-systems, is based on the interaction between localized transition dipole moments. The coupling gives rise to a splitting of the monomer state into a higher energy and a lower energy contribution. The resulting spectral shift value (Δν) is given by:

$$\Delta\nu = (N–1/N) \cdot M^2(1 – 3\cos^2\alpha) / hr^3;$$

where N is the degree of aggregation, h is Planck's constant, M is the transition dipole moment of the monomer, r is the center-to-center distance between molecules, and α is the tilt angle between the polarization axis of a unit molecule and the line connecting the molecular centers. When α is comprised between 90° and 54.7°, then Δν has a positive value which brings about blue shifts of the absorption wavelengths (*H*-type aggregates) (Figure 2.5a). In contrast, when α is comprised between 54.7° and 0°, then Δν has a negative value, resulting in red spectral shifts (*J*-type aggregates) (Figure 2.5b).

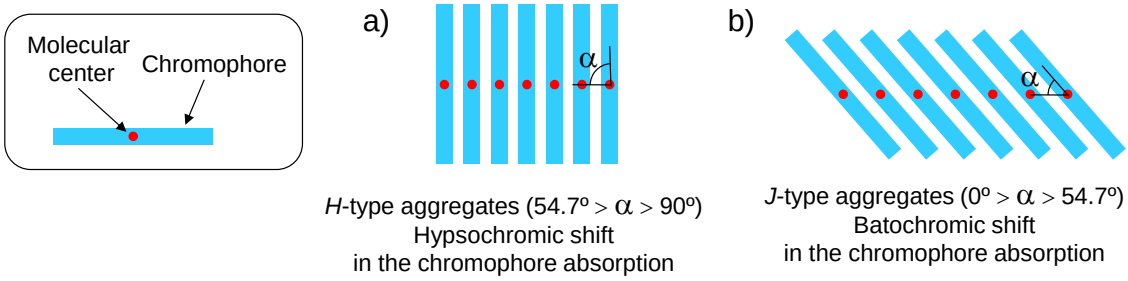

Figure S2.5 Schematic representation of the relative arrangement adopted by stacked chromophores giving rise to the formation of *H*-type (a) and *J*-type (b) aggregates.

---

136. A. W. Snow, in *The Porphyrin Handbook*; K. M. Kadish, K. M. Smith, R. Guillard, Eds.; Academic Press: San Diego, CA, 2003; Vol. 17, pp 129-176.

137. a) Katayose, M., Tai, S., Kamijima, K., Hagiwara, H., Hayashi, N. *J. Chem. Soc., Perkin Trans.* **1992**, *2* 403-409; b) Kroon, J. M., Koehorst, r. B. M., van, D. M., Sanders, G. M., Sudholter, E. J. R. *J. Mater. Chem.* **1997**, 7, 615-624.

138. a) McRae, E. G., Kasha, M. Enhancement of phosphorescence ability upon aggregation of dye molecules. *J. Chem. Phys*. 1958, 28, 721-722;. b) Kasha M., Rawls H. R., El-Bayoumi, M. A. *Pure Appl. Chem.* **1965**, 11, 371-392.

2.2 Exclusive case of bisadducts of C_{60} and Pc

2.2.1 Synthesis and characterization

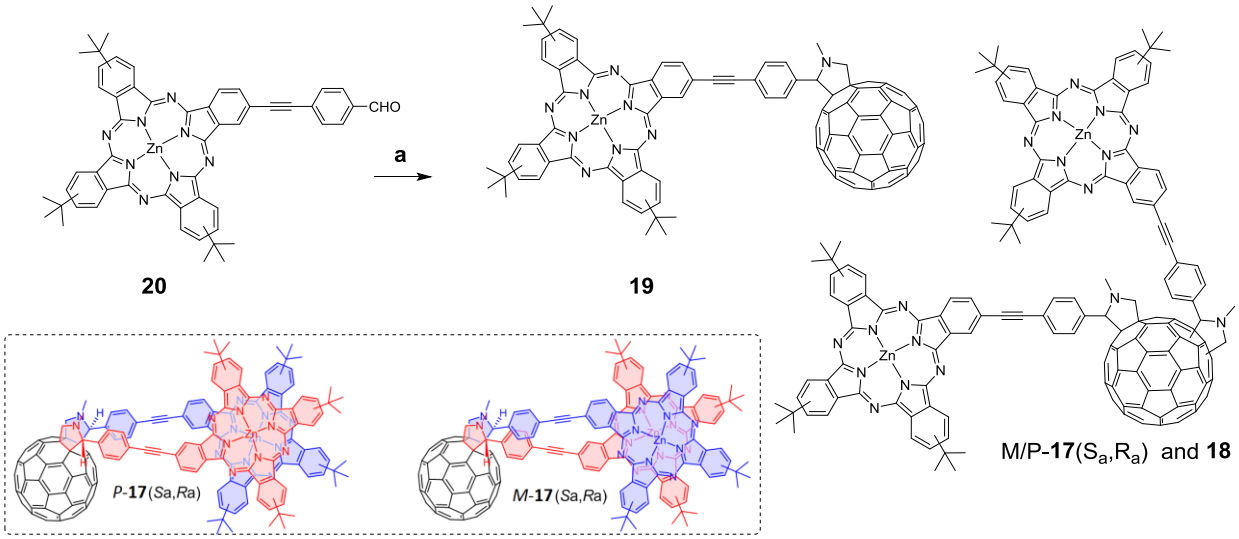

Scheme 2.2. Synthesis of Pc-based C_{60} monoadduct **19** and bisadducts *M*/*P*-1(S_a,R_a), **17** and 1**8**; a) C_{60} fullerene, *N*-methyl glycine, toluene, reflux, 12 hrs.

Pc_2-C_{60} bisadducts were synthesized via 1,3-dipolar cycloaddition reaction of (tri-*tert*-butyl)(benzaldehyde-4-ethynyl) Zn(II)Pc **20**[139], used as a mixture of regioisomers, with C_{60} fullerene in the presence of *N*-methyl glycine in refluxing toluene during 12 h (Scheme 2.2). Reaction mass was subjected to silica gel column chromatography affording three well-resolved green zones, besides the recovery of some unreacted C_{60} fullerene. Those zones were isolated in 29%, 14% and 23% yield and identified as Pc_2-C_{60} bisadducts *M*/*P*-**17**(S_a,R_a), Pc-C_{60} monoadduct **19**[139] and Pc_2-C_{60} bisadducts **18**, respectively. Briefly, Pc_2-C_{60} bisadducts *M*/*P*-**17**(S_a,R_a) bear the two Pc units in close proximity that enables their efficient π-π stacking (Scheme 2.2 - inset). The latter finds a bright resonance in the spectral and physicochemical properties of these compounds. In contrast, in Pc_2-C_{60} bisadducts **18** the two Pc units don't experience any intramolecular interactions. This allows an efficient separation of the compounds and their detailed spectrometric and spectroscopic characterization. Notably, products **17**-**19** were obtained as a mixture of regioisomers due to *tert*-Butyl substitution pattern at the Pc macrocycle (Figure 2.7).

---

[139] a) G. Bottari, D. Olea, C. Gómez-Navarro, F. Zamora, J. Gómez-Herrero, T. Torres, *Angew. Chem., Int. Ed.* **2008**, *47*, 2026 - 2031. b) G. Bottari, D. Olea, V. López, C. Gómez-Navarro, F. Zamora, J. Gómez-Herrero, T. Torres, *Chem. Commun.* **2010**, *46*, 4692-4694.

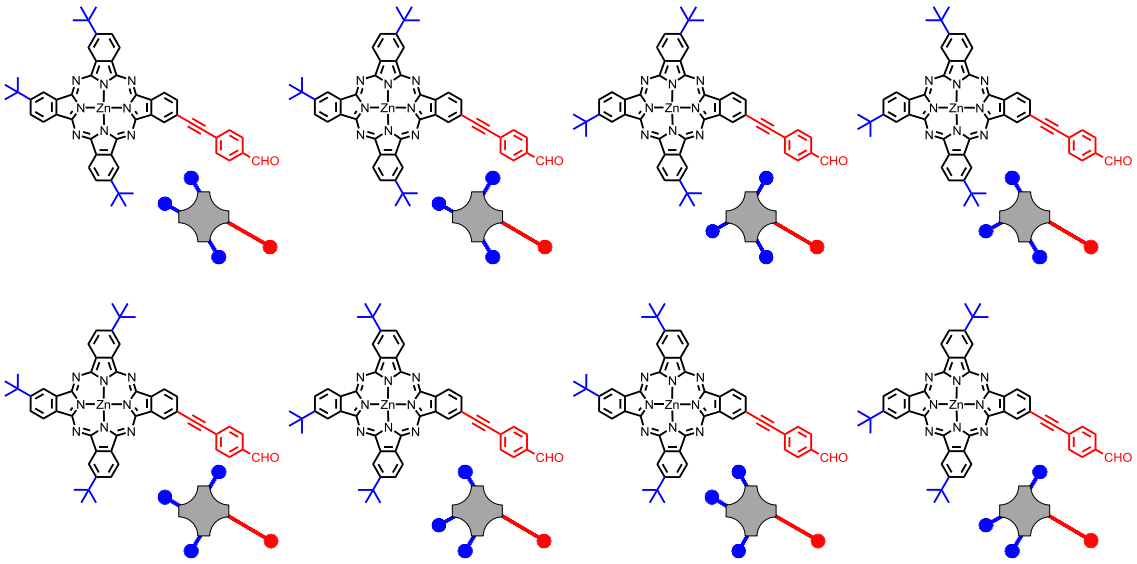

Figure 2.7. Molecular structures of the eight possible regioisomers of tri-*tert*-butyl Zn(II)Pc aldehyde **20**.

Whereas, bisadducts *M*/*P*-**17**(S_a,R_a) were obtained as a racemic mixture of the *M*-**17**(S_a,R_a) and *P*-**17**(S_a,R_a) enantiomers (Figure 6 - inset). Detailed explanation of their structure will be given in the Section 2.2.3 of this Chapter.

MALDI-MS study of the Pc_2-C_{60} bisadducts **17** and **18** revealed peaks of molecular ions at 2518 m/z, corresponding to the proposed structures (Figure 2.8). Interestingly, the same reaction was carried out with smaller content of Pc aldehyde **20** previously by our group.[139] In that case, the exclusive formation of monoadduct **19** and bisadducts **18**, as the major and minor products, was observed. Whereas the formation of bisadducts *M*/*P*-**17**(S_a,R_a) was not detected. Latter indicates the concentration of Pc aldehyde **20** to play a determining role in the formation of *M*/*P*-**17**(S_a,R_a) bisadducts and a consequent mechanism driven by supramolecular interactions between Pc units.

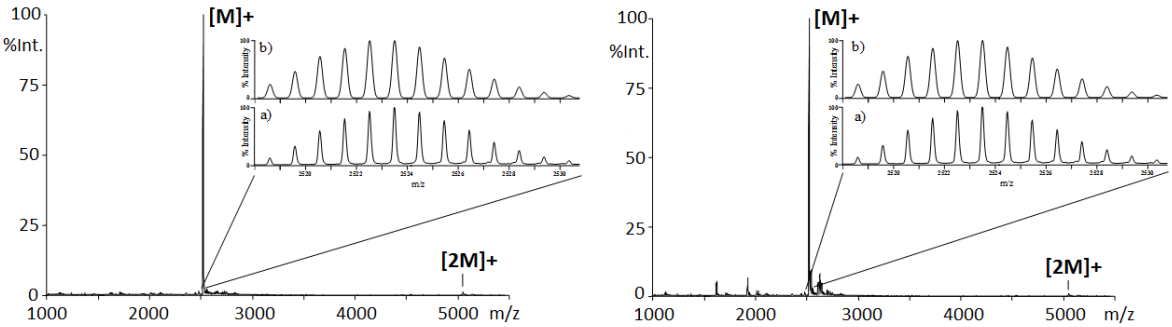

Figure 2.8. MALDI-TOF MS spectra (dithranol) of Pc_2-C_{60} bisadducts *M*/*P*-**17**(S_a,R_a) (left) and **18** (right). Inset: a) isotopic resolution of the MALDI-TOF main peak at 2523 m/z; b) calculated isotopic pattern for Pc_2-C_{60} bisadducts.

Important differences between racemate *M*/*P*-**17**(S_a,R_a) and Pc-C_{60} monoadduct **19** and Pc_2-C_{60} bisadducts **18** were also observed by low- and high-field ^{1}H NMR studies. Low field ^{1}H NMR studies of Pc_2-C_{60} bisadducts **17** and **18** revealed overlapped peaks at 9.5 – 7.5 ppm corresponding to aromatic protons and multiple peaks at 5.5 – 3.5 ppm attributed to methylene protons of pyrrolidine. N-methyl protons were found as multiplets in the range of 3.5 – 2.5 ppm (Figure 2.9 - left). All mentioned is in a good agreement with characteristic ^{1}H NMR spectrum of Pc-C_{60} monoadduct **19**.[139] Increased number of peaks in ^{1}H NMR spectra of bisadducts is probably caused by the presence of different regio- and/or stereoisomers within a specific C_{60} addition pattern. Due to poor informativity of the low-field ^{1}H NMR studies of Pc_2-C_{60} bisadducts **17** and **18** we turned to the high-field ^{1}H NMR spectroscopy. Herein, H_2@C_{60} analogs of adducts, namely compounds *M*/*P*-**17**(S_a,R_a)(H_2@C_{60}), **18**(H_2@C_{60}) and **19**(H_2@C_{60}), were prepared and investigated (Figure 2.9 - right).

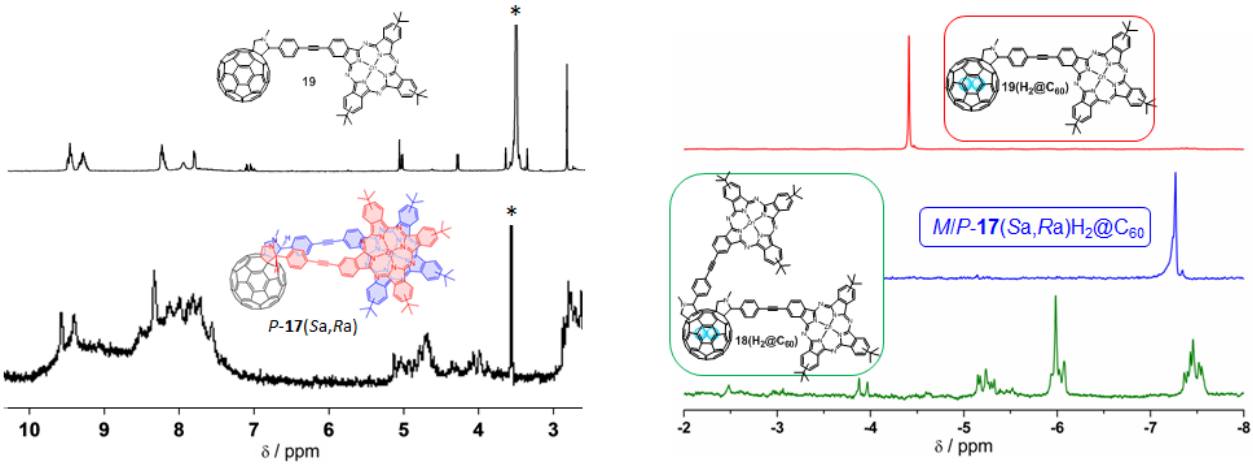

Figure 2.9. (Left) Low-field ^{1}H NMR spectra (THF-d_8, 25 °C) of fullerene monoadduct **19** and racemate *M*/*P*-**17**(S_a,R_a). (Right) High-field ^{1}H NMR spectra (toluene-d_8, 25 °C) of fullerene monoadduct **19**(H_2@C_{60}) (red), racemate *M*/*P*-**17**(S_a,R_a)(H_2@C_{60}) (blue) and fullerene bisadducts **18**(H_2@C_{60}) (green). Residual solvent peak are marked with asterisk.

In H_2@C_{60} derivatives, the chemical shift of the encapsulated hydrogen molecule is extremely sensitive to the magnetic field inside the fullerene cage which, in turn, is strongly influenced by

the exohedral modification of the endofullerene[140]. In the case of bisadducts **18**(H_2@C_{60}), more than 20 peaks with different intensities were observed in the spectral region between −2 and −8 ppm. This latter finding suggests that the magnetic field experienced by the encapsulated H_2 molecule in **18**(H_2@C_{60}) is somehow influenced not only by the fullerene addition pattern – otherwise maximum eight, high-field proton peaks should be observed accordingly to the eight possible C_{60} addition patterns – but also by the presence of different regio- and/or stereoisomers within each C_{60} addition pattern. On the other hand, the high-field ^{1}H-NMR spectrum of racemate *M*/*P*-**17**(S_a,R_a)(H_2@C_{60}) was considerably simpler showing a main peak at −7.27 ppm, which supports the hypothesis that *M*/*P*-**1**(S_a,R_a)(H_2@C_{60}) is a racemate. Additionally, few small side peaks could be observed close to the main peak probably due to the regioisomers arising from the different position of the three *tert*-butyl groups on each of the two Pc macrocycles. Similarly to *M*/*P*-**17**(S_a,R_a)(H_2@C_{60}), one main peak (−4.41 ppm) was also observed for the entrapped hydrogen molecule in **19**(H_2@C_{60}) as expected from the H_2@C_{60} monofunctionatization.

The UV-vis absorption features of C_{60} adducts *M*/*P*-**17**(S_a,R_a), **18** and **19**, and precursor aldehyde Zn(II)Pc **20** were then investigated in THF (Figure 2.10 - left). In the case of C_{60} adducts **18** and **19**, the important similarities between the UV-vis spectra of these two C_{60} adducts and C_{60}-free Zn(II)Pc **20** suggest negligible ground-state electronic communication i) between the Pc and the C_{60} moieties in derivatives **18** and **19** and ii) in the case of Pc_2-C_{60} bisadducts **18**, between the two Pc macrocycles which behave like electronically-independent moieties. On the contrary, and to our surprise, the UV/vis spectrum of Pc_2-C_{60} racemate *M*/*P*-**17**(S_a,R_a) was significantly different from the spectra of derivatives **18**-**19**. Bisadducts *M*/*P*-**17**(S_a,R_a) showed a *Q*-band with two broad and equally-intense absorptions maximizing at 640 and 670 nm, both weaker than the *B*-band at 341 nm (Figure 2.10 - left).

[140]. M. Murata, Y. Murata, K. Komatsu. *J. Am. Chem. Soc.* **2006**, 128, 8024 - 8033.

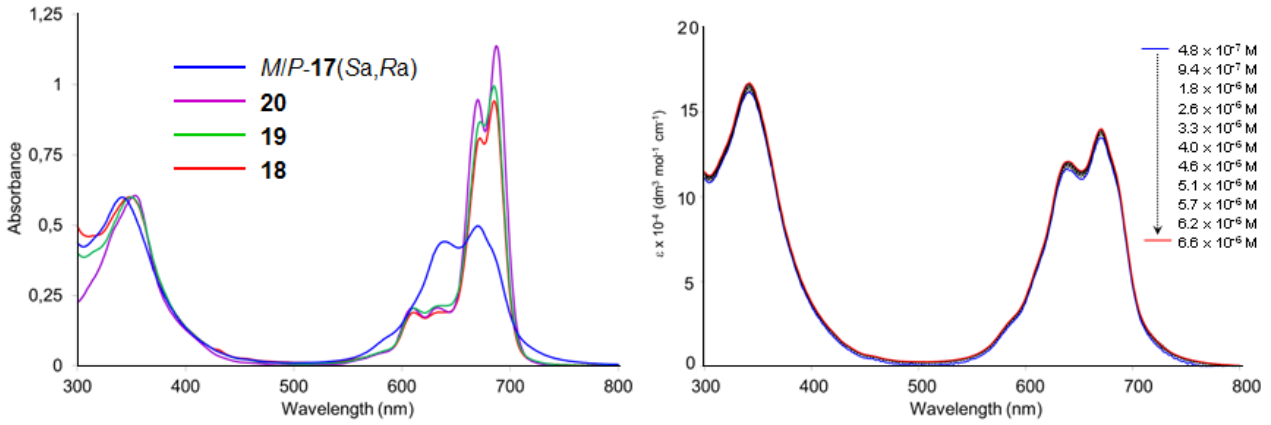

Figure 2.10. (Left) Normalized UV-vis spectra (THF) of C_{60} adducts **17**-**19** and aldehyde Zn(II)Pc **20**. (Right) Effect of dilution on the UV-vis absorption (THF, 25 °C) of Pc_2-C_{60} racemate *M*/*P*-**17**(S_a,R_a).

It is important to note that the Pc absorption bands, especially the *Q*-band, are strongly affected by the aggregation state of the Pcs in solution.[141] Concentration-dependent UV-vis studies on racemate *M*/*P*-**17**(S_a,R_a) in THF did not show significant changes in the shape and the position of the Pc *B*- and *Q*-bands (Figure 2.10 - right), thus suggesting that the observed absorptions arise from intramolecular π-stacking interactions. More precisely, the presence in the UV-vis spectrum of racemate *M*/*P*-**17**(S_a,R_a) of an intense and blue-shifted *Q*-band transition at 640 nm is a clear indication of an intramolecular *H*-type stacking arrangement of the two Pc macrocycles.[142]

2.2.2 Host-guest interactions with N-containing ligands

Possible break of inramolecular interactions between the two Zn(II)Pcs units in *M*/*P*-**17**(S_a,R_a) racemate could change drastically spectral properties of these compounds. Herein, we decided to study supramolecular interactions of Pc_2-C_{60} racemate *M*/*P*-**17**(S_a,R_a) with N-containing ligands by axial coordination of the nitrogen atom of the ligand to the Zn(II)Pc metal center.

With this aim, UV-vis titration experiments were carried out on racemate *M*/*P*-**17**(S_a,R_a) using pyridine, pyrazine and 1,4-diazabicyclo[2.2.2]octane (DABCO). These mono- and dinitrogenated ligands were chosen with the aim of "disrupting" the two Zn(II)Pcs units in *M*/*P*-**17**(S_a,R_a) racemate. Additionally, UV-vis titration experiments on Pc-C_{60} monoadduct **19** and Pc_2-C_{60} bisadducts **18** using the same kit of three nitrogenated ligands were carried out. For the two

[141]. A. Gouloumis, D. Gonzalez-Rodriguez, P. Vazquez, T. Torres, S. G. Liu, L. Echegoyen, J. Ramey, G. L. Hug, D. M. Guldi, *J. Am. Chem. Soc.* **2006**, 128, 12674 - 12684.

[142]. A. W. Snow, in *The Porphyrin Handbook*; K. M. Kadish, K. M. Smith, R. Guillard, Eds.; Academic Press: San Diego, CA, 2003; Vol. 17, pp 129-176.

latter C_{60} adducts, minor or insignificant changes in the shape and position of the Pc absorption bands were observed upon addition of any of the three ligands. Similarly, addition of pyridine or pyrazine to racemate *M*/*P*-**17**(S_a,R_a) did not cause any change in its UV-vis spectrum. On the other hand, and to our surprise, different results were obtained when racemate *M*/*P*-**17**(S_a,R_a) was titrated with DABCO, which has a N···N distance (2.6 Å) comparable to that in pyrazine (2.7 Å), but significantly higher basicity (p*Ka* = 8.7 *vs* 0.6), and, in turn, a better metal-ligand coordination ability. Titration curves shown on the Figure 11 (left) correspond to the addition of DABCO (THF, 2 x 10^{-2} mM) to a solution of *M*/*P*-**17**(S_a,R_a) (THF, 2 x 10^{-3} mM, blue spectrum) by 0.1 equivalents, up to a total of 2 equivalents of DABCO per 1 equivalent of a bisadduct. A gradual decrease in the intensity of the racemate *Q*-band transition at 640 nm was observed upon addition of DABCO accompanied by the simultaneous increase of the band at 670 nm. Multivariable analysis of the titration spectra afforded an association constant (K_a) for **DABCO**⊂*M*/*P*-**17**(S_a,R_a) of log K_a = 6.4 ± 0.3 in THF and at room temperature. Such high K_a value suggests an excellent complementarity between the tweezers-like geometry of *M*/*P*-**17**(S_a,R_a) resulting from the *H*-type stacked arrangement adopted by the two Zn(II)Pcs and DABCO. As a consequence of the complexation of DABCO into the binding pocket of *M*/*P*-**17**(S_a,R_a), π-stacking interactions between the two Pcs are disrupted giving rise to the observed changes in the *Q*-band absorption.

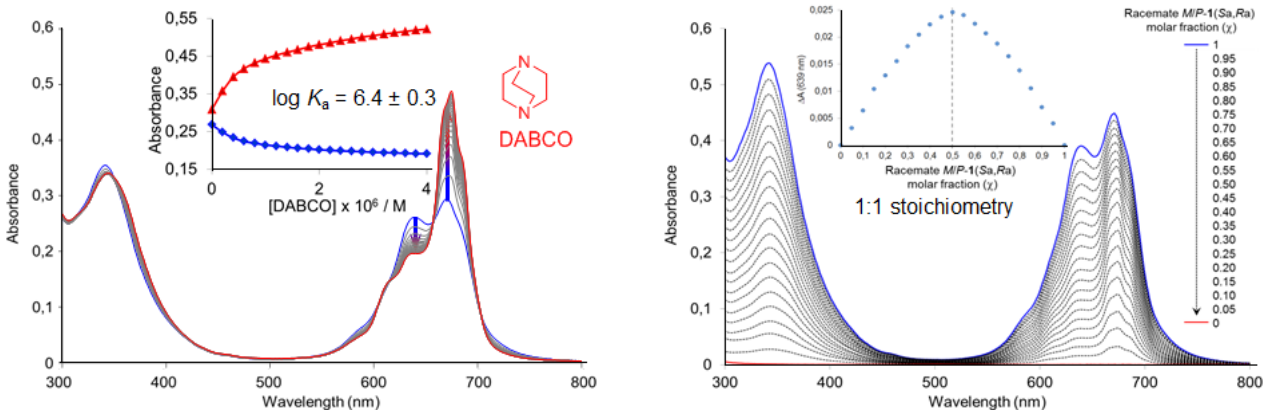

Figure 2.11. (Left) UV-vis titration of Pc_2-C_{60} racemate *M*/*P*-**17**(S_a,R_a) (THF, 2 x 10^{-3} mM, blue spectrum) with DABCO (THF, 2 x 10^{-2} mM) up to a total of 2 equiv (red spectrum). Inset: Binding isotherms at 640 (blue) and 670 nm (red). (Right) Absorption spectra (THF) obtained at different *M*/*P*-**17**(S_a,R_a):DABCO molar fractions (total concentration = 3 x 10^{-3} mM). Inset: Job's plot for the complexation of racemate *M*/*P*-**17**(S_a,R_a) by DABCO (THF, 639 nm) maximizing at χ=0.5, which indicates the formation of 1:1 supramolecular complex **DABCO**⊂*M*/*P*-**17**(S_a,R_a).

Well-defined isosbestic points at 350, 604, 656, and 704 nm suggests the formation of supramolecular complex **DABCO**⊂*M*/*P*-**17**(S_a,R_a). It's 1:1 stoichiometry was determined by Job's plot maximizing at a *M*/*P*-**17**(S_a,R_a) molar fraction (χ) of 0.5 (Figure 2.11 - right). The formation of 1:1 supramolecular complex **DABCO**⊂*M*/*P*-**17**(S_a,R_a) has been also proved by mass spectrometry revealing ESI-MS peak at 2635 m/z corresponding to [**DABCO**⊂*M*/*P*-**17**(S_a,R_a)]$^+$ molecular ion.

2.2.3 Control experiments

In the attempt to shed light on some of the key factors responsible for the amplification in the formation of racemate *M*/*P*-**17**(S_a,R_a), some control experiments were performed. Firstly, a reaction was carried out in which the volume of toluene used was increased ten times (*i.e.*, 150 mL, [**20**] = 0.3 mM) with respect to the standard reaction conditions. In the case of the "diluted" reaction, a 2% isolated yield of racemate *M*/*P*-**17**(S_a,R_a) was obtained, a value significantly lower than the 14% obtained in the "concentrated" reaction. Secondly, a reaction was performed under the standard reaction conditions, and DABCO added to the reaction mixture (**20**:DABCO molar ratio = 2:1). In this latter case, the 14% yield of the isolated bisadducts *M*/*P*-**17**(S_a,R_a) obtained under the standard reaction conditions dropped down to 4%. In the third control experiment, the standard reaction was carried out replacing Pc **20** for aldehyde-substituted Zn(II)Pc **23** which has six bulky 2,6-diphenylphenoxy substituents at the Pc periphery (Scheme 2.3). In this case, a UV-vis analysis of all the isolated products did not reveal the presence of any *H*-type Pc_2-C_{60} bisadduct.

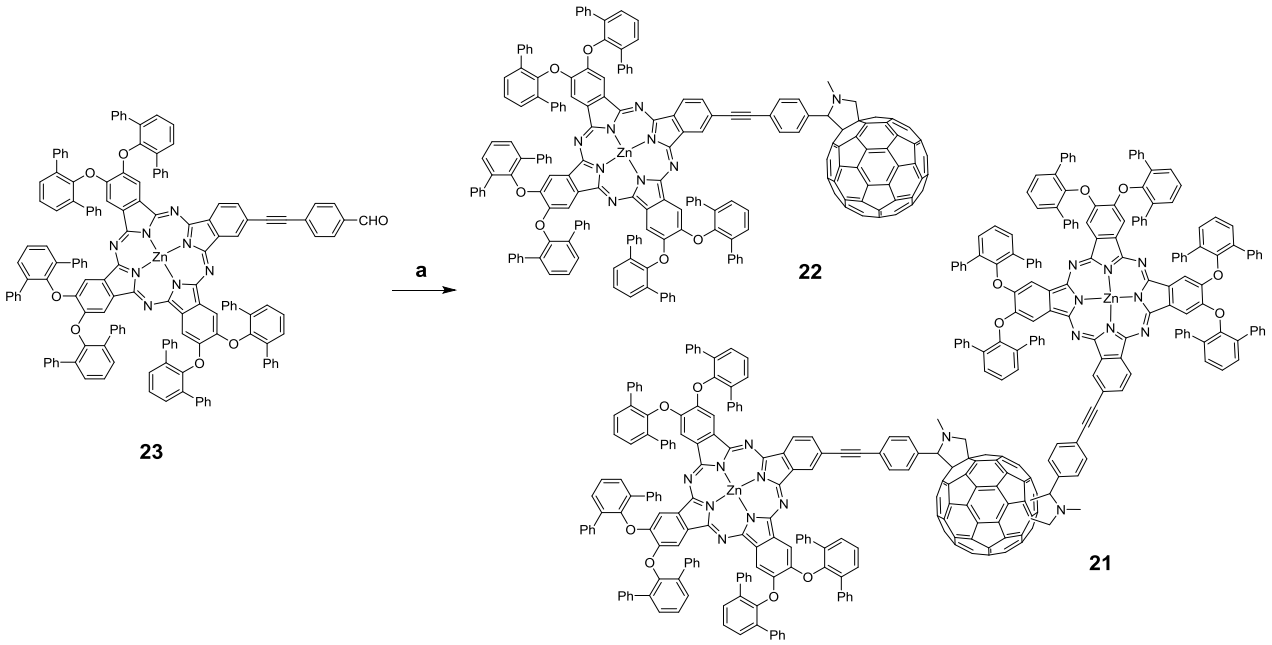

Scheme 2.3. Synthesis of Pc-based C_{60} monoadduct **22** and bisadducts **21**.

The results of the former two control experiments suggest that π-stacking interactions between Pc aldehydes **20** (or azomethyne ylide derivatives of **20**) must play a fundamental role in the formation of racemate *M*/*P*-**17**(S_a,R_a). Namely, when the concentration of these supramolecular Pc aggregates in solution was decreased, either by diluting the reaction or by addition of DABCO which hampers the Pc self-aggregation, the formation of *M*/*P*-**17**(S_a,R_a) was strongly reduced. The importance of Pc π-stacking interactions in the formation of racemate *M*/*P*-**17**(S_a,R_a) was further confirmed in the third control experiment in which the use of a bulky Zn(II)Pc derivative completely suppressed the formation of any Pc *H*-stacked C_{60} bisadduct. Unsurprisingly, the C_{60}-to-Pc aldehyde ratio in the reaction was also found to be crucial for the formation of racemate *M*/*P*-**17**(S_a,R_a). Thus, the formation of *M*/*P*-**17**(S_a,R_a) was not detected in a reaction carried out using Pc **20**, C_{60} fullerene and *N*-methyl glycine but in a different molar ratio (1:3:4, respectively) with respect to the standard reaction conditions (1:1.1:3, respectively) and at a lower concentration of aldehyde Pc **20** (0.4 mM *vs* 3 mM)[143]. In this case, the exclusive formation of Pc-C_{60} monoadduct **19** and Pc_2-C_{60} bisadducts **18**, as the major and minor products respectively, was observed.

[143]. Bottari, G., Olea, D., Gomez-Navarro, C., Zamora, F., Gomez-Herrero, J., Torres, T. *Angew. Chem. Int. Ed.* 2008, **47,** 2026-203.

2.2.4 Analysis of the selectivity of bisaddition

Bisaddition of prochiral azomethine ylides to C_{60} fullerene: an account of isomers

The 1,3 dipolar cycloaddition of the two azomethine ylides over C_{60} fullerene affords eight achiral C_{60} bisadducts accordingly to the eight C_{60} fullerene bisaddition patterns with the following nomenclature: *cis*-1, *cis*-2, *cis*-3, *e*, *trans*-1, *trans*-2, *trans*-3, and *trans-4* (Figure 2.12).[144]

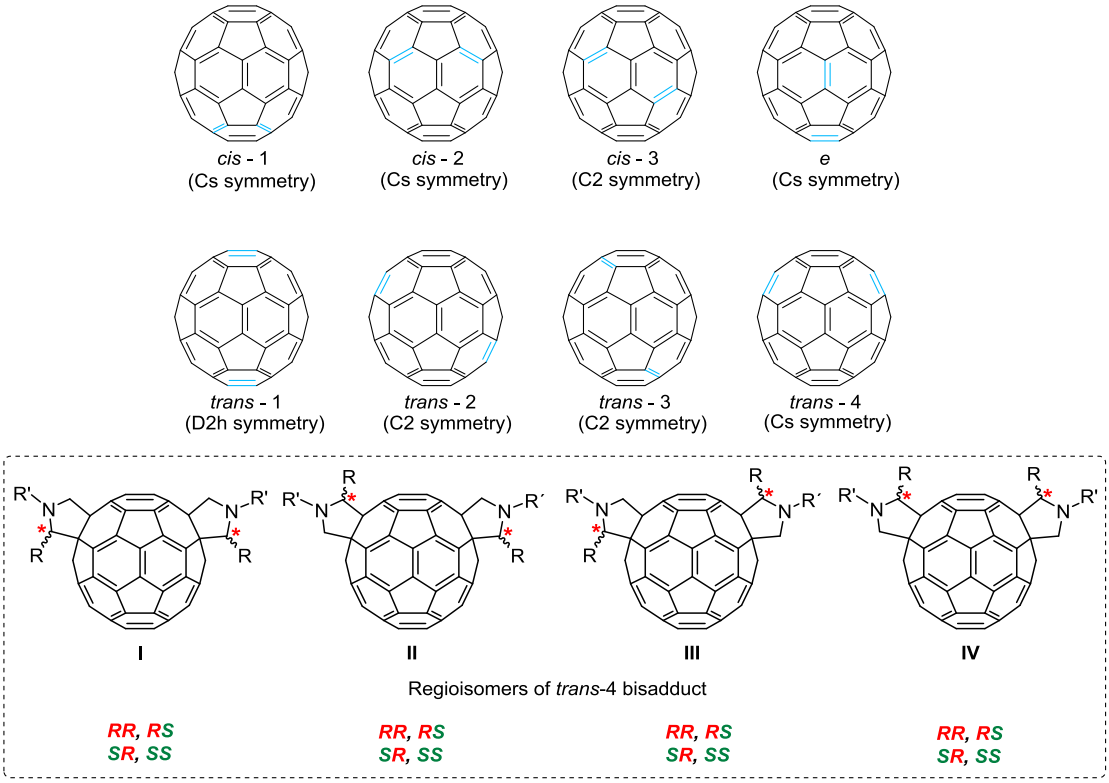

Figure 2.12. Eight C_{60} bisaddition patterns. Inset: four possible regioisomers for a *trans*-4 bisadduct and their possible enantiomeric configurations. The red asterisks indicate the stereogenic carbon atoms at the pyrrolidine ring.

When the reacting azomethine ylide is different to paraformaldehyde, the addition of two prochiral azomethine ylides to C_{60} gives rise to a racemic mixture of four enantiomeric C_{60} bisadducts for each of the eights addition patterns. For instance, there are four possible regioisomers for a *trans*-4 bisadduct identified as I, II, III and IV (Figure 2.12 - inset). Moreover, for each of the four regioisomers (I, II, III and IV), the configuration of each of the two stereogenic methine carbons can be either R or S. This implies that for each of the four regioisomers I-IV, four stereoisomers are possible depending on the configuration of the two

[144] Hirsch, A.; Lamparth, I.; Karfunkel, H. R. *Angew. Chem.,* **1994**, *106*, 453-455.

methine carbon atoms (*i.e. RR*, *SS*, *RS* and *SR*). Thus, each of the eight C_{60} addition patterns can theoretically form the maximum of 16 (*i.e.,* 2^4) isomers (Figure 2.14). The isomeric relationship between the 16 bisadducts within each of the eight C_{60} addition pattern takes into account "exclusively" the regio- and stereochemistry of the pyrrolidine addends and does not consider the presence of different regioisomers resulting from the different regiochemistry of the three peripheral *tert*-butyl groups on each of the two Pc units. Even though, the number of possible bisadducts increases to 32 (*i.e.*, 2 x 16) in the case of the "intrinsically" chiral *cis*-3*, trans*-2 and *trans*-3 C_{60} additions pattern considering the two enantiomers $^{f,s}A$ and $^{f,s}C$.

In summary, 20 isomers could be formed for each of the intrinsically chiral *cis*-3*, trans*-2 and *trans*-3 C_{60} addition patterns taking into account the two $^{f,s}A$ and $^{f,s}C$ enantiomers that each of these C_{60} addition patterns possesses. Only 16 isomers may take place for each of the *cis*-1, *cis*-2, *e* and *trans*-4 C_{60} addition patterns. Finally, 6 isomers are possible in the case of the *trans*-1 C_{60} addition pattern. This means that 130 isomers could theoretically be formed (*i.e.*, (20 x 3) + (16 x 4) + 6).

Bisaddition of prochiral azomethine ylides to C_{60} fullerene: yield calculation

According to the previous reports of Prato *et al.* on C_{60}-bisadducts of the *N*-methyl fulleropyrrolidine[145] and Nishimura *et al.* on on C_{60}-bisadducts of *N*-(m-TEG) fulleropyrrolidine [146], the *cis*-1 C_{60} addends are usually formed in the smallest relative percentage yield of 1.4-1.6% (Figure 2.13). Thus, the relative percentage yield of one of these 16 possible *cis*-1 isomers with respect to all the other bisadduct isomers would be ≈ 0.09% (*i.e.*, a sixteenth of 1.4%).

[145]. Kordatos, K., Bosi, S., Da Ros, T., Zambon, A., Lucchini, V. & Prato, M. *J. Org. Chem.* **66,** 2802-2808 (2001).

[146]. Nishimura, T., Tsuchiya, K., Ohsawa, S., Maeda, K., Yashima, E., Nakamura, Y. & Nishimura, J. *J. Am. Chem. Soc.* **126,** 11711-11717 (2004).

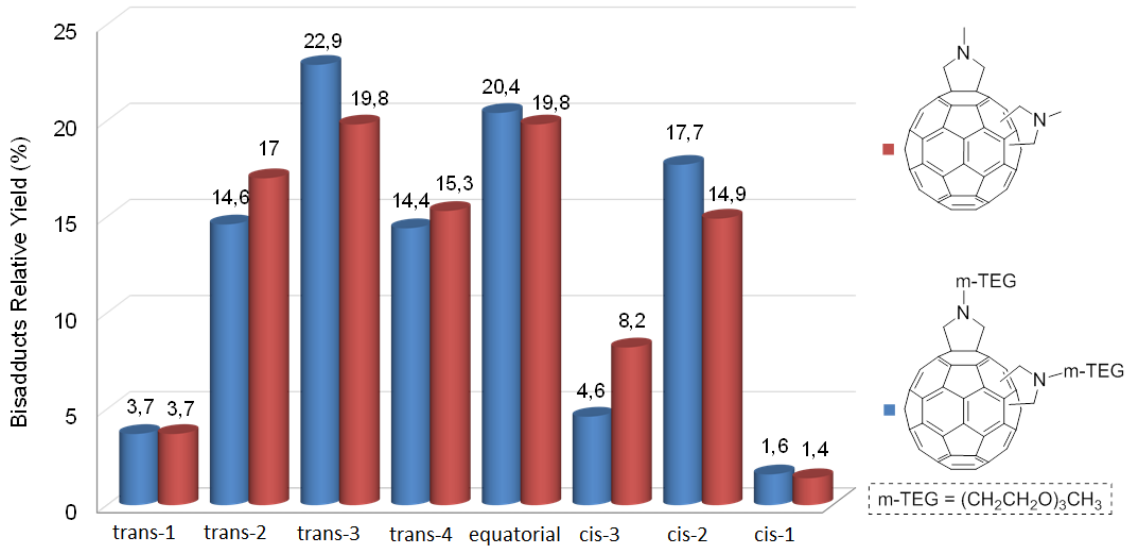

Figure 2.13. Relative yields (%) of the eight C_{60}-bisadducts of the *N*-methyl fulleropyrrolidine (red coloured bars) and the *N*-(m-TEG) fulleropyrrolidine**Ошибка! Закладка не определена.** (blue coloured bars).

In the case of the reaction carried out using Pc aldehyde **20**, *N*-methyl glycine and C_{60} in the condition reported above, an overall yield of 23% (based on the isolated product) was obtained for Pc_2-C_{60} bisadducts **18**.

Using the relative percentage yield of 1.4% reported by Prato *et al.* for the *N*-methyl *cis*-1 bisadducts, this would give rise to an expected yield for the Pc_2-C_{60} *cis*-1 isomers of 0.322% (*i.e.*, 1.4% of 23%). Considering that, when using a prochiral azomethyne ylide, 16 *cis*-1 isomers are theoretically possible. This would further reduce the yield of each one of these 16 *cis*-1 isomers down to 0.020% (*i.e.*, a sixteenth of 0.322%). This latter relative yield further decreases down to 0.005% (*i.e.*, a forth of 0.020%) for each of the four atropisomers *M*/*P*-**17**(*S*a,*R*a), *M*/*P*-**17**(*R*a,*R*a), *M*/*P*-**17**(*S*a,*S*a) and *M*/*P*-**17**(*R*a,*S*a) which could theoretically form. These four atropisomers have the same regio- and stereconfiguration at the two fulleropyrrolidine rings but different arrangement of the two Pc macrocycles due to the hindered rotation around the C–C single bonds of the spacers.

On the contrary, and to our surprise, the isolated yield of Pc_2-C_{60} *cis*-1 racemate *M*/*P*-**17**(*S*a,*R*a) was 14%, which represents a 2800–fold increase with respect to the 0.005% theoretical yield.

The remarkable amplification in the formation of Pc_2-C_{60} racemate *M*/*P*-**17**(*S*a,*R*a) is probably much greater than a 2800–fold increase considering that the relative yield of the *cis*-1 bisadducts in the case of 1,3 dipolar cycloaddition reactions involving prochiral azomethyne ylides, as in this

work, is expected to be significantly lower than that obtained for bisadducts reported by Prato and Nishimura, due to steric hindrance at the substituted C-2 positions of the two vicinal fulleropyrrolidine moieties for some of the *cis*-1 isomers.

Theoretical calculations on the Pc_2-C_{60} bisadducts

Theoretical calculations have been carried out to confirm the structure of enantiomers *M*- and *P*-**17**(S_a,R_a). Although, as mentioned above, the number of possible Pc_2-C_{60} bisadducts (*i.e.*, mixture of enantiomers, diastereoisomers and meso compounds) is 130, 116 of these 130 isomers are obtained as 58 pairs of enantiomers. Only one enantiomer has been modeled for each pair of enantiomers, so that the number of Pc_2-C_{60} bisadducts to be calculated was reduced to 72 structures. Moreover, Pc_2-C_{60} bisadducts are also obtained as a mixture of regioisomers arising from the different position of the three *tert*-butyl groups on each of the two Zn(II)Pc macrocycles. It is important to note that since the tri-*tert*-butyl Zn(II)Pc aldehyde **20** used for the 1,3 dipolar cycloaddition reaction on C_{60} is a mixture of eight regioisomers, the resulting Pc_2-C_{60} bisadducts are also obtained as a mixture of regioisomers arising from the different position of the three *tert*-butyl groups on each of the two Zn(II)Pc macrocycles. However, for the theoretical calculations only one of those Zn(II)Pc regioisomers has been considered. Finally, in the case of the three "inherently" chiral C_{60} addition patterns (*i.e.*, *cis*-3, *trans*-2 and *trans*-3) only the Pc_2-C_{60} isomers of the ^{f,s}*A* enantiomer have been modeled. Thus, molecular mechanics (MM+) calculation of 72 possible Pc_2-C_{60} bisadducts was performed showing that only two of these structures could give rise to an intramolecular π-stacked, *H*-type arrangement of the two Pc moieties, namely bisadducts *cis*-1 (A) and *cis*-1 (P,S_a,R_a) (Figure 2.14). Whereas for the other Pc_2-C_{60} bisadducts the distance between the two Pc planes in the minimized structures was either too large and/or their relative orientation inappropriate to give rise to any intramolecular *H*-type aggregate.

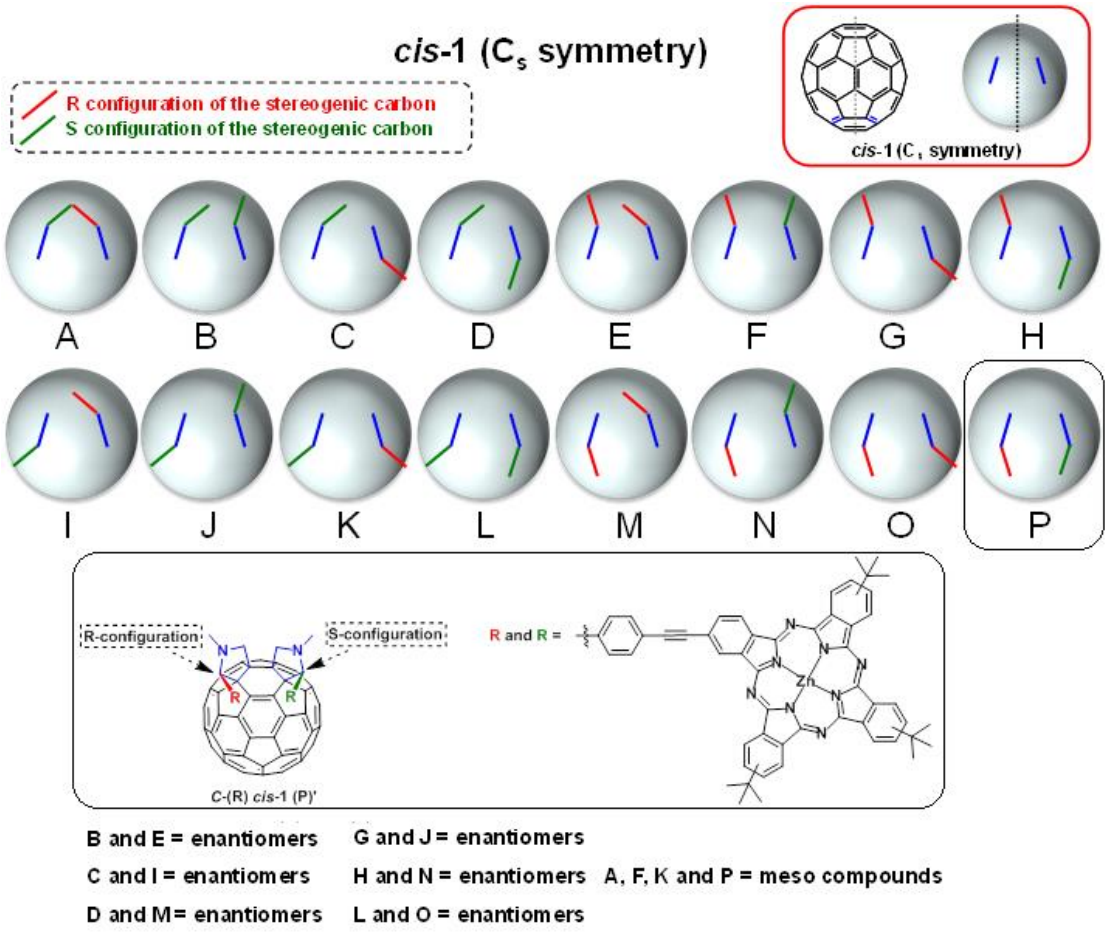

Figure 2.14. Schematic representation of the 16 possible *cis*-1 bisadduct isomers resulting from the addition to C_{60} fullerene of two prochiral azomethyne ylides, and their isomeric relationship. Each *cis*-1 isomer has been named by a letter from A to P for simplicity.

These two bisadducts were then selected together with three more structures chosen as references. Thus, geometry optimization at the PBE-D/TZP level was performed for the five MM+-minimized bisadducts *cis*-1 (A), *cis*-1 (K), *cis*-1 (P,*S*a,*R*a), *trans*-3 (C), and *e* (L) in which the six *tert*-butyl groups have been replaced by six hydrogen atoms. Resulting DFT-minimized bisadducts *cis*-1 (A)', *cis*-1 (K)', *cis*-1 (P,*S*a,*R*a)', *trans*-3 (C)' and *e* (L)' (Figure 2.15) and corresponding single-point calculations at SSB-D/TZP level provided useful information concerning relative energies of these bisadducts and their Zn···Zn distances (Figure 2.15 - inset). These studies showed that structure *cis*-1 (P,S_a,R_a), *i.e.* the corresponding bisadduct *P*-**17**(S_a,R_a), was significantly more stable (≈ 30–35 kcal mol^{-1}) than the other four computed bisadducts due to a combination of Pc-Pc π-stacking interactions and strain.

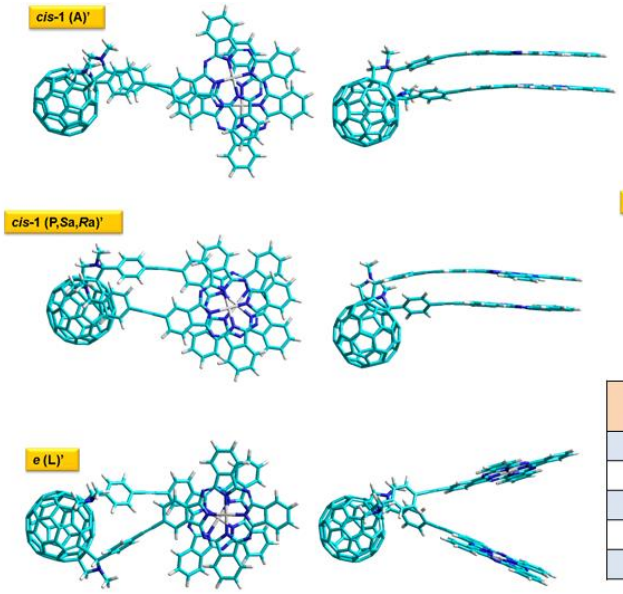

Pc_2-C_{60} bisadduct	Zn···Zn distance (Å)	DE^{PBE-D}	DE^{SSB-D}	$DE^{SSB-D\ (in\ Tol)}$
cis-1 (A)'	4.49	30.4	29.8	30.8
cis-1 (K)'	30.88	44.6	53.4	42.1
cis-1 (P,*Sa*,*Ra*)'	3.69	0.0	0.0	0.0
trans-3 (C)'	6.04	28.0	34.9	32.9
e (L)'	9.69	25.6	32.2	23.4

Figure 2.15. Representations (top view and lateral view) of *cis*-1 (A)', *cis*-1 (K)', *cis*-1 (P,*S*a,*R*a)', *trans*-3 (C)' and *e* (L)'[H] Pc_2-C_{60} bisadduct isomers obtained by DFT calculations. Inset: Relative energies (kcal mol^{-1}) and Zn···Zn distances (Å) for Pc_2-C_{60} bisadducts at PBE-D/TZP (gas phase) and SSB-D/TZP (gas phase and toluene) levels.

Detailed analysis of the chiral elements of atropisomers M/P-1(Sa,Ra), M/P-1(Ra,Ra), M/P-1(Sa,Sa) and M/P-1(Ra,Sa)

Some important points regarding the structural features of *P*-**17**(S_a,R_a) are worth mentioning. Bisadduct *P*-**17**(S_a,R_a), which at first glance could be erroneously considered a meso compound by looking exclusively at the regiochemistry of the C_{60} double addition and the configuration of its two stereogenic centers (Figure 2.14, model P), is instead a chiral molecule since it has no mirror plane and presents a right-handed (*P*) helical structure. Obviously, due to absence of any chiral bias, enantiomer *M*-**17**(S_a,R_a) (Scheme 2.2 - inset) is also formed together with *P*-**17**(S_a,R_a) leading to racemate *M*/*P*-**17**(S_a,R_a).

Moreover, it is worth noting that racemate *M*/*P*-**17**(S_a,R_a) presents a *cis*-1 C_{60} addition pattern. *cis*-1 C_{60} bisadducts are usually formed in the lowest relative yield with respect to the other C_{60} bisadducts (usually in a 1.4% relative yield in 1,3 dipolar cycloaddition reactions of untethered and non-prochiral azomethyne ylides to C_{60})[147,148], mainly due to the severe steric requirements imposed by the *cis*-1 bisaddition (Figure 2.13). Taking this into account, and considering that 16

147. Lu, Q., Schuster, D. I., Wilson, S. R. *J. Org. Chem.* **1996**, 61, 4764-4768.
148. Kordatos, K., Bosi, S., Da Ros, T., Zambon, A., Lucchini, V., Prato, M. *J. Org. Chem.* **2001,** 66**,** 2802-2808.

isomers are theoretically possible in the case of the *cis*-1 C_{60} bisaddition of two prochiral azomethyne ylides as in this work, a relative yield of 0.088% (*i.e.*, a sixteenth of 1.4%) should be expected for each of the 16 *cis*-1 isomers. In the case of racemate *M*/*P*-**17**(S_a,R_a), its relative yield would further decrease down to 0.022% (*i.e.*, a forth of 0.088%) considering that three more atropisomers, namely *M*/*P*-**17**(R_a,R_a), *M*/*P*-**17**(S_a,S_a) and *M*/*P*-**17**(R_a,S_a), could also theoretically form, each of them obtained as a racemic mixture of the *M* (Figure 2.13b-d,f-h) and *P* isomers. The four atropisomers have the same regiochemistry and stereoconfiguration at their two stereogenic centers but different spatial arrangement of the two Pcs due to their hindered rotation around two phenyl-ethynyl spacers. A comparison of the energetics of Pc_2-C_{60} bisadducts *P*-**17**(S_a,R_a), *P*-**17**(R_a,R_a), *P*-**17**(S_a,S_a), and *P*-**17**(R_a,S_a), which present similar distances between their quasi-parallel Pc planes, show that the latter three atropisomers are, respectively, 6.2, 6.5 and 24.6 kcal mol^{-1} higher in energy than atropisomer *P*-**17**(S_a,R_a). Beside energetics considerations, the partial stacked arrangement of the two Pcs in *P*-**17**(R_a,R_a), *P*-**17**(S_a,S_a) and *P*-**17**(R_a,S_a) could not explain the remarkable complexation ability of these Pc_2-C_{60} bisadducts towards DABCO – the three atropisomers have exceedingly large Zn···Zn distances of 5.9, 5.6 and 10.7 Å, respectively, *vs* 3.6 Å in the case of *P*-**17**(S_a,R_a). Moreover, the three latter atropisomers present α values, that is the tilt angle between the polarization axis of a Zn(II)Pc and the line connecting the two zinc metal centers, of ≈34.6º, 36.3º and 18.2º, respectively, values quite far from the ones typical of *H*-aggregates (54.7º > α> 90º; α for *P*-**1**(S_a,R_a) is 74.2º) and more proper of *J*-aggregates (0º > α> 54.7º).

Beside Pc π-stacking interactions, the role of other noncovalent forces in the formation of bisadducts *M*/*P*-**17**(S_a,R_a) such as electrostatic interactions between the azomethyne ylide zwitterions should not be discarded. Such electrostatic interactions should help stabilizing the π-stacked Pc dimer maintaining the two pendant azomethyne ylide moieties in close proximity, ultimately favoring their *cis*-1 addition to the C_{60} cage.

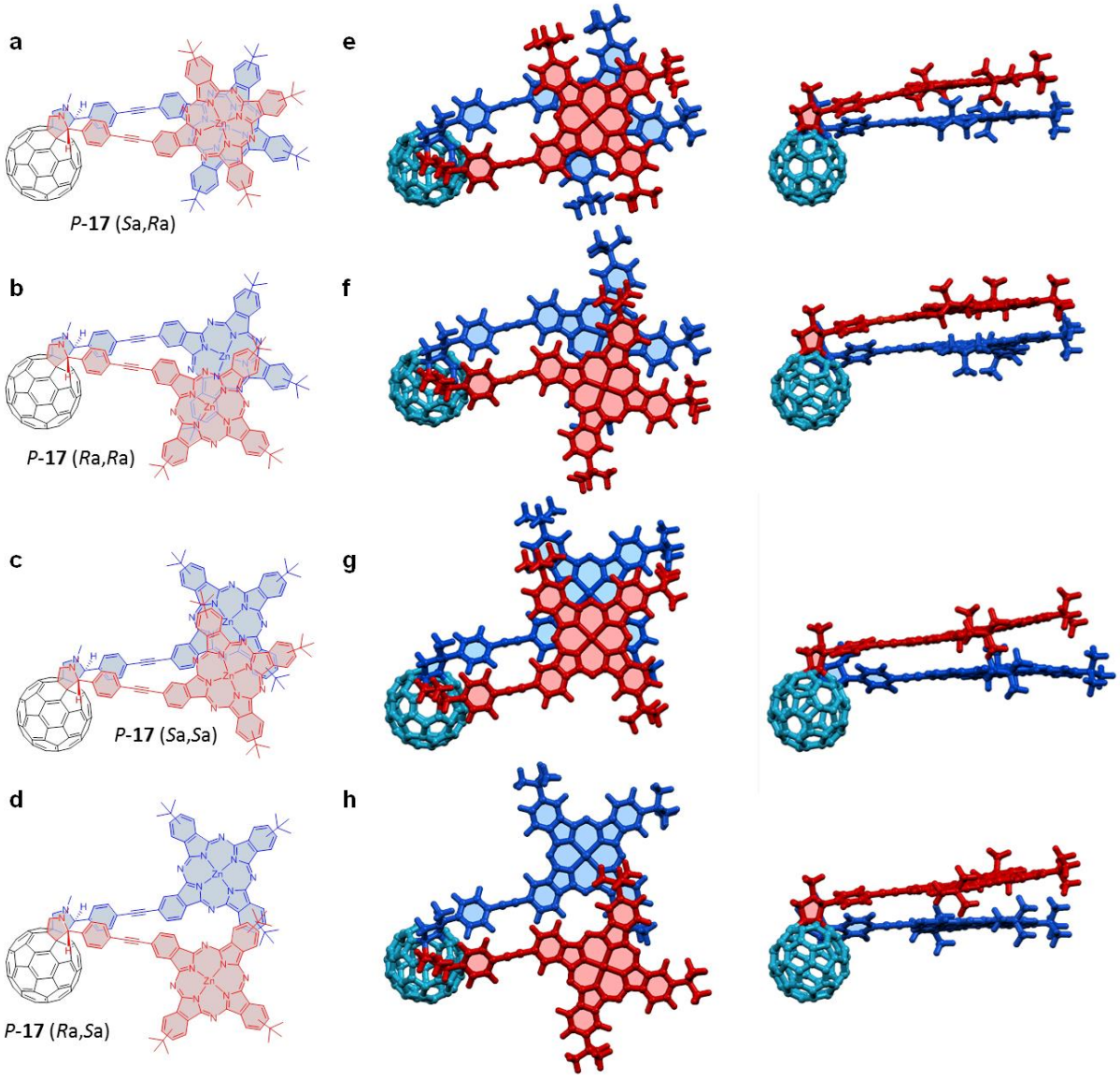

Figure 2.13. Molecular and DFT-minimized structures of atropisomers *P*-1(S_a,R_a), *P*-1(R_a,R_a), *P*-1(S_a,S_a), and *P*-1(R_a,S_a).

2.4 Summary and Conclusions

In this study we have demonstrated, for the first time, that noncovalent interactions between untethered and prochiral residues bearing large π-surfaces can be successfully used to promote the regio-, stereo- and atropselective synthesis of C_{60} bisadducts. Remarkably, using this "supramolecular-directed" approach, two bisadduct enantiomers presenting the sterically-demanding *cis*-1 C_{60} addition pattern could be obtained and greatly amplified from a complex mixture of over a hundred of C_{60} bisadducts from which the two enantiomers can be easily separated by simple silica gel column chromatography. This strategy takes advantage of noncovalent interactions between untethered phthalocyanine (Pc) species to boost (> 2800−fold) the formation of a pair of Pc_2-C_{60} bisadduct enantiomers which structure was determined by a combination of experimental techniques and theoretical calculations. Although supramolecular interactions have been widely used to construct complex architectures involving C_{60} fullerene, this is the first time that such noncovalent forces have been used to control the double functionalization of this carbon cage. We reckon that this "supramolecular" approach represents an important advance in the research area of the controlled multifunctionalization of fullerenes, which could be extended to other carbon nanoforms. Remarkably, and to our surprise, such untethered bisaddition reaction, not only proceeds with excellent regio- and stereoselectivity furnishing two enantiomers which present a *cis*-1 C_{60} addition pattern, but it is also highly atropselective as a result of the restricted rotation of the two Pc macrocycles in the products, representing the first example of atropselective reaction in fullerene chemistry.

2.5 Experimental Section

2.5.1 Materials and methods

Materials and methods used for identification of the compounds are similar to those described in the Experimental Section of Chapter 1.

For the **fluorescence** measurements, solutions containing *M*/*P*-**17**(*S*a,*R*a), **19**, **18** and reference compound were prepared and adjusted to exhibit identical absorbance of around 0.05 at the excitation wavelength of 611 nm. This ensures exclusive and likewise comparable excitation of the Zn(II)Pc chromophore as well as avoids inner filter effects that would result in intrinsic losses of the Zn(II)Pc fluorescence. The 611 nm excitation wavelength was selected since at this wavelength an isosbestic point was found upon the addition of DABCO allowing the comparability of fluorescence studies with and without the addition of DABCO.

Femtosecond transient absorption measurements were carried out with a CPA-2101 femtosecond laser (Clark MXR). The excitation wavelength was generated with an NOPA (Clark MXR). **Nanosecond transient absorption laser photolysis** measurements were performed with the output from the third harmonic (355 nm) of a Nd/YAG laser (Brilliant B, Quantel). The optical detection is based on a pulsed (pulser MSP 05 – Müller Elektronik-Optik) Xenon lamp (XBO 450, Osram), a monochromator (Spectra Pro 2300i, Acton Research), a R928 photomultiplier tube (Hamamatsu Photonics), and a 1-GHz digital oscilloscope (WavePro7100, LeCroy).

Pulse radiolysis measurements were performed with a LINAC electron accelerator (Titan Beta, TB-8/16-1S - Titan Cooperation). Electron pulses with a pulse width of 8 ns and a dose of 10 Gy were selected. The dose per pulse was measured with thiocyanate dosimetry[149]. The detection was performed by optical transient absorption technique consisting of an optional pulsed (Pulser 506 – PTI) 1000 W XBO lamp, a Spex 270 M monochromator (Spex Industries), an InGaAs photodiode and a 1.5 GHz digitizing oscilloscope (LC684DXL-LeCroy)[150].

[149]. Schuler, R. H., Patterson, L. K., Janata, E. *J. Phys. Chem.* **1980**, 84, 2088-2089.

[150]. Hug, G. L., Wang, Y., Schöneich, C., Jiang, P. Y., Fessenden, R. W. *Radiat. Phys. Chem.* **1999**, 54, 559-566.

The **association constant** (K_a) between Pc_2-C_{60} racemate *M*/*P*-1(*S*a,*R*a) and DABCO were calculated using the ReactLab™ EQUILIBRIA software through a global fitting of the four equilibrium titration measurements carried out.

Density functional calculations with inclusion of dispersion corrections in the density functionals have been carried out in collaboration with the group of Prof. Josep M. Poblet from Universitat Rovira i Virgili of Tarragona. The DFT-D3 method developed by Grimme has been used in combination with the PBE and SSB density functionals (PBE-D and SSB-D, respectively) and a basis set of triple-zeta quality (TZP)[151].

Tri-*tert*-butyl Zn(II)Pc aldehyde **20** [152] and 2-iodo-9,10,16,17,23,24-hexakis-(2',6'-diphenylphenoxy)-phthalocyaninato zinc(II) [153] were synthesized following some reported procedure. H_2@C_{60} fullerene was synthesized according to a reported procedure[154].

Pyridine, pyrazine and 1,4-diazabicyclo[2.2.2]octane (DABCO) were purchased from Aldrich. Pyridine and pyrazine were used without further purification whereas DABCO was recrystallized from absolute ethanol twice, and then dried under vacuum.

pyridine

p*Ka* = 5.1

pyrazine

p*Ka* = 0.6

N-N distance = 2.7 Å

DABCO

p*Ka* = 8.7

N-N distance = 2.6 Å

[151]. (a) Perdew, J. P., Burke K. & Ernzerhof, M. Generalized gradient approximation made simple. *Phys. Rev. Lett.* **77,** 3865–3868 (1996); (b) Swart, M., Solà M. & Bickelhaupt, F. M. A new all-round DFT functional based on spin states and S_N2 barriers. *J. Chem. Phys.* **131,** 094103 (2009); (c) Grimme, S., Antony, J., Ehrlich, S. & Krieg, H. A consistent and accurate ab initio parametrization of density functional dispersion correction (DFT-D) for the 94 elements H-Pu. *J. Chem. Phys.* **132,** 154104 (2010).

[152]. Bottari, G., Olea, D., Gomez-Navarro, C., Zamora, F., Gomez-Herrero, J. & Torres, T. *Angew. Chem. Int. Ed.* **47,** 2026-2031 (2008).

[153]. Ragoussi, M.-E., Cid, J. J., Yum, J.-H., de la Torre, G., Di Censo, D., Michael Grätzel, M., Nazeeruddin, M. K. & Torres, T. *Angew. Chem. Int. Ed.* **51**, 4375-4378 (2012).

[154]. Murata, M., Murata, Y. & Komatsu, K. *J. Am. Chem. Soc.* **128,** 8024-8033 (2006).

2.5.2 Synthetic procedures

General procedure for the synthesis of Pc-C_{60} monoadduct **19**, and Pc_2-C_{60} bisadducts M/P-**17**(Sa,Ra) and **18**:

A flask was charged under argon with C_{60} fullerene (36.0 mg, 0.05 mmol), *N*-methyl glycine (12.3 mg, 0.138 mmol) and dry toluene (15 mL) and the resulting solution ultrasonicated for 15 minutes at 40 ºC. After this, (tri-*tert*-butyl)(benzaldehyde-4-ethynyl) Zn(II)Pc **20** (40 mg, 0.046 mmol) was added and the resulting solution heated at 100 ºC under argon for 12 hrs. Silica gel column chromatography (toluene:EtOAc 25:1 v/v) was then carried out on the reaction mixture obtaining, besides the recovery of some unreacted C_{60} fullerene (3 mg, 0.004 mmol), Pc_2-C_{60} racemate *M*/*P*-**17**(*S*a,*R*a) (obtained as a mixture of the *M*-**17**(*S*a,*R*a) and *P*-**17**(*S*a,*R*a) enantiomers), Pc-C_{60} fullerene monoadduct **19** and Pc_2-C_{60} fullerene bisadducts **18** in this order of elution. Compounds *M*/*P*-**17**(*S*a,*R*a), **19** and **18** were finally triturated from MeOH obtaining for the three compounds a deep-green powder.

Alternatively, Pc_2-C_{60} fullerene bisadducts *M*/*P*-**17**(*S*a,*R*a) could also be purified by using a preparative TLC (toluene:EtOAc:pyridine 100:2:1 v/v/v). Interestingly, using preparative TLC as "stationary phase" and toluene:EtOAc:pyridine as "eluting phase" results in a change in the order of elution of compounds *M*/*P*-**17**(*S*a,*R*a) and **19** with respect to the silica gel column chromatography.

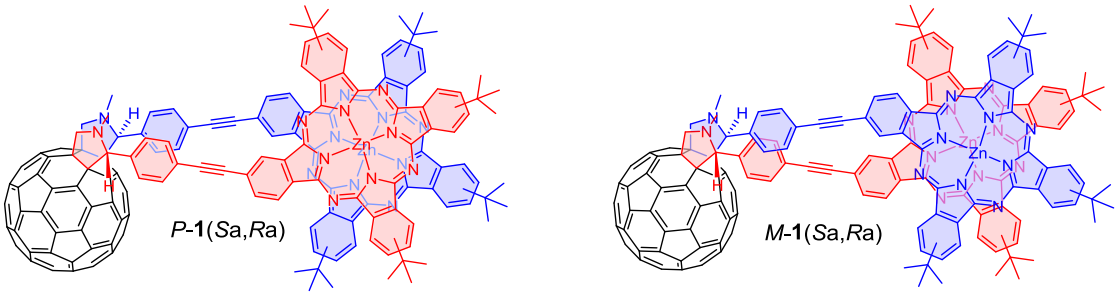

Yield and characterization of Pc_2-C_{60} racemate *M*/*P*-**17**(*S*a,*R*a):

Yield: 8.2 mg, 3.3 x 10^{-3} mmol (14%, based on half of the mmol of Pc-CHO **20** used, *i.e.*, 0.046/2 = 0.023 mmol); RF = 0.43 (toluene:EtOAc = 15:1); m.p. > 300 ºC; ^{1}H NMR (500 MHz, [D_8]THF, 25 ºC) δ 9.95-7.12 (m, 32H, C*H*$_{ArPc}$, C*H*$_{Ar}$), 5.18-3.74 (6H, C*H*$_{pyrrolidine}$), 3.03-2.41 (6H, NC*H*$_3$), 1.84 (s, 54H, C(C*H*$_3$)$_3$); FT-IR (KBr) ν (cm^{-1}) = 2956, 2779, 1738, 1610, 1495, 1389, 1331, 1255, 1150, 1089, 1053, 924, 832, 751, 693; UV/vis (THF): λ_{max} (log ε) = 341 nm (5.21), 640 nm (5.07), 670 nm

(5.14); MALDI-TOF MS (dithranol): *m/z* (% intensity) 2518.7-2530.7 (isotopic pattern) $[M]^+$ (100%), 5037.4-5055.4 (isotopic pattern) $[2M]^+$ (2%). HRMS (MALDI): calcd for $C_{170}H_{98}N_{18}Zn_2$ $[M]^+$: 2518,6799; found: 2518,6618.

Yield and characterization of Pc-C_{60} monoadduct **19**:

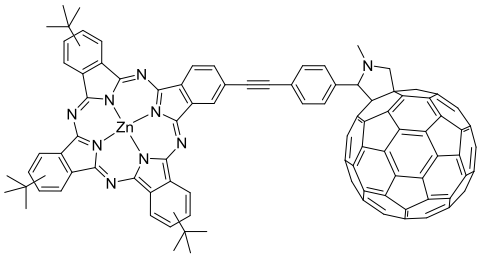

Yield: 21.5 mg, 1.3 x 10^{-2} mmol (28%, based on the mmol of Pc-CHO **20** used, *i.e.*, 0.046 mmol). ^{1}H NMR (300 MHz, [D_8]THF, 25 ^{o}C) δ 9.49 (m, 4H, CH_{ArPc}), 9.30 (m, 4H, CH_{ArPc}), 8.30 (m, 4H, CH_{ArPc}), 8.02 (d, 3*J*(H,H) = 7.2 Hz, 2H, CH_{Ar}), 7.88 (d, 3*J*(H,H) = 7.2 Hz, 2H, CH_{Ar}), 5.11 (s, 1H, C$H_{pyrrolidine}$), 5.07 (d, 2*J*(H,H) = 9.7 Hz, 1H, C*H*H$_{pyrrolidine}$), 4.32 (d, 2*J*(H,H) = 9.7 Hz, 1H, CH$H_{pyrrolidine}$), 2.89 (s, 3H, NCH_3), 1.84 (s, 27H, C(CH_3)$_3$); FT-IR (KBr) ν (cm^{-1}) = 2961, 2853, 2799, 1952 (weak), 1618, 1493, 1331, 1074, 916, 835, 758, 690; UV/vis (THF): λ_{max} (log ε) = 348 nm (4.55), 610 (4.07), 633 (4.02), 672 (4.69), 686 nm (4.76); MALDI-TOF MS (dithranol): m/z (% intensity) 1619.4-1628.3 (isotopic pattern) $[M]^+$ (100%), 3238.8-3254.6 (isotopic pattern) $[2M]^+$ (8%).

Yield and characterization of Pc_2-C_{60} bisadducts **18**:

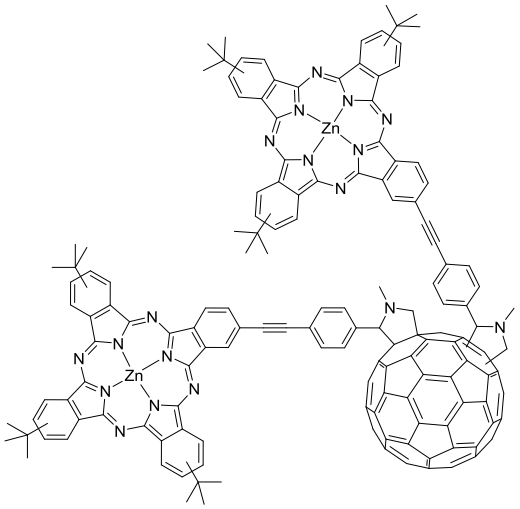

Yield: 13.2 mg, 5.2 x 10^{-3} mmol (23%, based on half of the mmol of Pc-CHO **20** used, *i.e.*, 0.046/2 = 0.023 mmol); RF = 0.14 (toluene:EtOAc = 15:1); m.p. > 300 ºC; ^{1}H NMR (500 MHz, THF-d_8, 25 ºC) δ 9.54-9.16 (m, 16H, CH_{ArPc}), 8.37-8.18 (m, 8H, CH_{ArPc}), 8.09-7.63 (m, 8H, CH_{Ar}), 5.38-3.67 (6H,

C$H_{pyrrolidine}$), 3.04-2.47 (6H, NCH_3), 1.84 (s, 54H, C(CH_3)$_3$); FT-IR (KBr) ν (cm^{-1}) = 2963, 2781, 1618, 1491, 1392, 1363, 1259, 1149, 1091, 1050, 923, 830, 749, 691; UV/vis (THF): λ_{max} (log ε) = 349 nm (5.35), 612 nm (4.88), 635 nm (4.89), 672 nm (5.50), 685 nm (5.59); MALDI-TOF MS (dithranol): *m/z* (% intensity) 2518.7-2530.7 (isotopic pattern) $[M]^+$ (100%), 5037.4-5055.4 (isotopic pattern) $[2M]^+$ (2%). HRMS (MALDI): calcd for $C_{170}H_{98}N_{18}Zn_2$ $[M]^+$: 2518,6799; found: 2518,6635.

*Synthesis and characterization of Pc **23**, Pc-C_{60} monoadduct **22**, and Pc_2-C_{60} bisadducts **21***

Synthesis of aldehyde-substituted Pc **23**

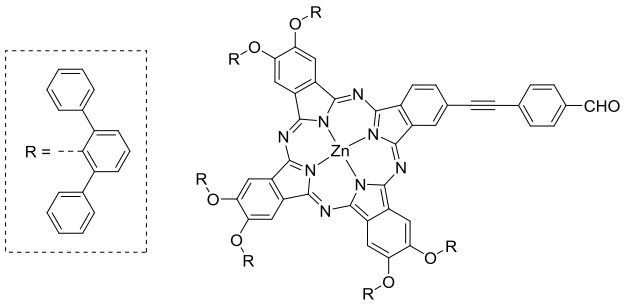

A flask was charged under argon with 2-iodo-9,10,16,17,23,24-hexakis-(2',6'-diphenylphenoxy)-phthalocyaninato zinc(II) (40 mg, 0.02 mmol) and CuI (0.35 mg, 0.002 mmol) and dry toluene (5 mL) added. NEt_3 (17 µL) was added to the solution while stirring, followed by addition of 4-(ethynyl)-benzaldehyde (2.9 mg, 0.02 mmol) and $PdCl_2(PPh_3)_2$ (0.5 mg, 7 x 10^{-4} mmol). The solution was left to stir at 45 ºC overnight. After this time, the solution was cooled down to room temperature and reduced in volume. The crude was purified by column chromatography in silica gel (DCM:THF 200:1) to obtain aldehyde-substituted Zn(II)Pc **23** which was triturated from hexane to obtain a green powder.

Yield and characterization of aldehyde-substituted Pc **23**:

Yield: 18.8 mg (47%); RF = 0.70 (DCM:THF = 200:1); m.p. > 300 ºC; ^{1}H NMR (400 MHz, THF-d_8, 25 ºC) δ 10.07 (s, 1H, C*H*O), 9.26 (s, 1H, CH_{ArPc}), 9.11 (d, *J*(H,H) = 8.0 Hz, 1H, CH_{ArPc}), 8.11 (d, *J*(H,H) = 8.8 Hz, 1H, CH_{ArPc}), 8.01 (d, *J*(H,H) = 8.4 Hz, 2H, CH_{Ar}), 7.91 (d, *J*(H,H) = 7.6 Hz, 2H, CH_{Ar}), 7.82-7.75 (m, 29H, CH_{ArPc}), 7.68-7.63 (m, 10H, CH_{ArPc}), 7.61-7.58 (m, 6H, CH_{ArPc}), 6.96-6.92 (m, 17H, CH_{ArPc}), 6.87-6.80 (m, 18H, CH_{ArPc}), 6.78-6.73 (m, 4H, CH_{ArPc}); UV/vis (THF): λ_{max} (log ε) = 363 nm (4.93),

614 nm (4.47), 640 nm (4.48), 677 nm (5.14), 699 nm (5.19); MALDI-TOF MS (DCTB): *m*/*z* 2168.6-2177.6 (isotopic pattern) $[M]^+$.

*Synthesis and characterization of Pc-C_{60} monoadduct **22**, and Pc_2-C_{60} bisadducts **21***

Pc-C_{60} monoadduct **22** and Pc_2-C_{60} bisadducts **21** were prepared using the same reaction conditions leading to the preparation of Pc-C_{60} monoadduct **19** and Pc_2-C_{60} bisadducts *M*/*P*-**17**(S_a,R_a) and **18**, only replacing Zn(II)Pc aldehyde **20** for Zn(II)Pc aldehyde **23**. Pc-C_{60} monoadduct **22** and Pc_2-C_{60} bisadducts **21** were isolated by column chromatography (toluene:EtOAc 25:1 v/v).

Yield and characterization of Pc-C_{60} monoadduct **22**:

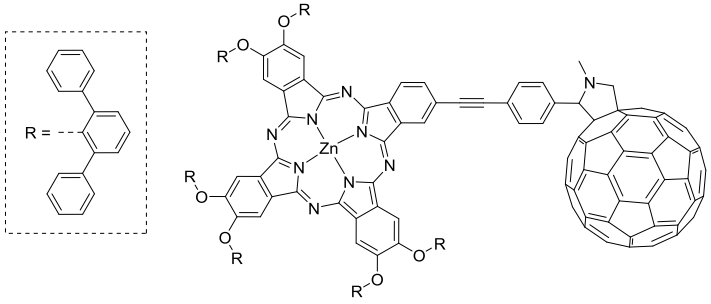

Yield: 15.1 mg (28%); RF = 0.85 (DCM:THF = 200:1); m.p. > 300 ºC; ^{1}H NMR (400 MHz, THF-d_8, 25 ºC) δ 9.21 (s, 1H, C*H*$_{ArPc}$), 9.08 (d, *J*(H,H) = 8.0 Hz, 1H, C*H*$_{ArPc}$), 8.07 (d, *J*(H,H) = 8.4 Hz, 1H, C*H*$_{ArPc}$), 7.80-7.73 (m, 4H, C*H*$_{Ar}$), 7.92-7.74 (m, 29H, C*H*$_{ArPc}$), 7.74-7.60 (m, 16H, C*H*$_{ArPc}$), 6.96-6.91 (m, 17H, C*H*$_{ArPc}$), 6.87-6.80 (m, 18H, C*H*$_{ArPc}$), 6.79-6.71 (m, 4H, C*H*$_{ArPc}$); 5.17 (s, 1H, C*H*$_{pyrrolidine}$), 5.14 (d, *J*(H,H) = 10.0 Hz, 1H, C*H*H$_{pyrrolidine}$), 4.40 (d, *J*(H,H) = 10.0 Hz, 1H, C*H*H$_{pyrrolidine}$), 2.91 (s, 3H, NC*H*$_3$); UV/vis (THF): λ_{max} (log ε) = 361 nm (4.66), 615 nm (4.14), 644 nm (4.08), 679 nm (4.82), 696 nm (4.84); MALDI-TOF MS (DCTB): *m*/*z* 2915.7-2924.7 (isotopic pattern) $[M]^+$.

Yield and characterization of Pc_2-C_{60} bisadducts **21**:

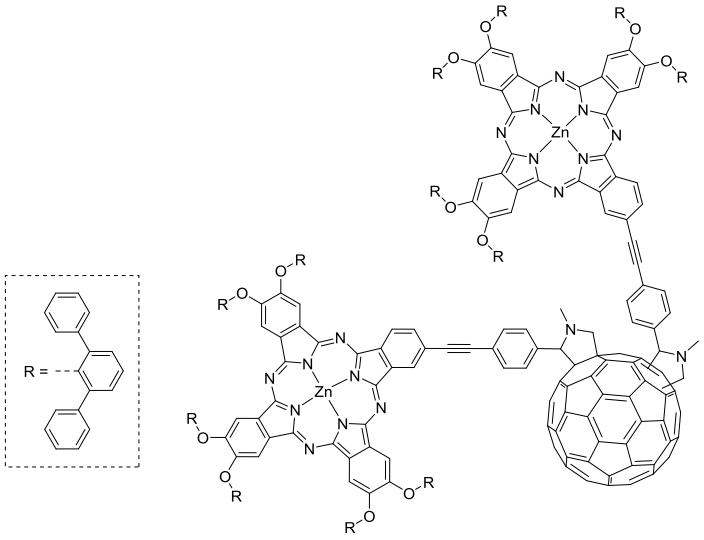

Yield: 16.0 mg (34%); RF = 0.80 (DCM:THF = 200:1); m.p. > 300 ºC; ^{1}H NMR (400 MHz, THF-d_8, 25 ºC) δ 9.30-9.04 (4H, CH_{ArPc}), 8.18-7.90 (2H, CH_{ArPc}), 7.81-7.73 (m, 8H, CH_{Ar}), 7.73-7.62 (m, 58H, CH_{ArPc}), 7.58-7.43 (m, 32H, CH_{ArPc}), 6.86-6.79 (m, 34H, CH_{ArPc}), 6.77-6.61 (m, 44H, CH_{ArPc}), 5.38-3.90 (6H, C$H_{pyrrolidine}$), 3.04-2.70 (6H, NCH_3); UV/vis (THF): λ_{max} (log ε) = 361 nm (5.45), 616 nm (4.93), 639 nm (4.90), 679 nm (5.61), 697 nm (5.69); MALDI-TOF MS (DCTB): *m*/*z* 5111.7-5125.8 (isotopic pattern) $[M]^+$.

Summary and conclusions

In the first chapter, synthesis and study of (Sub)Pc – EMF hybrids for tunable electron transfer has been discussed.

In the first section, we have successfully prepared four electron D-A ensembles built on metal-ligand coordination between C_{60} or $Sc_3N@I_h$-C_{80} featuring a pyridyl moiety, on one hand, and electron-donating or electron-accepting Zn(II)Pcs, on the other hand. Composition of supramolecular ensembles was Full-fledged photophysical assays with those two ensembles that contain $Sc_3N@I_h$-C_{80} **4** axially coordinated either to the electron-donating Zn(II)Pc **1** or to the electron-accepting Zn(II)Pc **2** revealed a switchable electron transfer reactivity.

Namely, spectroscopic and kinetic evidence for a Zn(II)Pc-to-$Sc_3N@I_h$-C_{80} a $Sc_3N@I_h$-C_{80}-to-Zn(II)Pc electron transfer – upon light excitation – was established as the major deactivation pathways in time–resolved pump probe experiments. In the case of the complexes between Zn(II)Pc **1** and fullerene derivatives **3** or **4**, PET from the Zn(II)Pc macrocycle to the fullerene moiety dominates the deactivation dynamics. Whereas, a $Sc_3N@I_h$-C_{80}-to-Pc charge transfer is observed for complex **2**/**4**, and no evidence of electron transfer was observed for complex **2**/**3**, in perfect agreement with electrochemical results obtained for derivatives **1**–**4**. This is, to the best of our knowledge, the first time that a fullerene-based molecular building block shows an electron transfer dualism. In the case of supramolecular complexes **1**/**4** and **2**/**4**, a switchable PET process is observed involving, for the first time, a fullerene-based molecule (**4**), which acts both as electron-acceptor or electron-donor as a function of the electronic nature of its supramolecular counterpart. Additionally, and importantly, this work involves, for the first time, the use of $Sc_3N@I_h$-C_{80} as an electron-accepting/-donating redox moiety, an EMF which is considered as the most abundant and readily available in bulk quantities by non-HPLC methods.

These findings, in combination with the small reorganization energy of fullerenes in electron transfer reactions, is likely to pave the road to the preparation of novel switching devices, solar energy conversion schemes, and logic gates based on $Sc_3N@I_h$-C_{80}, one of the most abundant and easy-to-purify fullerene. Particularly interesting is also the use of self-assembly *en-route* towards the preparation and study of a plethora of easy-to-prepare D-A constructs showing switchable electron transfer features.

In the second section, electron accepting SubPcs, bearing fluorine (**11**) or pentylsulfonyl substituents (**12**) on their periphery, have been used in combination with $La_2@I_h$-C_{80} and C_{60}

fullerenes to prepare a series of novel electron donor-acceptor conjugates by means of the Prato reaction. We have documented the comprehensive study of their photophysical properties by means of several steady-state and time-resolved assays.

In terms of electrochemical and steady-state absorption, our results reveal no appreciable electronic interactions between SubPcs and $La_2@I_h$-C_{80} / C_{60}fullerene moieties in the ground state. In the excited state, an intramolecular electron-transfer evolves from $La_2@I_h$-C_{80} to photo excited (perfluoro) or (pentylsulfonyl) SubPc unit upon photoexcitation at 530 or 568 nm, respectively.

Regarding SubPcs-C_{60} reference conjugates **5** and **7**, only a singlet-singlet energy transfer from SubPc to C_{60} takes place upon photoexcitation at 530 nm. Whereas, unambiguous intramolecular ultrafast charge separation (in the range from 0.6 to 4.1 ps) occurs between SubPcs and C_{60} moieties upon photoexcitation at either 320 or 387 nm to form the one-electron oxidized form of C_{60} and the one-electron reduced forms of the two different SubPcs. This is, to the best of our knowledge, the first case of an *intramolecular* oxidation of C_{60} as part of an electron donor-acceptor conjugate for advanced solar energy conversion schemes by means of only photoexcitation. The charge separated state lifetime is at this state rather short lived with values of up to 38 ps. Radical ion pair state lifetime could be extended by, possibly, changing the energetics / thermodynamics of charge recombination.

Resuming, subphthalocyanines were proved to be successful candidates for tuning electron transfer reactivity of fullerenes. Thus, replacing $La_2@I_h$-C_{80} by C_{60} in SubPc hybrids provided a promising way to tune electron-transfer *vs* energy-transfer. Most importantly, energy transfer within SubPc-C_{60} conjugates could be switched back to electron transfer of the opposite direction by a simple change of the excitation strength from 530 nm to 320 nm. Considering the short separations between the electron donors and acceptors in the reported systems, further optimisation of the charge-separated state lifetimes seems achievable through the tailored design of linkers between $La_2@I_h$-C_{80} and SubPcs.

In the second chapter we have demonstrated, for the first time, that noncovalent interactions between untethered and prochiral residues bearing large π-surfaces can be successfully used to promote the regio-, stereo- and atropselective synthesis of C_{60} bisadducts. Remarkably, using this “supramolecular-directed” approach, two bisadduct enantiomers presenting the sterically-

demanding *cis*-1 C_{60} addition pattern could be obtained and greatly amplified from a complex mixture of over a hundred of C_{60} bisadducts from which the two enantiomers can be easily separated by simple silica gel column chromatography. This strategy takes advantage of noncovalent interactions between untethered phthalocyanine (Pc) species to boost (> 2800−fold) the formation of a pair of Pc_2-C_{60} bisadduct enantiomers which structure was determined by a combination of experimental techniques and theoretical calculations. Although supramolecular interactions have been widely used to construct complex architectures involving C_{60} fullerene, this is the first time that such noncovalent forces have been used to control the double functionalization of this carbon cage. We reckon that this “supramolecular” approach represents an important advance in the research area of the controlled multifunctionalization of fullerenes, which could be extended to other carbon nanoforms. Remarkably, and to our surprise, such untethered bisaddition reaction, not only proceeds with excellent regio- and stereoselectivity furnishing two enantiomers which present a *cis*-1 C_{60} addition pattern, but it is also highly atropselective as a result of the restricted rotation of the two Pc macrocycles in the products, representing the first example of atropselective reaction in fullerene chemistry.